



**UNIVERSITÀ
DEGLI STUDI
DI UDINE**



Thesis submitted for the award of the degree of

DOCTOR OF PHILOSOPHY

in

ENVIRONMENTAL AND ENERGY ENGINEERING SCIENCE

from

UNIVERSITÀ DEGLI STUDI DI UDINE

XXVIII cycle

Homogeneous Gold Catalysis: understanding ligand and counterion effects, first steps in green chemistry.

Luca Biasiolo

Dr. Daniele Zuccaccia - Supervisor

Prof. Marco Bandini - Referee

Dr. Leonardo Belpassi - Referee

Prof.ssa Carla De Leitenburg - Examiner

Prof. Pietro Mastrorilli - Examiner

Prof.ssa Barbara Milani - Examiner

Summary

List of abbreviations and complexes numeration

List of publications

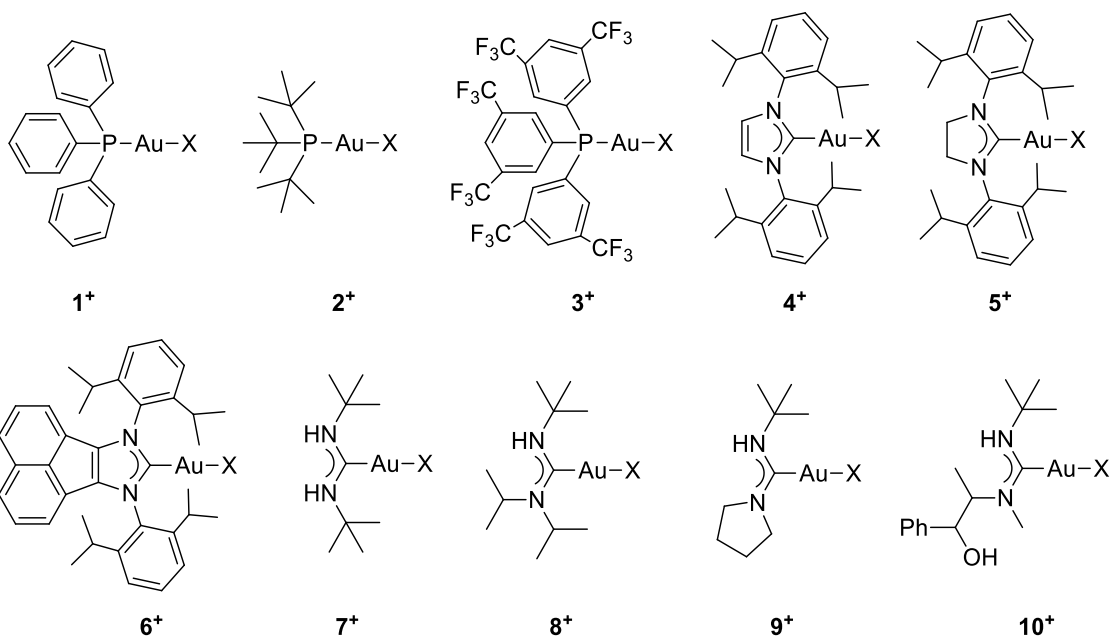
Abstract

Summary


1. Introduction	1
1.1 Transition metals in catalysis and sustainable process	3
1.1.1 Catalysis	3
1.1.2 Transition metals compounds	4
1.1.3 Green processes	7
1.2 Gold in catalysis and sustainable process	9
1.2.1 Story and properties of gold complexes	9
1.2.2 Gold Catalysis	14
1.2.3 Study of the Ion Pairs	19
1.2.4 Green gold applications	23
2. Results and Discussion	27
2.1 Role of the anion nature	29
2.1.1 Nucleophile effect	37
2.2 Functionalized carbene ligands to modify IP and catalytic activities	43
2.2.1 Nitrogen heterocyclic carbenes	43
2.2.2 Nitrogen acyclic carbenes	48
2.2.3 Importance of the anion position in catalysis.	55
2.3 Bonding characterization: Theory and Experimental Studies	59
2.4 Appropriate matching of Ligand (L) and Counterion (X ⁻)	68
2.4.1 Effect in methoxylation reaction	68
2.4.2 Effect in the cyclization of propargylamides	71
2.5 Hydration of alkynes	78
3. Conclusions and Perspectives	87
4. Experimental Part	93
4.1 General Procedures and Materials	95
4.2 Synthesis	95
4.3 Catalysis	112
4.3.1 Methoxylation of 3-hexyne catalysed by 4X	112
4.3.2 Methoxylation of 3-hexyne catalysed by 7-10X	127
4.3.3 Methoxylation of 3-hexyne catalysed by 1-4X	129
4.3.4 Cyclization of N-(prop-2-yn-yl)benzamide to 2-phenyl-5-vinylidene-2-oxazoline	134
4.4 4. NMR studies	139
4.4.1 4.1 Pre-equilibrium studies	139
4.4.2 ³¹ P NMR of 1-3X for ciclyzation	142
4.4.3 ³¹ P NMR of 1-3X for methoxylation	144
4.4.4 Intramolecular and Interionic Characterization.	146
4.4.5 4.5 EXSY NMR measurements and Eyring plots.	149
4.5 Computational Studies	155
4.5.1 Computational details for 4-10X complexes.	156
4.5.2 Computational details for 9L , 9'L and C₂H₂L systems	169
5. References	195

List of abbreviations and complexes numeration


BAR ^{F-}	tetrakis(pentafluorophenyl)borate
BF ₄ ⁻	tetrafluoroborate
BIAN	bis(imino)acenaphthene
CD	Charge Displacement
Cp	cyclopentadienyl
DCD	Dewar-Chartt-Duncanson
DCU	N,N'-Dicyclohexylurea
DFT	Density Functional Theory
L	general ligand
NAC	Nitrogen Acyclic Carben
NHC	Nitrogen Heterocyclic Carben, wen not otherwise specified it is refereeing to 1,3-bis(2,6-diisopropylphenyl)imidazol-2-ylidene
NO ₃ ⁻	nitrate
NOE	Nuclear Overhauser Effect
NTf ₂ ⁻	bis(trifluoromethanesulfonyl)amide
OAc ⁻	acetate
OTf ⁻	trifluoromethanesulfonate
OTs ⁻	p-toluenesulfonate
P(RO) ₃	tris(2,4-ditert-butylphenyl) phosphite
PAR ^F	tris(3,5-bis(trifluoromethyl)phenyl) phosphine
PF ₆ ⁻	hexafluorophosphate
PPh ₃	triphenylphosphine
P ^t Bu ₃	tri-tertbutyl phosphine
SbF ₆ ⁻	hexafluoroantimonate
SNHC	1,3-Bis(2,6-di-isopropyl-phenyl)dihydroimidazol-2-ylidene
TFA ⁻	trifluoroacetate
THT	tetrahydrothiophene
TOF	turnover frequency
TON	turnover number
X	general counterion




List of publications

- 1) G. Ciancaleoni, **L. Bisiolo**, G. Bistoni, A. Macchioni, F. Tarantelli, D. Zuccaccia and L. Belpassi, *Organometallics*, **2013**, *32*, 4444-4447. 


We have studied the ion pair structure of $[\text{NHCAu}(\eta^2\text{-3-hexyne})][\text{BF}_4]$ (NHC = nitrogen-heterocyclic carbene) by solution NOE NMR spectroscopy and relativistic DFT calculation. The neutral complexes $[\text{NHC-AuCl}]$ have been synthesized through an improved, silver-free one-pot synthesis, by reaction (in air and using solvents and substrates without any previous purification) of the appropriate $[\text{NHC(H)}]\text{Cl}$, gold precursor, and KHCO_3 . Ion pairs were generated in situ in NMR tubes. In our previous work, two main ion pair orientations were observed for unsaturated NHC ligands: one with the anion close to the carbene backbone (A, most populated) and another with the anion close to the alkyne (B). Here we focus on the effect of the carbene backbone on the ion pair structure, comparing the unsaturated NHC (1BF_4) with two different variants: a saturated NHC (2BF_4) and a polycyclic ligand with an extended aromatic system (3BF_4). For 2BF_4 , the A:B ratio remains almost the same as for 1BF_4 , while the ion pair structure of 3BF_4 becomes mainly nonspecific, with a slight preference for the orientation B. Both cases can be explained analyzing the DFT Coulomb potential map, which shows an attractive region on the backbone of 2BF_4 and a flat weak potential around the whole 3BF_4 .

- 2) **L. Bisiolo**, M. Trinchillo, P. Belanzoni, L. Belpassi, V. Busico, G. Ciancaleoni, A. D'Amora, A. Macchioni, F. Tarantelli and D. Zuccaccia, *Chem. Eur. J.* **2014**, *20*, 14594-14598. 


The intermolecular alkoxylation of alkynes is the oldest application of cationic gold(I) catalysts; however, no systematic experimental data about the role of the anion are available. In this contribution, the role of the anion in this catalytic reaction as promoted by a N-heterocyclic carbene-based gold catalyst, $[(\text{NHC})\text{AuX}]$ ($\text{X}=\text{BARF}^-$, BF_4^- , OTf^- , OTs^- , TFA^- , or OAc^-) is analyzed, through a combined experimental (NMR spectroscopy) and theoretical (DFT calculation) approach. The most important factor seems to be the ability to abstract the proton from the methanol during the nucleophilic attack, and such ability is related to the anion basicity. On the other hand, too high coordination power or basicity of the anion worsens the catalytic performance by preventing alkyne coordination or by forming too much free methoxide in solution, which poisons the catalyst. The intermediate coordinating power and basicity of the OTs^- anion provides the best compromise to achieve efficient catalysis.

- 3) **L. Bisiolo**, G. Ciancaleoni, L. Belpassi, G. Bistoni, A. Macchioni, F. Tarantelli and D. Zuccaccia, *Catal. Sci. Technol.* **2015**, *5*, 1558-1567. 

We elucidate the role of the ligand in determining the ion pair structure of the $[(\text{NAC})\text{Au}(\eta^2\text{-3-hexyne})]^+\text{BF}_4^-$ (NAC = Nitrogen Acyclic Carbene, also known as ADC = Acyclic Diamino Carbene) catalysts and how the position of the anion influences their catalytic performance, giving a detailed relationship between the ion pair structure, determined by ^{19}F , ^1H -HOESY NMR experiments and DFT calculations, and the catalytic activity in the intermolecular alkoxylation of alkynes. From our results, it is evident that if the anion is forced to be far from the catalytic site by ancillary ligand-anion hydrogen bonding interactions, the reaction slows down. On the contrary, if the anion is located near the alkynes the reaction is accelerated, coherent with the proposed active role of the anion in catalysis. These results open new opportunities in ligand design for the gold-mediated reactions in which the anion plays an important role during the catalysis.


- 4) G. Ciancaleoni, **L. Bisiolo**, G. Bistoni, A. Macchioni, F. Tarantelli, D. Zuccaccia and L. Belpassi, *Chem. Eur. J.* **2015**, *21*, 2467-2473. 

Even though the Dewar-Chart-Duncanson model has been successfully used by chemists since the 1950s, no experimental methodology is yet known to unambiguously estimate the constituents (donation and back-donation) of a metal-ligand interaction. It is demonstrated here that one of these components, the metal-to-ligand π back-donation, can be effectively probed by NMR measurements aimed at determining the rotational barrier of a C-N bond (ΔH_r^\ddagger) of a nitrogen acyclic carbene ligand. A large series of gold(I) complexes have been synthesized and analyzed, and it was found that the above experimental observables show an accurate correlation with back-donation, as defined theoretically by the appropriate charge displacement originated upon bond formation. The proposed method is potentially of wide applicability for analyzing the ligand effect in metal catalysts and guiding their design.


- 5) C. A. Gaggioli, G. Ciancaleoni, **L. Bisiolo**, G. Bistoni, D. Zuccaccia, L. Belpassi, P. Belanzoni and F. Tarantelli, *Chem. Commun.* **2015**, *51*, 5990-5993. 

We analyzed the ligand electronic effect in a gold(I)-catalyzed intramolecular alkyne hydroamination, through a DFT and charge-displacement function (CDF) study. We found that, in the presence of π -electron conjugation between the alkyne and the nucleophilic functionality, electron poor ligands modify the coordination mode and the geometric parameters of the substrate in such a way that, contrary to expectations, the activation barrier of the nucleophilic attack increases. This remarkable effect is


due to the competition between alkyne activation and nucleophile deactivation. The general relevance of these findings is highlighted.

6) **L. Biasiolo**, L. Belpassi, G. Ciancaleoni, A. Macchioni, F. Tarantelli and D. Zuccaccia, *Polyhedron* **2015**, *92*, 59. 


In the last years, it has been demonstrated that the anion plays a key role in gold(I) catalysis, affecting yield, regio- and stereo-selectivity of processes. In order to perform such activity, necessarily the anion has to locate itself close to the reaction center. In this contribution, the level of aggregation of cationic linear gold complexes bearing different ligands, such as phosphines and carbenes, is studied by diffusion PGSE (Pulsed field Gradient Spin Echo) NMR spectroscopy as a function of concentration and solvent. It is found that functional groups, which establish specific interactions with the anion, such as –NH or polarized –CH moieties, strongly influence the self-aggregation of gold(I) complexes: ion pairs are the predominant species in solution, but ion quadruples also form in apolar solvents only when –NH or polarized –CH moieties are present in the ligand. In the absence of those functional groups free ions are present in solution with a small amount of ion pairs. Interestingly, the presence of an extended aromatic group on the cation leads to dicationic adducts and ion triples, which are held together by π – π stacking interactions. When more than one functional group is present, ^{19}F , ^1H HOESY (Heteronuclear Overhauser Effect Spectroscopy) NMR experiments and DFT coulomb potential maps are used to check which group establishes the strongest interaction with the anion.

7) **L. Biasiolo**, A. Del Zotto and D. Zuccaccia, *Organometallics* **2015**, *34*, 1759. 

The effects of the ligand (L) and counterion (X^-) are considered the two most important factors in homogeneous gold catalysis, but a rational understanding of their synergy/antagonism is still lacking. In this work, we synthesized a set of 16 gold complexes of the type L-Au-X that differ as follows: (i) L = PPh_3 (**L1**), $\text{P}(\text{tBu})_3$ (**L2**), tris(3,5-bis(trifluoromethyl)phenyl)phosphine (PArF, **L3**), and 1,3-bis(2,6-diisopropylphenyl)imidazol-2-ylidene (NHC, **L4**), with the deliberate purpose of varying the electron withdrawing ability of the ligand, and (ii) $X^- = \text{BF}_4^-$, OTf^- , OTs^- , and TFA^- , which have various coordinating abilities, basicities, and hydrogen bond acceptor powers. All these catalysts were tested in two different model reactions: the cycloisomerization of *N*-(prop-2-ynyl)benzamide to 2-phenyl-5-vinylidene-2-oxazoline and the methoxylation of 3-hexyne. The main results are that the choice of the most efficient L-Au-X catalyst for a given process should not be made by evaluating the properties of L and X^- alone, but rather based on their best combination. For NHC-Au-X, the noncoordinating and weakly basic anions (such as BF_4^- and OTf^-) have been recognized as the best choice for the cycloisomerization of *N*-(prop-2-ynyl)benzamide. On the other side, the intermediate coordinating ability and basicity of OTs^- provide the best compromise for achieving an efficient methoxylation of 3-hexyne. A completely different trend is found in the case of complexes bearing phosphanes: OTs^- and TFA^- have been found to accelerate the cycloisomerization of *N*-(prop-2-ynyl)benzamide, and BF_4^- and OTf^- are suitable for the methoxylation of 3-hexyne. A possible explanation of the observed differences between phosphane and NHC ancillary ligands might be found in the higher affinity of the counterion (especially OTs^-) for the gold fragment for phosphane instead of NHC.

8) **L. Biasiolo**, L. Belpassi, C. A. Gaggioli, A. Macchioni, F. Tarantelli, G. Ciancaleoni, and D. Zuccaccia, *Organometallics*, **2016**, *35*, 595-604. 

The cyclization reaction of 2-(1-hexynyl)dimethylaniline (**S**) on gold(I) has been studied by NMR spectroscopy, in order to characterize the ion pair structure of the product, $[\text{LAuS}_c]\text{BF}_4$. The latter is a good model for the catalytic intermediate between the nucleophilic attack and the protodeauration step of a typical gold catalytic cycle. ^{19}F , ^1H HOESY NMR results demonstrate that in $[\text{LAuS}_c]\text{BF}_4$, with L being three different ligands, the anion mainly interacts with the ammonium moiety of the substrate, thanks to its formal positive charge, even if the ligand can tune the exact position of the anion. Furthermore, also gold chloride is able to promote the cyclization of **S**, forming $[\text{ClAuS}_c]$, which is the first example of a new class of precatalysts with potentially interesting catalytic properties. Preliminary data on its catalytic performances and a detailed DFT characterization of its electronic properties are presented, both of which indicate that S_c behaves as a carbene.

9) M. Trinchillo, P. Belanzoni, L. Belpassi, **L. Biasiolo**, V. Busico, A. D'Amora, L. D'Amore, A. Del Zotto, F. Tarantelli, A. Tuzi and D. Zuccaccia, *Organometallics* **2016**, accepted. 

Herein, we synthesized and characterized through NMR and X-ray techniques a new set of $[(\text{NHC})\text{-Au-X}]$ complexes (NHC = 1,3-bis(2,6-diisopropylphenyl)imidazol-2-ylidene), differing in the counterion X^- ($X^- = \text{OMs}^-$, NO_3^- , ClO_4^- , 2,2,3,3,4,4,5,5,6,6,7,7,7-tridecafluoroheptanoate (PFHp $^-$)). All of these complexes, together with those already known having NTf_2^- and phthalimide (ptm $^-$) as counterions, were tested as catalysts in the methoxylation of 3-hexyne. The results were analyzed together with those obtained previously. The values of activation parameters (ΔH^\ddagger and ΔS^\ddagger) for different anions are also reported. The overall catalytic and kinetic evidence, together with an extensive computational work, confirm the general mechanistic picture given recently in

which the anion plays an active role in all steps of the reaction mechanism: pre-equilibrium, nucleophilic attack, and protodeauration. Medium-coordinating anions (OMs^- , OTs^-) containing a highly symmetric anchoring group give the best catalytic performances. This is due to the following reasons: (a) the pre-equilibrium is shifted toward the outer sphere ion pair, (b) their characteristic basicity promotes the nucleophilic attack, and (c) the possible paths leading to the deactivation of the catalyst are inhibited. These highly symmetric tridentate anions destabilize the unreactive tricoordinated gold species, which instead may be formed by anions with a "planar" anchoring group, such as PFHp^- and TFA^- . A general trend between coordinating ability and catalytic performances in the alkoxylation of alkynes may be established only when the geometric features of the anion are taken into account. The role of the anion has been also investigated in connection with the nature of the nucleophile. In particular, when the alcohol is a poor nucleophile, a large difference in reactivity is observed, while the use of suitably functionalized alcohols, which may contribute to polarizing the $-\text{OH}$ bond through intramolecular interactions, flattens the anion effect.

Abstract

Since the last 20 years, homogeneous gold catalysis is receiving considerable attention and great efforts have been made to disclose the mechanism of the catalytic cycle and the role of many variables: nature of the ligand, structure of the catalyst, effect of the additives, etc. Although a wealth of empirical information on ligand effects is now available on homogeneous gold catalysis, the development of new L-Au-X catalysts and reactions continues to rely upon trial and error, and the outcome of the reaction is often unpredictable. The mechanistic understanding of the gold(I)-catalysed nucleophilic addition to a carbon-carbon unsaturated bond has been pursued and appreciably extended in this thesis by experimental and theoretical investigations. We focused our study on weak interactions and counterion effects with the aim to better understand these often not considered variables. We explained that the anion is influencing each single step of the catalysis and that it is modulating its role depending on its nature (coordination power and basicity) and position. Of course, its effect is also depending on the type of reaction and on which is the rate determining step of the latter. This deep study on the ligands and counterions role in gold homogeneous catalysis, matching both experimental and theoretical studies, allow us to setup a green, room temperature, acid-free, solvent-free and sustainable methodology for the hydration of alkynes. This reaction is generally working only with acidic additives and at high temperature, thereby here is reported for the first time an innovative way to perform it. These preliminary studies open new avenues to consider and rationalize the homogeneous gold catalysis, spreading light into the weak interactions that were underestimated in this field for a long time. This study clearly demonstrates that the interplay between ligand nature and anion effect is crucial in different steps of the catalytic cycle. The multiple roles played by counterions and L-Au⁺ fragments in chemical transformations require more comprehensive computational and experimental studies of the ligand/anion correlation.

Summary

The last few years countersigned the reincarnation of gold complexes as excellent catalysts in numerous homogeneous transformations involving the activation of carbon-carbon multiple bonds towards the attack of a large variety of nucleophiles, shedding the demons of inertness and preciousness (chapter 1.2). *Aurum* owes much of its fame to his *alkynophilicity* and a great deal of research has been focussed on exploring the kinetic and mechanistic studies. Although a wealth of empirical information on ligand effects is now available on homogeneous gold catalysis, the development of new [L-Au-X] catalysts (see abbreviations and catalysts numerations above) and reactions continues to rely upon trial and error, and the outcome of the reaction is often unpredictable. The mechanistic understanding of the gold(I)-catalysed nucleophilic addition to a carbon-carbon unsaturated bond has been pursued and appreciably extended in this thesis.

In chapter 2.1, we studied the role of the anion in the intermolecular alkoxylation of alkyne catalysed by gold(I) complexes ([NHC-Au-X], $X^- = \text{BAr}^{\text{F}-}, \text{BF}_4^-, \text{OTf}^-, \text{OTs}^-, \text{TFA}^-$ and OAc^-) through a combined experimental and theoretical approach. Coordination power or basicity of the anions are linked to the catalytic activities, as the key factor is the abstraction of the alcoholic proton. Too coordinating anions worsen the performances preventing the alkyne coordination or forming methoxide adduct poisoning the catalyst. Instead the intermediate features of OTs^- provides the best compromise to achieve an efficient catalyst.

In chapter 2.2, we have studied by solution NOE NMR spectroscopy and relativistic DFT the ion pair structures of NHC and NAC Au(η^2 -3-hexyne) compounds. We observed three main ion pair orientations: one with the anion close to the carbene backbone (**A**), one with the anion close to the alkyne (**B**), and another one with the anion close to the ligand's polar moieties (**C**). We related and rationalized these structural characterizations with the catalytic activity of the complexes. It has been found that when the anion is forced to be far from the catalytic site by ancillary ligand-anion hydrogen bonding interactions, the catalytic performances are deteriorated and *vice versa*.

In chapter 2.3, we demonstrate that the metal-ligand π back-donation can be indirectly measured by Exchange Spectroscopy NMR technique and theoretically quantified by Charge Displacement analysis. A series of ten bi-coordinate [(NAC)-Au-L] complexes have been synthesized *ad hoc* and used either to validate the method and to study the *trans* influence on the π back-donation component of the bond. The proposed method promises to be of general applicability and useful to rationalize ligand effect in catalysis. In chapter 2.4, we investigated the relationship between the ligand (L) and counterion (X^-) effects as a rational understanding of their synergy/antagonism was still missing. We synthesized a set of sixteen gold complexes of the type [(L)-Au-X] with the deliberate purpose of varying the electron

withdrawing ability of the ligand and the coordinating ability, basicity and hydrogen-bond acceptor power of the anion. All these catalysts were tested in two different model reactions: the cycloisomerization of N-(prop-2-yn-yl)benzamide to 2-phenyl-5-vinylidene-2-oxazoline and the methoxylation of 3-hexyne. The main results are that the choice of the most efficient [L-Au-X] catalyst for a given process should not be done by evaluating the properties of L and X⁻ alone, but rather based on their best combination.

In chapter 2.5, we design a green and sustainable protocol (room temperature and solvent, silver, and acid-free conditions) for the hydration of alkyne, promoted by NHC Gold catalysts, on the basis of previous chapters' information. In optimized conditions it is possible to reduce the catalyst loading up to 0.01 mol%, obtaining a very low E-factor (0.03) and high Effective Mass yield (96).ⁱ The solvent-free condition permit us to easily separate, by distillation, the liquid product from the catalyst and ionic additives used. This bring to high purity products and allow the recycle of the catalyst. All these factors are in the correct range for sustainable bulk chemicals production with homogeneous gold catalysts, a topic still considered a chimera in the literature.

This deep study on the ligands and counterions role in gold homogeneous catalysis, matching both experimental and theoretical studies, allow us to setup a green and sustainable methodology for the hydration of alkyne. This preliminary study opens new avenues to see and rationalize the homogeneous gold catalysis, bringing to light the weak interactions that were underestimated in this field for a long time.

To all whom supported me and made this became what it is now....

...thanks!!

I will personally thanks all of you.

ⁱ E-factor = (mass of waste / mass of desired product); Effective Mass Yield (EMY) = (mass of desired product / total mass of material used) %

1

Introduction

The most important function of a bibliographic entry is to help the reader obtain a copy of the cited work.

Daniel J. Bernstein

1.1 Transition metals in catalysis and sustainable process

1.1.1 Catalysis

A catalytic process is a chemical reaction where the addition of small amount of a substance, called catalyst, performs an increase of the reaction rate. Using a catalyst, the reaction occurs faster and with a smaller activation energy barrier (Figure 1). Moreover, as the catalyst is not consumed during the reaction it may continue to catalyse the conversion of further quantities of reagents.

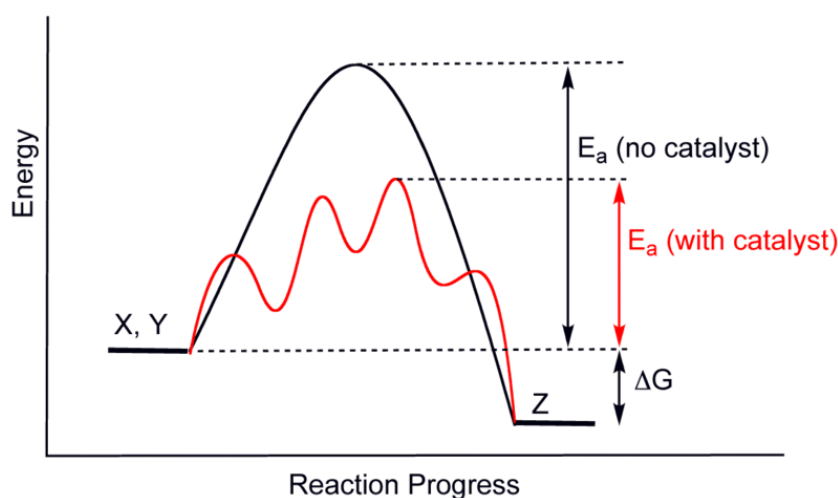


Figure 1. General reaction representation of the different activation energies with and without the use of a catalyst.

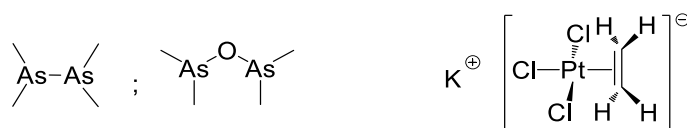
The catalyst is generally added to the reactants in its precursor form, as it is more stable and can be easily handled and stored, which has to be brought into an active form (formerly activated). During the catalytic cycle, the catalyst may be present in several intermediate forms but the most important factor is that the active catalyst will pass a number of times through this different states of the cycle remaining unaltered. The number of times that a catalyst goes through all the cycle is called turnover number (TON) and it represents the total number of substrate molecules that have been converted into product by the catalyst. Sometimes it could be found referred to a specific time as turnover frequency (TOF), especially when a deactivation process of the catalyst is possible during the cycle. There are two main macro classes of catalysis: homogeneous and heterogeneous, depending on whether catalyst and substrate exists in the same phase or not. It is clear that a wide range of molecules can act as catalyst and that their chemical nature is some time not well defined. Notwithstanding this, some species have emerged, throughout history, as favoured over others. The easiest and most ancient used are probably the proton acids catalysts, especially for the many reactions involving water (hydrolysis and its reverse). Also zeolites, higher-order oxides, nanoparticles and other multifunctional solid are often catalytically active and widely used.

Finally, transition metals are largely used especially for what concerns oxidation and hydrogenation reactions. The most significant application of these metals and their organometallics species is as catalysts in several organic reactions of industrial interest (from pharmaceutical to bulk chemistry).

1.1.2 Transition metals compounds

Transition metals (TM) are those elements with a partially filled *d* shell or which can give rise to cations with an incomplete *d* shell.¹ These elements need to complete their sub-shells with given or shared electrons, in order to generate stable compounds. Generally, the electrons provided by other atoms or molecules (that act as ligands) allow the metals to reach the electronic structure of the rare gas next to them in the periodic table. The transition metals consist of the 30 elements located in columns 3-12 on the periodic table and the 28 elements comprising the lanthanide and actinide series (inner transition metals). Unlike elements from the rest of the periodic table, transition metals are comfortable losing different numbers of electrons and generating compounds with high coordination numbers. The ability to have different types of cations is related to the organization of the *d* and *f* orbitals' electrons.

The first organometallic compound was discovered, as it often happens, studying other reactions. In 1757, Loius-Claude Cadet de Gassicourt² was trying to obtain a cobalt-containing invisible inks starting from smaltite and cobaltite, two cobalt salts that contain also Arsenic and that can develop As_2O_3 by thermal treatment. Mixing arsenic trioxide and potassium acetate Cadet discovered a malodorous red-brown liquid that was fuming as phosphorous. The Cadet's fuming liquid contained a mixture of cacodyl and cacodyl oxide which were the first organometallic substances prepared (Scheme 1, left). Since this discovery, the use of organometallic compounds has been important among chemists.



Scheme 1. Cadet's liquid (left) and Zeise's salt (right).

The discovery of Zeise's salt³ in 1825 was another key event in organometallic field. Investigating the reaction of $\text{K}_2(\text{PtCl}_4)$ in boiling ethanol W. C. Zeise observed a product containing ethylene. This was the first π -complex (Scheme 1, right) ever discovered and it received a great deal of attention because it was not so trivial to explain the molecular structure of this salt. Zeise's salt stimulated much scientific research in the field of organometallic chemistry, and would be essential in defining new concepts in chemistry such as *hapticity*.¹ Only with the advent of x-ray diffraction chemists were able to characterize it and,

using Dewar-Chatt-Duncanson (DCD) model, explained how the metal is coordinated to the double bond.^{4,5} In transition metal (M) complexes, the DCD model describes how the olefin acts as an electron donor and acceptor at the same time.

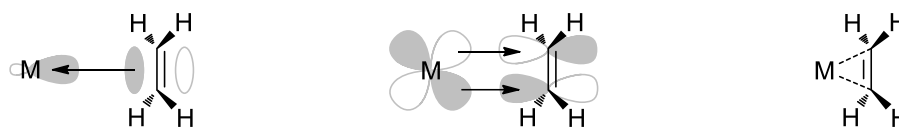


Figure 2. Interactions between a metal and its η^2 ligand.

According to the DCD model, the bond between an olefin and a transition metal is characterized by two factors: the σ -donation from the occupied π -bonding orbital of the olefin to the free d-orbital of the metal (Figure 2, left) and the π back-donation from the filled d-orbital of M to the empty π^* orbital of the olefin (center). This electron-transfer strengthens the metal-ligand bond and weakens the C-C bonds within the ligand. In the case of metal-alkenes and alkynes, the strengthening is reflected in bending of the C-C-R angles which assume greater sp^3 or sp^2 character, respectively. Thus strong π -backbonding causes a metal-alkene complex to assume the character of a metallacyclopropane (Figure 2, right).

In 1912, the Nobel Prize was assigned to Victor Grignard and Paul Sabatier for their research in the organometallic field. To date, Grignard reagents are probably the most know organometallic specie. In the Grignard reaction, aryl-, vinyl- or alkyl- magnesium halides react with an aldehyde or a ketone to form alcohols.⁶ The reaction is generally used to form new C-C bonds. The Grignard reagents have also been proven to undergo transmetalation in cross-coupling reactions, including palladium and other metals.⁷ In the early years of 1950, two individual groups⁸ reported that reduced iron reacts with cyclopentadiene forming a yellow, highly stable, powder. The structure of that new compound was determined by G. Wilkinson and later confirmed by NMR and X-ray crystallography.⁹ What was discovered was ferrocene (Figure 3), a very stable organometallic compound with a sandwich structure consisting of an iron(II) cation and two anionic cyclopentadienyl (Cp) rings. The two Cp rings have one negative charge each, reaching the aromaticity as now both have six π -electrons, and form bond with the metal interacting with all the five carbons (η^5).

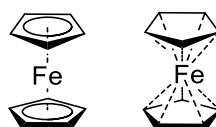
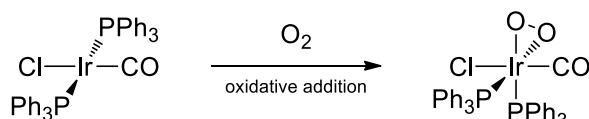


Figure 3. Ferrocene, nowadays representation (left) and as proposed by Wilkinson and Woodward in 1952(right).

The complex is nonetheless neutral as Iron has oxidation state +2, and this bring the complex configuration to 18 electrons. Complexes like that, generally called metallocenes, are used in different

reactions such as Ziegler-Natta polymerization¹⁰ and as agents in cancer treatment.¹¹ In 1961, L. Vaska reported a new organometallic iridium compound¹² with 16 valence electrons. *Vaska's complex* is considered coordinatively unsaturated and thus it can bind to 1 two-electron or 2 one-electron ligands to become electronically saturated (18 valence electrons). Upon oxidative addition, the iridium oxidation state goes from Ir(I) to Ir(III) and the four-coordinated square planar complex converts to an octahedral, six-coordinate ones. This complex is known for the reversible addition of O₂ and series of oxidative addition reactions due its coordinative unsaturation.

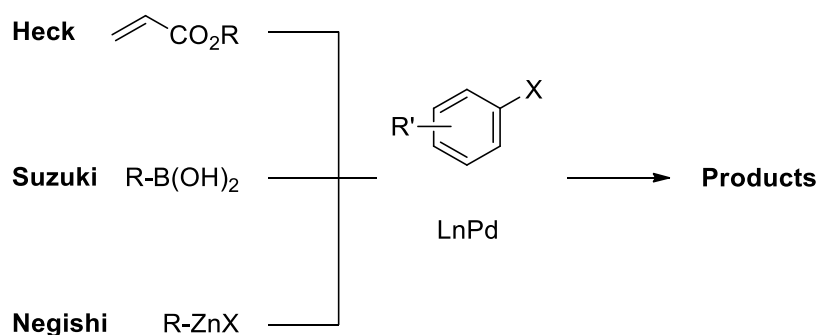


Scheme 2. Vaska's complex, square planar (left) and octahedral after oxidative addition (right).

After these initial discoveries, the interest around organometallic chemistry has increased exponentially and with that also the numbers of awards. K. Ziegler and G. Natta won the Nobel Prize¹³ in 1963 for their

“excellent work on organometallic compounds [... that leads] to new polymerization reactions and thus paved the way for new and highly useful industrial processes ”

This one was just the first of a long series, ten year after G. Wilkinson and E. O. Fischer won the Nobel Prize for sandwich compounds. In 2001 the Nobel Prize was awarded to W. S. Knowles, R. Noyori and K. B. Sharpless for their studies on the asymmetric hydrogenation catalysed by transition metals complexes. Just four years later another Nobel Prize was won for the metal-catalysed alkene metathesis by Y. Chauvin, R. Grubbs, and R. Schrock. Finally, in 2010 R. F. Heck, E. Negishi and A. Suzuki won the Nobel Prize for the palladium catalysed cross coupling reactions (Scheme 3.). Their observations revolutionized the way chemists conceptualized and constructed molecules, whilst simultaneously providing methods for previously impossible C-C bond forming processes.



Scheme 3. General reaction scheme for Heck, Suzuki and Negishi reactions.

Using more efficient catalytic systems (incorporating a plethora of ligands with different steric and electronic properties) it was possible to work under milder conditions and with lower Pd loadings. These powerful ligands ultimately led to the discovery of new cross-coupling reactions generating other bonds (e.g. C-N, C-O, C-S, and C-P) and widening the possible reactions. Nowadays these systems are still widely used by the industry in several applications (from fine chemical production to pharmaceutical and polymers chemistry) because by turning a reaction at lower temperature it is possible to save energy input. Furthermore, by improving the selectivity is possible to minimize the product distribution and therefore the separation problems and waste formation. The industrial interest around this subject has been a significant factor in the rapid development of this field.

1.1.3 Green processes

Starting from the end of 1900s USA and Europe, simultaneously, started to setup several laws to limit and regulate the industrial emissions. This led chemists to reconsider how they design chemical processes, not only focusing on hazardous products but also on the reduction of wastes and on the use of less noxious reagents. In 1998, Anastas and Warner set out 12 principles that are at the bases of the nowadays green chemistry philosophy.¹⁴ The green reactions should: maximize atom economy, minimize by-products and if they cannot be avoided they should have low toxicity, minimize the use of solvents (which make up the major mass in most chemical processes) or alternatively use safe and renewable one. Catalytic reactions are preferred, respect to stoichiometric, as are more selective (reducing the wastes) and generally works under mild conditions.

Palladium catalysed cross-coupling reactions are a perfect example of what a green process could be. Besides for their intrinsic atom economy these reactions, in the last years, has been developed also in a greener perspective. One of the first approaches was the substitution of the more reactive, but also more toxic and expensive, bromide and iodide reagents with their chloride analogues. Also the use of nontoxic reagents has been considered. For example, Stille couplings that use organostannanes has been largely supplanted by Suzuki coupling, which uses organoboron compounds that are much less toxic. Anyhow, much of the effort to decrease the environmental impact of cross-coupling reactions has focused on using more benign solvents, such ionic liquids¹⁵ or supercritical carbon dioxide.¹⁶ But the most likely alternative among the various available choices is water.¹⁷ The main problem remains the solubility of the substrates, to get around this issue the leading candidate technology appears to be the micellar catalysis, in which the reactants can be *solubilized* within the surrounding aqueous phase by the addition of *ad-hoc* surfactants.^{17b, 18}

Many other transition metals are used in green processes: Fe-TAMLs that are able to mimic both peroxidase and cytochrome P450 enzymes are used as green oxidation catalysts to clean the polluted water; Rh based catalysts have long been used in the hydrogenation of C-C bonds and so far have been optimized for by-product-free process that are extremely important in pharmaceutical and industrial sectors; palladacycles are used in many organic reactions as allylic rearrangements, allylic additions and aldol chemistry, since they may act as Lewis acid with no redox by-process that may occurs; a large series of transition metals are used with chiral ligands to perform enantioselective catalysis and have been optimized keeping in mind the green chemistry principles.¹⁹

1.2 Gold in catalysis and sustainable process

1.2.1 Story and properties of gold complexes

Metals have always played an important role in human history characterizing two of the three most important ages in the early civilization (Stone, Bronze and Iron Age). Nevertheless, even gold is following the mankind since the beginning of known history (being the first metal to be discovered, ca. 6000 BC) and it was always related to prosperity, authority, beauty and even magic. Over the past years, many wars, contentions and gold rushes were led for the desire to possess this extremely charming metal. Contemporary, also scientific discoveries came; alchemy, in particular, whose most known goal was the transmutation of metals into gold, is considered nowadays as the precursor of modern chemistry. The alchemists were not mistaken at all; they were just born in the wrong age. In 1941 gold was obtained by neutron bombardment of mercury but, unfortunately, all the gold isotopes produced were radioactive,²⁰ and in 1981 removing protons and neutrons from bismuth forming gold stable atoms.²¹

The interest around gold probably comes from its appearance and inertness towards oxidation in air or water; it is estimated that the 80% of gold found on Earth is in its elemental state (in the form of nuggets, veins, or as grains in rocks) whit its characteristic shining yellow colour. However, it is also quite rare, which contributes as well to its power of attraction, it was estimated that just 174100 tonnes of gold have been mined in human history, in terms of volume about a cube 21 m on a side (Figure 4).²²

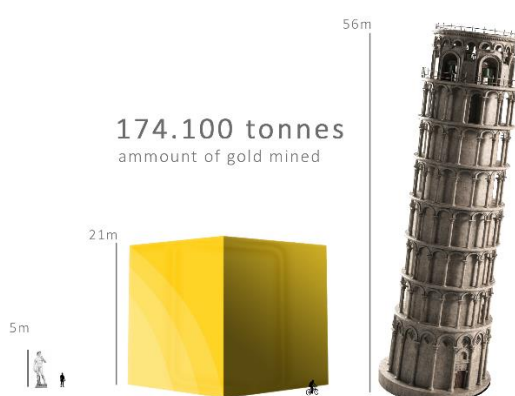


Figure 4. Representation of the amount of gold mined since now (center), compared with Michelangelo's David (left) and Tower of Pisa (right).

The main use of gold, nowadays, still remains in jewellery and decorative arts; due to its inertness and non-toxicity, gold is well suited either as base metal for various objects (for example fillings in dentistry), or as a protective coating on other more reactive materials (against radiation in the aeronautical/spatial industry and as heat shield in various high tech). It can be beaten into very thin sheets (gold leaves for

gilding) or made into thread (and used in embroidery) as it is the most malleable and ductile of all metals. However, because of its softness in pure state, it is often mixed with other metals (such as silver, copper, aluminum, nickel, palladium etc.) in order to modify its physical properties. Throughout the centuries, gold was also used as a medium of monetary exchange, in the form of coins or bullions, and formed the basis for the gold standard. The first use of gold as money was around 700 BC in Lydia (western Turkey); the first coin was simply stamped lumps of a 63% gold and 27% silver mixture known as *electrum*. Even today, gold is one of the most popular investments in the financial markets and many states hold gold in storage as a hedge against inflation or other economic disruptions. For instance, Banca D'Italia has about 2500 tons of gold lying in its vaults,²³ and with 3 times more tons, the Federal Reserve Bank of New York is the largest gold reserve in the world.²⁴

By a chemical point of view, gold has lived in the shadow of other metals for a long time, the same properties that distinguish it made people sceptical about its chemical reactivity. As far as organometallic chemistry is concerned, the role of gold has long been confined to its stoichiometric usage. This, combined to the preconception that it was an expensive metal, have detained its discovery as useful compound in chemical transformations. Gold is doubtless a rare metal, but also several other precious metals like rhodium, platinum, palladium, osmium, or iridium that are often used as catalysts and have comparable prices (Figure 5).²⁵

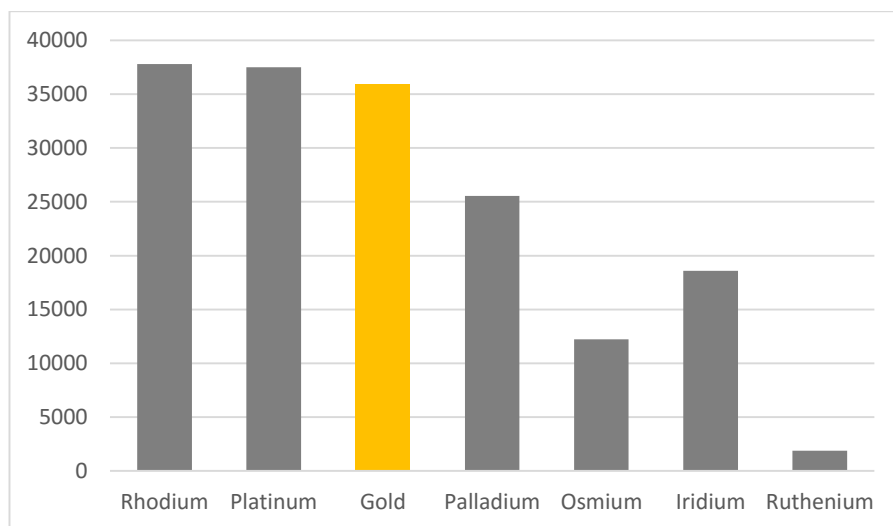
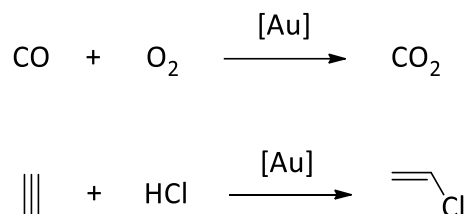


Figure 5. Chart of the prices (USD/Kg) of precious metals used in catalysis.

Gold is not entirely chemically inert, it readily dissolves upon exposure to aqua regia, which converts gold(0) into chloroauric acid, HAuCl_4 , or in basic aqueous cyanide solutions under aerobic conditions, which transforms gold(0) to $[\text{Au}(\text{CN})_2]^-$. The latter reaction is often used for gold extractions in gold mines. Interestingly, the properties of gold change drastically at higher oxidation states. It took as late as mid-1900s to have reports on the authentic potential of gold catalysts.²⁶ Since then, gold has found profound

application in heterogeneous catalysis and have a huge industrial importance nowadays,²⁷ two of the most used industrial applications are the low temperature oxidation of carbon monoxide and the hydrochlorination of ethyne to vinyl chloride (Scheme 4). In the later gold has replaced mercury in the industrial process (see chapter 1.2.4).



Scheme 4. Industrial applications of heterogeneous gold catalysis.

Nanoparticles catalysis, which is closely related to heterogeneous one, also played an important role in the development of new gold catalysis. As a matter of fact, gold nanoparticles are the most frequently used after the silicon ones.²⁸ Nevertheless, homogeneous gold catalysis, pretty much, remained in the cold until the last two decades when it started to blossom (see chapter 1.2.2).

Compared to other metals, cationic gold complexes, both Au(I) and Au(III) compounds, are superior Lewis acids for many transformations. Despite the others transition metal catalysts, their unique *alkynophilicity* coupled with reluctance to switch between oxidation states²⁹ premised the development of novel catalytic cycles, breaking the classical oxidative addition/reductive elimination pathways scheme common to many TM catalysts. As already mentioned their characteristic tolerance towards air and moisture and the nontoxicity, render these catalysts much user friendly and a premier choice for green chemistry. These unique properties of gold catalysts arise from the special nature of the metal center.

As depicted in chapter 1.1.2 the Dewar-Chatt-Duncanson model is typically used to describe the covalent bonding interaction between a transition metal complex and a ligand (alkene, alkyne, allene, etc...)³⁰ The molecular orbital picture consists of four components of which only two make significant contribution towards the total bond energy. The σ -symmetric L→Au bonding interaction and π -symmetric Au→L back-donation are the dominant bonding interactions for gold π complexes and result from overlap of the in-plane $\pi_{||}$ orbitals with the gold *d* orbitals. L→Au π -donation can also occur through the orthogonal, out-of-plane π_{\perp} orbitals, although this minor interaction is strongest for alkyne complexes in which the ligand serves as a four-electron donor. Overlap of an occupied *d* orbital on gold with the empty π_{\perp}^* orbital of the alkyne ligand can result in Au→L back-donation having δ symmetry, therefore representing only a weak interaction.

The high level computations for the parent gold-acetylene [(Au(C₂H₂))] and gold-ethylene [(Au(C₂H₄))] complexes revealed that the σ interaction (L→Au) accounted for 65% of the total bonding situation and

the π interaction ($\text{Au} \rightarrow \text{L}$) accounted for only 27% of the same.³¹ Meanwhile, analogous copper complexes were found to have a higher percentage of back bonding towards the total bonding energy.³¹ Spectroscopic studies suggested that the back bonding $\text{Au} \rightarrow \text{L}$ is minimal, as the stretching frequency of the carbon-oxygen bond (ν_{CO}) is greater than that of the free CO .³²

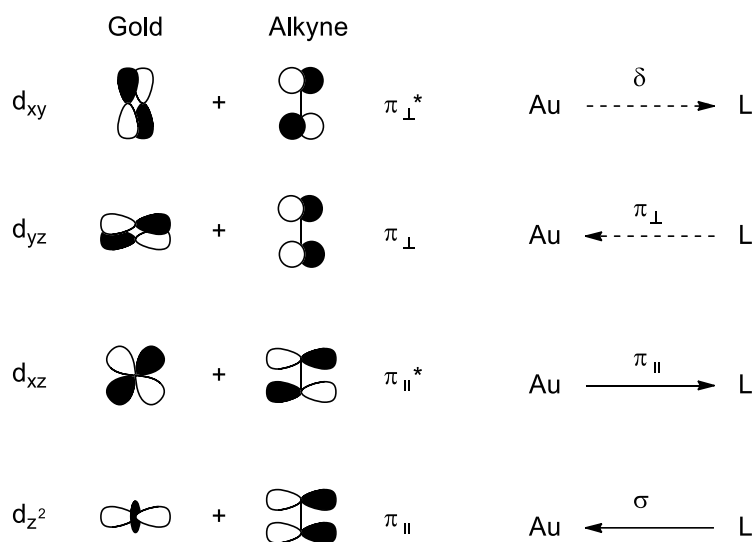


Figure 6. Qualitative orbital diagram

All these observations explain the higher activity of these systems. The lack of back bonding makes the unsaturated substrates electron deficient; thereby the possibility of an intramolecular or intermolecular nucleophilic attack is enhanced. However, computational studies observed a multiple bond character between the gold and the carbon atom suggesting the presence of a $\text{Au} \rightarrow \text{L}$ π back-donation, belying the previously accepted theory. The calculations carried out on the Au-CH_2^+ fragment showed that the bond energy of these species is surprisingly higher when compared to other late transition metal analogues.³³ In confirmation of that, Barysz and Pyykkö proposed that the species AuC^+ should have some triple-bond character³⁴ and later the mass spectroscopic evidences confirmed it.³⁵ Later, Tarantelli and his group employed computational methods and showed that both components could play comparable roles in bonding.³⁶ The charge displacement studies on realistic neutral (bearing Cl as ancillary ligand) and cationic (NHC) gold-ethylene/acetylene complexes revealed a covalent bonding picture in which π back-donation accounts for 25-50% of the orbital interaction. These findings are contrasting the absence of backing bonding. Thus, gold cationic species is able to drag the multiple bonded ligand towards nucleophilic attack by making it electron deficient (*pull effect*) yet are capable of stabilizing the developing positive charge on the vicinal carbene carbon (when the nucleophile is a double bond) by back-donation (*push effect*) of electrons. The *pull-push effect* whereby the gold at the same time activates and stabilizes the cationic center could be regarded as the key feature behind its unique success as carbophilic catalysts.

In addition, also the **relativistic effects** plays an important role in the chemistry of gold distinguish it from the other metals. Increasing the atomic nuclear charge (Z) throughout the periodic table, the electrons close to the nucleus, in s and to a smaller extent on p orbitals, are affected by a very high nuclear charge, and approaching the speed of light they need to be treated according to Einstein's theories of relativity. The direct consequence is that the radius of the $6s$ orbital result more contracted, lowering the distance of the electron from the nucleus and this effect is most pronounced for gold (Figure 7).³⁷

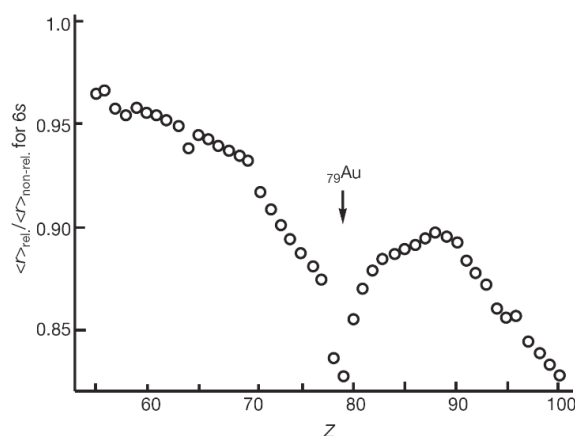


Figure 7. Calculated relativistic contraction of the $6s$ orbital.

Therefore, the d and f electrons are more shielded and occupy larger orbitals (Figure 8).³⁷ Both the relativistic effect and the lanthanide contraction synergistically decrease the size of the gold atom to that of the silver atom, which strongly affects its physical and chemical properties. In fact, gold has the electronic configuration $[Xe] 4f^{14} 5d^{10} 6s^1$, with a single $6s$ electron of the Au(0) it could be predicted that gold is a reactive metal for comparison with the very alkaline Cesium that has a similar electronic configuration ($[Xe] 6s^1$). However, as for gold this orbital is contracted and the $6s$ electron is closer to the inner shells, it does not easily take part in any kind of chemical reaction. Relativistic effects can also explain the unique and captivating yellow color of gold. As the energy of the $5d$ electrons is raised and the energy of the $6s$ electrons is lowered the light absorption (primarily due to the $5d \rightarrow 6s$ transition) takes place in the blue visual range (resulting in a yellowish golden color).³⁷ In contrast, silver absorbs in the ultraviolet region and has a metallic shine.

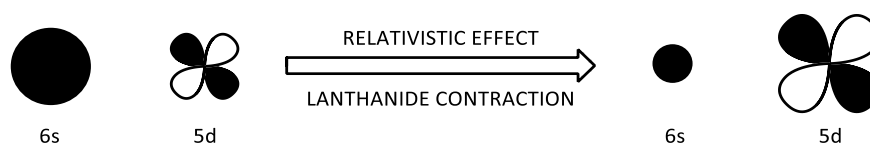
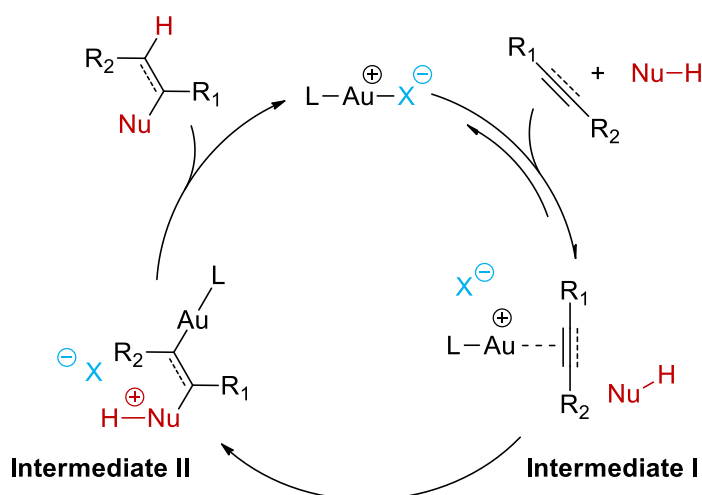


Figure 8. Effects of relativity and lanthanide contraction on outer-shell orbitals of gold.

Complexes of gold(I) due to their electronic configuration ($5d^{10} 6s^0$) are quite stable, they are dominantly linear two-coordinate complexes of the form $[L-Au-X]$.³⁸ Being a soft metal, the most favored ligands for gold are the soft ones like thiolates, thioethers (S), selenates (Se), phosphines (P) and carbenes (C).³⁹ Gold can arise also Au-Au interaction, which cannot be explained in terms of classical bonding, Schmidbaur⁴⁰ has called this effect *aurophilicity*. An interesting example of this effect was found by Puddephatt *et al.* when they observed an aurophilic bonding between Au(III) and Au(I).⁴¹ This interaction can modulate the properties of gold complexes both in solution and in solid state.

1.2.2 Gold Catalysis

In the last 20 years, gold catalysis is emerged as one of the most important innovations in organic synthesis, permitting to synthesize many common core structures of various natural products, pharmaceuticals and synthetic intermediates.⁴² The first breakthrough in gold catalysis occurred in 2000, when Hashmi and coworkers developed a new gold-catalyzed methodology for C-C bond formation.⁴³ Since then, cationic gold species started to be regarded as the most powerful catalysts for the electrophilic activation of unsaturated bonds (alkynes, allenes and alkenes) towards a variety of nucleophiles. Unlike many transition metal catalyzed reactions, gold catalysis does not require anhydrous and air free conditions. These distinctive characteristics are mostly due to the relativistic effect and to the unique properties of gold (see previous paragraph). Gold catalysis is widely used and great efforts have been made to optimize known reactions (hydroalkoxylation, hydroamination, hydration of alkynes, cycloisomerization of enynes and isomerization of allenyl esters) and to find new catalytic applications.

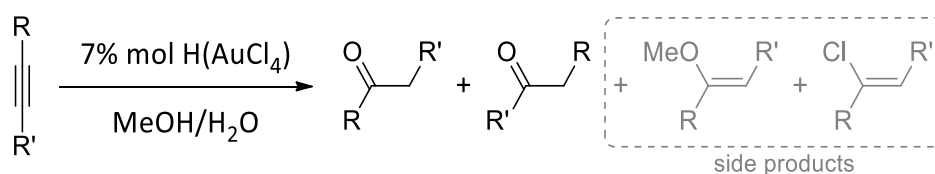


Scheme 5. General accepted mechanism for gold(I) catalysis.

Although gold(I) can catalyze many types of different transformations, most of them proceed through some very similar mechanistic steps. In the literature, it has been proposed that gold(I)-catalyzed nucleophilic addition reactions proceed through innersphere and outersphere mechanisms.⁴⁴ The generally accepted catalytic cycle can be simplified in two steps mechanism (Scheme 5).

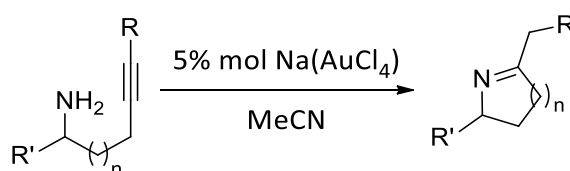
First, a cationic gold complex, $[(L)AuX]$, acts as Lewis acid to activate carbon-carbon multiple bonds and form a η^2 complex (Scheme 5, **intermediate I**). Whereupon, the nucleophile (NuH) may attack the activated substrate leading to the formation of **intermediate II** (Scheme 5). Then, the next step is the regeneration of the active species giving the final product. This happens usually by protodemetalationⁱⁱ from the organogold **intermediate II** (Scheme 5), although alternatively other electrophiles can be used to trap these derivatives or direct eliminations can take place.⁴⁵

The first remarkable report on gold catalysis came in 1976 when Thomas et al. developed the addition of methoxy and hydroxyl nucleophiles on alkynes by using catalytic amounts of hydrogen tetrachloroaurate.⁴⁶ The authors were able to identify even the by-product, which later became important in gold catalysis.



Scheme 6. First homogeneous gold catalyzed nucleophilic addition to alkynes.

In 1986, Utimoto and his group made another key discovery on the Lewis acid catalysis of gold,⁴⁷ describing the intramolecular hydroamination of alkynes catalyzed by sodium tetrachloroaurate. The new methodology was conducted in milder conditions and it showed a better selectivity with respect to the pre-existent palladium catalyzed reactions.



Scheme 7. Gold catalyzed hydroamination of alkynes (n=1, 2).

The early uses of gold to catalyze organic reactions were employing mostly inorganic gold salts as catalyst. An important key step for the synthesis of Au(I) complexes with binding organic ligands was the

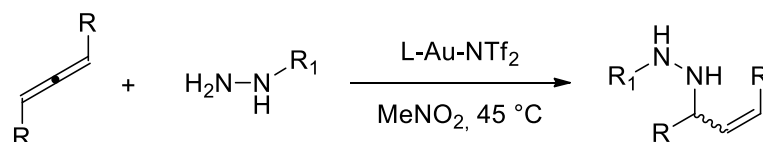
ⁱⁱ the substitution of proton with gold to regenerate the cationic gold active species

preparation of the sulfides gold(I) precursors. These complexes are prepared by the addition of a sulfide, typically dimethyl sulfide (DMS) ⁴⁸ or tetrahydrothiophene (THT), ⁴⁹ to an aqueous solution of tetrachloroauric acid (HAuCl₄). The coordinated sulfide in these gold(I) precursors can be readily replaced by any stronger coordinating ligand, such as phosphines, phosphites, or NHC's. Depending on the ligand environment, such complexes have found use in organic synthesis as homogenous catalysts and, also, in medicine (Auranofin).⁵⁰ The last fifteen year witnessed an exponential raise in activity in the area of gold

*“A change in paradigm has taken place. While the ancient alchemists investigated the question of how to make gold, now the question is **what to make with gold.**”*

catalysis and the substrate scope for these mild and selective catalytic systems has significantly been broadened. Several transformations are feasible for that system such as additions of carbon and heteroatom nucleophiles to unsaturated bonds, Friedel-Crafts reactions, cycloisomerization of enynes, carbonyl and imine activations and so on.^{42a} The mere multitude of publications and reviews that came out in this period testimony these facts and as Stephen Hashmi wrote in his review:

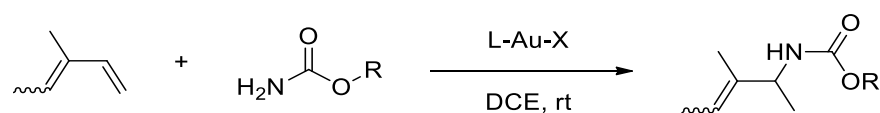
Even more groups are starting to focus their research on gold(I) catalysis because many information is still lacking. Recently, few in-depth kinetic and mechanistic studies on the gold(I)-catalyzed nucleophilic addition to a carbon-carbon unsaturated bond have been published. Although a wealth of empirical information on ligand effects is now available on homogeneous gold catalysis,⁵¹ the development of new catalysts and reactions continues to rely upon trial and error, and the outcome of the reaction is often unpredictable. Rational design of suitable ligands to achieve better efficiency is almost nonexistent in gold catalysis. For that reason, Xu and Hammond⁵² focus their study on the role of the ligand in gold(I) catalysis, concluding that it cannot be easily predicted but they were able to identify the most efficient class of ligands in each steps. They observe that electron-poor ligands are the best choice when the Rate Determining Step (RDS) is the preequilibrium or the attack. Those kind of ligands are able to activate more the substrate making more positive the gold fragment, as observed in the intermolecular hydroamination of allenes with hydrazide in the presence of [L-Au-NTf₂] (Scheme 8). Allenes are less reactive than alkynes toward nucleophilic attack and the electron-deficient hydrazide is a relatively weak nucleophile. These two characteristics make the activation of the substrate the RDS of the whole reaction.



Scheme 8. Hydroamination of allenes with hydrazide.

The same trend was recently confirmed also by Maier⁵³ and co-workers for another reaction where the RDS was supposed to be the attack. In the methoxylation of 3-hexyne the electron-poor ligands, such as (RO)₃P and PAR^F, were working better with respect to more electron-rich ligands, such as Ph₃P or Buchwald type phosphine. Instead, electron-rich ligands result the best choice when the protodeauration is the RDS. Investigating the cycloisomerization of N-(prop-2-yn-yl)benzamide to 2-phenyl-5-vinylidene-2-oxazoline Hammond et al. found that Cy₃P or Buchwald type phosphine (the more electron rich of the series) were improving the reaction rate, while PPh₃ and fluorinated phosphines were the worse choice for this catalysis. Maier studied the protodeauration performing a stoichiometrical experiment investigating the protonolysis of an already generated vinyl intermediate. Again, the more electron-rich ligands were the best choice to speed up the catalysis. These observations clearly demonstrated that a quantitative study of the ligand nature in L-Au-X complexes is fundamental to fully understand and rationalize their reactivity.

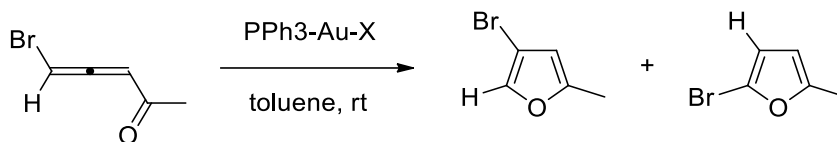
As we saw before, all the three key species of the catalytic cycle are charged species (Scheme 5) and, in fact, many ion pair effect were observed by several groups.⁵⁴ Trying to improve the hydroamination of 1,3-dienes (Scheme 9), He and his group observed that changing the counterion the activities of the catalyst were changing too.⁵⁵ The most basic and coordinating anion, such as TFA⁻, NO₃⁻ and OTs⁻ are not working at all; meanwhile the less basic and coordinating anions were working well and were following the basicity scale SbF₆⁻ < NTf₂⁻ < PF₆⁻ < BF₄⁻ < OTf⁻.



Scheme 9. Hydroamination of 3-methyl-1,3-pentadiene.

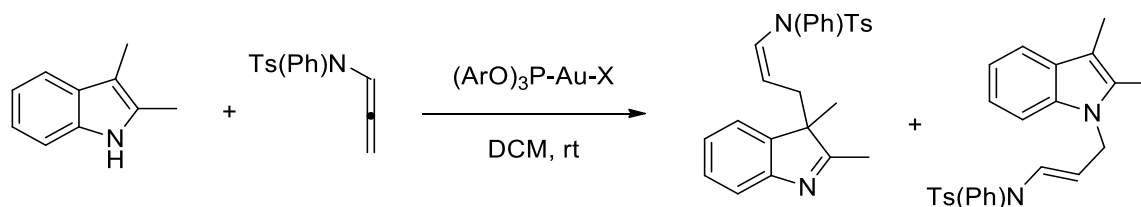
A very different trend was found by the group of Echavarren in 2014 studying the [2+2] cycloaddition of phenylacetylene and α -methylstyrene.⁵⁶ In summary, most basic anions were able to deprotonate the terminal alkyne generating more η^1 -phenylacetylene complex that was slowing down the reaction rate. Instead, BAr^F and SbF₆⁻ resulted to be the best choice (BAr^F > SbF₆⁻ > BF₄⁻ > NTf₂⁻ > PF₆⁻ > OTf⁻).

An ion pair effect was observed by Li also in the cycloisomerization of bromoallenyl ketones (Scheme 10) concerning the regioselectivity of the reaction.⁵⁷ They observed that SbF₆⁻ was producing selectively the 4-bromo derivate meanwhile, OTf⁻ was generating the 2-bromo derivate. Matching DFT and experimental data they concluded that the 1,2-Br migration (that allows to the formation of the 4-bromo derivate) is more favorable with three times lower activation barrier respect to 1,2-H shift. However, the 1,2-H shift, that brings to the production of the 2-bromo derivate, can be excellently assisted by the counterion, and using OTf⁻ it requires an even lower activation barrier.



Scheme 10. Cycloisomerization of bromoallenyl ketones

A similar trend was observed by Bandini and coworkers studying the site-selective functionalization of 2,3-disubstituted indoles with allenamides (Scheme 11).⁵⁸ The overall regiochemistry of the condensation is regulated by the nature of the gold counterion, spanning from absolute N(1)-alkylation using OTf⁻ to the corresponding regiospecific C(3)-functionalization when TFA⁻ was employed. As a matter of fact, with TFA⁻, they proposed the establishment of strong hydrogen bond interactions between the anion and the N(1)-H indole site, resulting in the nucleophilic activation of the heteroaromatic nucleus (mainly at the C(3)-position) and concomitant protection of the nitrogen.

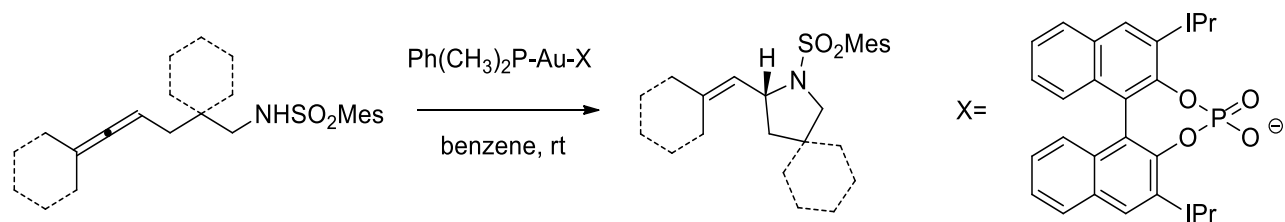


Scheme 11. Regioselective functionalization of 2,3-disubstituted indoles.

The nature of the anion not only modifies the products distribution but also the structure of the intermediates in the catalytic cycle. Gagné and coworkers concluded that less coordinating counterions (such as NTf₂⁻ and OTs⁻), respect to more basic ones (such as TFA⁻ and OAc⁻), were generating more, catalytic inactive, di-aurate species.⁵⁹

One of the most important ion pair effects, in gold catalysis, was observed in 2007 by Toste studying some enantioselective reactions catalyzed by gold(I) and gold(III).⁶⁰ This reaction exhibited a dramatic matched and mismatched pairing effect of the ligand and counterion, using both ligand and counterion in their (R)-enantiopure form, the resulting product was nearly racemic. Instead, using only the enantiopure counterion it was possible to achieve up to 96-99% of e.e. and open previously inaccessible transformations to asymmetric catalysis (

Scheme 12). In fact, it is generally accepted that for Au(I) catalysts it is difficult to transfer the chiral information from a ligand disposed 180° from the substrate. However, as they shows, a smart modification of the counterion can be used to circumvent this problem by introducing an additional source of chirality near the metal center.

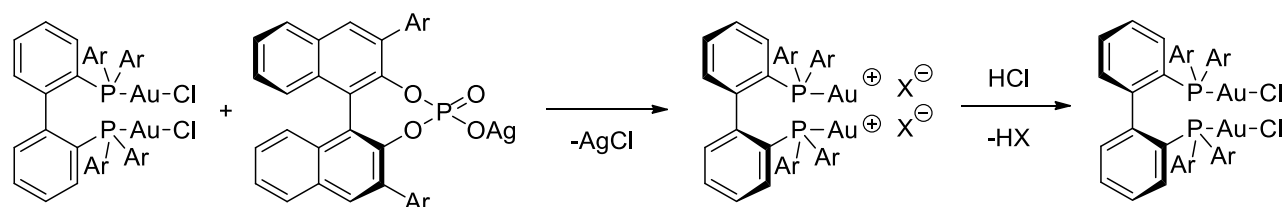


Scheme 12. Enantioselective hydroamination.

Moreover, it has been observed that such anions can influence also the structure of the catalyst.

Mikami's group was able to demonstrate that the axial chirality of biphenylgold complexes can be imprinted using phosphate chiral anions and that it can be memorized at room temperature even after the dissociation of chiral anions (

Scheme 13).⁶¹



Scheme 13. Anion imprinted chirality.

At the beginning of 2015, Bandini pointed out that although the importance of the anion is well recognized and it may seriously affect the catalysis, **its role** in each single step of the reaction mechanism **is still largely unknown**.⁵⁴ For all these reasons, the isolation and characterization of those charged intermediates, involved in the catalysis, became a fundamental step in order to better understand the full cycle,^{62, 63} and to shed more light on the role of the anion. It has become essential to characterize and study the structures of the ion pairs of the cationic gold species in solution.

1.2.3 Study of the Ion Pairs

Over the last few years, Macchioni and his collaborators have been developing investigative methodologies that mixing the complementary information from diffusion and Nuclear Overhauser Effect (NOE) NMR spectroscopy, disclose the structure of ion pairs in solution.^{64, 65}

The method has been successfully applied to investigate several classes of ionic transition metal complexes with different metals, ligands, and geometries. Remarkable results have been obtained for organometallic catalysts for alkene polymerization⁶⁶ and alkene/CO copolymerization⁶⁷ in terms of

explanation and, in some cases, correlation between the IP structure and the reactivity. NOE NMR spectroscopy, based on the detection of dipolar interactions, is ideal for measuring the spatial proximity of two (or more) NMR-active (I and S) nuclei, regardless of whether I and S are in the same molecular fragment (intramolecular) or belong to two different moieties (intermolecular). The relative anion-cation orientation(s) can be disclosed if: i) the NMR-active nuclei (especially with the high receptive H or F) are present in both ionic moieties; ii) they are not homogeneously distributed (non-equivalent) around the ionic moieties and iii) their maximum internuclear distance is no more than approximately 5 Å. The last is not a severe limitation, since ion-pairing effects are important almost exclusively when mainly contact ion pairs are present in solution. The NOE interionic contacts can be classified as strong, medium, or weak, according to the intensity of the crosspeaks (Figure 9). The potential of NOE NMR spectroscopic studies can be further exploited if they are paralleled with theoretical calculations. Recently, Tarantelli and Macchioni groups were focusing on $[L-Au-S]^+X^-$ IP (L = ancillary ligand, S = unsaturated substrate, and X^- = counterion), one of the key intermediates in the functionalization of double and triple C-C bonds and attempted to combine advanced NOE NMR spectroscopic measurements in solution and theoretical calculations made by DFT.

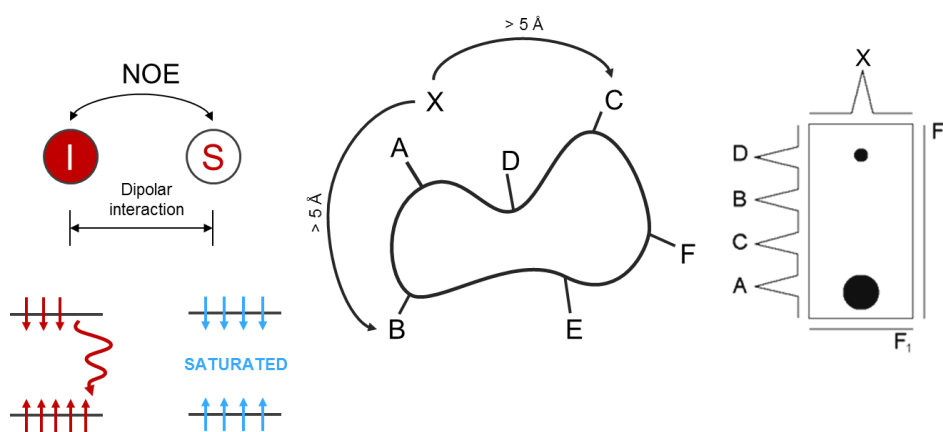


Figure 9. Representation of the HOESY NMR techniques.

In particular, they shown that analysis of the charge distribution on the cation is often sufficient to obtain a reliable indication of the most favored sites for anion-cation interactions. Their approach has therefore been to map the Coulomb potential, computed by relativistic Density Functional Theory (DFT) calculations, of $[(L)Au(S)]^+$ complexes in a region accessible to the anion and match this with the results of the experimental NMR measurements. A reasonable choice is to map the Coulomb potential on the electronic isodensity surface that is approximately tangent to the equivalent density surface of the isolated anion placed at the optimized geometry of the ion pair (Figure 10). This can be considered to yield a map of the potential on a boundary roughly corresponding to the steric dimension of the cation. When more quantitative information is required or some specific interactions between the anion and

cation exist, one has to resort to the analysis of the actual cation–anion potential energy surface. Typically, several, often computationally expensive, geometry optimizations within an appropriate solvation model are necessary.

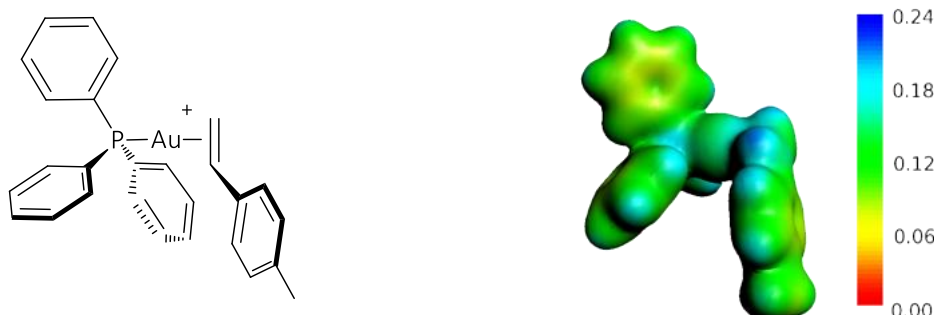


Figure 10. Example of CP map for the complex represented on the left. ⁱⁱⁱ

Concerning the NMR studies, the BF_4^- anion is ideal for this kind of investigation because of its unique properties: it contains NMR-active nuclei; it is less coordinating than most of the alkenes/alkynes, avoiding the problems arising from the anion/substrate competition; it is small enough to effectively probe the whole cation surface, minimizing the complications arising from steric hindrance; it is commonly used in catalysis. On the other hand, the Density Functional Theory (DFT) study allow to obtain information about the relative anion-cation position even if the anion does not possess any NMR active nucleus. Using this technique one can know the charge redistribution throughout all the complex, computed by relativistic Density Functional Theory (DFT) calculations, and obtain a map of the Coulomb potential around the cation that is useful to locate the most attractive regions. (Figure 10). Tarantelli and Macchioni groups demonstrated by ^{19}F , ^1H -HOESY NMR⁶⁸ how the anion position can be finely tuned by the choice of the ligand⁶⁹ and how the ion pair structure can be related with the electronic properties of the phosphorous-based ligand (Figure 11).^{70a}

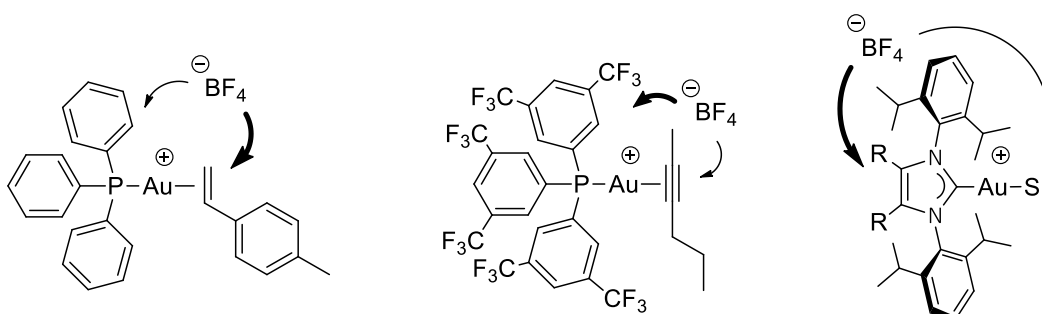


Figure 11. Previous studied systems, S = 2-hexyne, 4-methylstyrene, 4-methylpent-1-ene, tetramethylethylene; and R = H, Me.

ⁱⁱⁱ Coulomb potential of the cation fragments are mapped on an electronic isodensity surface ($\rho=0.007 \text{ e}/\text{\AA}^3$. Coulomb potential in a.u.). The isodensity value chosen is that approximately corresponding to tangent density surfaces for the isolated cation and anion placed at the optimized geometry of the ion pair. The most attractive regions on the surface are blue-colored

Up to now, all the qualitative and semi-quantitative comparisons between experimental NMR results and theoretical Coulomb maps have been successful.^{69, 70}

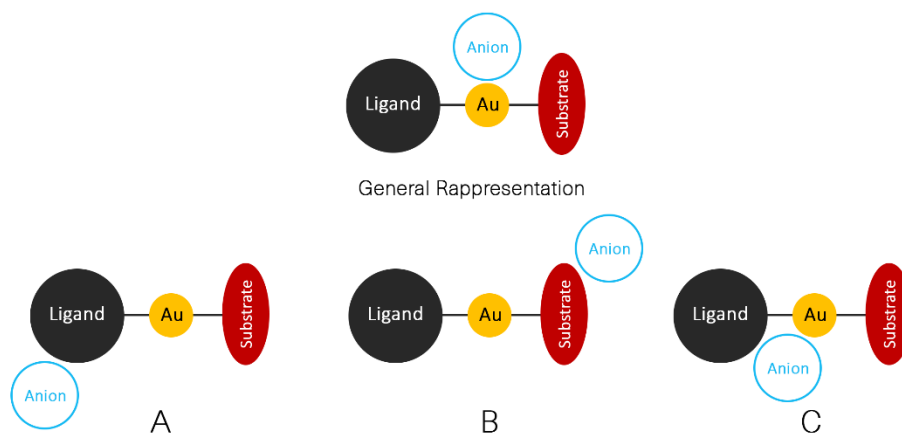


Figure 12. Different anion/cation orientation.

Such results show that the anion is not particularly attracted by the metal atom, where the positive charge is formally located (Figure 12), but it is located on the ligand-side when carbene ligands are used⁶⁹ and on the substrate-side in phosphine-gold complexes. Only the presence of a very acid proton, as the *ortho*-H of the $P(3,5-(CF_3)_2-C_6H_3)_3$ ligand (PAr^F), can force the anion to be close to gold atom (Figure 11, center). Summarizing they were able to find three different limit structures: (A) when the anion is placed on the ligand side, (B) when the anion is closer to the substrate and (C) when the anion is interacting with neighbouring groups on the ligand.

This technique represents, nowadays, the state of art for what concerns the study of Ion Pair in solution. However, this kind of study should be extended to other classes of ligands especially when particular functional group or charge, which may interact with the anion, are present. From this point of view, there is still a lot of information that may be obtained applying these systems to new complexes especially if related to their activity in catalysis that is still a missing point.

1.2.4 Green gold applications

The principles of green chemistry include waste prevention, renewable feedstocks, catalytic rather than stoichiometric reactions, safer solvents and reaction conditions, and increased energy efficiency. As we saw in chapter 1.2.2 gold catalysis could help in all these topics; contrarily to other metal catalyzed reactions that require high temperatures and long reaction times, gold compounds can work faster and at room temperature.⁷¹ Their room temperature activity has opened up new opportunities for pollution control applications.⁷² Due to their robustness, gold compounds can be also used in association with alternative solvents, which enable easy catalyst separation and recycle.⁷³ In addition, also the metal itself can be easily recycled in the same reaction or recovered generating new catalysts. Moreover, metallic gold is biocompatible and nontoxic, both gold(I) and gold(III) compounds have recently gained considerable attention due to their strong antiproliferative potency manifesting relevant anticancer properties against selected human tumor cell lines.⁷⁴

Indeed, it is recognized that gold catalysts could carry out processes for which no other catalyst has yet been identified and that they are now becoming interesting for commercial applications.⁷⁵ Gold is mostly used in the hydration and alkoxylation of alkynes that may also represent a model of modern, sustainable transformation in chemistry were the atom economy is preserved. These reactions are waste-free, use water/alcohol as reagent, and are catalytic.⁷⁶ Curiously, although these reactions has been known since the 19th century,⁷⁷ their potentials in organic synthesis have not been conveniently exploited. The reason may be found looking at the more active catalysts known to date. HgO-H₂SO₄ (Kucherov catalyst)⁷⁷ and HgO-BF₃ (Hennion-Nieuwland catalyst),⁷⁸ are both highly toxic mercury salts that must be used in combination with either Bronstead or Lewis acids.⁷⁹ Despite that, these catalysts were extensively used in high-scale industrial processes⁸⁰ until the discovery of the toxicity of mercury salts. Mercury intoxications may cause ataxia, general muscle weakness, narrowing of the field of vision, and damage to hearing and speech. In extreme cases, insanity, paralysis, coma, and death follow within weeks of the onset of symptoms.⁸¹

One of the most discussed mercury poisoning case was the one called **Minamata disease** caused by the release of methylmercury in industrial wastewater from the Chisso Corporation's chemical factory from 1951 to 1968. This highly toxic chemical was bioaccumulating in shellfish and fish in Minamata Bay area and then transferred to the local populace when eaten, resulting in mercury poisoning. The Chisso Minamata factory first started acetaldehyde production in 1932, producing 210 tons that year. By 1951, production had jumped to 6000 tons per year and reached a peak of 45245 tons in 1960.⁸² The company was having a great influence in Minamata city as over half of the city tax were paid from Chisso and its

employees.⁸³ As of March 2001, 2265 victims had been officially recognized as having Minamata disease (79% of whom had died) and over 10000 had received financial compensation from Chisso (Figure 13).⁸⁴

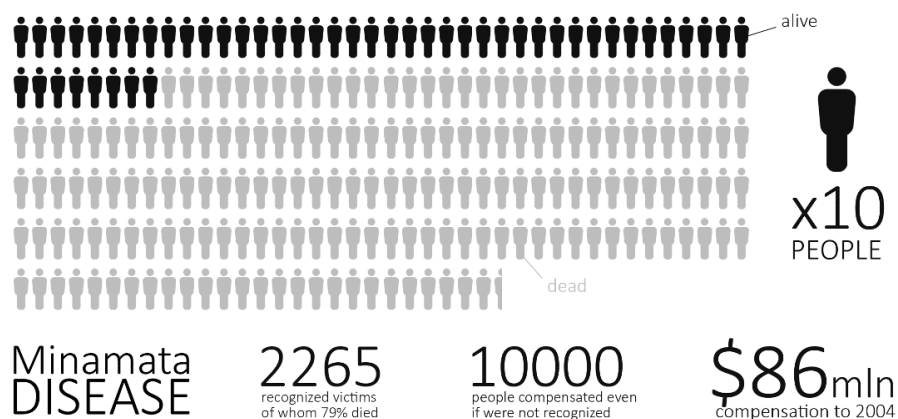


Figure 13. Graphic representation of the Minamata disease.

By 2004, Chisso Corporation had paid \$86 million in compensation, and in the same year was ordered to clean up its contamination.⁸⁵ A second outbreak of Minamata disease occurred in Niigata Prefecture in 1965. The original Minamata disease and Niigata disease are considered two of the Four Big Pollution Diseases of Japan. After that disaster the dangerousness of mercury was proven and several international protocols were signed for reducing the use and release of Hg.⁸⁶ Historically, Europe, followed by North America, has been the major region for anthropogenic Hg emissions. China is now the largest source of Hg emissions to the atmosphere (at least 700 tons per year) and the world’s largest consumer of Hg (>1000 t/year), which accounts for 50% of the global use.⁸⁷ The largest amount of mercury used is employed for producing polyvinyl chloride (PVC).⁸⁸

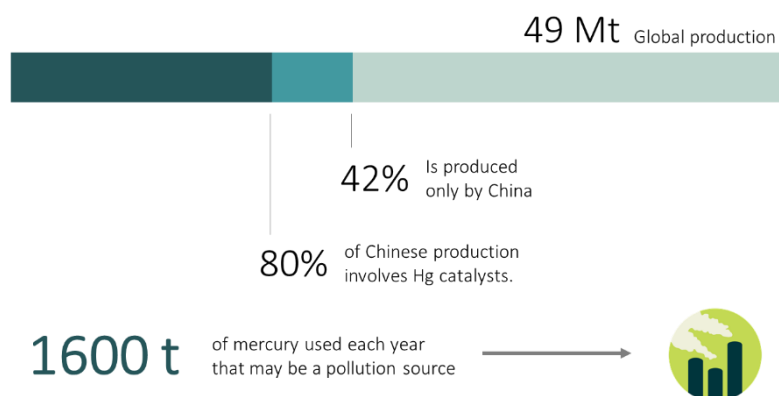


Figure 14. Graphical representation of Hg used for PVC production.

By the end of 2010, global production of PVC was 49 Mt/year,⁸⁸ China alone was producing the 42% of the global production and the 80% of that was made through the calcium carbide process (impregnated with HgCl_2 , used to ensure the reactivity and selectivity to form vinyl chloride monomer, VCM). It has been estimated that for the annual production of 16 Mt of PVC, through the calcium carbide process, >1600 tons of Hg is required.⁸⁹ Looking at these numbers it is clear that the interest for finding new catalytic systems for that kind of reactions is still high.

Alternative catalysts for the hydration of alkynes have been searched for over the past 30 years, including Brønsted acids, bases, and metal salts and complexes.^{76b} However, neither of them has been able to surpass the activity of those systems containing mercury salts. Among them, it is worth mentioning those systems where simple salts, such as PdCl_2 ⁹⁰ or Zeise's dimer $[\{\text{PtCl}_2(\text{C}_2\text{H}_4)\}_2]$,⁹¹ were used, along with the recently reported anti-Markovnikov hydration of alkynes catalysed by ruthenium complexes.^{76c} However, the use of acid promoters or heat the system, or both, are absolutely necessary in order to obtain good results. Only few examples can be found where simple alkynes are hydrated by using a transition metal species at room temperature without help of acidic additives.⁹²

Gold was firstly used in place of mercury for greening the chemistry process. The *alkynephilicity* of gold resembles that of mercury, and this behaviour has been attributed to the common electronic properties for these two elements in the valence shell, in part due to relativistic effects (see Chapter 1.2.1).³⁷ Thus, Utimoto⁹³ and Teles⁹⁴ applied gold salts and gold complexes as catalysts for the hydration of alkynes and, more recently, Hayashi and Tanaka⁹⁵, Laguna,⁹⁶ and others.⁹⁷

Notwithstanding its intrinsic green abilities, the use of gold in green chemistry has not been deeply investigated and it remained mostly confined to heterogeneous catalysis.⁹⁸ Friend and Min found that gold-based catalysts are promising for efficient oxidation of CO (Figure 15, top) and selective oxidation of propene (Figure 15, bottom).

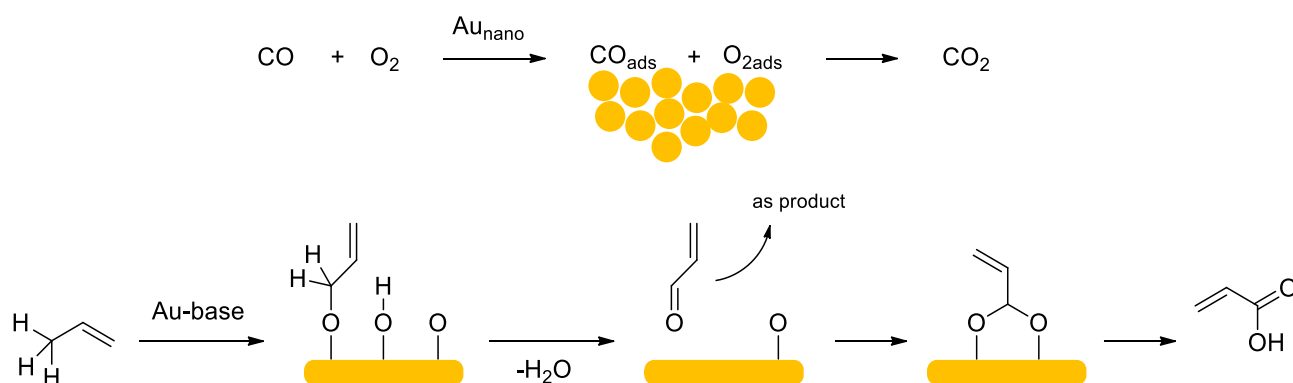


Figure 15. Heterogeneous use of gold in green chemistry.

The nanoscopic gold catalysts were active at much lower temperature compared to platinum-group catalysts for CO oxidation. Likewise, Au-based catalysts were effective for selective oxidation of propene, despite the very labile allylic hydrogen in this molecule.^{98a}

Concerning the homogeneous gold catalysis, only few examples are present in the literature. In 2009 Winter and Krause⁹⁹ proposed a new synthetic route for the cycloisomerization of functionalized allenes in water using HAuCl_4 as catalyst, most importantly the catalyst could be reused after the full conversion of the reagent. Also gold(I) catalysts have been investigated for their use in water, in 2007 Laguna *et al.*¹⁰⁰ achieved an efficient hydration of phenylacetylene in aqueous media using gold catalyst bearing a triphenylphosphane based ligand with $-\text{SO}_3\text{Na}$ substituents to promote its water solubility (Figure 16 left).

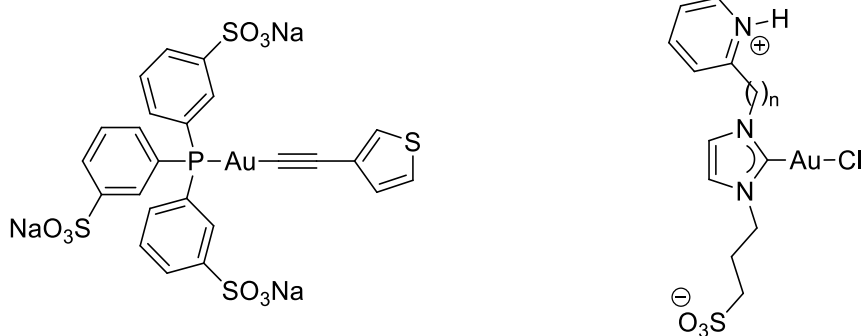


Figure 16. Water soluble gold complexes.

Few years later, a collaboration between Conejero, Michelet and Cadierno groups has brought to light that also NHC ligand, functionalized with proper groups (Figure 16 right), can be effective in water media proposing the intramolecular cycloisomerization of γ -alkynoic acids in a 1:1 toluene/water mixture.¹⁰¹ Earlier Tanaka *et al.* demonstrated how, adding acid promoters, triphenylphosphane gold complex can catalyse the intermolecular hydroamination of alkynes in solvent-free conditions.¹⁰²

Considering its doubtless green properties and these firsts results recently appeared in literature, one may conclude that gold can be a worthy, and probably under evaluated, choice to develop new green chemistry reactions.

2

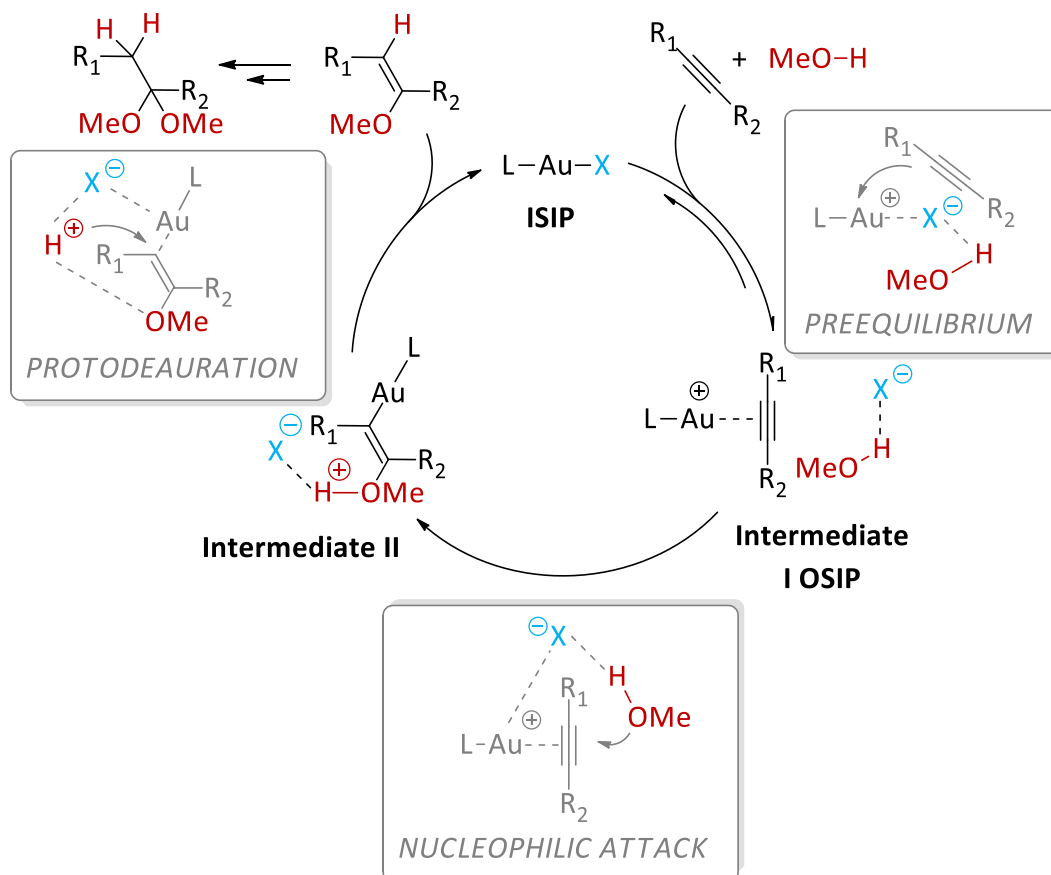
Results and Discussion

*Research is to see what everybody else has seen,
and to think what nobody else has thought.*

Albert Szent-Gyorgyi

2.1 Role of the anion nature

Homogeneous gold catalysis is now receiving a considerable attention and great efforts are being made to optimize known reactions and find new catalytic applications (chapter 1.2.2).^{42a} Recently, in-depth kinetic and mechanistic studies on the gold(I)-catalysed nucleophilic addition to a carbon–carbon unsaturated bond have been published, with the aim to understand the ligand effect⁵² and to isolate and characterize the intermediates involved in the catalytic cycle.^{62,63} However, as we saw in chapter 1.2.2 (Scheme 5), the main species of the cycle are all charged, and in fact many Ion Pair effects have already been observed. The anion can influence the catalytic activity,⁵⁵ the regioselectivity,⁵⁷ and even the stereoselectivity⁶⁰ of the process (chapter 1.2.2). Although the importance of the anion is well recognized, its role in each single step of the reaction mechanism is still largely unknown.



Scheme 14. Proposed mechanism for the methoxylation of 3-hexyne.

To shed more light on the anion nature effect, we decided to study the intermolecular alkoxylation of alkynes, one of the oldest applications of gold(I) catalyst along with hydration and hydrophenoxylation.¹⁰³ From the seminal work of Teles,⁹⁴ several other studies on these classes of reactions have been published, improving the activity¹⁰⁴ and clarifying the reaction mechanism.^{62b, 105}

Maier and Zhdanko have shown that when NHC is used as the ligand, the catalysed addition of methanol to 3-hexyne is of pseudo-zero order in 3-hexyne and pseudo-first order in methanol and catalyst.^{105a}

The gold metal fragment acts as a Lewis acid coordinating 3-hexyne (Scheme 14, **intermediate I**, Outer Sphere Ion Pair, **OSIP**), which subsequently undergoes a nucleophilic attack by MeOH, with the formation of an organogold intermediate (Scheme 14, **intermediate II**). The gold-carbon bond in the latter is typically cleaved by proton (protodeauration) to give the vinyl ether and regenerate the catalyst (Scheme 14, Inner Sphere Ion Pairs, **ISIP**).

The key gold-catalysed step is the formation of vinyl ether, while the addition of the second molecule of methanol, leading to the final product (acetal), seems to be very fast^{105b} and is generally considered a proton-catalysed process.^{105a} As no systematic experimental data about the role of the anion were available, we set a method to analyse in detail the role of the anion in different steps of this catalytic cycle by combining experimental and theoretical approaches. Choosing [(NHC)AuX], the mechanistic framework is largely simplified as the stability of the species [(NHC)Au(S)]X is well known and *gem*-diaurated species [(NHC-Au)₂S]X were not observed.^{105a}

We have considered a series of anions with increasing coordination ability:⁶⁴ BAr^{F-} [BAr^{F-}=tetrakis(3,5-bis(trifluoro-methyl)phenyl)-borate], tetrafluoroborate (BF₄⁻), trifluoromethanesulfonate (OTf⁻), *p*-toluensulfonate (OTs⁻), trifluoroacetate (TFA⁻) and acetate (OAc⁻).

All the catalysts [(NHC)AuX] (**4X**) have been synthesized from [(NHC)AuCl] through anion metathesis procedures, except for BAr^{F-} and BF₄⁻ as the ISIP complexes are not stable enough and [(NHC)Au(η²-3-hexyne)]X complexes (**4BAr^{F-}** and **4BF₄**,¹⁰⁶ respectively) have been used as catalysts (see Experimental Part for details and characterization of new complexes).

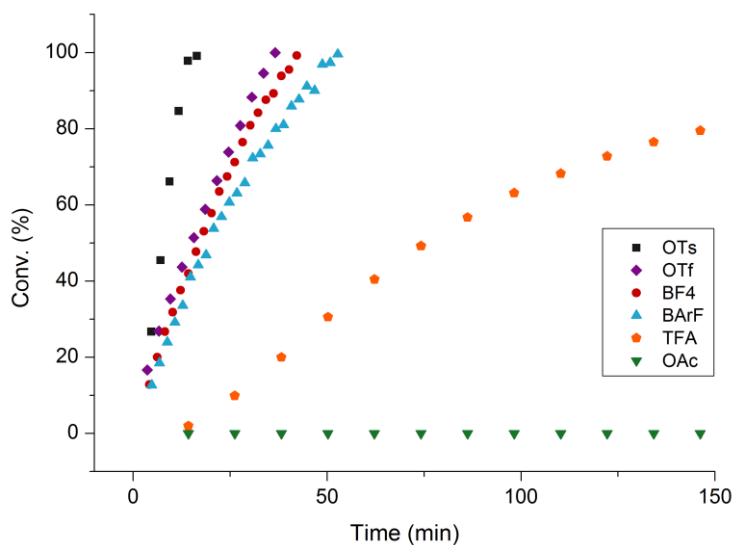


Figure 17. Alkoxylation of 3-hexyne with NHC-AuX catalysts.

The results for the alkoxylation of 3-hexyne with MeOH are shown in Figure 17 and Table 1.^{iv} The most active catalyst is the compound **4OTs**, followed by **4OTf**, **4BF₄**, **4BAr^F** and **4TFA**, which lead to complete conversion of 3-hexyne in 17, 33, 40, 48 and 266 minutes respectively (entries 1, 4, 5, 6 and 7 Table 1). The values of TOF are 5.6, 2.9, 2.4, 2.0 and 0.4 min⁻¹ for **4OTs**, **4OTf**, **4BF₄**, **4BAr^F** and **4TFA**, respectively, **4OAc** does not show any catalytic activity.

Very surprisingly, the trend of the TOF values does not reflect the coordinating power⁶⁴ of the anions. Usually, when the first catalytic step involves the competition between the substrate and the anion on the metal coordination vacancy, strong coordinating anions reduce the catalytic activity.¹⁰⁷ Indeed, from the mechanism depicted in Scheme 14, we may expect that non-coordinating anions should maximize the catalytic rate. On the other hand, the trend of TOF does not reflect the basicity of the anions¹⁰⁸ towards the abstraction of the alcoholic proton of the methanol neither before or after the nucleophilic attack. As a matter of fact, the best performing anion, OTs⁻,¹⁰⁹ possesses intermediate coordinating and basicity properties in the considered series of counterions. In order to get a deeper insight into these intriguing results, we analyzed the effect of the anion in the ISIP ⇌ OSIP pre-equilibrium step (Scheme 14).

Table 1. Alkoxylation of 3-hexyne with [(NHC)AuX]					
	Entry	Anion	Conv. [%]	t [min] ^[e]	TOF ^[f] [min ⁻¹]
[a]	1	OTs ⁻	99	17	5.6
	2 ^[c]	OTs ⁻	99	20	4.8
	3 ^[d]	OTs ⁻	99	22	4.3
	4	OTf ⁻	99	33	2.9
	5	BF ₄ ⁻	99	40	2.4
	6	BAr ^{F-}	99	48	2.0
	7	TFA ⁻	99	266	0.4
	8	OAc ⁻	0	-	-
[b]	9	OTs ⁻	99	18	5.3
	10	OTf ⁻	99	47	2.0
	11	BF ₄ ⁻	99	64	1.5
	12	BAr ^{F-}	99	89	1.1

Catalysis conditions: 30 °C, 3-hexyne (100 μL), **4X** loading (1 mol %), [a] CH₃OH (143 μL) or [b] CH₃OD (143 μL) in CDCl₃ (400 μL). [c] With 5% NBu₄OTs as additive. [d] With 15% pTsOH as additive. Conversions were determined by ¹H NMR spectroscopy, using TMS as internal standard, as average of three runs. [e] time for 95% conversion. [f] TOF= ([acetal] / [4X])/t at 95% of conversion.

^{iv} Under our conditions, the formation of 3-hexanone, due to the presence of traces of water, is less than 2% with respect to the initial concentration of 3-hexyne.

The equilibrium is shifted to OSIP when weakly and non-coordinating OTf^- , BF_4^- and BARF^- anions are considered.¹⁰⁶ This means that the concentration of ISIP is constant during the reaction, leading to a linear profile of the conversion against time (Figure 17).

Differently, for **4TFA** (Figure 17) the reaction rate is not constant, but it lowers when the time is around 90 minutes. Recording the ^{19}F NMR spectrum at different reaction times, we observed the disappearance of the broad resonance at -74.8 ppm and simultaneously the formation of a sharp new resonance at -76.2 ppm assigned to the trifluoroacetic acid TFAH (Figure 18). Dissolving **4TFA** in CDCl_3 with 400 eq. of methanol, the same phenomenon is observed, with the total disappearance of the NMR signal relative to **4TFA** within one hour (Figure 18). If 3-hexyne is added to the solution after three hours (at complete formation of TFAH), no catalytic activity was observed. These experimental results can be explained by assuming an acid-base reaction between TFA^- and MeOH , giving TFAH and MeO^- , which, in turn, probably poisons the catalyst forming the catalytically inert $[(\text{NHC})\text{Au}-\text{OMe}]$ species.¹⁰⁵

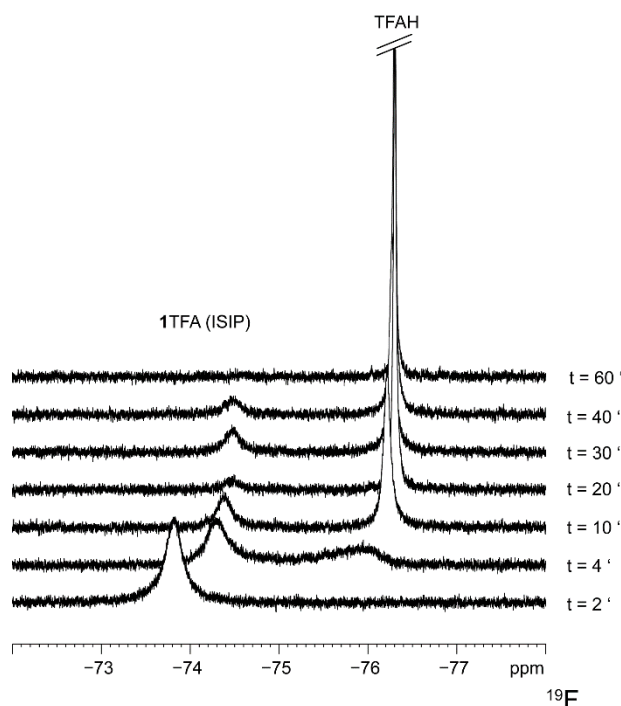


Figure 18. ^{19}F NMR spectra of **4TFA** (CDCl_3 , 1mM) in presence of 400 eq of methanol, recorded at different times.

For **4OAc**, which does not show any catalytic activity (Figure 17), the reaction with MeOH is very slow (30% of acetic acid is formed within 48 hours, Figure 19). In this case, the ISIP is predominant in solution due to the strong coordinating ability of the anion.

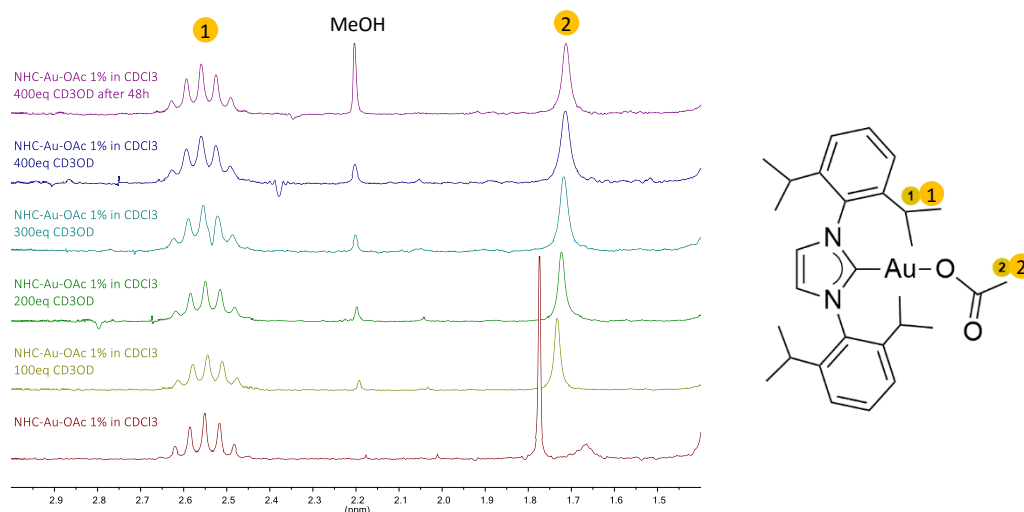


Figure 19. ^1H NMR spectra of **4OAc** (CDCl_3 , 1 mM) in presence of an increasing concentration of methanol at different time.

Finally, for **4OTs**, in the ^1H NMR spectra recorded during the catalysis, the resonances of the tosylate anion closely resemble those of NBu_4OTs (compare Figure 20a and Figure 20c), which indicates that the anion is not coordinated to the metal. Since the pre-equilibrium is completely shifted toward the ISIP in absence of methanol (compare Figure 20b and Figure 20d), we can surmise that methanol may help the de-coordination of the anion, probably through the formation of a hydrogen bond.¹¹⁰ Therefore, the anion can be considered always not-coordinated to the metal. The importance of the pre-equilibrium step is demonstrated by the fact that the addition of an external salt such as NBu_4OTs (5%) reduces the TOF from 5.6 to 4.8 min^{-1} , likely because of the shift of the ISIP/OSIP equilibrium toward the ISIP.

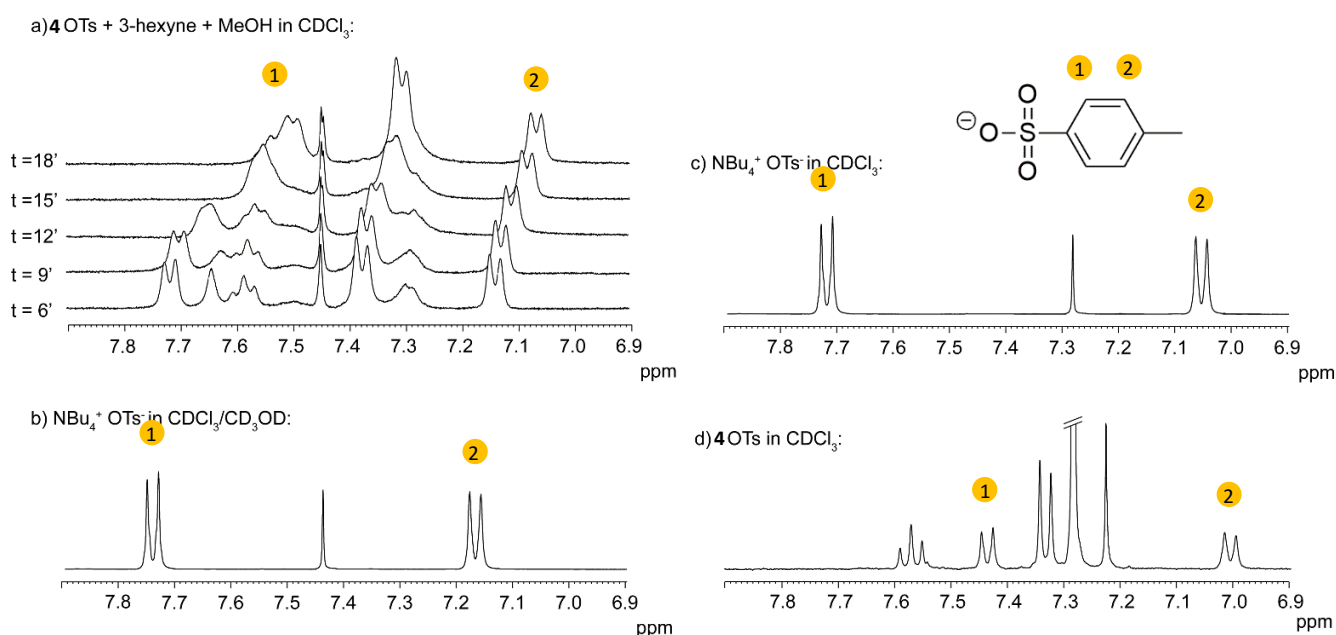


Figure 20. a) Aromatic region of ^1H NMR spectra recorded at different reaction times (indicated at the side of the spectra, in minutes) during the alkoxylation of 3-hexyne catalysed by **4OTs**; b) ^1H NMR spectrum of NBu_4OTs in $\text{CDCl}_3/\text{CD}_3\text{OD}$; c) ^1H NMR spectrum of NBu_4OTs in CDCl_3 ; d) ^1H NMR spectrum of **4OTs** in CDCl_3 .

We have determined the order of reaction with respect to **4OTs**, which resulted to be 1 (Table 2), the same order has been observed for non coordinating anions,^{105a} confirming that only one gold atom is involved in the RDS of the reaction. However, the latter can be either the nucleophilic attack or the protodeauration (Scheme 14).

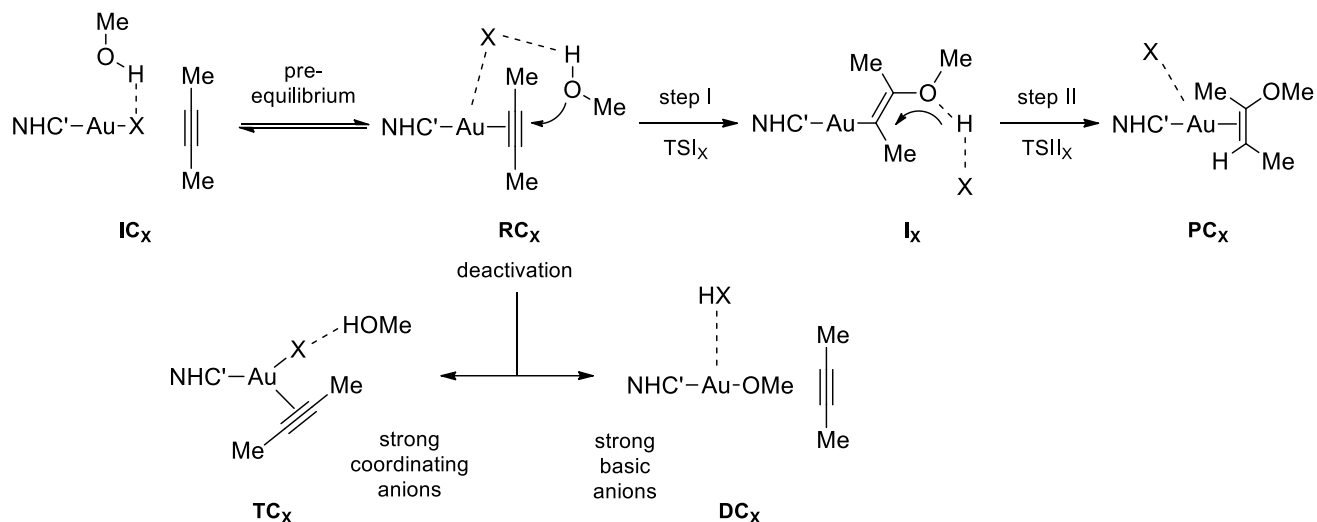
Table 2. Reaction order with respect to 4OTs				
Entry	Au [mol%]	Conv. [%]	t [min] ^[a]	TOF ^[b] [min ⁻¹]
1	0.5	97	33	5.8
2	1	99	17	5.6
3	1.5	98	11	5.8
4	2	99	7	6.8

Catalysis conditions: 30 °C, 3-hexyne (100 μL), NHC-Au-OTs (mol%), methanol (143 μL) in CDCl₃ (400 μL). Conversions were determined by ¹H NMR spectroscopy, using TMS as internal standard, as average of three runs. [a] Time for 95% conversion. [b] TOF= (n_{acetal} / n_{4OTs}) / t [min] at 95% of conversion.

To identify the RDS, different catalytic conditions have been tested. In presence of pTsOH (15%) and **4OTs**, the reaction is decelerated and the TOF changes from 5.6 to 4.3 min⁻¹ (entries 1 and 3, Table 1). In addition, using CH₃OD instead of CH₃OH, we observe a slight reduction of the TOF, which shifts from 5.6 to 5.3 min⁻¹ (compare entries 1 and 9, Table 1), giving a Kinetic Isotopic Effect (KIE)¹¹¹ equal to 1.1. For **4OTf**, **4BF₄** and **4BAr^F**, the KIE resulted equal to 1.4, 1.6 and 1.8 respectively (entries 4/10, 5/11, 6/12, Table 1). These values of KIE point out that, under our conditions, the rate-limiting step is the nucleophilic attack of the methanol.¹¹² However, the small increase of the KIE on going from more coordinating anion (OTs⁻) to non-coordinating one (BAr^{F-}), may indicates that the importance of protodeauration step in the mechanism increases from OTs⁻ to OTf⁻, from OTf⁻ to BF₄⁻ and from BF₄⁻ to BAr^{F-}. In agreement with our findings, Zhdanko and Maier showed clearly that the reaction rate of the hydroalkoxylation of 3-hexyne by methanol (in methanol), is independent from the amount of acid, excluding the protodeauration as the RDS.^{105a} We also note that the RDS strongly depends on the reaction conditions and on the reactants. In a recent paper by Straub and co-workers¹¹³ a KIE of 3 to 5 is observed for the hydration of terminal alkynes conducted in methanol, while the group of Gagné and Widenhoefer reported a KIE of 5.3 for the gold-catalysed intramolecular hydroalkoxylation of 2,2-diphenyl-4,5-hexadien-1-ol to a 2-vinyltetrahydrofuran derivative.¹¹⁴ These authors suggest that protonolysis of the gold-carbon bond was the RDS in both cases.

From the computational point of view, the role of the anion has been usually recognized only in the protodeauration step,¹¹⁵ acting as a *proton shuttle*, or forming weak interactions with the substrate, changing the enantioselectivity.¹¹⁶ However, since under our catalytic conditions the nucleophilic attack is the RDS, an active role of the anion is expected also within this step. We focused our study on the attack

of the first methanol molecule, as we mentioned the addition of the second molecule of methanol is shown to be fast.^{105b} The complex $[(\text{NHC}')\text{AuOTs}]$, ($\text{NHC}' = 1,3\text{-dimethylimidazol-2-ylidene})$ 2-butyne and methanol as models for the catalyst, substrate and nucleophile, respectively, have been selected (Scheme 15).



Scheme 15. Role of the anion (X) in the reaction mechanism between 2-Butyne and methanol catalysed by the $[(\text{NHC}')\text{Au-X}]$ complex.

In particular, we decided to investigate the OTs^- anion because, unexpectedly, it is the most efficient in spite of its stronger coordinating ability with respect to BF_4^- and $\text{BAr}^{\text{F}-}$, moreover no DC_{OTs} or TC_{OTs} were observed during the catalysis because its intermediate coordinating and basicity ability (Figure 20). According to recent benchmark papers, we used density functional theory (DFT) in combination with the BP86 exchange-correlation functional to optimize the geometries and the double-hybrid functional B2PLYP to compute the corresponding energy.^{117, v}

For the pre-equilibrium, the electronic energy of the complex $[(\text{NHC}')\text{AuOTs}] \cdot (2\text{-butyne})$ is 3.6 kcal/mol lower than that of $[(\text{NHC}')\text{Au}(\eta^2\text{-2-butyne})]\text{OTs}$, which indicates that the alkyne substitution of the coordinated OTs^- is somewhat unfavourable. Interestingly, when one molecule of methanol is introduced in the system, the difference between $[(\text{NHC}')\text{AuOTs}] \cdot (2\text{-butyne}) \cdot (\text{MeOH})$ (IC_{OTs}) and $[(\text{NHC}')\text{Au}(\eta^2\text{-2-butyne})]\text{OTs} \cdot (\text{MeOH})$ (RC_{OTs}) lowers to 2.7 kcal/mol, thanks to the hydrogen bond formation between the methanol and the anion ($\text{O}_{\text{OTs}}\text{-H}_{\text{MeOH}} = 1.780 \text{ \AA}$). In the RC_{OTs} configuration, the anion weakly interacts with gold ($\text{Au-O}_{\text{OTs}} = 3.283 \text{ \AA}$) and the methanol is positioned at the opposite side of the alkyne with respect to the gold. RC_{OTs} is a particularly suitable reactant complex configuration for the *anti*-periplanar addition of the nucleophile, which is the most favoured mechanism according to previous studies.^{105a}

^v If other functionals, as M-06 or B2PLYP-D3, are used to compute the energies, only small differences can be found. Also the inclusion of the solvent (COSMO) does not alter the path significantly.

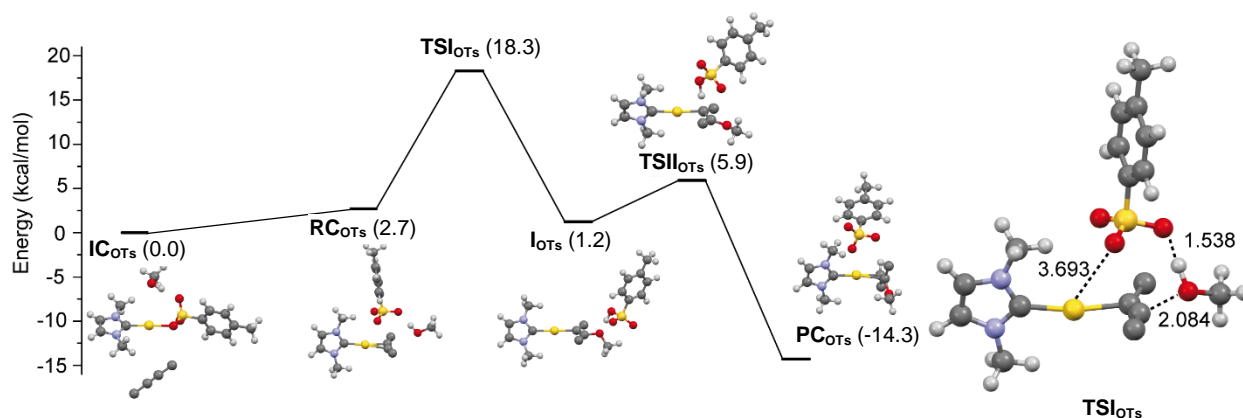


Figure 21. DFT-calculated profile for the reaction between 2-butyne and methanol, catalyzed by (NHC')AuOTs (*left*). Geometrical structure of TSIOTs, with relevant distances in Å (*right*). The structures of the species are also shown. The protons of 2-butyne have been omitted for clarity.

Starting from **RCOTs**, the methanol can approach the carbon atom coordinated to gold, passing through a transition state (**TSIOTs**), with an activation barrier of 15.6 kcal/mol (computed with respect to **RCOTs**). Note that removing the anion from the catalytic cycle, the σ -coordinated gold(I) vinyl ether (**IOTs** like structure of Figure 21) is not stable. In the transition state geometry, the distance between the methanol and the carbon atom is 2.084 Å (Figure 21, right), with the anion facilitating the attack in two ways: i) it acts as a template, keeping the reactive methanol molecule in the right position for the addition, and, simultaneously; ii) it “activates” the nucleophile through an hydrogen bond that is shorter than in **RCOTs** ($O_{OTs}-H_{MeOH} = 1.538$ Å).

The product of the attack is a metal σ -coordinated vinyl ether (**IOTs**), with the hydrogen of the methanol completely transferred to the anion ($O_{OTs}-H_{MeOH} = 1.035$ Å), giving a neutral molecule of *p*-toluenesulfonic acid. The acid easily donates the hydrogen to the carbon coordinated to gold (**TSIIOTs**) acting as an efficient proton shuttle between the methanol and the substrate (activation barrier 4.7 kcal/mol with respect to **IOTs**). The product of the protodeauration step is a π -coordinated vinyl ether (**PCOTs**). In **PCOTs** the gold atom is not equidistant from the two carbons, but it is at a larger distance from the carbon that underwent the nucleophilic attack (Au-C2 = 2.209 Å, Au-C1 = 2.430 Å). The same asymmetry has been experimentally observed, too.¹¹⁸ Now the vinyl ether can de-coordinate and be substituted by another molecule of alkyne.^{vi}

From the structure of **TSIOTs**, the experimentally observed anion effect (Figure 17) can be rationalized on the basis of the coordinating and basicity properties of the different anions. The most important factor seems to be the ability to abstract the proton from the methanol, and this ability is proportional to the anion basicity. Coherently with this picture, the performances of **4BF₄** and **4BAR^F** are worse than those of

^{vi} Noteworthy, all the complexes considered in Figure 21 have the same number of atoms, minimizing the entropy problem. An estimation of the entropic contribution can be found in the Experimental Part.

4OTs, because such anions more difficultly form the corresponding acids HBF_4 and HBAr^{F} . On the other hand, too high coordination or basicity power of the anion worsens the catalytic performances, preventing the alkyne coordination (as in the case of OAc^-) or forming too much free MeO^- in solution, which poisons the catalyst (as in the case of TFA^-).

2.1.1 Nucleophile effect

The experimental data confirmed by DFT calculations (see previous paragraph) suggested that an extra molecule of nucleophile could help the attack to the coordinated alkyne bound to a gold cationic framework, or support the proton shuttle, when weakly coordinating anions are employed. A systematic experimental study of the role of the anion in connection with the nature of the nucleophile is not present in the literature. For this purpose, we analysed both **4OTs** (where anion plays an active role) and **4BAr^F** (where anion does not enter into the reaction mechanism) in the alkoxylation of 3-hexyne, in which different nucleophiles were screened. Among them, triethylene glycol monomethyl ether (Gly-OMe) is a better nucleophile than methanol for its capacity to polarize the attack (or the proton shuttle). On the contrary, 2,2,2-trifluoroethanol (TFE), benzyl alcohol (BnOH), and 2,6-dimethoxyphenol (2,6-(OCH_3)PhOH), were chosen as nucleophiles poorer than methanol.

Table 3. Alkoxylation of 3-hexyne					
Entry	Nucleophile	Catalyst	Conv. [%] ^a	t [min] ^b	TOF [min ⁻¹] ^c
1	TFE ^d	4OTs , 4BAr^F	0	-	-
2	Gly-OMe ^e	4OTs	98	345	0.28
3		4BAr^F	98	476	0.20
4	BnOH ^f	4OTs	99	78	1.2
5		4BAr^F	99	1619	0.06
6	2,6-(OCH_3)PhOH ^g	4OTs	18	5430	0.003
7		4BAr^F	0	-	-

Catalysis conditions: 30 °C, 3-hexyne (0.88 mmol, 100 μL), 1 mol% catalyst in CDCl_3 (400 μL). [a] Determined by ^1H NMR using TMS as internal standard; averaged values of three runs. [b] Time for 95% of conversion or at the highest conversion registered. [c] $\text{TOF} = (n_{\text{product}} / n_{\text{catalyst}}) / t$ (min) at 95% of conversion. [d] 2,2,2-trifluoroethanol (3.52 mmol, 256 μL). [e] Triethylene glycol monomethyl ether (1.16 mmol, 186 μL), 3-hexyne (0.29 mmol, 33 μL). [f] Benzyl alcohol (1.16 mmol, 120 μL), 3-hexyne (0.29 mmol, 33 μL). [g] 2,6-dimethoxyphenol (0.88 mmol, 136 mg), 3-hexyne (0.22 mmol, 25 μL), TOF calculated at 18 min.

Using TFE as nucleophile, both complexes **4OTs** and **4BAr^F** do not promote any reaction (Table 3, entry 1). When the alkoxylation of 3-hexyne is performed with a functionalized alcohol such as Gly-OMe, the

overall reaction is strongly slowed down, and complexes **4OTs** and **4BAr^F** promote full conversion in similar reaction time (Table 3, entries 2 and 3) while in the case of methoxylation the reaction times were different (17 and 48 min for **4OTs** and **4BAr^F** respectively, Table 1, entries 1 and 6). On the other hand, performing the reaction with BnOH proceeded efficiently using **4OTs**, whereas in the case of **4BAr^F** the almost complete formation of the final product was achieved after a much higher reaction time (Table 3, entries 4 and 5). Finally, using **4OTs** an incomplete and slow conversion of substrate was observed upon addition of 2,6-(OCH₃)PhOH (the poorest nucleophile here employed), while the reaction failed completely in the presence of **4BAr^F** (Table 3, entries 6 and 7). Taken all together, these experimental evidences reveal that the character of the nucleophile significantly modifies the impact of the anion effect in the catalytic reaction.

With functionalized nucleophiles (*e.g.*, Gly-OMe) the O-H bond may be polarized *via* specific intramolecular interactions, suppressing the anion effect. The role of the anion is crucial in presence of soft nucleophiles (as compared to methanol, *e.g.*, benzyl alcohol and 2,6-dimethoxyphenol) which are less able to attack the coordinated substrate and need to be activated. The use of TFE as nucleophile even inhibits the reaction, most probably due to the presence of the strongly electron withdrawing -CF₃ group, that may in principle either decrease the nucleophilic character of the -OH group or favor the formation of CF₃CH₂O⁻ in solution, leading to catalyst deactivation **DC_x**.

We studied the activation of the nucleophile in the RDS step for two different nucleophiles: TFE, in combination with the OTs⁻, as it was not reacting with respect to MeOH, and Gly-OMe in the absence of the anion, because of its unchanging activity in combination with different anions (Table 3). First, we focus on the activation of TFE nucleophile by hydrogen-bond acceptor ability of OTs⁻ anion, in spite of the structural similarity with MeOH, it is not able to react with 3-hexyne to give the product (see Table 3, entry 1). Here, the electron withdrawing -CF₃ group may i) induce a stronger acidity to the -OH group so that the proton can be easily removed in the presence of an anion and the resulting methoxy leads to catalyst deactivation; ii) reduce the nucleophilic ability of the -OH group in such a way that is not able to attach the triple bond of the substrate.

The calculated initial complex **IC_{TFE}**, reactant complex **RC_{TFE}**, intermediate **I_{TFE}**, transition state **TS_{preeqTFE}** for the preequilibrium step and transition state **TS_{TFE}** for the TFE nucleophile attack to butyne in the presence of the OTs⁻ anion are shown in Figure 22.

Similarly to MeOH, the most stable species has been calculated to be the anion-coordinated initial complex (**IC_{TFE}**), which has been taken as the zero point energy, with the 2-butyne in the second coordination sphere weakly interacting with the NHC ligand. In the reactant complex (**RC_{TFE}**) the anion acts as a template and holds the TFE nucleophile in the right position for an outer sphere attack. In **RC_{TFE}** one of the basic atom of the anion weakly interacts with the metal center (Au...O = 3.284 Å), while forming an hydrogen bond with the nucleophile. The O(OTs⁻)...H(OTFE) distance is 1.679 Å, shorter than that in

$\mathbf{RC}_{\text{MeOH}}$ (1.780 Å), due to the presence of the electron withdrawing CF_3 group which leads to a stronger interaction between the alcoholic proton and the basic oxygen atom of the anion. The reaction of \mathbf{RC}_{TFE} formation from the initial complexes \mathbf{IC}_{TFE} is endothermic by +2.4 kcal/mol, with an activation barrier of 9.1 kcal/mol. The formation of the catalytically inactive \mathbf{DC}_{TFE} complex from the \mathbf{IC}_{TFE} is calculated to be also endothermic by +6.9 kcal/mol, with an activation barrier of 13.2 kcal/mol. So this deactivation path (throughout the formation of alkoxyde) is even less accessible here than what was found above for MeOH (we recall that the $\mathbf{DC}_{\text{MeOH}}$ energy of formation from $\mathbf{IC}_{\text{MeOH}}$ is 2.4 kcal/mol and the activation energy is 9.6 kcal/mol). In the \mathbf{TS}_{TFE} for the nucleophilic attack of TFE to the butyne-coordinated species \mathbf{RC}_{TFE} the bond between the gold center and the carbon atom on which the nucleophile attacks (C1) is elongated (2.719 Å) while that between gold and C2 is 2.094 Å. The distance between oxygen of OTs^- and the metal center is 3.916 Å, larger than that calculated for MeOH (3.693 Å), and the incipient abstraction of the TFE hydrogen by OTs^- is more pronounced ($\text{CF}_3\text{CH}_2\text{O}-\text{H} = 1.081$ Å, $\text{CF}_3\text{CH}_2\text{OH}\cdots\text{O}(\text{OTs}^-) = 1.398$ Å) in this case due to the presence of the CF_3 group leading to a more acidic proton. This larger “acid-like” character of OTs^- , apparently indicating a larger activation of the TFE by HB acceptor property of the anion, results however in a higher activation barrier (18.6 kcal/mol) with respect to MeOH (15.6 kcal/mol, from \mathbf{RC}_{OTs} to \mathbf{TS}_{OTs}) for the nucleophilic attack, showing an intrinsically poor nucleophilic character of TFE.

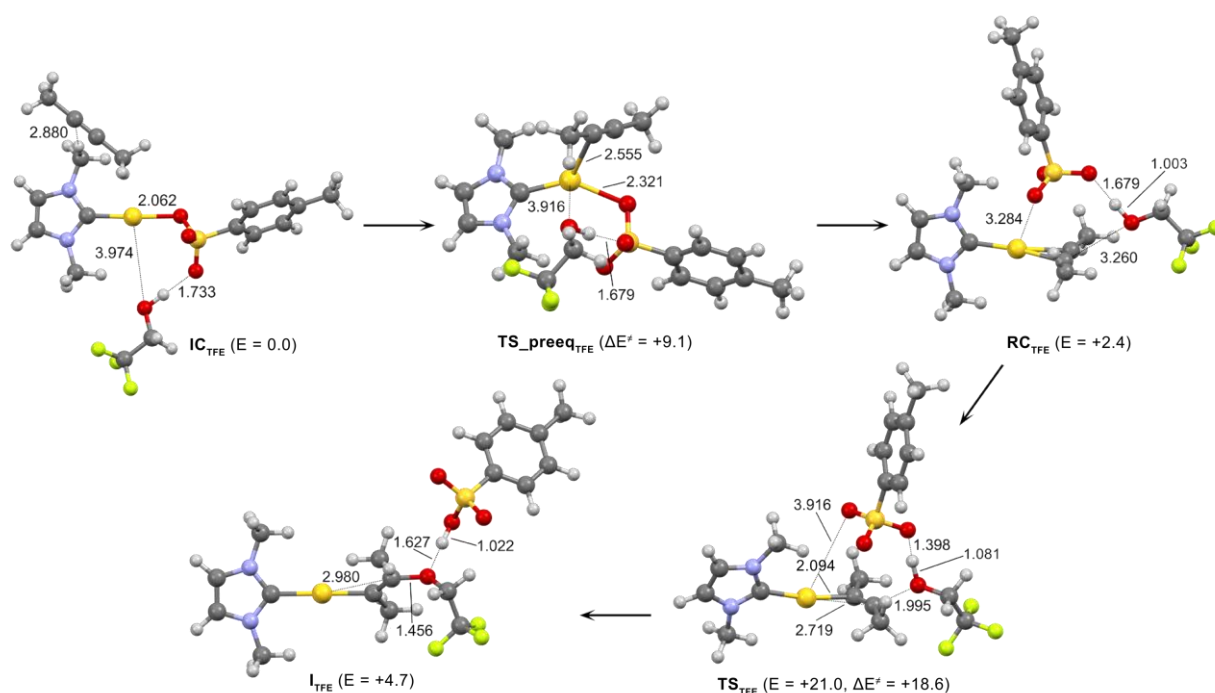


Figure 22. Initial complex \mathbf{IC}_{TFE} , reactant complex \mathbf{RC}_{TFE} , intermediate \mathbf{I}_{TFE} , transition state $\mathbf{TS}_{\text{preeq}_{\text{TFE}}}$ for the preequilibrium step and transition state \mathbf{TS}_{TFE} for the trifluoroethanol nucleophile attack to butyne in the presence of the OTs^- anion. Energies values (kcal/mol) refer to \mathbf{IC}_{TFE} , taken as zero. Bond lengths are in Å.

The transition state \mathbf{TS}_{TFE} evolves with the formation of the intermediate complex \mathbf{I}_{TFE} where the hydrogen of trifluoroethanol has been completely abstracted by OTs^- ($\text{CF}_3\text{CH}_2\text{O}\cdots\text{H} = 1.627 \text{ \AA}$ and $\text{H}-\text{O}(\text{OTs}) = 1.022 \text{ \AA}$). The overall activation barrier from \mathbf{IC}_{TEF} to \mathbf{I}_{TEF} is 21.0 kcal/mol.

From these results we conclude that: i) in the pre-equilibrium step for TFE the \mathbf{RC} formation is favored over the \mathbf{DC} formation, thus precluding a catalyst poisoning through alkoxy deactivated species; ii) in the nucleophilic attack step the OTs^- anion acts as a hydrogen-bond acceptor, enhancing the nucleophilicity of the attacking trifluoroethanol, nevertheless the latter is remaining scarcely nucleophilic. These findings suggest that a too low nucleophilic power rather than a catalyst poisoning is the reason why TFE is not experimentally active when both $\mathbf{4OTs}$ and $\mathbf{4BAR}^{\text{F}}$ are employed as catalyst.

Finally, we studied the nucleophilic attack of Gly-OMe to 2-butyne via auto-activation through $\text{OH}\cdots\text{O}$ hydrogen bond in order to rationalize its observed similar reaction time in combination with different anions. Gly-OMe can be found in many different rotational conformers, and three possible stable conformations are conceivable with the alcoholic hydrogen forming an internal hydrogen bonds (HB) with the oxygen atom of one of the two ethylene glycol groups (1-O and 2-O) or with the oxygen of the ether group (3-O). Only these three conformations have been considered in the calculations and the one with the smaller activation barrier is reported here (see Experimental Section for the others). We start our study from the reactant complex $\mathbf{RC}_{\text{Gly-OMe}}$ since no anion is taken into account in order to verify that the addition to butyne may take place via an auto-activation. In the $\mathbf{RC}_{\text{Gly-OMe}}$ complex (Figure 23) the Gly-OMe is held in a suitable position for the outer sphere nucleophilic attack through formation of a HB between the oxygen atom of the ether group and one hydrogen of the butyne ($\text{H}_{\text{butyne}}\cdots\text{3-O}(\text{OMe}) = 2.328 \text{ \AA}$) while the distance between the Gly-OMe oxygen which performs the nucleophilic attack and the C1 carbon of the butyne is 3.420 \AA . The alcoholic hydrogen in Gly-OMe forms in turn an internal HB with the ethylene glycol oxygen atom (2-O) that lies at 2.157 \AA from it. This latter distance becomes shorter in $\mathbf{TS}_{\text{Gly-OMe}}$ ($\text{OH}\cdots\text{2-O}$ (ethylene glycol) = 1.940 \AA) with $\text{O}-\text{H} = 1.002 \text{ \AA}$ which is only slightly elongated with respect to that in the $\mathbf{RC}_{\text{Gly-OMe}}$ complex (0.984 \AA). A peculiar feature of the $\mathbf{TS}_{\text{Gly-OMe}}$ structure is the almost co-planar approach of the oxygen atom of the nucleophile towards the substrate C1 carbon (dihedral angle $\text{Au-C2-C1-O} = 174.5^\circ$), at a variance with the substantial out-of-plane approach found in the \mathbf{TS} structures for the MeOH and TFE nucleophilic attack to 2-butyne mediate by the OTs^- anion (dihedral angle $\text{Au-C2-C1-O} = 155.1^\circ$ and 153.8° , respectively), a constraint due to the anion template effect. The calculated activation barrier is 10.4 kcal/mol, indicating an efficient auto-activation of the nucleophile, which may be then ascribed not only to the possibility of forming internal hydrogen bond but also to the possibility of allowing a co-planar nucleophilic attack, which seems to stabilize the transition state.

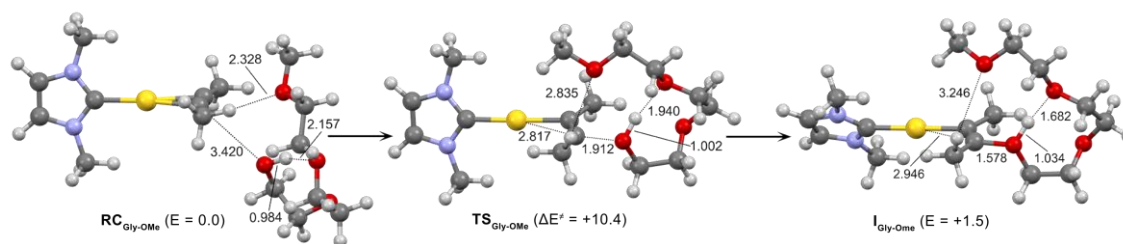


Figure 23. Reactant complex $RC_{\text{Gly-OMe}}$, intermediate $I_{\text{Gly-OMe}}$ and transition state $TS_{\text{Gly-OMe}}$ for the triethylene glycol monomethyl ether nucleophile attack to 2-butyne without the anion. Energies values (kcal/mol) refer to $RC_{\text{Gly-OMe}}$, taken as zero. Bond lengths are in Å.

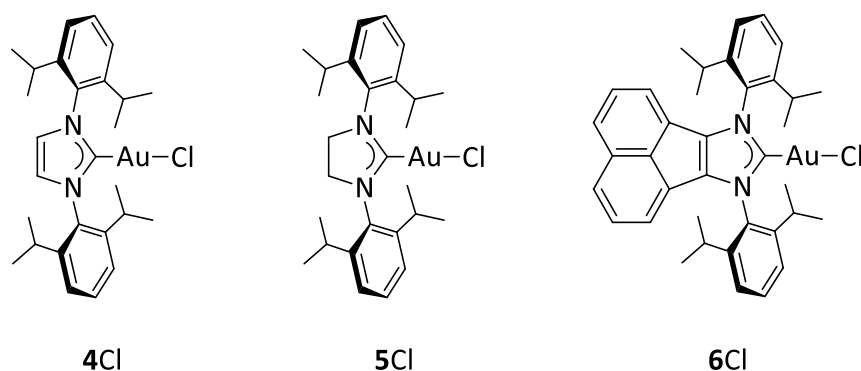
$TS_{\text{Gly-OMe}}$ evolves with the formation of the intermediate $I_{\text{Gly-OMe}}$ which is less stable than $RC_{\text{Gly-OMe}}$ by 1.5 kcal/mol. The intermediate structure is very similar to that of the transition state, with much reduced C1...O (1.578 Å) and OH...2-O(ethylene glycol) (1.682 Å) distances, and an elongated O-H bond (1.034 Å). These results clearly show that Gly-OMe as nucleophile is auto-activating for the alkyne attack via both internal HB formation and structural flexibility that releases steric constraints and allows a co-planar substrate attack. Here the activation of OH via the HB acceptor ability of the anions are not needed, in agreement with the Gly-OMe experimentally observed activity which remains almost constant independently of the used anion (Table 3, entries 2 and 3).

In conclusion, we showed that the anion properties, both coordination ability and basicity, have a great and under evaluated impact on the catalytic performances of gold complexes, and the “classical” non-coordinating anions (as BF_4^-) may be not always the best choice. Intermediate coordinating and basicity power of the anion OTs^- provides, under the specific experimental conditions employed, the best compromise to achieve an efficient catalyst: the preequilibrium with this anion is shifted toward the OSIP, deactivation of catalyst to a gold-methoxide is prevented and its characteristic basicity promotes the nucleophilic attack. This study clearly demonstrates that the anion can play an effective role in different steps of the catalytic cycle, including the overall important nucleophilic attack.¹¹⁹ Finally, the counterion effects can be modulated by the choice of the nucleophile. When the alcohol is a poor nucleophile as in the case of benzyl alcohol the reactivity increases (about 20 folds) on going from BAR^F^- to OTs^- . Using methanol this difference was smaller and flattened due to the formation of hydrogen bonding with a second alcohol molecule that improves the nucleophilicity of the attacking methanol. On the other hand, the use of suitably functionalized alcohols that contribute to the polarization of the -OH bond through intramolecular interactions (this is the case of Gly-OMe) flatten the effect of the anion (BAR^F^- and OTs^- show analogous catalytic performances). Alcohols with too low nucleophilic power (as TFE) is not active when both $4OTs$ and $4BAR^F$ are employed as catalyst.

2.2 Functionalized carbene ligands to modify IP and catalytic activities.

2.2.1 Nitrogen heterocyclic carbenes

In the previous chapter, we have demonstrated that the anion can assist the nucleophilic attack of the nucleophile on the substrate (chapter 2.1). In order to extend our knowledge about the relationship between the anion/cation orientations and the catalytic performances of gold complexes, we explored a new series of organogold species bearing NHC carbene ligands with a modified ligand structure. The aim is to produce different charge distribution and, consequently, different ion pair structures pushing the anion closer to the reaction site. From previous work we observed that for the *classical* unsaturated $[(\text{NHC})\text{-Au}(\eta^2\text{-2-hexyne})]\text{BF}_4$, the anion is strongly attracted by the hydrogen atoms on the imidazole ring.^{69b} The substitution of such hydrogen atoms with methyl groups only moderately reduces this interaction in $[\text{NHC-Au}(\eta^2\text{-alkene})]\text{BF}_4$ related complexes.^{69b} Here we study the influence of eliminating the unsaturation using the saturated heterocyclic carbene $[(\text{sNHC})\text{-Au}(\eta^2\text{-3-hexyne})]\text{BF}_4$ (Scheme 16, **5BF₄**), in order to reduce the affinity of the hydrogen atoms of the imidazole ring toward the anion. We also explore the opposite direction, studying the effect of an extended aromatic π -system of the ligand¹²⁰ with $[\text{NHC}(\text{BIAN})\text{-Au}(\eta^2\text{-3-hexyne})]\text{BF}_4$ (Scheme 16, **6BF₄**). In fact, it is known that such polycyclic aromatic system in Pd(II) and Pt(II) complexes delocalizes the charge so effectively as to make the ion pair structure completely unspecific.¹²¹ For a strict comparison between the complexes also $[(\text{NHC})\text{-Au}(\eta^2\text{-3-hexyne})]\text{BF}_4$ (Scheme 16, **4BF₄**) was synthesized and studied.

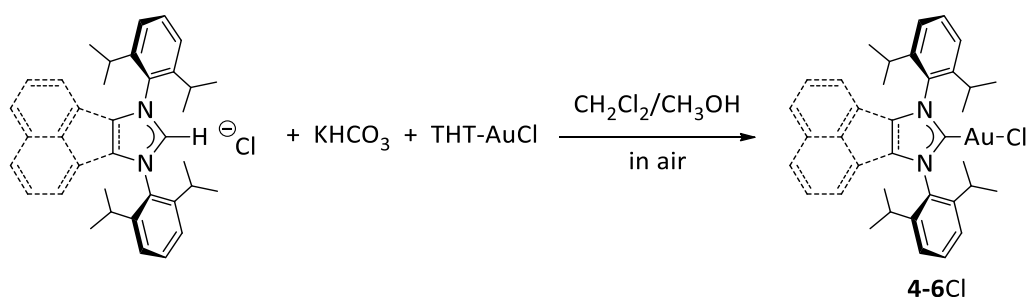


Scheme 16. Structure of the NHC gold precursors.

During this study, we also setup an improved strategy to synthesize NHCs gold chloride complexes. Generally, such species are prepared by deprotonation of imidazolium salts $[\text{NHC}(\text{H})]\text{Cl}$ with a strong base, followed by the addition of a gold source.^{122, 123} Since this method requires moisture- and air-free conditions, due to the presence of a free carbene, different approaches have been developed in the last

years. One of them is the synthesis of [(NHC)AgCl] complexes¹²⁴ as carbene transfer agents, which are able to transfer the carbene to a gold(I) precursor *via* trans-metallation reaction, with precipitation of silver chloride. Decomposition of silver adducts can reduce the yield and purity of the final gold complexes, and recrystallization is always necessary. Recently [NHC(H)]HCO₃ salts have been used for the synthesis of gold complexes,¹²⁵ even if the carbonate salt is highly hygroscopic and very dry conditions are required.

We obtained the NHC carbene gold precursors **4-6Cl** in high yield and purity and without successive crystallization with a simple one-pot methodology (meanwhile also Nolan and co-workers published a similar procedure).¹²⁶ Stirring [NHC(H)]Cl salt, KHCO₃ and THT-AuCl together in CH₂Cl₂/CH₃OH mixture in air without any distillation of solvents and without drying the KHCO₃ (Scheme 17, see the Experimental Part for details), yields directly the desired gold precursors.



Scheme 17. One-pot synthesis of [NHC-AuCl] precursor **4-6Cl**.

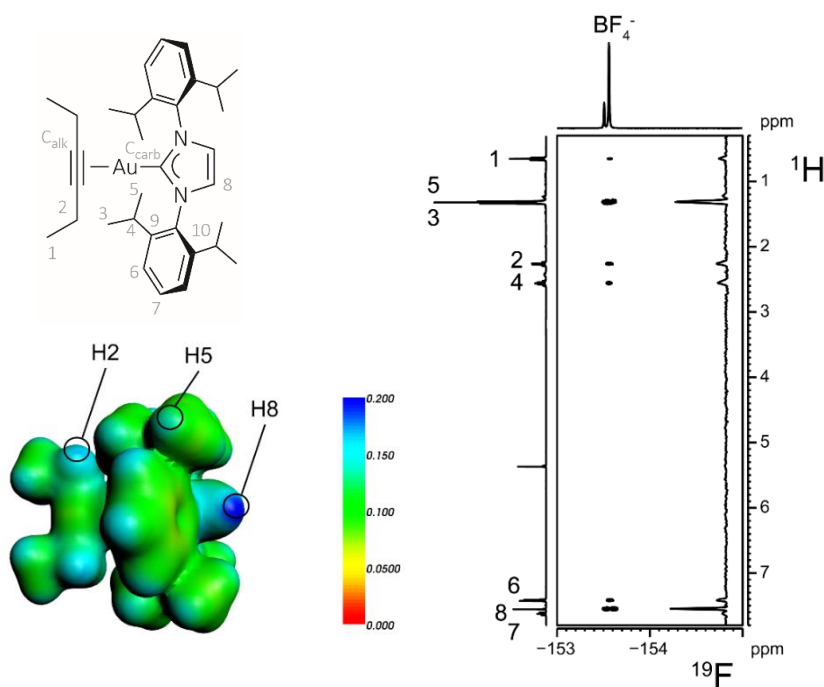


Figure 24. (Left) Coulomb potential map (in a.u.) of **4**⁺, mapped on an electronic isodensity surface (0.007 e/Å³; (Right): ¹⁹F, ¹H-HOESY NMR spectrum (376.65 MHz, 297 K, CD₂Cl₂) of complex **4**BF₄.

Subsequently, cationic bis-coordinate gold(I) complexes **4-6**BF₄, were generated in a NMR tube by the reaction of the parent [(NHC)AuCl] complexes with AgBF₄ in CD₂Cl₂, in the presence of 3-hexyne. From ¹H, ¹³C, ¹H-COSY, ¹H-NOESY, ¹H,¹³C-HMQC NMR, and ¹H,¹³C-HMBC NMR spectroscopies all proton and carbon resonances belonging to the different fragments were assigned (see the Experimental Part).

The interionic structure has been studied combining the ¹⁹F, ¹H HOESY NMR technique and relativistic DFT calculations. The latter were performed using the ADF (Amsterdam Density Functional) package, at the TZ2P/BLYP/ZORA¹²⁷ level (see chapter 4.5 for further details), including explicitly the conductor like screening model (COSMO,¹²⁸ with ε = 8.93) to include solvent effect.

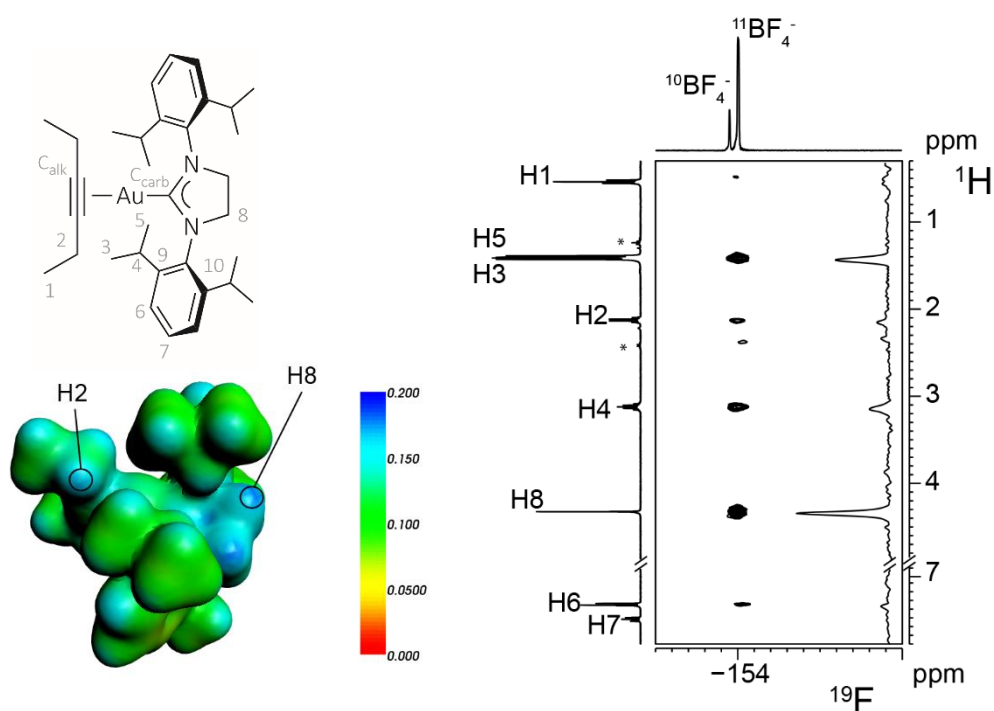


Figure 25. Left: Coulomb potential map (in a.u.) of **5**⁺, mapped on an electronic isodensity surface (0.007 e/Å³; right: ¹⁹F, ¹H-HOESY NMR spectrum (376.65 MHz, 297 K, CD₂Cl₂) of complex **5**BF₄. *denotes the resonances of free 3-hexyne (Apparently, the anion interacts also with the protons of free 3-hexyne but this contact can be reasonably explained by a fast exchange between the coordinated and free 3-hexyne: the anion interacts only with the coordinated alkyne, but because of the exchange, the NOE is indirectly transferred also to the free one; the total Overhauser effect is the sum of the cross peaks with free and coordinated alkyne).

From previous studies¹²⁹ on [(NHC)Au(S)]BF₄ ion pairs we found that two important ion-pair relative orientations are possible, **A** and **B**, in which the anion is located near NHC and S, respectively (see chapter 1.2.3 for further details). Other orientations seem to be disfavoured; the orientation in which the anion is located near gold is underprivileged because the aryl moieties with hindered ortho-substituents introduce steric hindrance above and below the metal center.^{67,130} Since the protons of the imidazole ring of the NHC ligand are slightly acidic, they carry some additional positive charge and may act as anchoring point for the anion, thus favouring orientation **A**.

This is confirmed by analysing¹³¹ the NOE contacts for **4BF₄** (Figure 24), the most intense contact is with H8 (Table 4) and it is representative for orientation **A**, whereas the contact H2/F (representative for the orientation **B**) is weaker. The weakness of H6/F and H7/F contacts indicates that the ion pair structure can be well described by either orientation **A** or **B**. The ratio between H8/F and H2/F is 1.00:0.18, leading to a **A:B** ratio of 85:15 (Table 4). As expected, it is very similar to that measured for [(NHC)-Au(η^2 -2-hexyne)]BF₄.^{69b}

Table 4. Relative NOE intensities determined by arbitrarily fixing the largest intensity of the NOE(s) between the anion fluorines and the cation protons to 1.				
	4BF₄	5BF₄^a	5BF₄	6BF₄
H1	0.13	0.10	0.17	0.49
H2	0.18	0.39	0.32	1.00
H3				0.34
H5	0.50 ^b	0.40 ^b	0.37 ^b	0.50
H4	0.23	0.32	0.27	0.89
H6	0.17	0.10	0.10	0.46 ^c
H7	0.08	0.04	0.05	0.26
H8	1.00	1.00	1.00	0.24
H9	-	-	-	0.46 ^c
H10	-	-	-	0.37
A:B	85:15	72:28	76:24	27:73 ^d
[a] Isolated ion pairs. [b] H3/F and H5/F contacts partially overlap. [c] H6/F and H9/F contacts partially overlap. [d] In this case the conformations A and B are not enough to fully describe the ion pair structure, see text.				

Figure 25 shows the ¹⁹F-¹H HOESY spectrum for **5BF₄**. The most intense interaction is H8/F, and the general pattern is very similar to that for **4BF₄**. Performing ¹⁹F, ¹H-HOESY NMR experiment on the isolated ion pairs **5BF₄** gives essentially the same results, within the experimental error. The **A:B** ratio is around 76:24 (Table 4). Mapping the Coulomb potential of the **5⁺** cation shows that H2 and H8 are indeed the most attractive regions of the cation, with a slight predominance of H8.^{vii} This map is in qualitative agreement with the experimental **A:B** ratio and comparison of the potential maps of **5⁺** and **4⁺** shows that the partial saturation of the NHC ring only slightly reduces the accumulation of positive charge on the ligand backbone, thus giving a similar **A:B** ratio (Table 4).

^{vii} A 76:24 ratio is consistent with a small difference in energy between the two conformations, around 0.7 kcal/mol.

Figure 26 shows the ^{19}F - ^1H HOESY spectrum for 6BF_4 . In this case, all the interionic interactions are of comparable intensity. In fact, the weakest is H8/F (H8 is the most “internal” proton of the BIAN system), with relative intensity 0.24. This means that there is no single favored conformation and many anion/cation relative orientations are possible. The most intense contact is with H2, and, among the carbene ligands we have studied up to now, this is the first time that the conformation **B** is favored, even if slightly, over the **A** one. This aspecific ion pair structure is a direct consequence of the extended aromaticity on the backbone of the carbene, which makes the Coulomb potential quite flat throughout the cation. This is seen in the Coulomb map of 6^+ , where the regions around the 3-hexyne, the carbene ring and the aromatic fragment of NHC show essentially the same small potential value.

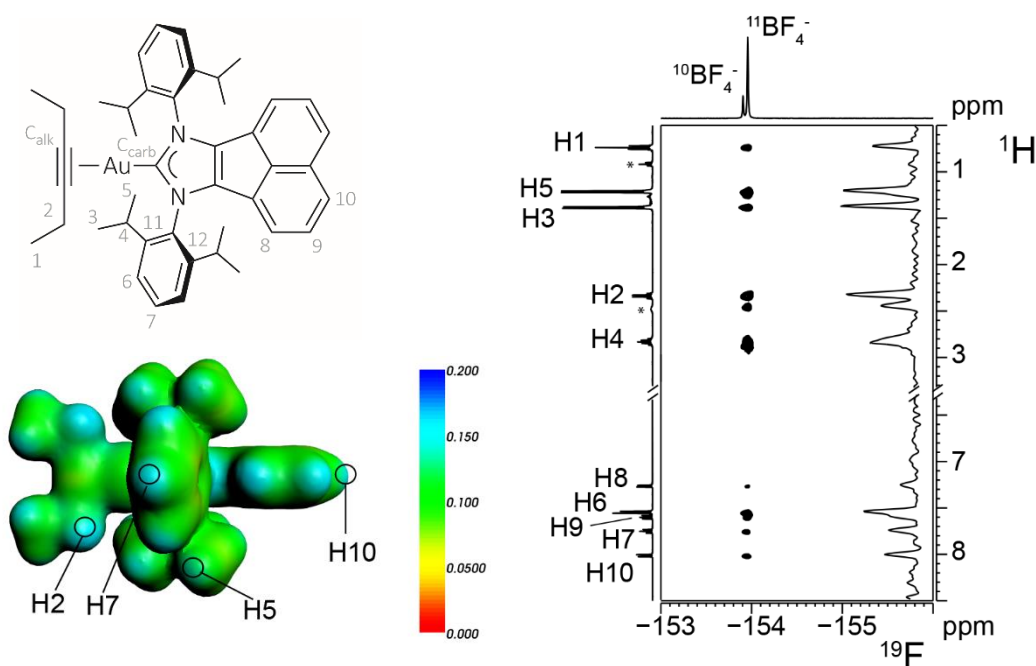
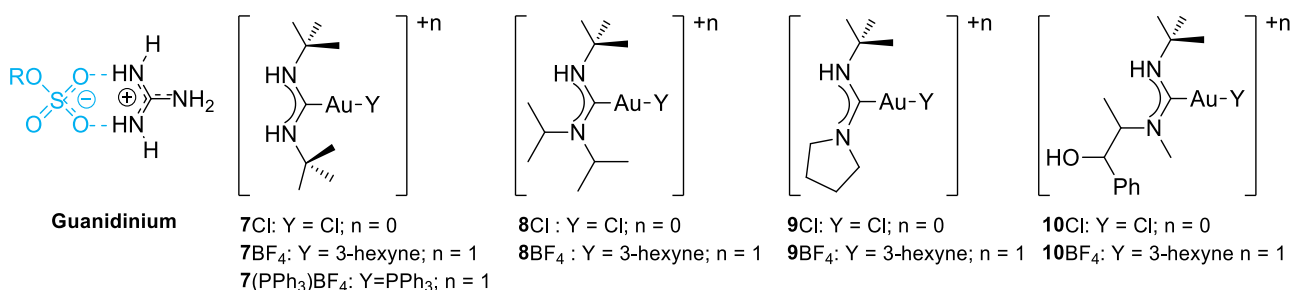


Figure 26. Left: Coulomb potential map (in a.u.) of 6^+ , mapped on an electronic isodensity surface ($0.007 \text{ e}/\text{\AA}^3$); right: ^{19}F , ^1H -HOESY NMR spectrum (376.65 MHz, 297 K, CD_2Cl_2) of complex 6BF_4 . *denotes the resonances of free 3-hexyne.

The NOE results on the saturated NHC show that the removal of the unsaturation is not enough to markedly influence the ion pair structure and the anion still prefers to stay on the carbene-side. On the other hand, the extended aromaticity of an acenaphtene-based NHC makes the ion pair structure aspecific, with only a small preference for the substrate side. These results underline that the structure in solution of $[(\text{NHC})\text{Au}(\text{S})]\text{BF}_4$ ion pairs cannot be easily tuned and meaningful modifications can be achieved only through large alterations of the NHC backbone. Gold complexes containing phosphorous-based ligands show a more marked ligand influence on the ion pair structure in solution^{70, 129}

2.2.2 Nitrogen acyclic carbenes

We just saw that the Ion Pair orientation was not drastically changing by removing the aromaticity on the NHC backbone and that using a BIAN functionalized ligand results in a nonspecific IP. Thereafter, with the deliberate purpose of influencing the ion pair structure of the complex, we chose another class of carbene ligands synthesizing four [(NAC)AuCl] (**7-10Cl**) precatalysts (also known as Acyclic Diamino Carbene, ACD)^{132,133} (Scheme 18), differing in the number and the position of the -OH and -NH moieties, and also in the steric hindrance around them. In particular, the structure of complex **7Cl** (Scheme 18) having a [NHR-(C=Au)-NHR]⁺ moiety recalls the urea and the guanidinium functional groups, two structures widely used for anion recognition.^{134,135} In complex **8Cl**, one nitrogen bears two *iso*-propyl groups, which create a steric hindrance around the -NH group, likely weakening the interaction with the anion. Complex **9Cl** is similar to **8Cl**, but the steric hindrance around -NH is reduced. Finally, complex **10Cl** bears an additional -OH moiety, another suitable anchoring point for the anion introducing a competition between the amine and the alcoholic groups (Scheme 18). The neutral compounds **7-10Cl** were synthesized using procedures similar to those reported in the literature^{133f} (see Experimental Part for details). **7-10BF₄** complexes were generated in a NMR tube after the addition of AgBF₄ to a solution of neutral precursors **7-10Cl** in the presence of 3-hexyne (solvent = CD₂Cl₂). All attempts to isolate complexes **7-10BF₄** failed and led to the formation of metallic gold. In the case of **3BF₄**, also the *in situ* characterization failed, due to the rapid decomposition of the complex to metallic gold, even at low temperature.



Scheme 18. Structure of guanidinium, **7-10Cl**, **7-10BF₄** and **7(PPh₃)BF₄** complexes.

All the proton and carbon resonances belonging to the different fragments were assigned through ¹H, ¹³C, ¹H-COSY, ¹H-NOESY, ¹H,¹³C-HMQC NMR, and ¹H,¹³C-HMBC NMR spectroscopies (see Experimental Part).

A marked difference in the presence of different rotamers of the carbene moiety in **7Cl** and **7BF₄** can be evidenced. In **7Cl**, as reported by Hashmi et al. for similar complexes, two different rotamers exist in solution (approximately 1:1 ratio), one of which is relative to the complex with the two *tert*-butyl groups pointing toward gold (*syn-syn*), and the other one with one *tert*-butyl group in *anti* position to the gold (*syn-anti*).^{133f} In the former, the two sides of the carbene are magnetically equivalent and the two *tert*-

butyl groups give only one NMR signal, whereas in the latter there is no symmetry and the two *tert*-butyl moieties give two different signals.

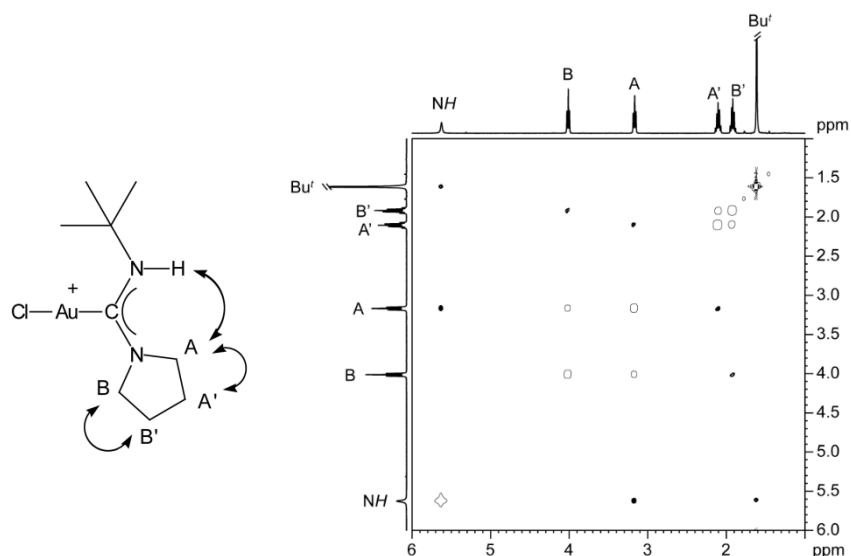


Figure 27. ^1H -NOESY NMR spectrum of complex **9Cl** (400.13 MHz, CDCl_3 , $T = 298\text{ K}$).

On the contrary, for **7BF₄** only the *syn-syn* rotamer existing, as proved by the presence of only one signal for the *tert*-butyl groups. In the case of **9Cl**, a 180° rotation around the C-N(pyrrolidine) bond does not originate any rotamer because the pyrrolidine moiety is symmetrical. Nonetheless, such a rotation can be easily proved by ^1H EXSY (EXchange Spectroscopy) NMR, while ^1H NMR NOESY experiments on **9Cl** does not show any indication of the rotation around the C-N(H)(*t*Bu) bond at room temperature (Figure 27). The singlet relative to the *tert*-butyl group has a NOE contact only with the NH. The absence of NOE with protons A, A', B and B' demonstrates that the NH(*t*Bu) group does not rotate around the N-C bond. The broad signal due to NH interacts only with protons A, thus confirming the structure depicted in the left side of Figure 27.

It is interesting to note that the ^{19}F NMR chemical shift of BF_4^- strongly depends on the cation, being -149.7, -153.3 and -152.2 ppm for **7BF₄**, **8BF₄** and **10BF₄**, respectively. For comparison, the NMR resonances of the anion in $[\text{LAu}(\eta^2\text{-3-hexyne})]\text{BF}_4$ complexes, falls between -154 and -155 ppm (L = phosphine or NHC,^{69b,70} see Experimental Part). The relative anion/cation orientation in solution of **7BF₄**, **8BF₄** and **10BF₄** complexes has been investigated by ^{19}F , ^1H -HOESY NMR spectroscopy (Figure 28) in CD_2Cl_2 at room temperature. NMR spectrum of **7BF₄** exhibits a very strong contact between the fluorine nuclei of the BF_4^- and the protons directly bound to the nitrogen atoms (H4), a medium contact with the protons of the *tert*-butyl groups (H3), and very weak, almost undetectable, contacts with the 3-hexyne (H1 and H2) (Figure 28a). A quantitative analysis of interionic NOE intensities was carried out taking into account that the volumes of the crosspeaks are proportional to $(n_{\text{H}} * n_{\text{F}})/(n_{\text{H}} + n_{\text{F}})$, where n_{H} and n_{F} are the number of

magnetically equivalent H and F nuclei, respectively.¹³¹ The results are reported in Table 5. The H4/F contacts results to be 10 and 30 times more intense than H3/F and H2/F, respectively.

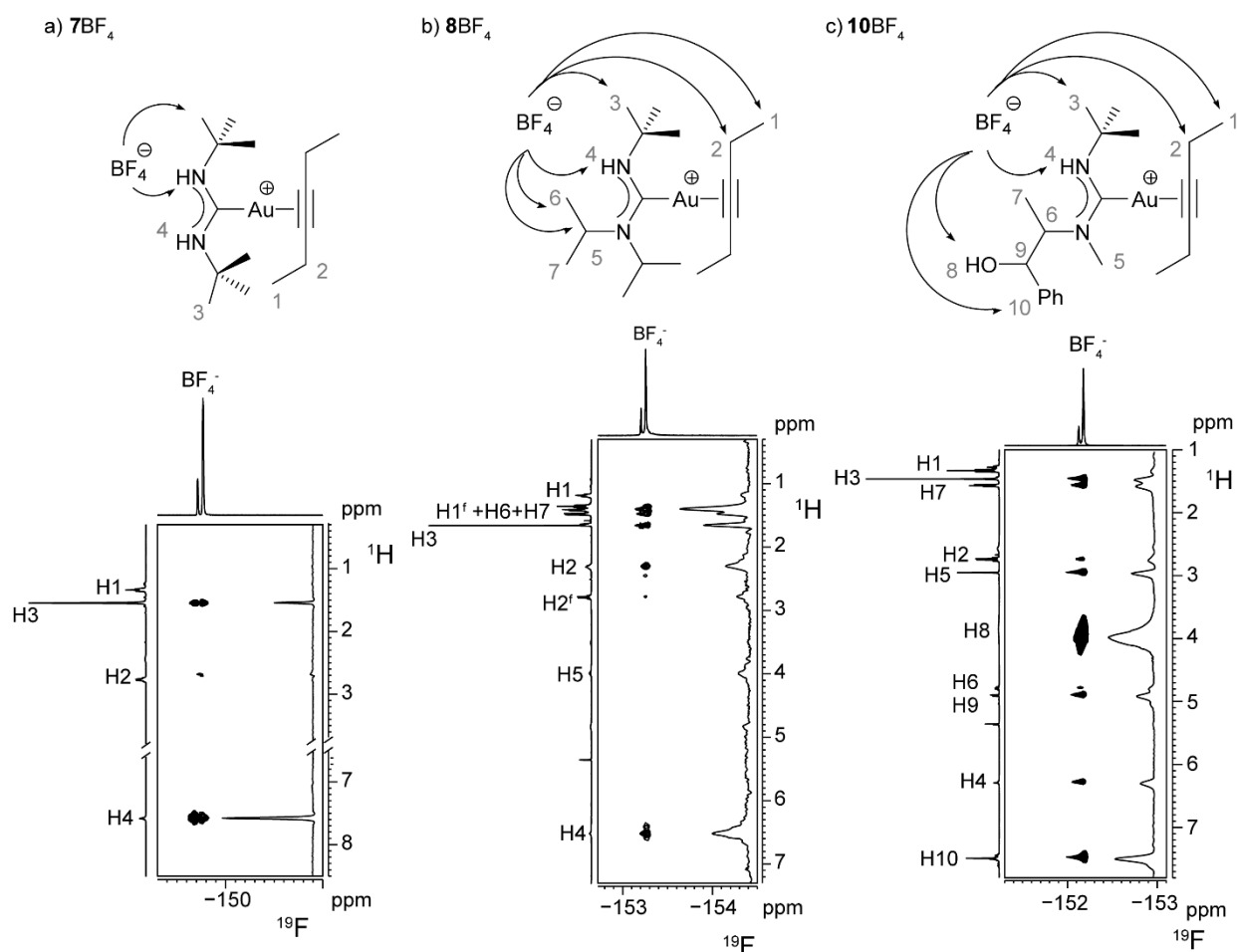


Figure 28. ^{19}F , ^1H -HOESY NMR spectrum (376.65 MHz, 298 K, CD_2Cl_2) of complexes 7BF_4 (a), 8BF_4 (b) and 10BF_4 (c). H1^f and H2^f are relative to the free 3-hexyne, in dynamic equilibrium with the coordinated one.

^{19}F , ^1H -HOESY NMR spectrum of 8BF_4 show strong contacts between F atoms of the BF_4^- and the proton directly bound to the nitrogen atoms (H4), a medium contact with other protons of NAC ligand (H3, H6 and H7). In this case, also medium contacts with the 3-hexyne (H1 and H2) are observed (Figure 28b), making the NOE pattern much less selective than in the case of 7BF_4 . From the quantitative point of view, the H2/F contact is 8-fold less intense than the H4/F one (Table 5). 10BF_4 has an hydroxyl group (H8) on one “side arm” of the carbene and an amine proton (H4), both of which are able to establish a hydrogen bond with the anion. The ^{19}F , ^1H -HOESY NMR spectrum clearly shows that H8/F is the most intense contact (Figure 28c), almost 8-fold more intense than H4/F. As in the case of 7BF_4 , the contact between the hexyne and the anion is very low, with a relative intensity of 0.03. For comparison, it can be useful to remember

that in the case of **1**BF₄ the most intense NOE contact is between the anion and the CH₂ on the backbone of the carbene, while the relative intensity of the NOE with the 3-hexyne is 0.4 (Table 4).

Table 5. Relative NOE intensities determined by arbitrarily fixing the largest NOE contact to 1.				
Signal	Relative intensity			
	7BF₄	8BF₄	9BF₄	10BF₄
H1	0.01	0.12	-	0.02
H2	0.03	0.27	-	0.03
H3	0.11	0.25	-	0.06
H5	-	0.30	-	0.11
H4	1.00	1.00	-	0.13
H6	-	0.18 ^a	-	0.08
H7	-		-	0.11
H8	-	0.09	-	1.00
H9	-	-	-	0.11
H10	-	-	-	0.16
A:B:C	97:3	79:21	85:15 ^b	11:3:86 ^c
[a] H6/F and H7/F contacts partially overlap; [b] estimated; [c] in this case the conformations A and B are not enough to fully describe the ion pair structure, see text.				

In order to study the interaction between the anion and the carbene with two -NH moieties in methanol, the ion pair structure of **7**(PPh₃)BF₄ has been studied in deuterated methanol by ¹⁹F, ¹H- HOESY NMR (see Experimental Part). The spectrum of **7**(PPh₃)BF₄ in methanol-d₄ demonstrates that the anion-cation interaction is so strong to exist also in a polar solvent such as methanol. The -NH moiety is not visible in the spectrum, probably because a H/D exchange with the solvent occurs. Remarkably, the *syn-anti* rotamer is not present even in this case and NOE contact between BF₄⁻ and the two equivalent *tert*-butyl groups are consistent with the ion pair structure of **7**BF₄ in CD₂Cl₂. A weak NOE contact is visible between BF₄⁻ and the two *tert*-butyl groups of the carbene (Figure 29). A very small contact is visible at 4.70 ppm, but it does not correspond with any signal; this contact could be due to the -NH moiety, which is almost completely deuterated by H/D exchange with the solvent, but the remaining traces of -NH are expected to give an intense NOE contact (Figure 29). Consistently, it is known that in the case of the cationic guanidinium-like structures (HN-CR-NH)⁺, as the one present in **7**BF₄ and **7**(PPh₃)BF₄, the two cooperative hydrogen bonds with an anion are so strong that the methanol is generally not enough to break the ion pair.^{135, 136}

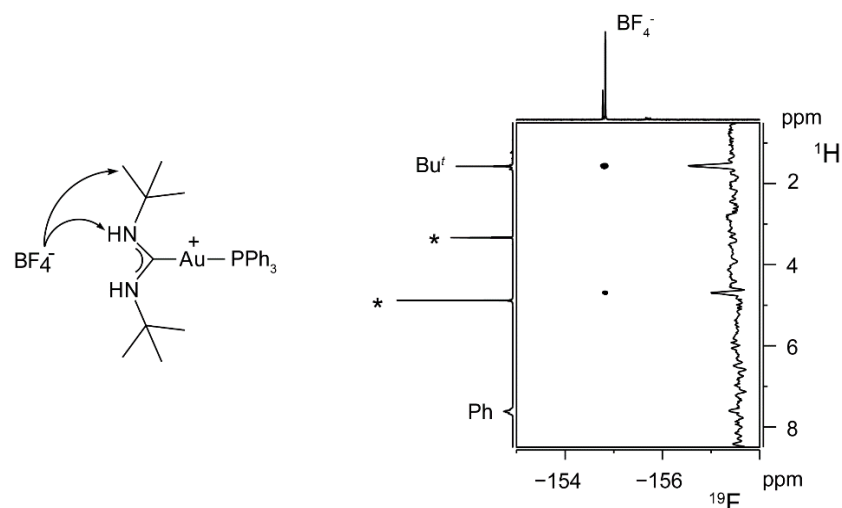


Figure 29. ^{19}F , ^1H -HOESY NMR spectrum (376.65 MHz, 298 K, CD_3OD) of complexes **7**(PPh_3) BF_4 .

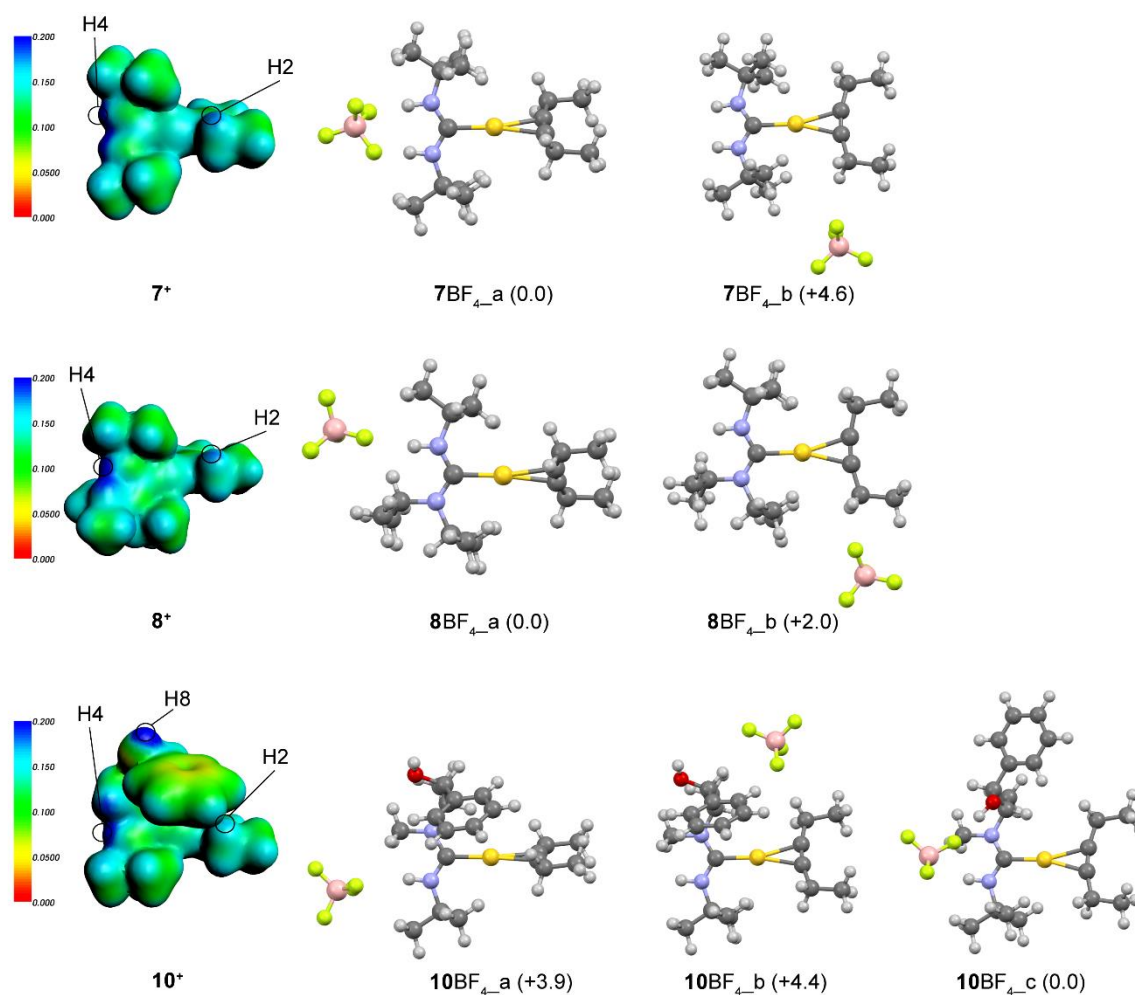


Figure 30. Left side: Color-coded representation of the Coulomb potential on an electronic isodensity surface ($\rho = 0.007 \text{ e}/\text{\AA}^3$) of the cationic complexes **7** $^+$, **8** $^+$ and **10** $^+$. The regions corresponding to relevant part of the molecules are evidenced. Right side: DFT-optimized ion pair structures for the systems **7** BF_4 , **8** BF_4 and **10** BF_4 . The relative energies of the conformations are in parentheses and are expressed in kcal/mol.

The easiest way to rationalize the anion/cation relative orientation by DFT calculations is mapping the Coulomb potential of the sole cation,¹²⁹ as explained in chapter 1.2.3. Calculations were performed including explicitly the conductor like screening model (COSMO, $\epsilon = 8.93$) to include the solvent effect. Such maps for **7**⁺-**10**⁺ cations (left side Figure 30) show clearly that H4 (the hydrogen bound to the nitrogen atom) is always one of the most attractive regions (blue colored) of the cation. In **8**⁺, H4 is buried in the steric hindrance of the iso-propyl group. In **10**⁺, also H8 (the hydrogen bound to the oxygen) has a comparable Coulomb potential. On the other side, for all the complexes the protons of the hexyne (H2) are poorly attractive for the anion (Figure 30). In order to quantify the energy difference between different ion pairs structures, the ion pairs **7BF₄**, **8BF₄** and **10BF₄**, have been fully optimized starting from several different geometrical configurations that only differ for the BF₄⁻ position (right part Figure 30). In the case of **7BF₄**, the anion is strongly bound to the NAC due to the presence of two H-bonds (**7BF₄_a**). The other accessible structure, that is the one with the anion in the alkyne position (**7BF₄_b**), is +4.6 kcal higher in energy. In the case of **8BF₄**, in which the NAC has only one hydrogen capable of giving hydrogen bond, the difference in energy between the structures with anion in the NAC and in the alkyne position is roughly halved, with the first that is however still the most stable configuration. Finally, in the case of **10BF₄**, we have found three possible optimized configurations, and in the most stable one the anion is close to the -OH moiety (**10BF₄_c**). The latter is 3.9 kcal/mol more stable than the configuration having the anion interacting with the -NH group (**10BF₄_a**) and 4.4 kcal/mol with respect to the configuration having the anion close to the alkyne (**10BF₄_b**) (Figure 30).

Coulomb potential maps and ion pair optimizations together with the different degree of selectivity in the HOESY spectra of **7BF₄**, **8BF₄** and **10BF₄** makes clear that the ion pair structures of the three compounds are markedly different. A convenient way to describe such structures for linear gold(I) salts is to quantify the two main structures, with the anion close to the ancillary ligand (structure **A**) or to 3-hexyne (structure **B**), as already reported for similar complexes.⁷⁰ Specifically, **7BF₄** shows an exceptional ion pair selectivity, with the anion interacting almost exclusively with the two -NH¹³⁷ of the NAC (Figure 28a and Figure 30), and an **A:B** ratio of 97:3 can be calculated.^{viii} The high stability of this ion pair structure can be easily explained by the presence of two cooperating hydrogen bonds, forming a cyclic structure similar to that formed by guanidinium-based anion receptors,^{134, 135} in which two fluorine atoms of the anion interact with the two coplanar -NH moieties. The presence of such a strong interaction is evidenced also by the NMR shift of the fluorine nuclei (-149.7 ppm) which is considerably lower than that with other ligands. Moreover, the supramolecular cycle given by the two hydrogen bonds stabilizes the *syn-syn* structure so much to make the C-N rotational barrier insurmountable at room temperature and inhibiting the

^{viii} Assuming that the minimum distance between the anion and the cation is the same in both the orientations, the abundances have been estimated by the normalized NAC/anion and alkyne/anion NOE intensities. For the NAC-side orientation the protons showing the largest NOEs have been selected as the probes instead of the sum of the intensities in the assumption that a single anion orientation is present on the side of the ligand, while H2 have been chosen as the probes of the alkyne side orientation.

formation of the *syn-anti* rotamer, as experimentally evidenced. DFT studies fully confirm this structure, evidencing a very attractive potential on the -NH region (Figure 28) and a large energy difference between the DFT-optimized **7BF₄_a** and **7BF₄_b** (4.6 kcal/mol, Figure 30).

In the case of **8BF₄**, which has only one -NH moiety, the ¹⁹F, ¹H-HOESY NMR is much less selective (Figure 28), and the H2/F contact is clearly visible and measurable. In this case, the A:B ratio can be estimated as 79:21. The latter is very similar to those previously obtained for complexes bearing the NHC ligand. Looking at the DFT-optimized structure of the cation, the -NH still presents a very attractive potential (Figure 30), but it is partially buried in the steric hindrance of the isopropyl group bound to the other nitrogen. This is reflected on a smaller difference of energy between the DFT-optimized structures **8BF₄_a** and **8BF₄_b** (2.0 kcal/mol, Figure 30).

For the last compound, **10BF₄**, having a hydroxyl group on one arm of the carbene, the most intense NOE contact is between the anion and the -OH (Figure 28). In this case the A:B ratio is not enough anymore to exhaustively describe the ion pair structure in solution, but adding the configuration with the anion close to the hydroxyl group (C), and using H8/F, H4/F and H2/F as probes for the ratio of the configurations, the A:B:C ratio is 11:3:86. This is in good agreement with DFT studies, according to which the -NH and -OH regions have similar attractive potentials, but the -OH is less sterically hindered than the -NH. Consequently, DFT-optimized conformation **10BF₄_c** is the most stable one, by 3.9 and 4.4 kcal/mol with respect to **10BF₄_a** and **10BF₄_b**, respectively. Interestingly, the ¹⁹F NMR shift nicely correlates with the anion/cation specific interactions present in solution: indeed, it is -149.7 for **7BF₄** (two -NH...F-BF₃ interactions), -152.2 ppm for **10BF₄** (one strong -OH...F-BF₃ interaction), -153.3 ppm for **8BF₄** (one weak -NH...F-BF₃ interaction) and between -154 and -155 in absence of hydrogen bonding interactions.⁷⁰ Unfortunately, the low stability of **9BF₄** did not allow us to experimentally characterize its ion pair structure, but the corresponding Coulomb map (Figure 31) allows us to predict it: the -NH is again the most attractive region of the cation and a good -NH...F-BF₃ interaction can be expected. The pyrrolidine cycle on the other nitrogen creates some steric hindrance around the -NH, but less than the isopropyl group in **8BF₄**. For this reason, we expect an A:B ratio intermediate between those of **7BF₄** and **8BF₄**.

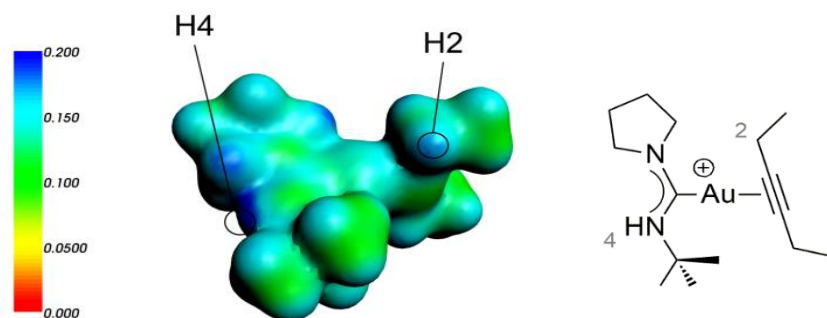
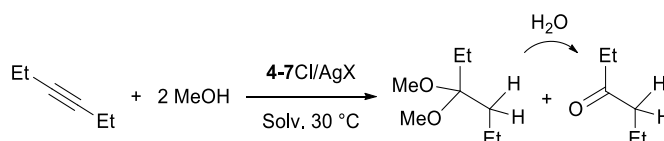


Figure 31. Color-coded representation of the Coulomb potential on an electronic isodensity surface ($\rho=0.007 \text{ e}/\text{Å}^3$) of the cationic complex **9⁺**. The regions corresponding to relevant part of the molecule are evidenced.

2.2.3 Importance of the anion position in catalysis.

In chapter 2.1 we proposed that, in the intermolecular methoxylation of alkynes (Scheme 19), the anion assists the nucleophilic attack of methanol (which is the rate determining step, RDS) through the formation of a hydrogen bond, and it is not only a *proton shuttle*, as proposed in previous works.^{115,138} Clearly, in order to exploit its role, the anion has to be located close to the unsaturated substrate. This prompted us to search a relationship between the anion/cation relative orientation and the catalytic activity of gold complexes. Complexes **7-10Cl** have been tested in such reaction, in the presence of different silver salts to generate the active catalyst *in situ*. For further details, see the Experimental part.



Scheme 19. Methoxylation of 3-hexyne promoted by **7Cl-10Cl**/silver salt.

Table 6. Gold(I) catalysed alkoxylation of 3-hexyne					
Entry	Cat.	AgX	Conv. (Yield) [%] ^[c]		TOF ₃₀ [min ⁻¹] ^[d]
			90 min	180 min	
1	7Cl	BF ₄ ⁻	24 (21)	43 (34)	0.30
2	8Cl	BF ₄ ⁻	59 (55)	91 (87)	0.83
3 ^[a]	8Cl	BF ₄ ⁻	33(26)	54(48)	0.35
4	9Cl	BF ₄ ⁻	28 (23)	44 (37)	0.43
5	10Cl	BF ₄ ⁻	30 (20)	52 (42)	0.36
6	7Cl	OTf ⁻	50 (47)	77 (73)	0.73
7	8Cl	OTf ⁻	83 (79)	99 (96)*	1.60
8	9Cl	OTf ⁻	58 (44)	84 (69)	0.88
9	10Cl	OTf ⁻	57 (54)	91 (88)	0.66
10 ^[b]	7Cl	BF ₄ ⁻	20 (11)	37 (24)	0.26
11 ^[b]	8Cl	BF ₄ ⁻	75 (68)	99 (94)*	1.06
12 ^[b]	9Cl	BF ₄ ⁻	39 (34)	62 (56)	0.43
13 ^[b]	10Cl	BF ₄ ⁻	77 (71)	97 (90)*	1.23

Catalysis conditions: 30 °C, 3-hexyne (100 μL), Cat/AgX (1 mol%), CH₃OH (143 μL), CDCl₃ (400 μL), [a] performed with 5 mol% of N,N'-Dicyclohexylurea as additive, [b] CD₃OD (543 μL). [c] Conversions and TOF₃₀ were determined by ¹H NMR spectroscopy, using TMS as internal standard, as average of three runs. [d] TOF₃₀= (n product /n catalyst)/(30 min). * the catalysis reached full conversion before 180 min.

A typical catalytic run was performed mixing 3-hexyne and methanol in the presence of the catalyst precursor (1 mol%) and a silver salt (1 mol%) at 30 °C in CDCl₃ or CD₃OD. **7Cl**/AgBF₄, **9Cl**/AgBF₄ and **10Cl**/AgBF₄ reaches similar conversions (24-30%) in 90 minutes (entry 1, 4 and 5, Table 6), whereas catalyst **8Cl**/AgBF₄ reaches 59% in the same reaction time (entry 2, Table 6) using CDCl₃ as solvent (Figure 32). It is interesting to note that the catalytic rate of **9Cl**/AgBF₄ decreases slowly after the first hour, when the conversion is just 20%. Comparing the value of the initial turnover frequency TOF₃₀ (calculated after 30 minutes), we can see that catalysts **7Cl**/AgBF₄, **9Cl**/AgBF₄ and **10Cl**/AgBF₄ are almost similar while catalyst **8Cl**/AgBF₄ is two time faster (entries 1, 4, 5 and 2 respectively, Table 6).

When the catalysis is carried out using **8Cl**/AgBF₄ as catalyst and N,N'-Dicyclohexylurea (DCU) as additive, the reaction rate decreases reaching a value similar to that shows using catalysts **7Cl**/AgBF₄, **9Cl**/AgBF₄ and **10Cl**/AgBF₄ (compare entry 3 with entries 1, 4 and 5, Table 6).

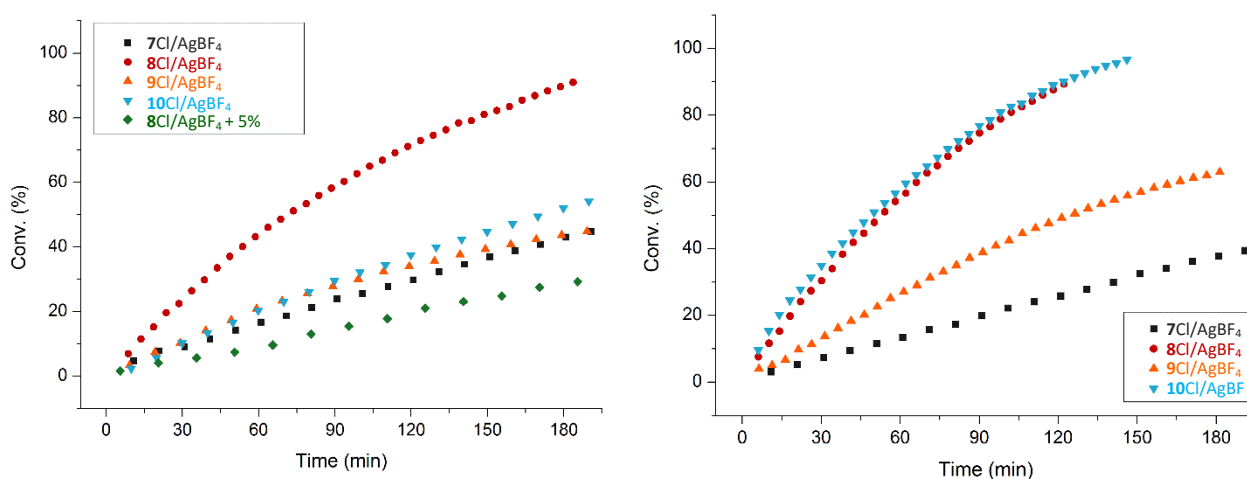


Figure 32. Alkoxylation of 3-hexyne with methanol catalyzed by 7Cl-10Cl complexes activated with AgBF₄ in CDCl₃ (left) and CD₃OD (right).

As we previously saw in chapter 2.2.2, the ion pair structure and the alkyne-gold bond in **7Cl-10Cl**/AgX catalysts are expected to be of key importance in the RDS of the alkoxylation, namely the nucleophilic attack of the first molecule of methanol on the triple bond. It has been already reported on the role of the anion during such step,¹³⁷ demonstrating that it establishes a hydrogen bond with the alcoholic proton of the methanol, which results activated, as we have seen in chapter 2.1. Obviously, in order to do that, the anion must be located close to the 3-hexyne. On the other hand, the acidity of the [LAu]⁺ fragment is important to activate the triple bond: the more acidic the metal fragment is, the more electronic density is transferred from the alkyne to the gold, likely with a proportional C≡C activation (chapter 1.2.1).⁵² Our detailed DFT studies (chapter 2.2.2) demonstrate that all the considered cations behave similarly in the interaction with 3-hexyne. In particular they present the same electron withdrawing ability towards

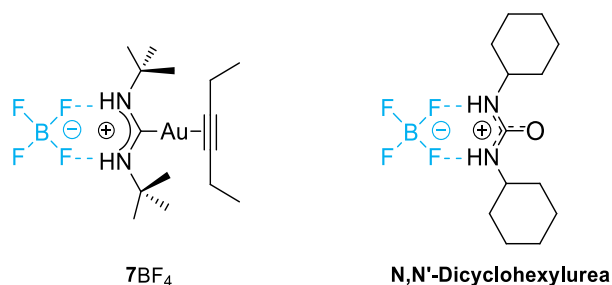
3-hexyne with an almost identical alkyne \rightarrow gold net donation. Remarkably, also the amount of gold \rightarrow alkyne π back-donation, which can be qualitatively estimated by the alkyne bending,¹³⁹ seems to be the same for all the systems (Table 7).

Table 7. Interaction energies and important geometrical parameters				
Complex	E_{int} (kcal/mol)	C-N (Å)	N-C-N (°)	C-C\equivC (°)
7⁺	-43.6	1.341	115.9	13.1
8⁺	-40.8	1.349	118.9	13.0
9⁺	-41.0	1.347	117.6	13.0
10⁺	-42.1	1.341	117.6	13.0

In the case when the system shows slight asymmetries, we reported the average of the values.

If we also consider that the geometry of the attack is *anti*-periplanar and, consequently, there is no direct interaction between the methanol and the steric hindrance of the ligand, this electronic similarity of **7⁺**-**10⁺** cations suggests that they would activate the 3-hexyne with the same efficiency and should catalyse the alkoxylation of hexyne with the same performances. Assuming this hypothesis, we can ascribe any difference in the catalytic performances to the anion.

Comparing catalytic and HOESY results, a trend appears evident: the complexes for which a strong anion-ligand hydrogen bond is possible (i.e. **7BF₄**, **9BF₄** and **10BF₄**) have similar and low catalytic rates. On the contrary, the complex in which the hydrogen bond donor is sterically hindered and shows the lowest A:B ratio (**8BF₄**) exhibits the highest catalytic performances. This is consistent with the *scenario* previously depicted, according to which the anion has a beneficial role in activating the methanol lowering the activation barrier of the attack: if a specific interaction, stronger than the anion/methanol one, keeps the anion far from the catalytic center, it cannot play its role of activator and the reaction slows down.



Scheme 20. Representation of the anion interactions with **7BF₄** and DCU.

Using N,N'-Dicyclohexylurea (DCU), which possesses a functional group able to interact with the counterion such as **7BF₄** (Scheme 20), as additive with the catalyst **8Cl/AgBF₄**, it likely keeps the anion far

from the catalytic center, slowing down the catalysis and giving performances similar to those of **7Cl/AgBF₄** and **10Cl/AgBF₄**.

An additional proof of the anion role comes from the presence of OTf⁻ instead of BF₄⁻ when the pre-catalysts is activated with AgOTf there is a systematic increase of the performances of two/three times (compare entries 1, 2, 4 and 5 with 6, 7, 8 and 9 in Table 6) in chloroform. The increase of the TOF₃₀ values are due to the fact that more basic anions can activate the methanol to a higher degree (as we have seen in the chapter 2.1 for NHC ligand) but the trend among the considered catalysts is the same.

Using methanol as the solvent instead of chloroform usually produces the separation of organometallic ion pairs in free ions.¹⁴⁰ Analysing the catalytic results in methanol, it is evident that **8Cl/AgBF₄** and **10Cl/AgBF₄**, whose TOF₃₀ values were very different in CDCl₃, have now the same activity. Since the corresponding active species, **8BF₄** and **10BF₄**, are likely present in methanol as free ions,^{ix} and since DFT studies revealed that **8⁺** and **10⁺** have the same acidity (Figure 60 left), their similarity in catalysing the reaction is reasonable and confirms that the differences in CDCl₃ are due to the nature of the anion.

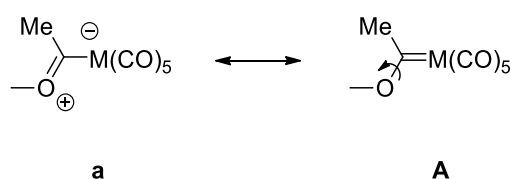
On the other hand, **7Cl/AgBF₄**, bearing a guanidinium-like moiety, shows lower TOF₃₀ values in CD₃OD with respect to those of **8Cl/AgBF₄** and **10Cl/AgBF₄**. NMR studies confirm that, differently from **8BF₄** and **10BF₄**, **7BF₄** is likely present as an ion pair having the anion close to the -NH moieties. The acidity of gold in the ion pair is smaller than in the cation (Figure 60 right) due to the *neutral* character of the complex, therefore the alkyne will be less activated and less prone to the nucleophilic attack of the methanol. **9Cl/AgBF₄** shows a catalytic activity that is intermediate between those of **7Cl/AgBF₄** and **8Cl/AgBF₄**. Since the corresponding Coulomb potential map of **9BF₄** (Figure 31) indicates that the -NH moiety is more exposed and more prone to the interaction with the anion than in the case of **8BF₄** and **10BF₄**, we can expect that **9BF₄** is present in solution as a mixture of free ions and ion pairs, giving an intermediate activity.

^{ix} This assumption cannot be verified because the [LAu(3-hexyne)]⁺ cannot be studied in methanol since it undergoes nucleophilic attack from the solvent.

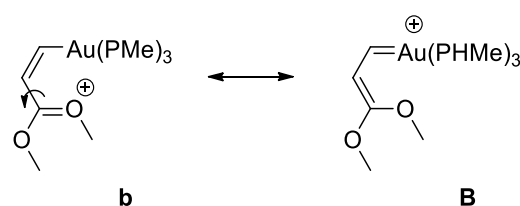
2.3 Bonding characterization: Theory and Experimental Studies

In chapter 1.2.2 we introduced how the ligands can influence the catalyst reactivity depending on their donation and back-donation properties. Concerning gold(I) catalysis (Scheme 5) is generally accepted that electron poor ligands work better when the RDS is the attack and that electron rich ones work better when the RDS is the protodeauration.^{52,105a} It is logical that a fully comprehension and characterization of the bond nature is nowadays becoming essential for organometallic chemists, and as a matter of fact, the Dewar-Chatt-Duncanson (DCD)^{141,142} model has been high in chemists' favour.¹⁴³ As we described in chapter 1.1.2, it gives a simple picture of the bond between an unsaturated substrate and a transition metal in terms of σ donation and π back-donation. Despite its popularity, the evaluation of the relative contribution of its two components still remains a challenge. Indeed, available experimental techniques, including the popular Tolman¹⁴⁴ and Lever^{145,146} Electronic Parameters, do provide an estimate of the net donor power of a ligand, but cannot disentangle the DCD components. More recent efforts aimed at extracting the electronic properties of N-heterocyclic carbene (NHC) ligands from experimental observables^{147,148,149,150} are very relevant here, but if and how an experimental observable depends on the DCD bonding components remains very difficult to ascertain.^{150,151} Tarantelli and Belpassi, building upon an unambiguous definition of the donation and back-donation charges based on the Charge Displacement Function (CDF),¹⁵² have recently demonstrated that the DCD components can be disentangled and effectively extracted by looking at simple experimental observables.^{139,153} It was then argued that the approach can in principle be used to identify experimental observables that selectively depend on a specific DCD component and we build here on that principle.

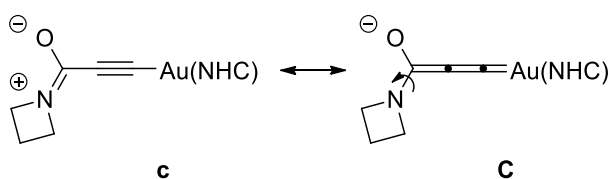
a) Fischer, 1967



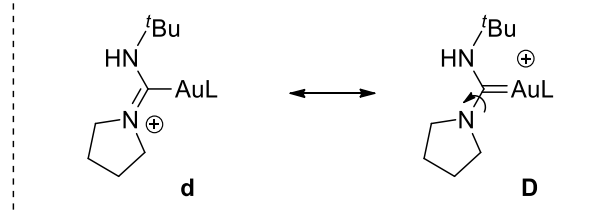
b) Furstner, 2009, $\Delta G_r^\ddagger = 11$ kcal/mol



c) Hashmi, 2013, $\Delta G_r^\ddagger = 16.6$ kcal/mol



d) this thesis, $\Delta G_r^\ddagger = 17.2-18.8$ kcal/mol, 10 examples



Scheme 21. Comparison between previous experimental works (panels a-c) and this thesis (panel d).

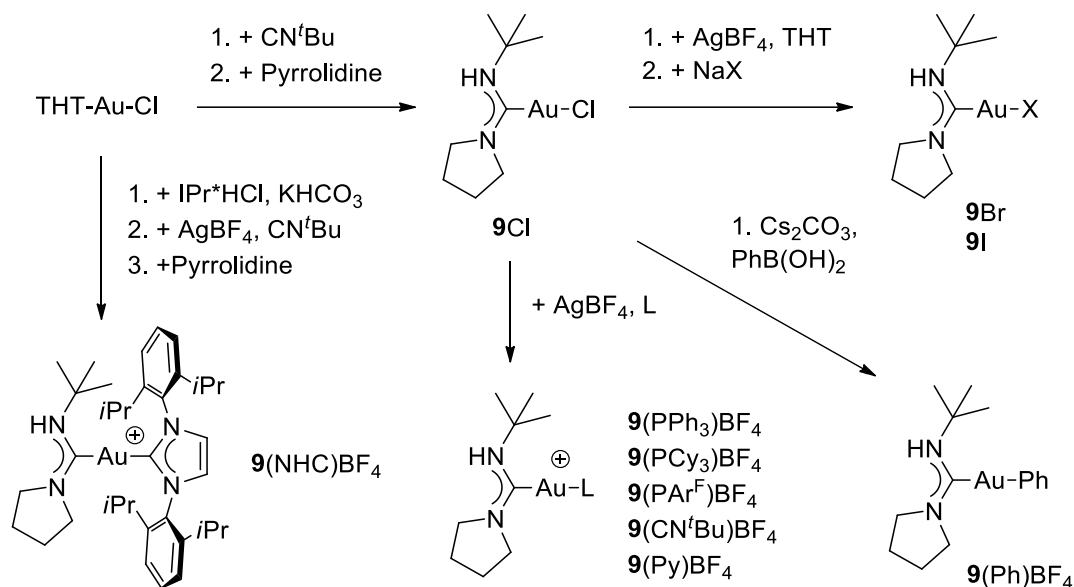
A seminal work, more than 50 years ago,^{154,155} by Fischer and Maasböl related qualitatively the rotation of the heteroatom-carbenic carbon bond to the extent of back-donation in Fischer's carbenes (Scheme 21a). On similar grounds, the groups of Fürstner¹⁵⁶ and Hashmi¹⁵⁷ have recently synthesized and characterized catalytic intermediates of Au(I) bearing σ -bonded organic substrates (Scheme 21b,c), with the aim of analyzing the nature of the Au(I)-C bond. These gold-carbenoids intermediates are receiving increasing attention^{63b,158,159,160,161,162,163} because the gold-carbene vs gold-stabilized carbocation character may be selectively tuned by the proper choice of the ancillary ligand (L)^{164,165,166,167} opening the way to a new rational ligand-controlled gold catalysis. The Au-C bonds in Scheme 21b,c can be described with two limit resonance structures: one implying a pure C \rightarrow Au σ donation with the formal positive charge located on the heteroatom of the substrate^x (cationic structure), the other implying also a complete Au \rightarrow C π back-donation and having the formal positive charge on the metal (carbenic structure). One may expect that the relative importance of these two limit structures is related to the proper rotational barrier of a C-C bond for **b/B** or C-N bond for **c/C** Scheme 21b,c). A systematic analysis based on this approach appears very promising to reveal the metal-carbon bond order but, to the best of our knowledge, it was applied only to the two systems of Scheme 21b,c. This prompted us to look for a class of Au-carbene compounds suitable to be investigated and our choice fell on [LAu(NAC)]⁺⁰ (NAC = Nitrogen Acyclic Carbene)^{133f, 168} since: i) such complexes are stable; ii) being acyclic, they undergo rotation of the C-N bond; iii) they can be easily synthesized; finally, iv) the complexes present two limit structures, with the double bond localized between the gold and the NAC (**D**, Scheme 21d) or between the carbon and the nitrogen bearing the pyrrolidine (**d**, Scheme 21d).^{xi}

We synthesized ten [(NAC)Au-L]⁺⁰ complexes (Scheme 22 and Experimental Part for further details), with L varying among different classes of ligands, to study and evaluate the rotational barrier of the C-N(pyrrolidine) (Scheme 21d) bond through a Variable Temperature EXchange Spectroscopy (VT-EXSY) NMR¹⁶⁹ and a detailed theoretical analysis of the CDF and its DCD components. Our selection of the ancillary ligands covers many classes of ligands commonly used in coordination and organometallic chemistry. Some of these ligands give rise to effective catalysts and find a wide range of applications in gold(I) catalysis. All complexes have been fully characterized by NMR (Experimental Part) and are

^x The X-ray crystal structure of the related complex [(Ph)(NMe₂)C]AuCl shows that the C-N distance is 1.262 Å, which is particularly short and essentially double. This is an indication that in such case the resonance structure with the formal charge on the nitrogen is particularly stable. Please, see Schubert, U., Ackermann, K. & Aumann, R. Chloro-[dimethylamino (phenyl) carbene] gold(I), ClAuC(C₆H₅)N(CH₃)₂. *Cryst. Struct. Comm.* **1982**, *11*, 591 – 594.

^{xi} A third resonance structure exists, which is similar to **d** but the double bond is localized between the carbon and the nitrogen atom bearing the *tert*-butyl group. Likely, the ligand effect will be the same, or proportional, for the two different C-N bonds.

present in solution as a single isomer, since rotation of the $-\text{NH}(t\text{Bu})$ moiety is prevented by the severe steric hindrance between the pyrrolidine and its *tert*-butyl group.



Scheme 22. Synthetic routes for the complexes 9L. PAr^{F} indicates *tris*[(3,5-(trifluoromethyl)phenyl)phosphine], NHC indicates 1,3-Bis(2,6-diisopropylphenyl)imidazol-2-yliden).

Moreover, the 180° rotation of the pyrrolidine moiety around the C-N bond, accessible at room temperature, does not alter the molecule at all. The rotation rate constant (k_r) of the pyrrolidine, which is related to the C-N bond order,¹⁷⁰ has been obtained using the VT-1H-EXSY NMR technique, which already proved to be effective in the measurement of activation parameters.^{66e,171, 172} The measurement of k_r is based on the exchange of the non-equivalent protons A and B of the pyrrolidine ring, due to the rotation around the C-N bond. This gives two off-diagonal peaks in the 2D spectra (Figure 33), whose volume is related to the rotation rate (Experimental Part). Measuring k_r at different temperatures, $\Delta H^{\ddagger r}$ can be evaluated through a simple Eyring plot (Experimental Part).

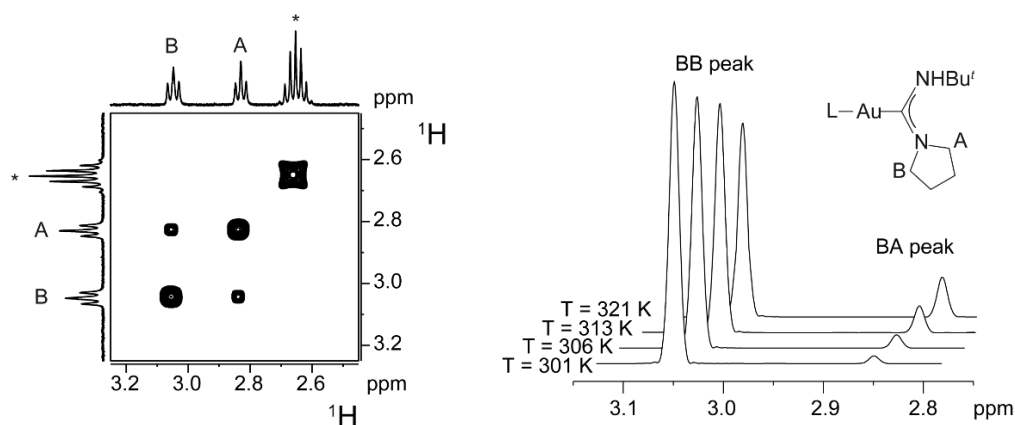


Figure 33. VT-1H-EXSY NMR spectrum of $9(\text{NHC})\text{BF}_4$ (left) and stacked traces extracted at $\delta\text{H} = 3.05$ ppm from EXSY NMR spectra recorded at different temperature (right), for further info see Experimental Part.

The activation enthalpy (ΔH_r^\ddagger) presents a significant ligand effect, going from 17.6 (for **9Cl**) to 20.0 (for **9(PAr^F)BF₄**) kcal/mol (Table 8), while the entropic contribution is small with all the ligands (below 4 cal/Kmol, Table 1), consistently with an intramolecular process. Experimental results show an evident differentiation between anionic L ($\Delta H_r^\ddagger < 18.5$ kcal/mol) and neutral ones ($\Delta H_r^\ddagger > 19.5$ kcal/mol). Such a difference can be explained considering that anionic ligands make the metal more electron-rich, favoring structure **D**. Notably, the trend among anionic ligands well correlates with the kinetic *trans* effect ($\text{Cl}^- < \text{Br}^- < \text{I}^- < \text{Ph}^-$).¹⁵⁴

On the contrary, ΔH_r^\ddagger does not correlate (correlation coefficient of linear regression, R^2 , is of 0.753, Figure 34) with the Tolman Electronic Parameter, TEP,¹⁴⁴ that measure the electron donor ability of the ligands.^{xii,173} For example, the experimental results reveal that complexes **9(PPh₃)BF₄** and **9(PCy₃)BF₄** have very similar values of ΔH_r^\ddagger but the difference in the TEP values is significant (2068 cm^{-1} and 2056.4 cm^{-1} , respectively). Similarly, the compound with pyridine, **9(Py)BF₄**, presents a ΔH_r^\ddagger close to that bearing the NHC, **9(NHC)BF₄**, but a TEP value considerably higher (by about 21.5 cm^{-1}).¹⁷⁴ A detailed theoretical analysis of these contrasting considerations appears highly desirable.

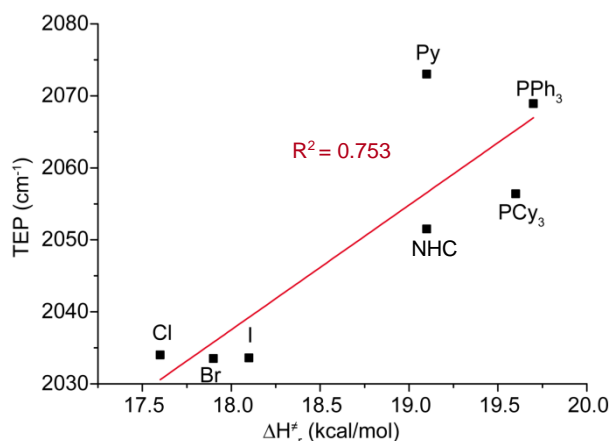


Figure 34. Correlation between C-N rotational barrier (ΔH_r^\ddagger) and Tolman Electronic Parameter (TEP).

Our aim here is to provide a quantitative picture of the relation between the nature of the Au-C bond, its bond order and the barrier to rotation, ΔH_r^\ddagger . It is well known that the analysis of simple structural data, such as the Au-C distance, is of little help^{152,165,175} and a more stringent analysis is thus required. We base this on the well-established definition of the donation and back-donation charges provided by the analysis of the symmetry components of the CDF^{153a,36,129} (see Experimental Part).

In order to apply this approach, we need to refer to more symmetric model systems $[\text{LAu}(\text{NAC}^{\text{sym}})]^{+0}$ (**9'L**) in which we substitute the NAC moiety with a simplified symmetric version $(\text{NHMe})_2\text{C}$, having two -NHMe moieties bound to the carbenic carbon atom (indicated hereafter as **NAC^{sym}**, Figure 35).

^{xii} The TEP is 2034.0 for Cl⁻, 2033.5 for Br⁻, 2033.6 for I⁻, 2051.5 for IPr, 2056.4 for PCy₃, 2068.9 for PPh₃, 2073 for Py, and 2071 cm^{-1} for $(\text{C}_6\text{H}_4\text{F})_3\text{P}$. Please, see Ref. 144 and Ref.174.

Table 8. Experimental activation parameters (ΔH_r^\ddagger and ΔS_r^\ddagger) of the rotation around the C-N bond for [LAu(NAC)] ⁺⁰ complexes 9X . CT_{tot} , CT_{don} and CT_{back} values (in electrons) for model complexes 9X' , [LAu(NAC ^{sym})] ⁺⁰ .					
L	Complex 9Y		Complex 9'Y		
	ΔH_r^\ddagger (kcal/mol)	ΔS_r^\ddagger (cal/K×mol)	CT_{tot}	CT_{don}	CT_{back}
Cl	17.6	1.2	0.102	0.210	-0.108
Br	17.9	2.3	0.114	0.219	-0.105
I	18.1	2.2	0.132	0.230	-0.098
PPh ₃	19.7	3.6	0.247	-	-
PCy ₃	19.6	3.3	0.220	-	-
PAr ^F	20.0	3.9	0.269	-	-
CNBU ^t	19.6	3.1	0.202	0.247	-0.045
Py	19.1	3.8	0.229	0.286	-0.057
NHC	19.1	3.2	0.174	0.226	-0.052
Ph	18.3	1.2	0.106	0.198	-0.092

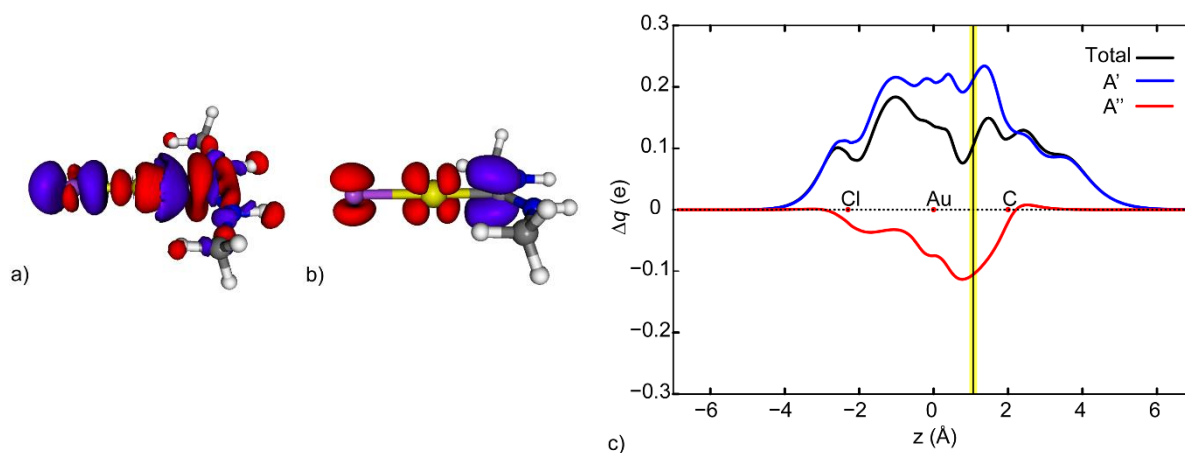


Figure 35. Three dimensional plots of the electron density difference for A' (a) and A'' (b) symmetry for complex 9'Cl (left, red isosurfaces identify charge depletion area, blue isosurfaces charge accumulation, density value at the isosurface: ± 0.002 e/(a.u.)³) and charge displacement curves for complex 9'Cl (right, the vertical yellow band identifies a suitable boundary between AuCl and NAC^{sym} fragments).

In this way, most of the complexes present a symmetry plane passing through the metal center and the N-C-N atoms of NAC^{sym} and this allows us to use C_s symmetry (with A' and A'' irreducible symmetry representations) to separate the DCD components of the CDF. In all the cases, the fragments used are [LAu]⁺⁰ and [NAC^{sym}], with the aim to analyze the charge displacement between the metal fragment and the carbene. It should be stressed that the introduction of NAC^{sym} does not alter significantly the

properties of the Au-C bond: both Au-C distances and interaction energies for the two series of complexes, $[\text{LAu}(\text{NAC})]^{+/0}$ and $[\text{LAu}(\text{NAC}^{\text{sym}})]^{+/0}$, show a stringent linear correlation (Figure 36).

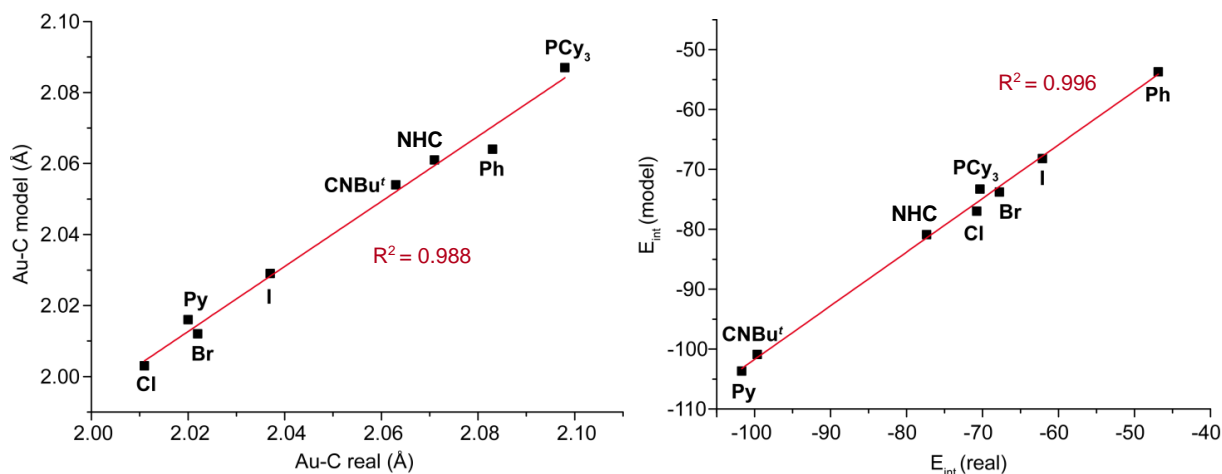


Figure 36. Correlation between: the Au-C_{NAC} bond distances real vs model (left) and the $[(\text{L})\text{Au}]^+$ -NAC interaction energies, E_{int} (right).

Complexes $\mathbf{9}'(\text{PPh}_3)\text{BF}_4$, $\mathbf{9}'(\text{PCy}_3)\text{BF}_4$, $\mathbf{9}'(\text{PAr}^{\text{F}})\text{BF}_4$, bearing phosphine ligands, do not possess the symmetry plane, due to the *helical* orientation of substituents at the phosphorous. In these cases only the net $\text{NAC} \rightarrow \text{Au}$ charge transfer (CT) can be reported (Table 8).

The 3D contour plot of the electron density difference, related to the A' symmetry (Figure 35a), shows a depletion of electron density at the carbenic carbon (red isosurface) exactly in the region of the donating lone-pair and an accumulation (blue isosurface) in the Au-C region toward the gold site (this symmetry correlates with the donation component involving the occupied σ orbital of the NAC^{sym} described by the lone pair of the carbenic carbon and the partially empty σ orbitals of AuCl). In case of A'' symmetry (Figure 35b) a clear charge depletion is present only at the site of AuCl accompanied by a corresponding significant accumulation at the carbenic site (back-donation component).

The two symmetry CDFs give the desired quantitative picture of the nature of the Au-C bond. They clearly show two charge fluxes moving in opposite directions across the whole molecular space, in the expected correspondence with their respective symmetries. By fixing a boundary plane to separate the fragments within the complex (Figure 35c and Experimental Part) one can extract suitable numerical values of CT between the metal fragment and NAC^{sym} . In this case (complex $\mathbf{9}'\text{Cl}$) the net CT (CT_{tot}) from NAC^{sym} to AuCl is 0.102 electrons, resulting from a donation of 0.210 e and a back-donation of 0.108 e. The results for all complexes ($\mathbf{9}'\text{L}$) are summarized in Table 8 (the corresponding CDFs are reported in the Experimental Part). The range of variation of the DCD components of the bond is significant. The ligand of complexes $\mathbf{9}'(\text{Py})\text{BF}_4$ and $\mathbf{9}'\text{Ph}$ induce the largest and smallest σ -acidity to the metal fragment ($[\text{LAu}]^{+/0}$), respectively.

The back-donation, CT_{back} , varies from -0.045 to -0.108 e for complexes $\mathbf{9}(\text{CN}^t\text{Bu})\text{BF}_4$ and $\mathbf{9}\text{Cl}$, respectively.

Our most important question now is whether a demonstrable relationship exists between CT_{back} and ΔH_r^\ddagger and Figure 37 (left) shows that a linear correlation indeed exists for all complexes ($\mathbf{9}Y$) with a correlation coefficient of 0.971. Compounds with a smaller C-N rotational barrier show a larger back-donation component of the Au-C bond (larger magnitude of CT_{back}) and *vice-versa*. This finding is nicely confirmed by theoretical calculations. The computed rotational barrier vs CT_{back} presents the same linear trend (Figure S17, SI Plot 43 pag 183?). Note that, extending the range of ligands, including for instance the carbonyl complex $[\text{COAu}(\text{NAC})]^+$ (where the back-donation ability of the metal fragment is almost vanishing, CT_{back} is just of 0.02 e), the linear correlation is preserved (R^2 is 0.991, Experimental Part).^{xiii} It is important to note that the rotational barrier does not show any correlation with the donation component CT_{don} ($R^2=0.397$, see Figure S18? in Experimental Part) and, therefore, only a poor correlation with the overall net donation ($R^2=0.889$, see Figure S19? in Experimental Part).

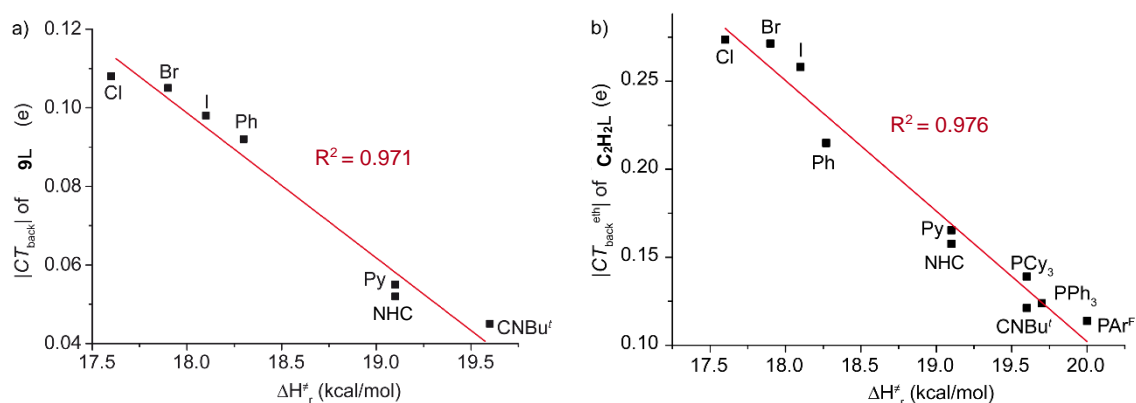


Figure 37. Linear correlations of the C-N rotational barrier (ΔH_r^\ddagger for $\mathbf{9}L$) vs the absolute value of: the CT_{back} for $\mathbf{9}'L$ (left) or $CT_{\text{back}}^{\text{eth}}$ in C_2H_2L (right) model systems.

It is somewhat unsatisfactory that the three phosphorus ligands in $\mathbf{9}(\text{PPh}_3)\text{BF}_4$, $\mathbf{9}(\text{PCy}_3)\text{BF}_4$ and $\mathbf{9}(\text{PAR}^F)\text{BF}_4$ which induce strong net acidity at the metal fragment, escape the previous analysis. We can however, adopt a different, indirect approach, which includes all the ligands and, at the same time, provides a powerful, independent, verification and generalization of the correlation between rotational barrier and ability of the metal fragment $[\text{LAu}]^{+/0}$ to give back-donation. We analyzed theoretically a different series of complexes, C_2H_2Y , of structure $[\text{LAu}(\text{C}_2\text{H}_2)]^{+/0}$, where the ligands L are the same as in the corresponding $\mathbf{9}Y$ series, while ethyne replaces NAC^{sym} . As we pointed out previously, Tarantelli and Belpassi have demonstrated¹⁵³ that the distortion of ethyne from linearity upon coordination to a metal center depends very precisely on the metal $\rightarrow (\text{C}_2\text{H}_2) \pi$ back-donation ($CT_{\text{back}}^{\text{eth}}$), with a small contribution of the $(\text{C}_2\text{H}_2) \rightarrow$

^{xiii} Our attempts to synthesize $[(\text{CO})\text{Au}(\text{NAC})]^+$ failed, leading to the decomposition of the product.

M σ donation ($CT_{\text{don}}^{\text{eth}}$), and an even smaller contribution of an electrostatic term [see Eq. (5), Eq. (6) in Experimental Part]. We have computed ethyne distortion and total CT and, from these, extracted the two DCD components of the gold-ethyne bond for the entire L series ($\text{C}_2\text{H}_2\text{Y}$) (see Table 9).

As Figure 37 (right) shows, the correlation between the π back-donation and the experimental ΔH_r^\ddagger of complexes **9Y** is indeed very good and the data for phosphine ligands fit the model nicely. The implications of this finding are remarkable. It clearly suggests that the ligand effect on the π basicity of the metal is very similar across different substrates, even having very different π accepting properties. It is indeed noteworthy that the magnitude of back-donation to ethyne almost doubles compared to NAC, but the various ligands induce the same ordering of back-donation amount in both series (Figures 4a and 4b). There are a number of other interesting observations that are worth pointing out. We can see again, for example, that complexes bearing Py and NAC have very different $CT_{\text{tot}}^{\text{eth}}$ but similar $CT_{\text{back}}^{\text{eth}}$ values (and so similar ΔH_r^\ddagger). The fluorinated phosphine PAr^{F} induces the smallest back-donation from the *trans* ligand, in accord with its highest ΔH_r^\ddagger . Comparison of PPh_3 and PCy_3 leads to the firm conclusion that the fragment $[(\text{PR}_3)\text{Au}]^+$, has the same back-donation-inducing ability with either an alkylic or aliphatic substituent R.

Table 9. $CT_{\text{tot}}^{\text{eth}}$, $\Delta\theta$, $\Delta\theta_{\text{elect}}$ and $CT_{\text{back}}^{\text{eth}}$ values for $[\text{LAu}(\text{C}_2\text{H}_2)]^{+/0}$ model systems.				
L	$CT_{\text{tot}}^{\text{eth}}$ (e)	$\Delta\theta$ (°)	$\Delta\theta_{\text{elect}}$ (°)	$CT_{\text{back}}^{\text{eth}}$ (e)
Cl	0.007	18.35	0.41	-0.273
Br	0.015	18.25	0.39	-0.271
I	0.030	17.44	0.33	-0.258
PPh_3	0.144	11.95	2.71	-0.124
PCy_3	0.128	11.75	2.82	-0.121
PAr^{F}	0.163	11.58	2.85	-0.114
CN^tBu	0.125	12.61	2.86	-0.134
Py	0.112	14.99	3.22	-0.166
NHC	0.071	14.03	2.66	-0.165
Ph	0.026	14.59	0.33	-0.215

This result is somewhat surprising, considering the different net donor ability of PPh_3 and PCy_3 and the net acidity of the corresponding fragments (CT_{tot} is 0.128 and 0.144 electrons, respectively), and indicates clearly that the gold atom “mediates” the electronic interplay between the two ligands, making intuitive predictions on the ability of a ligand to stabilize the carbenic structure unreliable. Consistently with our results, recent experimental data do indeed indicate that aromatic and alkyl phosphines behave similarly

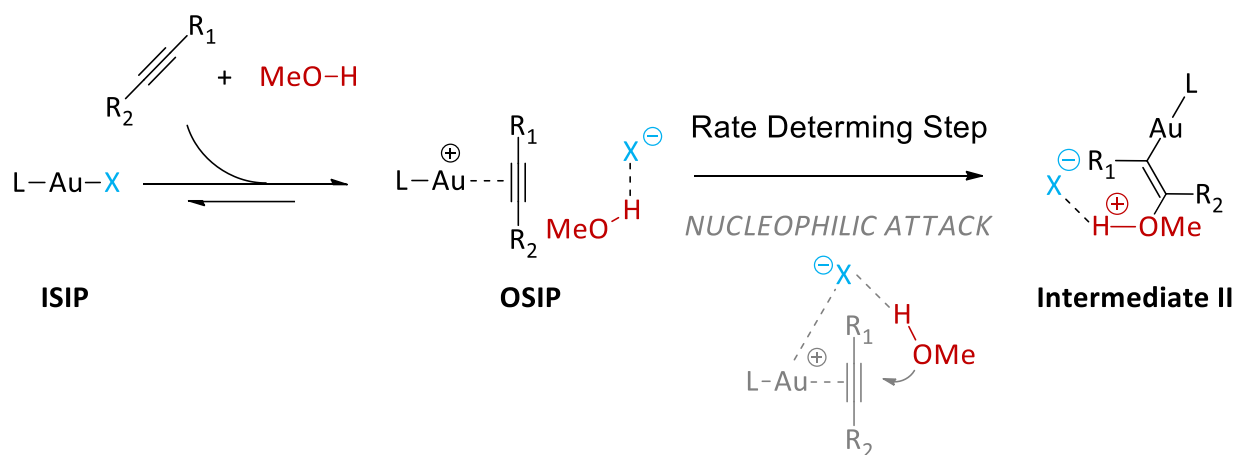
when employed for tuning the carbocation vs carbenoid character of catalytic intermediates of Au(I).^{156,165,166,176}

In summary, we have discovered that an experimental observable determined by NMR techniques, the proper rotational barrier of the C-N bond of a NAC ligand bound to a metal (gold in our case), provides a selective measurement of one DCD bonding component, the metal-to-substrate π back-donation. This opens the possibility to characterize the electronic structure of the gold metal fragment by actually measuring how its π basicity is affected by the nature of the coordinated ligands. We hope that this method shall contribute to a more rational control of ligand electronic effects in the design of new catalysts. Furthermore, in view of the recent advances in the synthesis of different metal complexes of acyclic carbenes,¹⁶⁸ one can easily envisage a broader applicability of the method to other metal systems.

2.4 Appropriate matching of Ligand (L) and Counterion (X⁻)

2.4.1 Effect in methoxylation reaction

In chapters 2.1 and 2.2 we proposed for the first time that, in the alkoxylation of 3-hexyne, the anion was not only acting as proton shuttle effecting only the protodeauration step but that it had an active role even during the attack. We observed that OTs⁻ was the most suitable anion for NHC-containing catalysts (complexes **4**⁺, Scheme 28, chapter 4.2). In the same period Maier and Zhdanko, instead, observed that OTf⁻ was the best compromise for PPh₃ based catalysts.⁵³ To complete and rationalize these findings, complexes **1-3X** (Scheme 28, chapter 4.2) have been tested as catalysts in the methoxylation of 3-hexyne (Scheme 14 and Table 10) in the same experimental conditions of our previous work. A typical catalytic run was performed by mixing 3-hexyne and methanol in the presence of the active catalyst (X⁻ = OTs⁻, TFA⁻) or the catalyst precursor **1-3Cl** and the appropriate silver salt (X⁻ = BF₄⁻, OTf⁻), at 30 °C in CDCl₃. In Table 2, the already mentioned results concerning complexes **4X** have been added for useful comparison.



Scheme 23. Preequilibrium and nucleophilic attack for methoxylation of 3-hexyne, the complete cycle can be found in chapter 2.1.

Complexes **2BF₄** and **3BF₄** promoted full conversion of the precursors within 120 minutes (Table 10, entries 2 and 3), whereas catalyst **1BF₄** in the same reaction time promoted only 36% conversion (Table 10, entry 1).

When the catalytic process was carried out using **1-3OTf** as the catalysts, an overall neat increase of the reaction rate was observed. Again, the complex bearing PPh₃ (**1OTf**) gave the poorest result, as only 84% conversion was recorded within 120 min. By contrast, the reaction catalyzed by **2OTf** and **3OTf** reached full conversion in 61 and 52 minutes, respectively (Table 10, entries 5, 6, and 7).

Replacing OTf⁻ with a more coordinating and basic anion such as OTs⁻, lower activity was exhibited by all catalysts (**1-3OTs**). Thus, 70, 82 and 94% conversion was recorded for **1OTs**, **2OTs** and **3OTs**, respectively, after 120 min of reaction time (Table 10, entries 9, 10 and 11).

Table 10 - Gold(I) catalyzed methoxylation of 3-hexyne in chloroform				
Entry	Catalyst	Time (min)	Conv. ^[a] (%)	TOF _i ^[a,b] [min ⁻¹]
1	1BF₄	120	36	0.31
2	2BF₄	118	>98	2.72
3	3BF₄	120	>98	1.43
4	4BF₄	42	>98	2.86
5	1OTf	120	84	0.97
6	2OTf	61	>98	5.84
7	3OTf	52	>98	3.45
8	4OTf	33	>98	3.46
9	1OTs	120	70	0.69
10	2OTs	120	82	2.43
11	3OTs	120	94	2.37
12	4OTs	18	>98	5.06
13	1TFA	120	5	0.05 ^[c]
14	2TFA	120	4	0.04 ^[c]
15	3TFA	120	1	0.03 ^[c]
16	4TFA	120	72	0.60

Catalysis conditions: 30 °C, 3-hexyne (100 μL, 0.88 mmol), catalyst 1 mol% (or 1:1 L-Au-Cl/AgX), CH₃OH (143 μL, 4 eq), in CDCl₃ (400 μL). [a] Conversions and TOF_i were determined by ¹H NMR spectroscopy as average of three runs. [b] TOF_i = (n_{product}/n_{catalyst})/time (at 30% conversion). [c] In order to calculate the TOF_i value, the catalytic process was followed until 30% conversion was reached.

Finally, using TFA⁻ as counterion, the reaction rate for all catalysts **1-3TFA** slowed down further, and only small amounts of product (≤ 5%) were detected after 120 minutes (Table 10, entries 13, 14, and 15).

Comparing the values of the initial turnover frequency TOF_i (Table 10 and Figure 38), one can observe that all complexes bearing phosphines (**1-3X**) follow the same trend, although with different magnitudes. While only a slight difference has been observed by replacing BF₄⁻ with OTs⁻, OTf⁻ derivatives showed a 2-3 times increase of the catalytic activity. **1-3TFA** are the worst catalysts, as judged by their extremely low TOF_i values. Contrarily, complexes **4X** follow a different trend, as the performance increases on going from BF₄⁻ to OTf⁻ and then to OTs⁻, but it finally collapses in the case of TFA⁻ (entries 4, 8, 12 and 16 in Table 10, Figure 38).

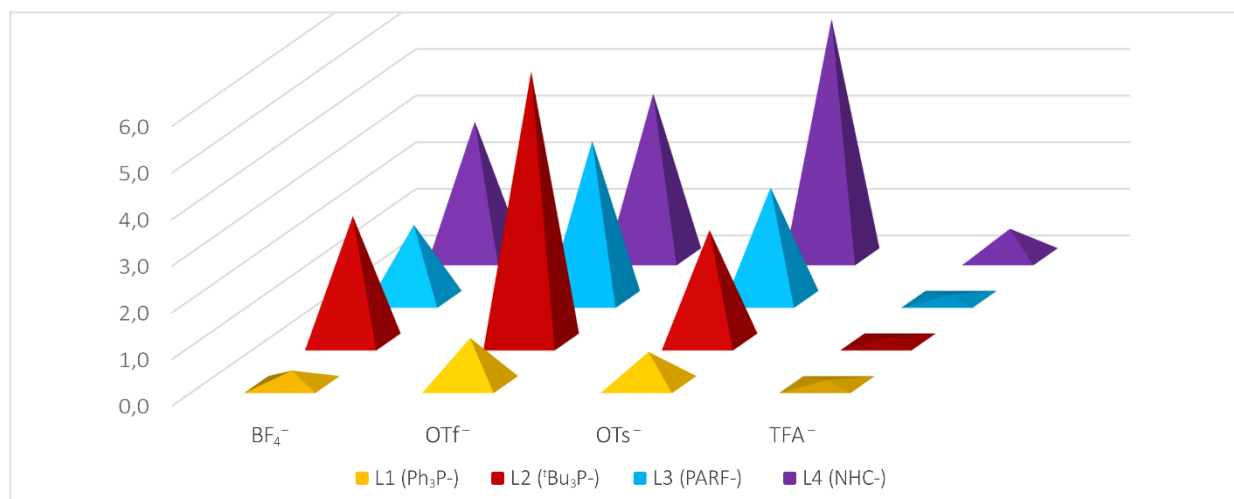


Figure 38. TOFi values for methoxylation of 3-hexyne promoted by 1-4X ($X^- = \text{BF}_4^-, \text{OTf}^-, \text{OTs}^-, \text{TFA}^-$).

The alkoxylation of alkynes has been deeply studied by several groups,¹⁰⁵ and the accepted mechanism was shown and fully described in chapter 2.1 (Scheme 5). In the presence of certain phosphines the formation of the gem-diaurated species¹⁷⁷ was observed, that causes a different kinetic profile of the reaction for different L ligands. The detailed study of the kinetic profile has led to the conclusion that, in the catalytic cycle, only one gold atom is involved and that the RDS of the reaction is the attack of methanol on the ISIP (Scheme 5) both for phosphine⁵³ and NHC ligands (chapter 2.1). A notable anion effect was observed, particularly in the initial steps of the reaction: pre-equilibrium $\text{ISIP} \rightleftharpoons \text{OSIP}$ and activation of methanol during the nucleophile attack (Scheme 14).

In the nucleophilic attack step, the anion acts as a template, holding the methanol in the right position for the outer-sphere attack and as a hydrogen-bond acceptor, improving the nucleophilicity of the attacking methanol.

In particular for NHC complexes, the intermediate coordinating ability and basicity of OTs^- affords the best compromise to achieve an efficient catalyst. Thus, in the presence of this anion the pre-equilibrium is shifted towards the OSIP and its characteristic basicity promotes the nucleophilic attack (much better than less basic BArF^- [tetrakis[3,5-bis(trifluoromethyl)phenyl]borate], BF_4^- , and OTf^- anions). Concerning **1X**, it has been found that OTf^- is the best anion and it has been suggested that OTs^- is too coordinating to **1**⁺, reducing the amount of OSIP in solution.⁵³

Analyzing our results, it should be noted that for all **1-4X** complexes the catalytic performances improve replacing BF_4^- with OTf^- , as expected, due to the higher basicity and hydrogen-bond acceptor powers of the latter. However, if the basicity of the anion is further increased (OTs^-), opposite trends can be observed in function of the ligand L. Thus, while a decrease of catalytic efficiency was measured for all species bearing phosphines (**1-3**), a significant increase was obtained for NHC.

In order to understand these differences, at first we deeply investigate the ISIP \rightleftharpoons OSIP equilibrium (Scheme 14) during the reaction, recording ^{31}P NMR spectra at different reaction times. We found that OTs^- tends to re-enter gradually in the first coordination sphere of gold (ISIP) whilst the reaction proceeds and the amount of alkyne and methanol is decreasing (Figure 39 and Experimental Part). We can ascribe the different catalytic behavior observed for **1-3**OTs, with respect to **4**OTs, to the higher coordination power of OTs^- when phosphines rather than NHC is bound to gold. However, it is also possible that OTs^- shows different ability to acts as a template (holding the methanol for the outer-sphere attack and as hydrogen-bond acceptor) when NHC is replaced with phosphines.

Finally, the very high tendency of TFA^- to coordinate to gold and its high basicity deeply undermine catalyst efficiency for all species bearing phosphines (**1-3**), preventing alkyne coordination and forming free MeO^- in solution, which poisons the catalyst (Chapter 2.1 and Experimental Part) as observed for **4X**.¹⁷⁸

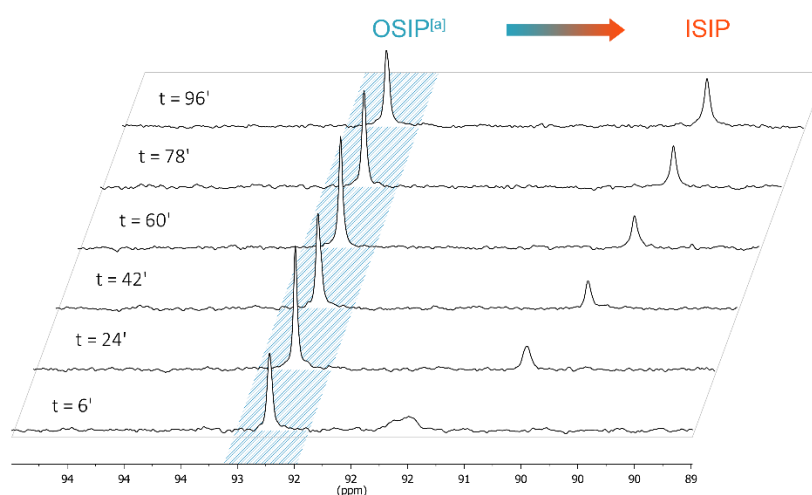
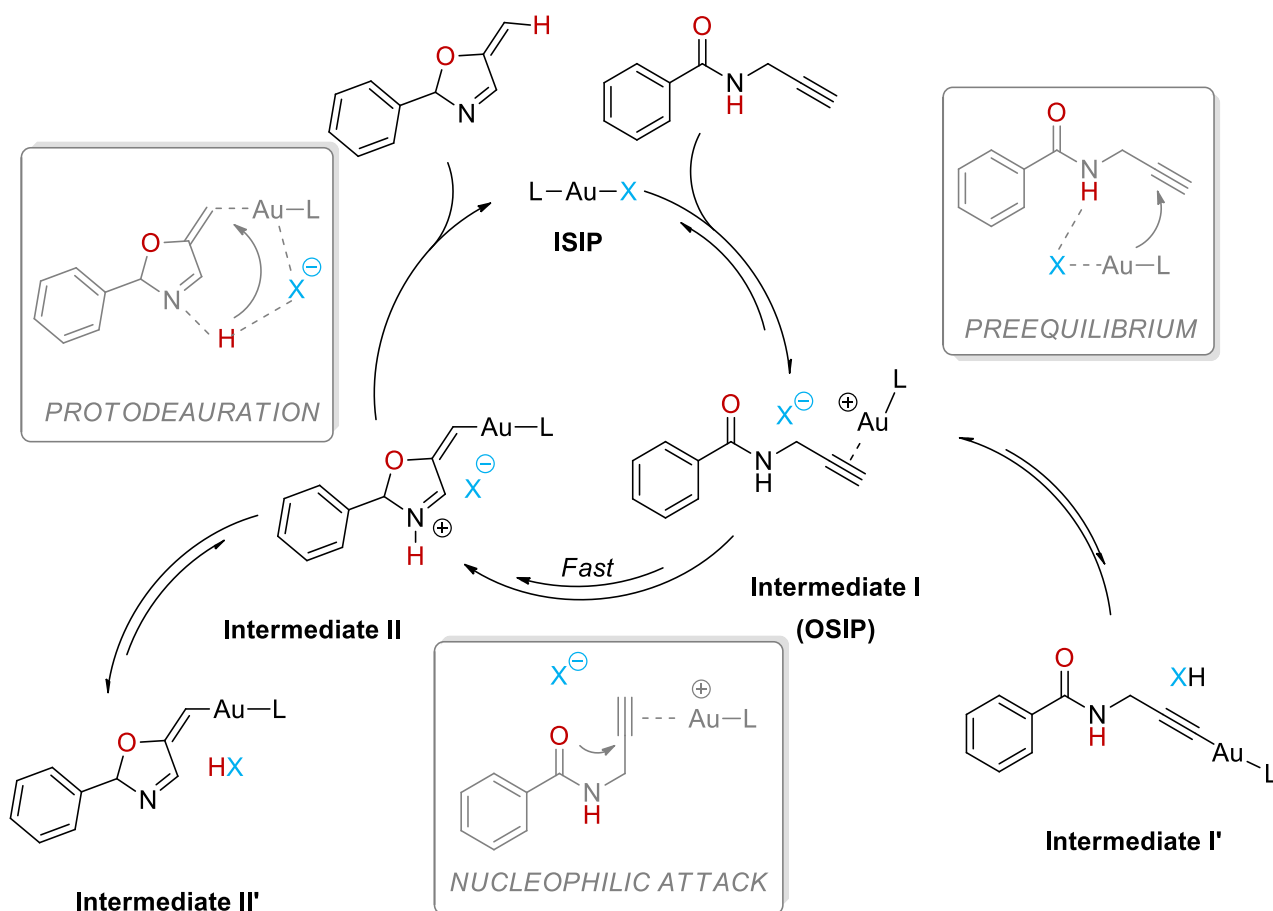


Figure 39. ^{31}P -NMR spectra recorded at different reaction times for methoxylation of 3-hexyne conducted with 2OTs. [a] and/or *gem*-diaurated^{105a} (see Experimental Part)

2.4.2 Effect in the cyclization of propargylamides

In the previous paragraph we shed some light on the ligand effect over the counterion effect studying the methoxylation of 3-hexyne, where the attack is the rate determining step. The natural consequence is to find and investigate also a catalysis where the RDS is, instead, the nucleophilic attack. The cycloisomerization of N-propargylcarboxamides is a well-studied gold-catalyzed reaction in which protodeauration is considered the slow step (Scheme 24).^{179a-d} A pseudo-first order kinetic with respect to the catalyst concentration is observed,¹⁸⁰ and the key vinyl gold intermediate (Scheme 24), **intermediate II/II'** has been identified in the case of NHC-Au(I) ^{181c,d} and $\text{PPh}_3\text{-Au(I)}$ ^{180,52} by Hashmi and

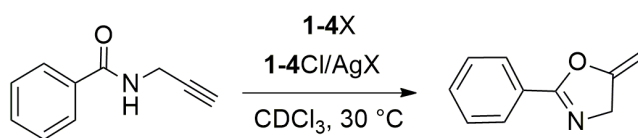
Hammond groups, respectively, and by Ahn¹⁸² and coworkers in the case of gold(III). These observations induce to believe that the passage from **intermediate I** to **intermediate II**, with the formation of the vinyl gold complex, is fast and thus it is not the rate-determining step.



Scheme 24. Proposed mechanism for cyclization of N-(prop-2-ynyl)benzamide to 2-phenyl-5-vinylidene-2-oxazoline.

In the **intermediate II**, the gold-carbon bond is cleaved by a proton (protodeauration, RDS) to give the final product and regenerate the catalyst (Scheme 24, **ISIP** = Inner Sphere Ion Pair). Accordingly, it was found that the additives that are good hydrogen-bond acceptors increase the efficiency of this reaction, because they can act as proton shuttle.¹⁸³

All complexes **1-4X** (Scheme XX, $X^- = BF_4^-, OTf^-, OTs^-, TFA^-$) have been tested as catalysts in the cyclization of propargylamide (Scheme 25 and Table 11). The isolated species were employed in the case of all trifluoroacetates, *p*-toluenesulfonates and **3-4OTf**, whereas in all other cases the catalyst was prepared *in situ* in a NMR tube by mixing equimolar amounts of the precursor **1-4Cl** and the appropriate silver salt in $CDCl_3$.



Scheme 25. Cyclization of N-(prop-2-yn-yl)benzamide to 2-phenyl-5-vinylidene-2-oxazoline.

Table 11 - Gold(I) catalysed cyclization of N-(prop-2-yn-yl)benzamide				
Entry	Catalyst	Time (min)	Conv.^[a] (%)	TOF_i^[a,b] [min⁻¹]
1	1BF₄	114	>98	1.88
2	2BF₄	84	>98	1.94
3	3BF₄	120	55	1.25
4	4BF₄	99	>98	1.86
5	1OTf	120	78	1.40
6*	1OTf	120	85	1.31
7	2OTf	120	83	0.92
8	3OTf	120	50	0.74
9	4OTf	120	89	1.29
10	1OTs	63	>98	4.16
11	2OTs	40	>98	3.67
12	3OTs	120	53	0.76
13	4OTs	120	65	0.84
14	1TFA	120	63	1.07
15	2TFA	73	>98	3.89
16	3TFA	120	22	0.13 ^[c]
17	4TFA	120	56	0.54

Catalysis conditions: 30 °C, N-(prop-2-yn-yl)benzamide (80 mg, 0.5 mmol), catalyst 1 mol% (or 1:1 L-Au-Cl/AgX) in CDCl₃ (500 μL). [a] Conversions and TOF_i were determined by ¹H NMR spectroscopy as average of three runs. [b] TOF_i = (n_{product}/n_{catalyst})/time (at 30% conversion). [c] In order to calculate the TOF_i value, the catalytic process was followed until 30% conversion was reached. *using isolated **L1**-Au-OTf as catalyst.

A typical catalytic run was performed by mixing N-(prop-2-yn-yl)benzamide in the presence of 1 mol% catalyst (or 1:1 L-Au-Cl/AgX) at 30 °C in CDCl₃. The progress of the reaction was monitored by NMR spectroscopy (see Experimental Part for details). Quantitative (>98%) conversion of the substrate into 2-phenyl-5-vinylidene-2-oxazoline was reached in 114, 84 and 99 min by using **1BF₄**, **2BF₄** and **4BF₄**, respectively (Table 11, entries 1, 2, and 4). Much less efficiently, **3BF₄** promoted the formation of the reaction product in only 55% yield after 120 min (Table 11, entry 3).

By changing the anion from BF₄⁻ to OTf⁻, a slight decrease of the catalytic efficiency for all the catalysts was observed (Table 1, entries 5-8 vs. 1-4). Again the complex bearing PAR^F (**3OTf**) showed to be the less active catalyst within the series **1-4OTf** (Table 11, entry 7).

In order to verify that *silver effects*¹⁸⁴ are negligible in our catalytic conditions also isolated **1OTf** was employed as catalyst giving similar conversion of **1Cl**/AgOTf (Table 11).

Turning into a more basic and coordinating anion such as OTs⁻, very different catalytic performances were observed within the series **1-4OTs**. Thus, a complete conversion was obtained in the case of **1OTs** and **2OTs** after 63 and 40 min, respectively (Table 11, entries 9 and 10). On the other hand, **3OTs** and **4OTs** gave performances comparable with that of **3OTf** (Table 11, entries 7, 11, and 12). It is worth noting that the catalytic activity of **4OTs** is very similar to that of **3OTs**, while when the anion is BF₄⁻, **4BF₄** shows the same high efficiency of **1BF₄** and **2BF₄**, differently from **3BF₄** (Figure 40).

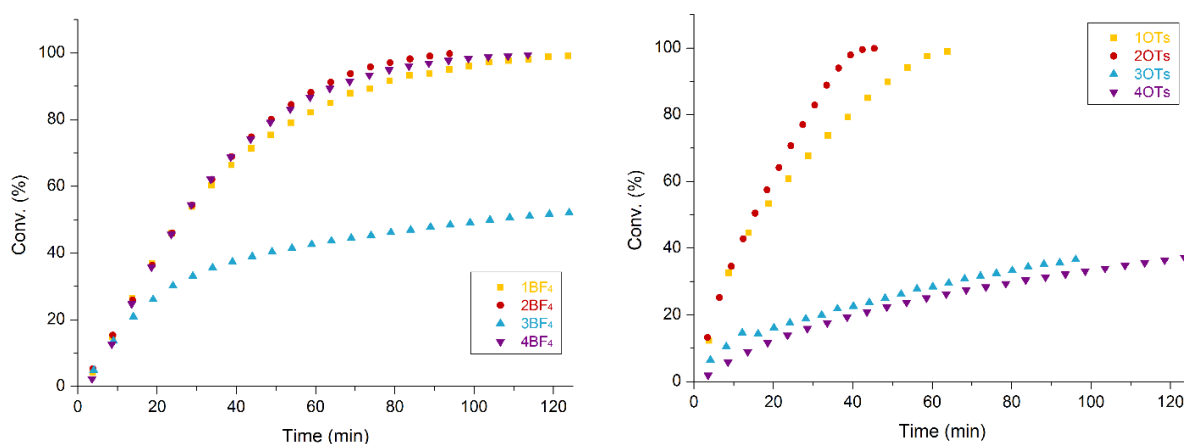


Figure 40. Propargylamide cyclization performed by **1-4BF₄** (left) and **1-4OTs** (right) complexes.

Finally, in the case of TFA⁻, the most coordinating and basic anion of the four screened in this work, generally low catalytic performances were observed, with the exception of **2TFA** which allows complete formation of 2-phenyl-5-vinylidene-2-oxazoline in a short reaction time.

Comparing the value of the initial turnover frequency, TOF_i (Table 11 and Figure 41), one can see that for catalysts bearing triphenylphosphine (Table 11, entries 1, 5, 9 and 13) the best anion is OTs⁻ followed, in the order, by BF₄⁻, OTf⁻ and TFA⁻. The range of TOF_i values varies from 1.07 to 4.16 min⁻¹. With the exception of **2TFA**, an analogous trend can be observed for catalysts **2X** (Table 11, entries 2, 6, and 10). At difference with **1TFA**, complex **2TFA** exhibits about the same high performance of **2OTs**, the TOF_i values being 3.67 and 3.89 min⁻¹, respectively. By contrast, for **3X** and **4X** series, the catalytic activity decreases following exactly the increasing basicity of the anion. In fact, the TOF_i values are 1.25, 0.74, 0.76 and 0.13 min⁻¹ for **3BF₄**, **3OTf**, **3OTs**, and **3TFA**, respectively and 1.86, 1.29, 0.84 and 0.54 min⁻¹ for **4BF₄**, **4OTf**, **4OTs**, and **4TFA**, respectively.

To confirm that the organogold intermediate is actually present in our catalytic mixture, ³¹P NMR spectra have been recorded during the catalysis for complexes **1-3X** (X⁻ = BF₄⁻, OTf⁻, OTs⁻, TFA⁻). ³¹P NMR

monitoring indicated that the resting state for the gold catalyst is a vinyl gold complex, **intermediate II/II'**. At high conversions, also the coordination of the product is observed (see Experimental Part for details). Therefore, it is reasonable to assume that the protodeauration step is slow and consequently it is the RDS for all **1-4X** catalysts in our reaction conditions (Table 11).

In literature it is suggested that two important factors should be taken into account in order to rationalize the activity of L-Au-X compounds: i) the breaking of the Au-C bond, that is related to the nature of the ligand L^{52, 185} and ii) the ability of the counterion to promote the proton-shuttle¹¹⁵ that is related to acid-base nature¹⁰⁸ and hydrogen-bond acceptor powers of X⁻.¹⁸³

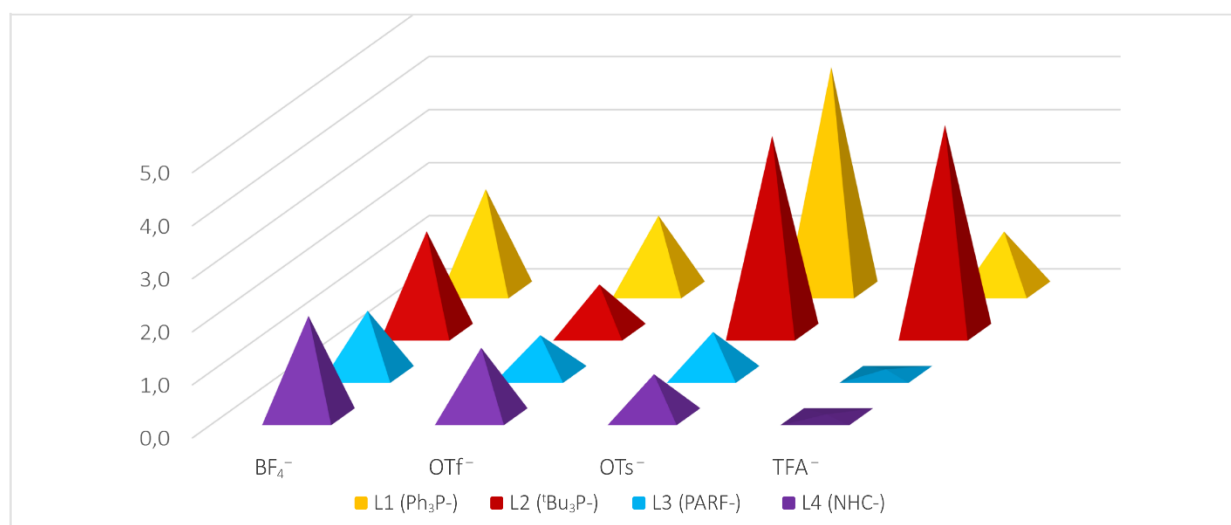


Figure 41. TOF_i values for propargylamide cyclization promoted by **1-4X** (X⁻ = BF₄⁻, OTf⁻, OTs⁻, TFA⁻).

Concerning the first point if we compare the results obtained using **1-4BF₄** catalysts (BF₄⁻ is a poor basic and non-coordinating anion¹⁸⁶) we observed that compound **3BF₄**, bearing the most electron withdrawing ligand (PARF), is by far the worst catalyst within the series (Table 11, entry 3 vs. entries 1, 2 and 4), presumably because it renders more stable the Au-C bond.¹⁷⁹ On the contrary, **1BF₄**, **2BF₄** and **4BF₄** showed higher activity, but with almost negligible differences in their performances.^{144, xiv}

In order to verify the importance of the acid-base nature and hydrogen-bond acceptor powers of the counterion (second point) we can consider the series of complexes **4X** (X⁻ = BF₄⁻, OTf⁻, OTs⁻, TFA⁻). It can be seen that the catalyst activity is related to the basic strength of the anion (Table 11, entries 4, 8, 12, and 16). Performances of the catalysts decrease gradually with increasing basicity and hydrogen-bond acceptor power of X⁻ (basic strength: BF₄⁻ < OTf⁻ < OTs⁻ < TFA⁻). The plausible scenario for **4X** is that too basic anions with higher hydrogen-bond acceptor power (OTs⁻ and TFA⁻) do not easily release the proton to gold thus slowing the reaction rate.

^{xiv} This finding contrasts with the fact that PPh₃ is less electron donating than P(tBu)₃ and NHC: see Ref. 173.

In the case of phosphine complexes **1-2X** ($X^- = OTf^-, OTs^-, TFA^-$), the catalytic activity of each compound quite follows the basicity scale of X^- and medium-high basic and hydrogen-bond acceptor OTs^- and TFA^- anions give better results (Table 11, entries 9, 10, 13 and 14).

A possible explanation can be found in the coordination properties (affinity) of medium-high coordinative OTs^- and TFA^- anions towards Au.¹⁸⁷

In the case of **1X** and **2X** complexes, the best anion is by far OTs^- and TFA^- respectively, probably because during the proton shuttle the anion can interact with the Au atom. This interaction weakens both Au-C and H-X bonds simultaneously, accelerating the reaction (Scheme 24, protodeauration). A similar trend was recently observed by Xu and Hammond.¹⁸³ They observed that the addition of NaOTs or HCOONa to a catalytic chloroform solution of **1OTf**/N-propargylcarboxamides increases the catalytic performances by 3.9 and 1.4 times, respectively. Unlike OTs^- , there are not many examples in gold catalysis in which TFA^- results to be the best choice.⁵⁸

Finally, the behaviour of **3X** is similar to the related NHC ones (**4X**). In this case, the interionic structure of OSIP [PARF-Au-(2-hexyne)BF₄] shows that the anion has a strong tendency to interact with the highly positively charged *ortho*-proton of the aryl fragment (3,5-CF₃-C₆H₃) rather than with the gold atom.^{70b} This evidence suggests that Au...X interaction is less probable during the protodeauration.

On the basis of all these observations, a general trend can be drawn as follows. When the coordination of the anion to gold during the protodeauration step (Scheme 24) is not favored, the catalytic performances follow the basicity of the anion. This is the case of complexes **3X** and **4X** (Figure 41). As a confirmation, the interionic structure of NHC-Au(3-hexyne)BF₄ OSIP, determined by ¹⁹F-¹H HOESY experiment and explained by DFT calculation of Coulomb Potential, suggests that the counterion does not easily interact with the gold fragment.¹⁰⁶ On the other hand, when X^- coordination to gold is possible, a balance between basicity and hydrogen bond acceptor power versus coordination ability of the anion is observed. This is the case of complexes **1X** and **2X**, where the ion pair structures of strictly related compounds **L1**-Au-(η^2 -Me-styrene)BF₄ and **L2**-Au-(η^2 -3-hexyne)BF₄ suggest that the counterion can interact with the gold atom.^{69, 70a, 188} The results here presented show that the anion properties, both coordination ability and basicity (hydrogen-bond acceptor power), have a great impact on the "proton shuttle ability"¹¹⁵ of the counterion, and, more importantly, this ability depends on the ligand L present in the cationic gold fragment.

In summary, the catalytic results obtained studying the gold-catalysed cycloisomerization of N-(prop-2-yn-yl)benzamide show that ligands with lower electron withdrawing ability generally accelerate the reaction, but the exact order cannot be trivially anticipated because match/mismatch of ligand and anion properties is present. Taking into account the most used catalysts **1X** and **4X**, it can be concluded that the intermediate coordinating ability and hydrogen bond power of OTs^- provides the best results within the **1X** series (PPh₃ ligand), while BF₄⁻ or OTf⁻ is the best choice for the **4X** series (NHC ligand).

From the results here reported, it is evident that the correct choice of the ligand L, in order to increase the performances of gold(I) complexes L-Au-X in catalysis, strongly depends on the nature of the anion X⁻ and *vice versa*.

For NHC compounds, non-coordinating and weakly basic anions (such as BF₄⁻) may be the best choice for a reaction in which the RDS is the protodeauration, as in the case of the cycloisomerization of N-propargylcarboxamides. On the other side, the intermediate coordinating ability, basicity and hydrogen-bond acceptor property of OTs⁻ provides the best compromise to achieve an efficient catalyst in the methoxylation of 3-hexyne, where the RDS is the nucleophile attack helped by the counterion. In the case of complexes bearing phosphines, a complete different behaviour has been outlined. Thus, an intermediate-high coordination ability of the anion combined with its relatively high basicity and hydrogen-bond acceptor property (OTs⁻ and TFA⁻) has been found to accelerate the cycloisomerization of N-(prop-2-yn-yl)benzamide. Instead, a medium-low coordination power and a weak basicity of the anion (BF₄⁻ and OTf⁻) is suitable for the methoxylation of 3-hexyne. A possible explanation can be found in the higher affinity of the counterion (especially OTs⁻) towards the gold fragment when the ancillary ligand L is a phosphine with respect to NHC: higher gold affinity accelerates the reaction in which the RDS is the protodeauration but inhibits it when the RDS is the nucleophilic attack, due to the shift of the ISIP-OSIP equilibrium (Scheme 24) in favour of ISIP.

This study clearly demonstrates that the interplay between ligand nature and anion effect is crucial in different steps of the catalytic cycle. The multiple roles played by counterions and L-Au⁺ fragments in chemical transformations require a more comprehensive computational and experimental studies of the ligand/anion correlation.

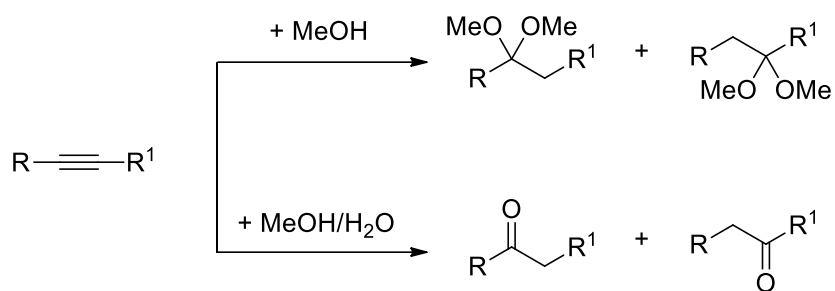
2.5 Hydration of alkynes

Since the 12 principles of Green Chemistry¹⁴ were established, 15 years ago, chemists have been interested in developing more efficient and environmentally friendly synthetic protocols.¹⁹ Several metrics to assess the greenness of any given chemical process (e.g., atom economy, Effective mass yield [EMY], E-factor, etc) have been developed.¹⁸⁹

The use of catalyst is, also, highly desirable in a Green Chemistry context; thus, terms such as turnover number (TON) and turnover frequency (TOF) have shown to be useful to describe the efficiency and sustainability of catalytic reactions. An additional target of Green Chemistry has been to minimize the use of auxiliary substances and to perform the process in mild conditions, if possible at room temperature without any need of protecting atmosphere. In this context, the development of solvent-free reactions has greatly contributed to reduce the environmental impact of chemical processes. In addition, the possibility to use recyclable catalysts can greatly improve the sustainability of the whole process.

During the last 10 years, gold has become a powerful tool in organic chemistry,¹⁹⁰ however, most of the gold-catalysed transformations proceed under unsustainable, from a green chemistry point of view, conditions requiring relatively high catalyst loadings (1–10 mol%) and affording low TON values (in the range 10–100). Moreover, the use of organic solvents and/or silver salt as halide scavenger, also represent a drawback. Protocols describing the use of lower catalyst loadings, room/lower temperature, solvent/silver free conditions and recyclable catalysts are limited.^{104d aggiornare,191} Therefore, designing new efficient and sustainable processes represents a fundamental challenge in the future of gold-based catalysis.

The hydration of alkynes is an important reaction in organic chemistry, and one of the most straightforward and environmentally friendly methods to form the carbon-oxygen bond. This reaction is noticeable in terms of sustainability as it satisfies both *carbon efficiency* and *atom economy* rules. The hydration of alkynes is a well known reaction¹⁹² for which toxic mercury salts were initially used as catalysts. Many other metals were then tested, in order to avoid the use of mercury(II) salts, but gold(III)¹⁹³, Pt(II),¹⁹⁴ Ag(I),¹⁹⁵ Ru(II)¹⁹⁶ showed to be less efficient. Nevertheless, few years later, studying the gold(I) catalysed methoxylation of alkynes in acidic media, Teles^{94a} found out that, in presence of water, the reaction was leading to ketones (Scheme 26).



Scheme 26. Methoxylation and hydration of alkynes catalysed by Au(I).

Tanaka extended this preliminary work by testing several alkynes, both terminal and internal, and different acids.^{104a} TON and TOF values of 1000 and 1000 h⁻¹, respectively, were obtained under optimized conditions (methanol as the solvent, 70°C, 50 mol% of strong Brønsted acid as the co-catalysts) using PPh₃-Au⁺ as the catalyst (Table 12).^{xv} Concerning the E-factor and Effective mass yield (EMY), the calculated values were around 22 and 5, respectively. Afterwards, Nolan was able to further optimize the reaction conditions reducing the catalyst loading up to 10 ppm, for the internal alkynes, using dioxane, high temperature and NHC ligands (instead of phosphines).^{104b}

Table 12. Principal parameters for hydration of alkynes								
	Tanaka ^{104a}	Nolan ^{104b}	Wu ¹⁹⁸		Li ¹⁹⁹		<i>This work</i>	
Solvent	MeOH	Dioxane	MeOH	<i>neat</i>	MeOH	MeOH ^a	<i>neat</i>	<i>neat</i> ^b
TON	1000	84000	20	11	200	1200	1000	5000
TOF (h ⁻¹)	1000	4500	1	0.5	10	10	500	500
T (C°)	70	120	<i>RT</i>	<i>RT</i>	120	120	<i>RT</i>	<i>RT</i>
Silver additives	NO	YES	NO	NO	YES	YES	NO	NO
Acid additives	YES	NO	NO	NO	NO	NO	NO	NO
Other add.	NO	NO	YES	YES	NO	NO	YES	YES
Reusable	NO	NO	NO	NO	YES	YES	YES	YES
E-factor	22	8	17	5	2	2	0.1	0.03
EMY	5	15	10	67	34	35	90	97

a= 6 recycle b= 5 recycle

The decrease of catalyst loading and the use of acid-free conditions were of great impact, concerning environmental friendly reactions, but unfortunately, the use of 1,4-dioxane and silver salt matched with the high temperature, up to 120 °C, made this effort partly fruitless with an E-factor and EMY of 8 and 15, respectively. Several other papers have been appeared dealing with the use of Au(I) and Au(III) catalysts but, to the best of our knowledge, a complete rationalization and optimization of the hydration of alkynes

^{xv} Hayashi and Tanaka (see ref 104a) reported low catalyst loadings (100 ppm) and low amounts of acid promoter (4 mol %) only for the hydration of 1-octyne. For all other alkynes, catalyst loadings typically range from 0.2 to 1 mol % and acid loadings from 25 to 50 mol %.

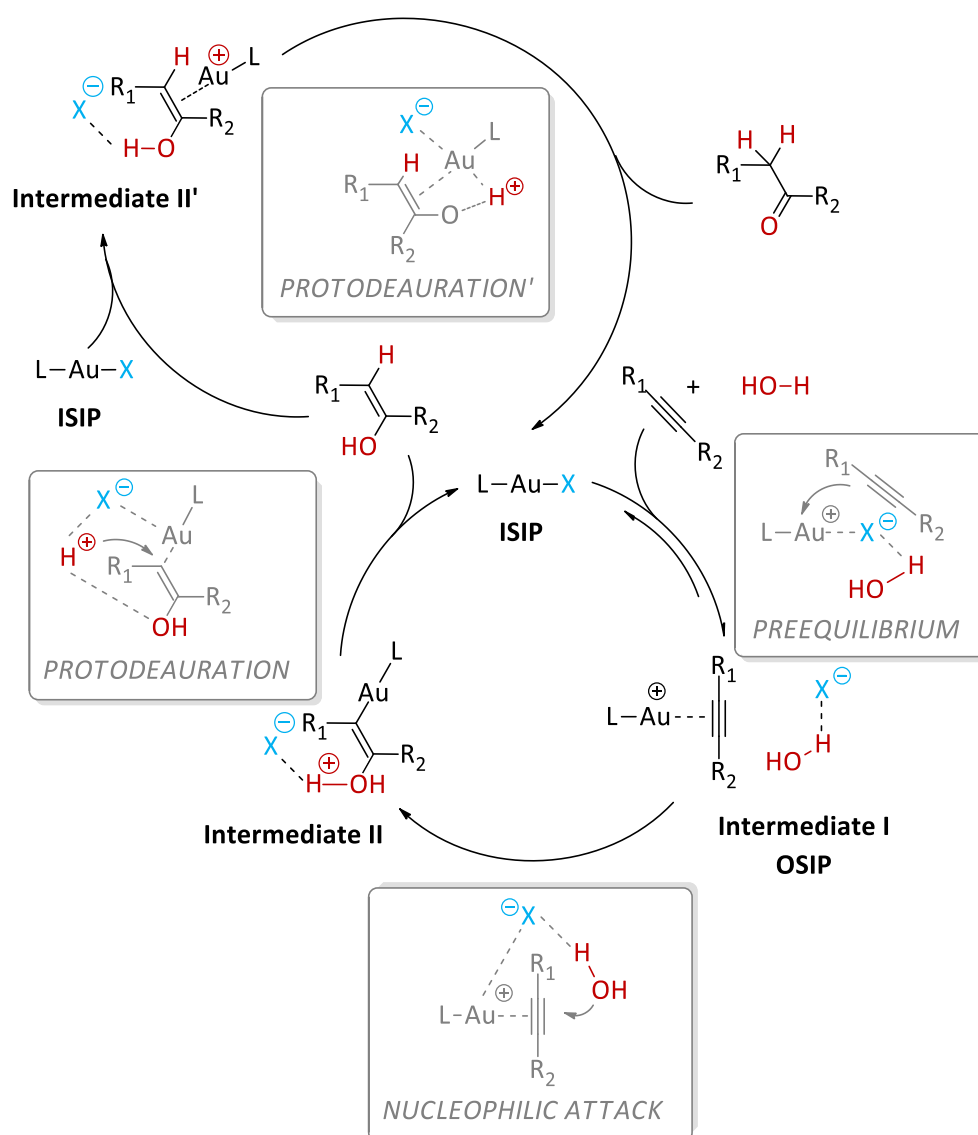
using greener conditions is still absent in the literature.¹⁹⁷ Hu and Wu¹⁹⁸ put a first brick along that direction performing the hydration of several terminal alkynes, at room temperature in acid-free and silver free condition (E-factor and EMY were around 17 and 10, respectively). Even if most of their trials were run using methanol as the solvent, they succeeded to obtain 57% of conversion in neat condition after 24h using a ionic additive ($\text{KB}(\text{C}_6\text{F}_5)_4$). Unfortunately, both TON and TOF were very low, even if the high EMY value of 67 was achieved (Table 12).

In the gold catalysed hydration of alkynes, the recycling of the catalyst has been poorly investigated in the literature. Nevertheless, in a recent work,¹⁹⁹ AuNHC@porous organic polymers have been synthesized and employed in the hydration of alkynes with the aim of recycling the catalysts. Although the system is moderately active (TON on the order of 10^2 - 10^3 , E-factor around 2 and EMY around 35) the use of high temperatures (120°) and the large volume of diethyl ether (around 30 times the volume of the product) necessary to separate the product from the catalyst made the process only partially sustainable.

Concerning the mechanistic aspects, some theoretical papers have appeared in the literature in order to rationalize the behaviour of the gold catalyst in the hydration of alkynes conducted in protic solvents and acidic conditions. Summarizing, it has been found that: i) the water attack can proceed via inner sphere (*syn*-attack) but the presence of other water (or alcohol) molecules²⁰⁰ favour the outer sphere mechanism (*anti*-attack); ii) the first proton transfer can be done by the gold atom²⁰⁰ or other water²⁰¹ or alcohol²⁰² molecules (the energy barrier is lower when the attack is assisted by water even when compared with the anion-assisted one); iii) the second proton transfer needs the attendance of another water molecule and/or the coordination of the vinyl-alcohol through the oxygen atom.¹⁹⁸ It is generally accepted that the RDS is the proton transfer, but the presence of proper solvent and/or acidic media may promote the proton shuttle leading to a switch of the RDS. In this context, in the strictly related methoxylation of alkynes, we found that the role of the counterion (see chapter 2.2.3 and rif 54) is crucial during both nucleophilic attack (see chapter 2.1) and protodeauration steps (see chapter 2.4) The intermediate coordination ability and basicity of sulfonated counterions gave the best results under our conditions.¹⁷⁸ It has also been observed that the addition of ionic additives can increase the rate of the catalytic reaction.^{105a, 183}

Starting from these considerations, we set up the silver-free synthesis of NHC-Au-X [NHC=(1,3-bis(2,6-diisopropylphenyl)-imidazol-2-ylidene, $\text{X}^- = \text{BF}_4^-, \text{OTf}^-, \text{ClO}_4^-$ and OTs^-) pre-activated complexes (see the Experimental Section), and investigated their catalytic activity in the solvent free hydration of 3-hexyne at room temperature, and with suitable additives (in particular NBu_4OTf). Kinetic experiments coupled with DFT calculations allowed us to shed some light on the mechanism of alkyne hydration in apolar, aprotic, and neutral conditions. This study highlighted again the crucial role of the counterion in all the different steps of the catalytic cycle.

Optimizing the conditions, it was possible to avoid the use of acids and solvents, to work at room or mild temperature (50°C), and to reduce the catalyst loading up to 0.05 mol%, leading to high TON (10^3) and TOF (10^2 h^{-1}) values. The silver and solvent free conditions gave us the possibility to reach very low E-factor (0.03-010) and high EMY (90-96) values (Table 12). Finally, the absence of the solvent allowed us to simply separate the liquid product from both solid catalyst and ionic additives by distillation. This opened the way to: a) obtain the product with high purity and b) recycle the catalyst (up to five times) without loss of activity. All these factors (low E-factor, high EMY and catalyst recyclability) are in the correct range for a sustainable production of bulk chemicals with homogeneous gold catalysts, a topic that is still considered a chimera in the literature.²⁰³



Scheme 27. Proposed mechanism for the hydration of alkynes.

The compounds NHC-Au-X ([NHC = (1,3-bis(2,6-di-isopropylphenyl)-imidazol-2-ylidene), X⁻ = ClO₄⁻, BF₄⁻, OTf⁻ and OTs⁻) were synthesized according to the procedure developed by Nolan and co-workers²⁰⁴ that avoids the use of a silver salt, by addition of HX to NHC-Au-CH₂-(C=O)CH₃ acetyl complex.

Complexes NHC-Au-X have been tested as catalysts in the hydration of internal and terminal alkynes. A typical catalytic run was performed by mixing the alkyne and 1.1 equivalent of H₂O in the presence of the catalyst (0.2, 0.1 or 0.05 mol%) and a proper additive (up to 5%) at 30, 40 or 50 °C. At the beginning of the reaction, two phases are present due to the low miscibility of water and alkynes, while during the proceeding of the reaction the formation of a single phase is observed due to the miscibility of the residual water in the formed ketone.

Table 13. Gold(I) catalysed hydration of 3-hexyne ^a . Exploiting the role of the counterion				
entry	Catalyst loading	NHC-Au-X	conversion ^b (%)	time ^c (h) (TOF ^d)
1	0.1	BF ₄	<1	24
2 ^e	0.1	BF ₄	<1	24
3	0.1	ClO ₄	<1	24
4	0.1	OTf	>99	16 (63)
5	0.1	OTs	<1	24
6 ^e	0.1	OTs	<1	24

^a Catalytic conditions: 30 °C, 3-hexyne (1.75 mmol, 200 μL), H₂O (1.92 mmol, 35 μL). ^b Determined by ¹H NMR, averaged value of three measurements. ^c Time necessary to reach the reported conversion. ^d TOF = (n_{product} / n_{catalyst})/t(h) at the reported conversion. ^e 50 °C.

The progress of the reaction was monitored by NMR spectroscopy. Complexes bearing BF₄⁻, ClO₄⁻ or OTs⁻ as counterion were inefficient at 30 °C showing no conversion after 24h. Instead, quantitative (>99%) conversion of the 3-hexyne into 3-hexanone was reached within 16h by using NHC-Au-OTf (Table 13). In order to better compare the catalytic activity in different conditions, the TOF value [TOF (h⁻¹)=(number of mole of product)/mole of catalyst)/time] was taken into account (Table 13).

The TOF obtained by using NHC-Au-OTf was 63 h⁻¹, a value higher with respect to those reported in the literature in neat conditions and room temperature.¹⁹⁸ Even by increasing the temperature up to 50 °C, the catalysts bearing BF₄⁻ and OTs⁻ ions failed to promote the reaction. This surprising and important finding suggests a specific role of the anion during the reaction. In fact, OTs⁻ is the best counterion when NHC is used as ligand in the related methoxylation of alkynes (see chapter 2.1). It is likely that the slightly basic BF₄⁻ is not able to promote both nucleophilic attack and proton shuttle, despite in the preequilibrium step the catalyst is in the active form (OSIP, Scheme 27). This result confirms previously experimental and theoretical observations in the methoxylation of alkynes. When poor-coordinating and

poor basic anions are employed, it is supposed that a second methanol molecule is involved in the mechanism.

In the apolar and biphasic conditions of the catalysis, it is unlikely that a second molecule of water is involved in the mechanism. On the other hand, we have previously observed from NMR experiment, corroborate by DFT calculations, that OTs⁻ is too coordinating for the NHC-Au⁺ cation in the absence of a proton donor like methanol (see chapter 2.1). It is possible that in the neat hydration of alkynes the catalyst in the preequilibrium step is shifted towards the non active form (ISIP, Scheme 27) when OTs⁻ is employed. Thus, the intermediate coordinating and basic nature of OTf⁻ provides the best compromise in our reaction conditions.

Table 14. Gold(I) catalyzed hydration of 3-hexyne ^a . The role of additives				
Entry	Catalyst	Additive	Conversion^b (%)	Time^c (h) (TOF^d)
1	0.1	5% BMIMOTf	<1	24
2	0.1	5% NH ₄ OTf	>99	16 (63)
3	0.1	5% NBu ₄ OTf	>99	2 (495)
4	0.1	5% NBu ₄ OTf + 15% of 3-hexanone	97	2 (493)
4	0.1	2.5% NBu ₄ OTf	97	2.5 (388)
5	0.1	1% NBu ₄ OTf	97	3 (323)
6	0.1	0.5% NBu ₄ OTf	97	6 (162)

^a Catalytic conditions: 30 °C, 3-hexyne (1.75 mmol, 200 μL), H₂O (1.92 mmol, 35 μL). ^b Determined by ¹H NMR, averaged value of three measurements. ^c Time necessary to reach the reported conversion. ^d TOF = (n_{product} / n_{catalyst})/t(h) at the reported conversion.

It is known that ionic additives (in particular NBu₄OTf) can improve some catalytic processes promoted by gold, such as the cycloisomerization of N-(prop-2-ynyl)benzamide to 2-phenyl-5-vinylidene-2-oxazoline, the methoxylation of 3-hexyne, the intermolecular hydroamination of alkynes, the cycloisomerization of allenone, the cyclization of 4-pentynoic acid, and the synthesis of α-pyrone. On the other hand, only acidic additives are used to increase the catalytic performances of gold in the hydration of alkynes^{104a}, and no information is available for other ionic additives.

In Table 14, the results obtained using NHC-Au-OTf as the catalyst and triflate salts as additives are reported. As can be seen by comparing the results obtained without additives (Table 13, entry 4), BMIMOTf (1-Butyl-3-methylimidazolium trifluoromethanesulfonate) stops the reaction. The use of NH₄OTf does not correspond to a substantial effect on catalysis, and complete conversion is achieved within 16 h (compare entry 2 in Table 14 with entry 4 in Table 13). On the other hand, NBu₄OTf increases the catalytic performances and full conversion was obtained in only 2h (compare entry 3 in Table 14 with entry 4 in

Table 13). It can be stressed that the addition of 5% of NBu₄OTf causes an increase of TOF of about an order of magnitude (from 63 to 495 h⁻¹).

Reasonably, the cationic fragment NBu₄⁺ increases the solubility of the salt in 3-hexyne, while the water-soluble NH₄⁺ ion is not present in the organic phase where the reaction takes place. On the other hand, the ionic liquid BMIMOTf, which is immiscible with 3-hexyne, most presumably prevents the distribution of water in the organic phase (water is completely distributed in the ionic liquid). A clear trend was observed by changing the amount of NBu₄OTf from 0 to 5%: between 5 and 2.5% there is only a slight decrease of TOF (from 495 to 408 h⁻¹), while a substantial decrease was detected on going from 2.5% to lower values. As a matter of fact, 5% of NBu₄OTf turns out to be the best choice.

In order to evaluate the potentially benefit effect of the product (3-hexanone) during the catalysis, we added 15% of 3-hexanone directly from the beginning (entry 4, Table 14), but no substantial differences on the retention time were observed, thus indicating that the effect of ionic additives is more marked.¹⁸³

Table 15. Gold(I) catalyzed hydration of alkynes ^a . Catalyst loading, temperature and Kinetic Isotopic effects.						
entry	catalyst	Alkyne	T (°C)	Additive	conversion ^b (%)	time ^c (h) (TOF ^d)
1	0.2	3-hexyne	30	5% NBu ₄ OTf	>99	1 (495)
2	0.05	3-hexyne	30	5% NBu ₄ OTf	>99	4 (495)
3	0.1^e	3-hexyne	30	0% NBu ₄ OTf	42	24 (17)
4	0.1^e	3-hexyne	30	5% NBu ₄ OTf	>99	5 (194)
5	0.05	3-hexyne	40	5% NBu ₄ OTf	93	3 (620)
6	0.05	3-hexyne	50	5% NBu ₄ OTf	95	1.5 (1267)
7	0.05	4-octyne	40	5% NBu ₄ OTf	89	5 (356)
8	0.05	4-octyne	50	5% NBu ₄ OTf	82	3.5 (469)
9	0.1	1-hexyne	40	5% NBu ₄ OTf	25	8 (32)
10	0.1	Ethynylbenzene	40	5% NBu ₄ OTf	27	30 (10)
11	0.25	Ethynylbenzene	50	5% NBu ₄ OTf	>99	24 (17)

^a Catalytic conditions: alkyne (1.75 mmol, 200 μL), H₂O (1.92 mmol, 35 μL). ^b Determined by ¹H NMR, averaged value of three measurements. ^c Time necessary to reach the reported conversion. ^d TOF = (n_{product} / n_{catalyst})/t(h) at the reported conversion. ^e Reaction performed with D₂O instead of H₂O.

We have determined the order of reaction with respect to the catalyst. In the presence of NHC-Au-OTf and 5% NBu₄OTf the catalysis was carried out by changing the catalyst loading (entries 1-2, Table 15 and entry 3, Table 15) from 0.05 to 0.2 mol% observing a pseudo-linear correlation between the average rate [3-hexyne]₀/t versus [NHC-Au-OTf]. This trend suggests a 1st order dependence on catalyst as recently reported in the literature in the case of the methoxylation of alkynes promoted by NHC gold

complexes.^{105a} Thus, it can be argued that only one gold atom is involved in the rate determining step of the reaction.

However, the RDS can be either the nucleophilic attack or the protodeauration (Scheme 27). The Kinetic Isotopic Effect (KIE)¹¹¹ has been measured in different catalytic conditions. Using D₂O instead of H₂O, we observed a reduction of the TOF, which shifted from 62 to 17 h⁻¹ (compare entry 3 in Table 3 and entry 4 in Table 1), giving a Kinetic Isotopic Effect (KIE) equal to 3.7. In presence of NBu₄OTf (5%), the reaction is decelerated and the TOF decreases from 495 to 194 h⁻¹ (entries 1 and 3, Table 15) when D₂O is employed instead of H₂O, giving a KIE of 2.6. These KIE values suggest that, under our conditions, the turnover-limiting step is the proton shuttle (Scheme 27) in both conditions. However, the small decrease of the KIE when ionic additives are used may indicate a specific role of NBu₄OTf during the protodeauration step. In a recent paper by Straub,¹¹³ a KIE of 3-5 is observed for the hydration of terminal alkynes conducted in methanol, while Gagné and Widenhoefer reported a KIE of 5.3 for the gold-catalyzed intramolecular hydroalkoxylation of 2,2-diphenyl-4,5-hexadien-1-ol to a 2-vinyltetrahydrofuran derivative.¹¹⁴ These authors suggested that protonolysis of the gold-carbon bond was the turnover-limiting step in both cases. Preliminary DFT calculations seem to confirm the experimental findings. Complex [NHCAuOTf] (NHC = 1,3-dimethylimidazol-2-ylidene) has been chosen as a model for the catalytically active species, 2-butyne and H₂O have been selected as substrate and nucleophile, respectively, for the calculations. The influence of the OTf⁻ ion on the catalytic efficiency of [NHCAuOTf] in the water addition to 2-butyne process under examination has been thoroughly analysed. The role of the anion is emphasized in all the steps of the pathway, which are the pre-equilibrium, the nucleophilic attack of water to the Au-butyne complex and both proton transfers to the unsaturated carbon atom (protodeauration and protodeauration', Scheme 2). As previously observed for related alkoxylation of alkynes, in the nucleophilic attack two beneficial roles of the anion can be envisaged: (i) it holds the reactive water molecule in the right position for an anti-periplanar addition, acting as a template (Scheme 27); (ii) it enhances the nucleophilicity of the attacking water through the HOH...OTf⁻, which induces a polarization on the oxygen. For the protodeauration, the fact that anions can assist and facilitate proton transfers by lowering the energy barriers is well-known in the literature.¹¹⁵ In our calculation the proton is found between the OTf⁻ ion, oxygen and C2 (carbon not bonded to oxygen), therefore the first proton transfer takes place in one step. On the other hand, the second proton shuttle (Scheme 27) is much more difficult and the hydrogen bond ability and basicity of OTf⁻ is not sufficient to abstract the second proton from enol substrate (intermediate OSIP'). Preliminary calculations indicate that also the gold atom can participate in this step: a formal oxidative addition of HOTf to the gold (I) fragment followed by an easy insertion of the hydride into gold-C2 can take place, with an activation barrier for this protodeauration step larger than that of the nucleophilic attack, thus indicating the latter as the rate determining step of the overall mechanism.

We then studied the effect of the temperature and also screened different alkynes to verify the scope of this methodology. The increase of temperature has, as expected, a beneficial effect. When 3-hexyne is employed as the substrate and NBu_4OTf (5%) as the additive, an increase of the temperature by 10 °C resulted in a decrease of the reaction time of about 1h (from 30 to 40 °C) and about 1.5h (from 40 to 50 °C), while the TOF increased from 495 to 620 to 1267 h^{-1} (entries 2, 5 and 6, Table 15). Both internal alkynes with a higher molecular weight and terminal alkynes are less active than 3-hexyne (entries 7-11, Table 15). For 4-octyne, this could be due to the lower solubility of water in the organic phase, while for terminal alkynes it is known that they are less active in the nucleophilic attack reactions. It should be emphasised, however, that the TOF values here obtained are in line with those reported in the literature when protic solvents and Bronsted acids are employed.^{104a}

The use of neat conditions and solid additives has allowed us to easily recover the product at the end of the reaction by simple vacuum distillation. The product 3-hexanone was separated and obtained with an excellent degree of purity, without the need for chromatography or other similar dispendious techniques. Contemporarily, the catalyst/additive solid mixture can be easily separated from the product and can be reused by simple re-addition of 3-hexyne and water. We reused the catalyst up to 5 times, without loss of activity, reaching a final TON of 5000 at RT. This procedure gives us the possibility to obtain outstanding EMY and E-factor values (97 and 0.03, respectively). All these factors combined (low E-factor, high EMY, and recyclability) are in the correct range for sustainable production of bulk chemicals with homogeneous gold catalysts.

3

Conclusions and Perspectives

The reader's challenge is to replicate the experiment by reading the poem and to draw their own conclusions.

John Barton

In this thesis work we extended the mechanistic investigation of gold(I)-catalysed nucleophiles addition to unsaturated carbon-carbon bonds. As introduced in chapter 1.2.2, the generally accepted catalytic cycle consists of a three steps mechanism (preequilibrium, nucleophilic attack and protodeauration, Scheme 5), where all the three main gold containing species are charged. We succeeded in adding more information about the weak interactions and counterion effects that were no available before.

In chapter 2.1, we clearly demonstrated that the anion can play an effective role acting in different steps of the catalytic cycle. Both coordination ability and basicity have a great and under evaluated impact on the catalytic performances of gold complexes. Moreover, also the nature of the nucleophile is related to the anion effect. Considering the alkoxylation of alkynes our findings can be summarized with three limit cases (**Figure 45**). When the nucleophile cannot help itself (case 1), we observed a pure anion effect. The *classical* non-coordinating anions were the worst choice slowing down the reaction rate (for BArF^- no reaction at all was observed). Intermediate coordinating and basicity power of the anion OTs^- provides the best compromise to achieve an efficient catalyst: the preequilibrium with this anion is shifted toward the OSIP, deactivation of catalyst to a gold-methoxide is prevented and its characteristic basicity promotes the nucleophilic attack furthering a template between the complex and the nucleophile. When MeOH is used, the anion effect is mediated by the nucleophile itself that is more assisting the nucleophilic attack than less basic/coordinating anions (case 2). Finally, when a suitably functionalized alcohols is used (case 3) the anion effect is flattened as the nucleophile is much more able to help the nucleophilic attack.

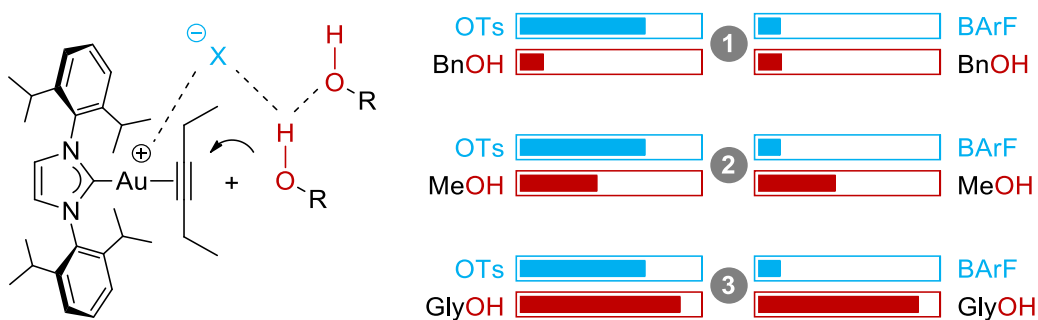


Figure 42. Role of the anion and the nucleophile in the methoxylation of 3-hexyne.

From our knowledge, not only the anion basicity and the coordination ability are important factors, but also the position seems to be crucial. Altering the backbone of NHC ligands could be a way to modify the Ion Pair (IP) structure of the complexes thus moving the anion closer or farther from the reaction site. In chapter 2.2, we have described the IP structure for different $[(\text{NHC})\text{-Au}(3\text{-hexyne})]\text{BF}_4$ complexes. Removing the aromaticity is not enough to markedly influence the ion pair structure and the anion still prefers to stay on the carbene-side. On the other hand, the extended aromaticity of an acenaphtene-based NHC makes the ion pair structure aspecific, with only a small preference for substrate side. The results underlined that ion pairs cannot be easily modified without large alterations of the NHC backbone.

For these reason we tried another carbene class, synthesizing four NAC based complexes baring different -NH and -OH polar moieties. We demonstrated that the ion pair structure of the gold complexes can be tuned by modifying the functional groups of the NAC ligand (Figure 43), and, more importantly, that the differences dramatically influence the catalytic performances of the NAC-gold catalysts. When the anion is forced to be far from the catalytic site by ancillary ligand-anion HB interactions, the catalytic performances are deteriorated and *vice versa*. The use of a polar solvent, that may break the IP, or specific additives, that may trap the anion, can flatten the differences between this set of catalysts (**7⁺**-**10⁺**).

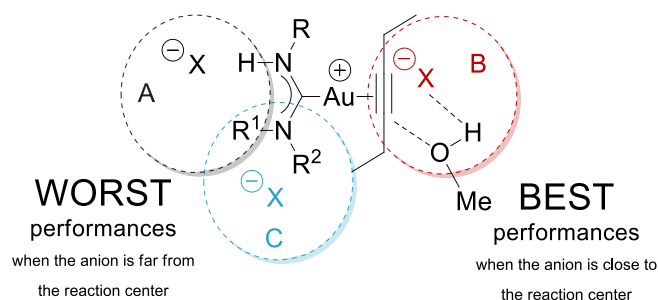


Figure 43. Rationalization of the catalysis performance depending on the anion position for NAC complexes.

The comparison between those complexes was possible because DFT calculations allowed us to give insights on the ion pair structures and to make sure, by the CDF approach, that the **7-10⁺** cations had the same acidity. Any catalytic activity variation was ascribed to the different ion pair structure.

Characterizing complex **9⁺** we have discovered that the rotational barrier of the C-N bond of the NAC ligand bound to gold (a NMR experimental observable) provides a selective measurement of one DCD bonding component, the metal-to-substrate π back-donation (**Figure 44** and chapter 2.3). This opens the possibility to characterize the electronic structure of the gold metal fragment by actually measuring how its π basicity is affected by the nature of the coordinated ligands. Thus it is possible to achieve a more rational control of ligand electronic effects when design new catalysts.

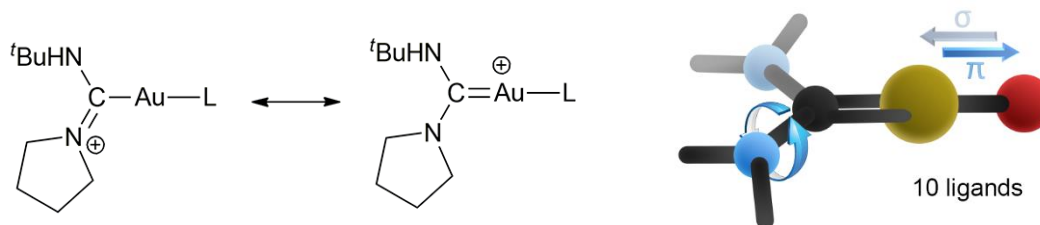


Figure 44. Resonance structures for complex **9⁺** and relationship of C-N rotational barrier with π back-donation on ligand.

In chapter 2.4 we demonstrated that the correct choice of the ligand L, in order to increase the performances of gold(I) complexes in catalysis, strongly depends on the nature of the anion X^- and *vice*

versa. When the Rate Determining Step (RDS) is the nucleophilic attack (as in the methoxylation of 3-hexyne) and NHC ligands are used, intermediate coordinating ability, basicity and hydrogen-bond acceptor property of OTs⁻ provides the best activities. Differently when phosphine ligands are used, we demonstrated by NMR experiments that OTs⁻ is interacting more with the gold cation and consequently the best results are achieved with OTf⁻ anion.(Figure 45).



Figure 45. Intuitive representation of ligand/anion effects in the methoxylation of 3-hexyne.

On the contrary, when the RDS is the protodeauration (as in the cyclization of propargylamides), the NHC carbene based complexes are following the basicity scale and non-coordinating and weakly basic anions (such as BF₄⁻) are the best choice; the more basic ones are strongly interacting with the proton removing it from the cycle and stabilizing the organogold species (INTERMEDIATE II, Scheme....). In the case of complexes bearing phosphanes, a complete different behaviour has been outlined. Thus, an intermediate-high coordination ability of the anion combined with its relatively high basicity and hydrogen-bond acceptor property (OTs⁻ and TFA⁻) has been found to accelerate the cycloisomerization of N-(prop-2-yn-yl)benzamide (Figure 46).



Figure 46. Intuitive representation of ligand/anion effects in the cyclisation of propargylamide.

A possible explanation can be found in the higher affinity of the counterion (especially OTs⁻) towards the gold fragment when the ancillary ligand L is a phosphane with respect to NHC: higher gold affinity accelerates the reaction in which the RDS is the protodeauration but inhibits it when the RDS is the nucleophilic attack, due to the shift of the ISIP-OSIP equilibrium (Scheme 1) in favour of ISIP.

This study clearly demonstrates that the interplay between ligand nature and anion effect is crucial in different steps of the catalytic cycle. However, the multiple roles played by counterions and L-Au⁺ fragments in chemical transformations require a more comprehensive computational and experimental studies of the ligand/anion correlation.

New and important information regarding the role of the anion, the effect of the ligand and the interplay between them have been obtained. Possible future developments, concerning homogeneous gold(I) catalysis, should include: the extension of the anion and ligand classes, pointing to different electronic and steric properties; and the study of more attractive reactions, from both the academic and industrial point of view. The same experimental and theoretical approach, set up for gold(I), may be used to explain the chemical reactivity of gold(III) complexes that more and more often are used as catalysts to find new frontiers in modern chemistry. Finally, the information obtained by our synergic approach may be the key to develop more green and sustainable conditions, for homogeneous gold catalysis-

A first steps in this direction are depicted in chapter 2.5. Taking advantage of counterion optimization we design a green and sustainable protocol (room temperature and solvent, silver, and acid-free conditions) for the hydration of alkyne, promoted by NHC Gold catalysts. It is possible to reduce the catalyst loading, obtaining a very low E-factor and E_{MY}. The solvent-free condition permit us to easily separate, by distillation, the liquid product from the catalyst. This leads to high purity products and allow the recycle of the catalyst. All these factors are in the correct range for sustainable bulk chemicals production with homogeneous gold catalysts, a topic still considered a chimera in the literature.

4

Experimental Part

A man of genius makes no mistakes; his errors are volitional and are the portals of discovery.

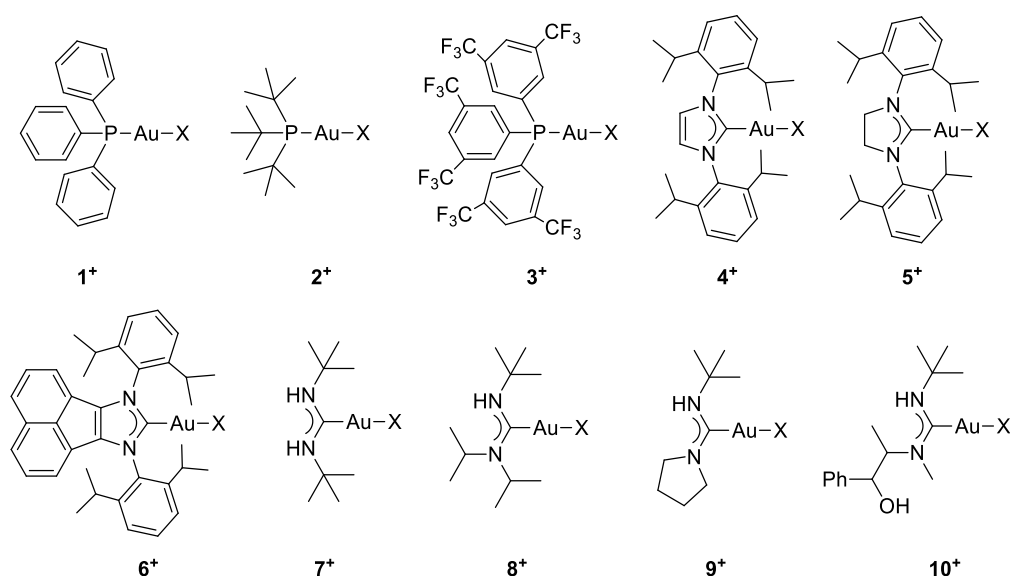
James Joyce

4.1 General Procedures and Materials

HAuCl_4 , tetrahydrothiophene (THT), 1,3-Bis(2,6-di-*i*-propyl-phenyl)imidazolium chloride $[\text{NHC(H)}]\text{Cl}$, 1,3-Bis(2,6-di-*i*-propylphenyl)-dihydroimidazolium chloride $[\text{sNHC(H)}]\text{Cl}$, *tert*-Butylisocyanide, *tert*-Buthylamine, diisopropylamine, pyrrolidine, (1R,2S)-(-)-Ephedrine, AgBF_4 , AgOTf , N,N'-dicyclohexylurea (DCU), triphenylphosphine and 3-hexyne were purchased from Ricci Chimica, Strem Chemicals and Sigma Aldrich and used without further purification. AgBF_4 was charged in Schlenk flask and stored under nitrogen atmosphere at -20°C . $[\text{NHC(H)}]\text{Cl}$ ²⁰⁵ and $[\text{NHC(BIAN)H}]\text{Cl}$,¹²⁰ $[(\text{THT})\text{AuCl}]$,⁴⁹ $[(\text{Ph}_3\text{P})\text{AuCl}]$,²⁰⁶ $[(\text{tBu}_3\text{P})\text{AuCl}]$,²⁰⁷ $[(\text{PAR}^F)\text{AuCl}]$,^{70b} $[(\text{NHC})\text{AuCl}]$,¹²⁶ and N-(prop-2-yn-1-yl)benzamide²⁰⁸ were synthesized according to the literature methods. All manipulations of moisture-sensitive materials were performed in flamed Schlenk glassware on a Schlenk line, interfaced to a high vacuum pump, or within a nitrogen filled glove box. All the new compound were characterized in solution by ^1H , ^{13}C , ^{19}F , ^{31}P NMR spectroscopies. One- and two dimensional ^1H , ^{13}C , ^{19}F NMR spectra were measured on Bruker AC-200 and Bruker DRX 400 spectrometers. Typical mixing times were 600 ms for the Overhauser experiments and within the range 20-400 ms for EXSY experiments. Referencing is relative to TMS (^1H and ^{13}C), CCl_3F (^{19}F) and 85% H_3PO_4 (^{31}P). The elemental analyses were carried out with a Carlo Erba 1106 elemental analyser.

4.2 Synthesis

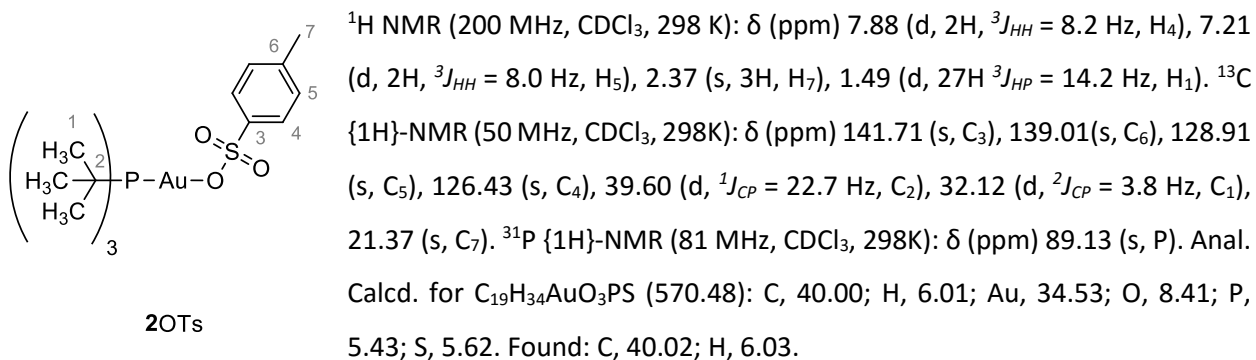
All the complexes used in this work are here reported (Scheme 28), 10Tf ,²⁰⁹ 10Ts ,^{97a} 1TFA ,²¹⁰ 40Tf ,²¹¹ 40Ac ,²¹² 4BF_4 ,¹⁰⁶ and 40Tf^{211} were prepared as previously reported.



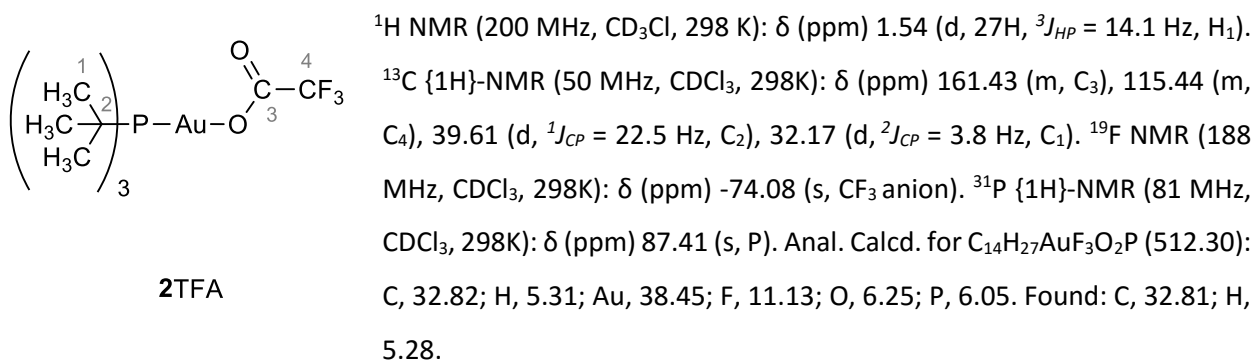
Scheme 28. Representation of all the complexes use in this work.

Some of the catalysts, when not otherwise specified, were generated *in situ* starting from their chloride precursor by addition of the proper silver salt.

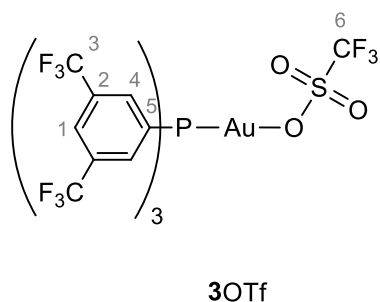
Synthesis of [(tri-tert-butylphosphine)gold(I)] p-toluenesulfonate (2OTs). [(^tBu₃P)AuCl] (48 mg, 0.11 mmol) was dissolved in 5 mL of CH₂Cl₂/acetone (5:1). Subsequently, 1.1 eq (0.12 mmol) of AgOTs was added, leading to the precipitation of AgCl. The reaction mixture was stirred in the dark overnight, and then dried. After the addition of 2 mL of fresh dichloromethane, the mixture was filtered on Celite® pad, washed with 3x1 mL of CH₂Cl₂, concentrated under vacuum and then *n*-pentane (4 mL) was added, resulting in the formation of precipitate. The resulting solid was filtered off and washed with 3x2 mL of *n*-pentane. Then dried under vacuum to afford the product as a white powder (yield 86%).



Synthesis of [(tri-tert-butylphosphine)gold(I)] trifluoroacetate (2TFA). [(^tBu₃P)AuCl] (35 mg, 0.08 mmol) was dissolved in 4 mL of CH₂Cl₂/acetone (5:1). Subsequently, 1.2 eq (0.10 mmol) of AgTFA was added, leading to the precipitation of AgCl. The reaction mixture was stirred in the dark overnight, and then dried. After the addition of 2 mL of fresh dichloromethane, the mixture was filtered on Celite® pad, washed with 3x1 mL of CH₂Cl₂, concentrated under vacuum and then *n*-pentane (4 mL) was added, resulting in the formation of precipitate. The resulting solid was filtered off and washed with 3x2 mL of *n*-pentane. Then dried under vacuum to afford the product as a white powder (yield 60.7%).



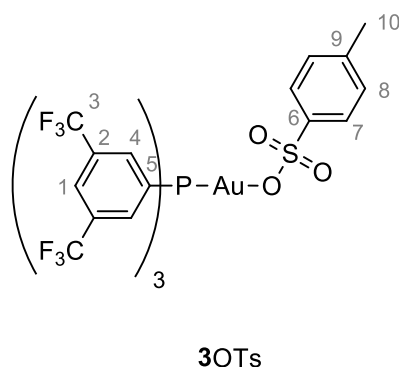
Synthesis of [tris(3,5-bis(trifluoromethyl)phenyl)phosphine gold(I)] trifluoromethanesulfonate (3OTf). [(PArF)AuCl] (100 mg, 0.11 mmol) was dissolved in 4mL of CH₂Cl₂. Subsequently, 1.1 eq (0.12 mmol) of AgOTf was added, leading to the precipitation of AgCl. After 1 h at room temperature, the reaction mixture was filtered on Celite® pad, washed with 3x1 mL of CH₂Cl₂, concentrated under vacuum and then *n*-pentane (4mL) was added, resulting in the formation of precipitate. The resulting solid was filtered off and washed with 3x2 mL of *n*-pentane. Then dried under vacuum to afford the product as a white powder (yield 91%).



¹H NMR (200 MHz, CD₂Cl₂, 298 K): δ (ppm) 8.27 (s, 3H, H₁), 8.04 (d, 6H, ³J_{HP} = 13.5 Hz, H₄). ¹³C{¹H}-NMR (50 MHz, CD₂Cl₂, 298K): δ(ppm) 133.34 (dq, ²J_{CF} = 34.7 Hz, ³J_{CP} = 12.8 Hz, C₂), 134.29 (dq, ²J_{CP} = 15.3 Hz, ³J_{CF} = 3.3 Hz, C₄), 128.62 (m, C₁), 128.41 (d, ¹J_{CP} = 67.6 Hz, C₅), 125.27 (q, ¹J_{CF} = 273 Hz, C₃). 120.40 (q, ¹J_{CF} = 318 Hz, C₆). ¹⁹F NMR (188 MHz, CD₂Cl₂, 298K): δ (ppm) -63.38 (s, CF₃), -77.04 (s, CF₃ anion). ³¹P {¹H}-NMR (81 MHz, CD₂Cl₂, 298K): δ (ppm) 30.53 (s, P). Anal. Calcd. for C₂₅H₉AuF₂₁O₃PS (1016.31): C,

29.54; H, 0.89; Au, 19.38; F, 39.26; O, 4.72; P, 3.05; S, 3.16. Found: C, 29.59; H, 0.88.

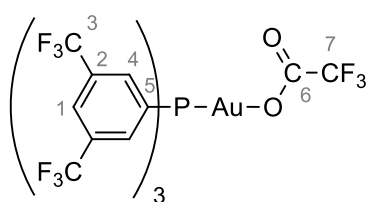
Synthesis of [tris(3,5-bis(trifluoromethyl)phenyl)phosphine gold(I)] p-toluenesulfonate (3OTs). [(PArF)AuCl] (100 mg, 0.11 mmol) was dissolved in 5mL of CH₂Cl₂/acetone (5:1). Subsequently, 1.1 eq (0.12 mmol) of AgOTs was added, leading to the precipitation of AgCl. The reaction mixture was stirred overnight, and then dried. After the addition of 2 mL of fresh dichloromethane, the mixture was filtered on Celite® pad, washed with 3x1 mL of CH₂Cl₂, concentrated under vacuum and then *n*-pentane (4mL) was added, resulting in the formation of precipitate. The resulting solid was filtered off and washed with 3x2 mL of *n*-pentane. Then dried under vacuum to afford the product as a white powder (yield 93%).



¹H NMR (200 MHz, CDCl₃, 298 K): δ (ppm) 8.22 (s, 3H, H₁), 7.97 (d, 6H, ³J_{HP} = 13.5 Hz, H₄), 7.85 (d, 2H, ³J_{HH} = 7.3 Hz, H₇), 7.26 (d, 2H, ³J_{HH} = 7.4 Hz, H₈), 2.40 (s, 3H, H₁₀). ¹³C {¹H}-NMR (50 MHz, CDCl₃, 298K): δ (ppm) 142.02 (s, C₆), 139.26 (s, C₉), 134.53 (dq, ²J_{CF} = 34.8 Hz, ³J_{CP} = 12.5 Hz, C₂), 133.61 (dd, ³J_{CF} = 3.2 Hz, ²J_{CP} = 15.4 Hz, C₄), 129.21 (s, C₈), 128.86 (d, ¹J_{CP} = 64.8 Hz, C₅), 127.79 (m br, C₁), 126.38 (s, C₇), 122.03 (q, ¹J_{CF} = 273.7 Hz, C₃), 21.40 (s, C₁₀). ¹⁹F NMR (188 MHz, CDCl₃, 298K): δ (ppm) -63.88 (s, CF₃). ³¹P {¹H}-NMR (81 MHz, CDCl₃, 298K): δ (ppm) 32.45 (s,

P). Anal. Calcd. for $C_{31}H_{16}AuF_{18}O_3PS$ (1038.43): C, 35.86; H, 1.55; Au, 18.97; F, 32.93; O, 4.62; P, 2.98; S, 3.09. Found: C, 35.90; H, 1.58.

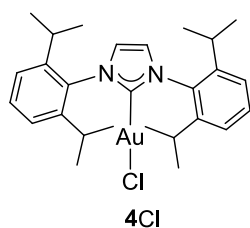
Synthesis of [tris(3,5-bis(trifluoromethyl)phenyl)phosphine gold(I)] trifluoroacetate (3TFA). [(PArF)AuCl] (71.7 mg, 0.08 mmol) was dissolved in 4 mL of CH_2Cl_2 /acetone (5:1). Subsequently, 1.2 eq (0.10 mmol) of AgTFA was added, leading to the precipitation of AgCl. The reaction mixture was stirred overnight, and then dried. After the addition of 2 mL of fresh dichloromethane, the mixture was filtered on Celite® pad, washed with 3x1 mL of CH_2Cl_2 , concentrated under vacuum and then *n*-pentane (4 mL) was added, resulting in the formation of precipitate. The resulting solid was filtered off and washed with 3x2 mL of *n*-pentane. Then dried under vacuum to afford the product as a white powder (yield 60.7%).



3TFA

1H NMR (200 MHz, CD_2Cl_2 , 298 K): δ (ppm) 8.25 (s, 3H, H_1), 8.06 (d, 6H, $^3J_{HP} = 13.2$ Hz, H_4). ^{13}C { 1H }-NMR (50 MHz, CD_2Cl_2 , 298K): δ (ppm) 161.60 (m, C_6), 134.01 (m br, C_4), 133.93 (dq, $^2J_{CF} = 34.7$ Hz, $^3J_{CP} = 12.5$ Hz, C_2), 128.96 (d, $^1J_{CP} = 65.1$ Hz, C_5), 128.05 (m br, C_1), 122.36 (q, $^1J_{CF} = 272.9$ Hz, C_3), 115.19 (m br, C_7). ^{19}F NMR (188 MHz, CD_2Cl_2 , 298K): δ (ppm) -63.35 (s, CF_3), -74.01 (s, CF_3 anion). ^{31}P { 1H }-NMR (81 MHz, CD_2Cl_2 , 298K): δ 30.97 (s, P). Anal. Calcd. for $C_{26}H_9AuF_{21}O_2P$ (980.26): C, 31.86; H, 0.93; Au, 20.09; F, 40.70; O, 3.26; P, 3.16. Found: C, 31.84; H, 0.92.

Synthesis of [(NHC)AuCl] (4Cl). A Schlenk flask was charged, under air, with 276 mg of [NHC(H)Cl] (0.65 mmol), 208 mg of [(THT)AuCl] (0.67 mmol) and 90 mg of finely ground K_2CO_3 (0.65 mmol). were added in a Schlenk tube with a 5:1 solution of CH_2Cl_2 /MeOH. The reaction mixture was stirred at room temperature for 3 days. The reaction mixture was filtered on Celite® pad, dried under vacuum and then 2 mL of pure CH_2Cl_2 was added. Subsequently the addition of 8 mL of *n*-pentane resulted in the formation of a precipitate. The resulting solid was filtered off and washed with 3x3 mL of *n*-pentane. Then dried under vacuum to afford the product as a white powder, 143 mg (97%).

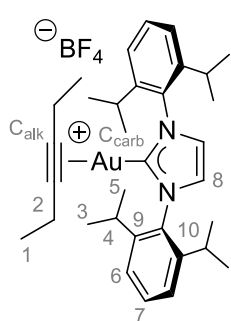


4Cl

1H NMR (200 MHz, CD_2Cl_2 , 293 K): δ (ppm) 7.57 (t, 2H, $^3J_{HH} = 7.8$ Hz, $CHAr$), 7.35 (d, 4H, $^3J_{HH} = 7.8$ Hz, $CHAr$), 7.24 (s, 2H, CH_{imid}), 2.56 (sept, 4H, $^3J_{HH} = 6.9$ Hz, $CH(CH_3)_2$), 1.34 (d, 12H, $^3J_{HH} = 6.9$ Hz, $CH(CH_3)_2$), 1.23 (d, 12H, $^3J_{HH} = 6.9$ Hz, $CH(CH_3)_2$). ^{13}C -{ 1H }-NMR(50 MHz, CD_2Cl_2 ,293 K): δ (ppm) 175.7 (s, $C-Au$), 146.4 (s, CAr), 134.6 (s, CAr), 131.2 (s, CAr), 124.8 (s, CAr), 123.9 (s, C_{imid}), 29.4 (s, $CH(CH_3)_2$),

24.7 (s, CH(CH₃)₂), 24.3 (s, CH(CH₃)₂). Anal. Calcd. for C₂₇H₃₆AuClN₂ (621.01): C, 52.22; H, 5.84; Au, 31.72; Cl, 5.71; N, 4.51 Found: C 52.33; N 4.60; H 5.91.

Synthesis of [(NHC)Au]BF₄ (4BF₄). In a Schlenk tube with a 2 mL of CH₂Cl₂ were added 111 mg of 4Cl (0.18 mmol), 40 μL of 3-esyne (0.36 mmol) and finally 60 mg of AgBF₄ (0.31 mmol). The reaction mixture was stirred at room temperature for 1 h. The later was filtered on Celite® pad and then the volume was reduced to minimum. The subsequent addition of *n*-pentane, 5 mL, resulted in the formation of a precipitate. The resulting solid was filtered off and washed with 3x3 mL of *n*-pentane, dried under vacuum to afford the product as a white powder, 129 mg (95%).

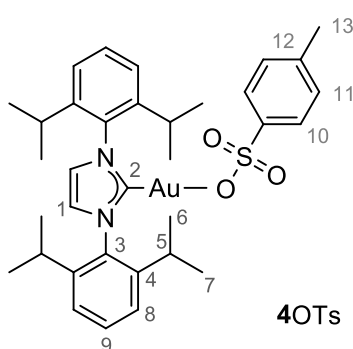


4BF₄

¹H NMR (400 MHz, CD₂Cl₂, 298 K): δ (ppm) 7.62 (t, 2H, ³J_{HH} = 7.9 Hz, H₇), 7.55 (s, 2H, H₈), 7.41 (d, 4H, ³J_{HH} = 7.8 Hz, H₆), 2.56 (sept, 4H, ³J_{HH} = 7.0 Hz, H₄), 2.26 (m, 4H, H₂), 1.34 (d, 12H, ³J_{HH} = 7.0 Hz, H₃), 1.31 (d, 12H, ³J_{HH} = 7.5 Hz, H₅), 0.64 (t, 6H, ³J_{HH} = 7.5 Hz, H₁). ¹⁹F NMR (376.42 MHz, CD₂Cl₂, 297 K): δ (ppm) -153.56 (br, ¹¹BF₄), -153.51 (br, ¹⁰BF₄). ¹³C-{¹H} NMR (100.5 MHz, CD₂Cl₂, 297 K): δ (ppm) 178.03 (s, C_{carb}), 146.22 (s, C₉), 133.41 (s, C₁₀), 131.84 (s, C₇), 125.37 (s, C₆), 125.00 (s, C₈), 87.68 (s, C_{alk}), 29.27 (s, C₄), 24.82 (s, C₃), 24.20 (s, C₅), 15.16 (s, C₂), 13.50 (s, C₁). Anal. Calcd for C₃₃H₄₆AuBF₄N₂ (754.50) C, 52.53; H, 6.15; Au, 26.11; B, 1.43; F, 10.07; N, 3.71. Found:

C, 52.50; H, 6.18; N, 3.74.

Synthesis of [(NHC)Au]OTs (4OTs). [(NHC)AuCl] (100 mg, 0.161 mmol) was dissolved in the minimal amount of CH₂Cl₂. Subsequently, 1.1 eq (0.177 mmol) of AgOTs was added, leading to the precipitation of AgCl. After 1 h at room temperature, the reaction mixture was filtered on Celite® pad, washed with 3x1 mL of CH₂Cl₂, concentrated under vacuum and then *n*-hexane (4mL) was added, resulting in the formation of precipitate. The resulting solid was filtered off and washed with 3x2 mL of *n*-hexane. Then dried under vacuum to afford the product as a white powder (yield 93%).

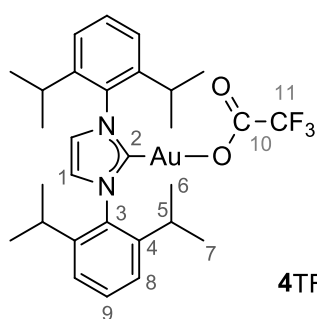


4OTs

¹H NMR (400 MHz, CDCl₃, 298 K): δ (ppm) 7.55 (t, 2H, *J*_{3^{HH}} = 7.8, H₉), 7.39 (d, 2H, *J*_{3^{HH}} = 7.3, H₁₀), 7.31 (d, 4H, d, 2H, *J*_{3^{HH}} = 7.9, H₈), 7.21 (s, 2H, H₁), 6.98 (d, 2H, *J*_{3^{HH}} = 7.4, H₁₁), 2.47 (sept, 4H, *J*_{3^{HH}} = 6.8, H₅), 2.32 (s, 3H, H₁₃), 1.29 (d, 12H, *J*_{3^{HH}} = 6.8, H₆), 1.21 (d, 12H, *J*_{3^{HH}} = 6.8, H₇). ¹³C-{¹H}-NMR (400 MHz, CDCl₃, 298 K): δ (ppm) 164.56 (s, C₂), 145.69 (s, C₄), 133.86 (s, C₉), 131.12 (s, C₃), 128.87 (s, C_{Ar}-OTs), 126.42 (s, C_{Ar}-OTs), 124.57 (s, C₁), 123.59 (s, C₈), 123.20 (s, C_{Ar}-OTs) 29.05 (s, C₅), 24.32 (d,

C6-7), 21.58 (s, CH₃-OTs). Anal. Calcd. for C₃₄H₄₄AuN₂O₃S (757.76): C, 53.89; H, 5.85; Au, 25.99; N, 3.70; O, 6.33; S, 4.23. Found: C, 53.91; H, 5.84; N, 3.6.

Synthesis of [(NHC)Au]TFA (4TFA). [(NHC)AuCl] (100 mg, 0.161 mmol) was dissolved in the minimal amount of CH₂Cl₂. Subsequently, 1.1 eq (0.177 mmol) of AgTFA was added, leading to the precipitation of AgCl. After 1 h at room temperature, the reaction mixture was filtered on Celite® pad, washed with 3x1 mL of CH₂Cl₂, concentrated under vacuum and then n-hexane (4mL) was added, resulting in the formation of precipitate. The resulting solid was filtered off and washed with 3x2 mL of n-hexane. Then dried under vacuum to afford the product as a white powder (yield 87%).

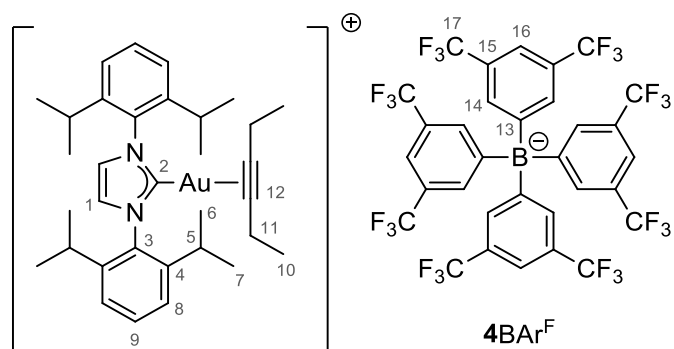


4TFA

¹H NMR (400 MHz, CD₂Cl₂, 298 K): δ (ppm) 7.58 (t, 2H, *J*_{3^{HH}} = 7.8, H9), 7.37 (d, 4H, *J*_{3^{HH}} = 7.7, H8), 7.28 (s, 2H, H1), 2.56 (sept, 4H, *J*_{3^{HH}} = 6.9, H5), 1.35 (d, 12H, *J*_{3^{HH}} = 6.8, H6), 1.24 (d, 12H, *J*_{3^{HH}} = 6.8, H7). ¹⁹F NMR (400 MHz, CD₂Cl₂, 298 K): δ (ppm) -73.89 (s, CF₃). ¹³C{¹H}-NMR (400 MHz, CD₂Cl₂, 298 K): δ (ppm) 166.01 (s, C2), 162.11 (bs, C15), 146.46 (s, C4), 134.44 (s, C9), 131.27 (s, C3), 124.85 (s, C1), 124.37 (s, C8), 116.50 (s, C14), 29.49 (s, C5),

24.52 (d, C6-7). Anal. Calcd. for C₂₉H₃₇AuF₃N₂O₂ (699.58) C, 49.79; H, 5.33; Au, 28.16; F, 8.15; N, 4.00; O, 4.57. Found: C, 49.82; H, 5.84; N, 3.86.

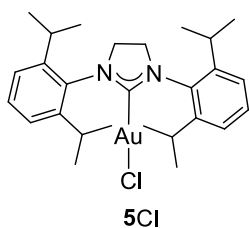
Synthesis of [(NHC)Au]BAR^F (4BAR^F). [(NHC)AuCl] (49.7 mg, 0.08 mmol) and 3-hexyne (14 μL, 0.12 mmol) were added in a Schlenk tube in 1 mL of CH₂Cl₂. Subsequently AgBF₄ (23 mg, 0.12 mmol) was added. The reaction mixture was stirred at room temperature for 15 min observing the precipitation of AgCl. The reaction mixture was filtered on Celite® pad, washed with 3x1 mL of CH₂Cl₂, concentrated under vacuum and then NaBAR^F (77.8 mg, 0.09 mmol) was added, resulting in the formation of a thin new precipitate. The reaction mixture was filtered again on Celite® pad, washed with 3x1 mL of CH₂Cl₂, concentrated under vacuum and then n-pentane (4mL) was added, resulting in the formation of precipitate. The resulting solid was filtered off and washed with 3x2 mL of n-pentane. Then dried under vacuum to afford the product as a mild-yellow powder (yield 85%).



^1H NMR (CD_2Cl_2 , 400 MHz, 298 K): δ (ppm) 7.72 (bs, 8H, H14), 7.57 (t, $J_3^{\text{HH}} = 7.8$ Hz, 2H, H9), 7.56 (bs, 4H, H16), 7.43 (s, 2H, H1), 7.37 (d, $J_3^{\text{HH}} = 7.6$ Hz, 4H, H8), 2.51 (sept, $J_3^{\text{HH}} = 6.8$ Hz, 4H, H5), 2.30 – 2.07 (m, $J_3^{\text{HH}} = 7.3$ Hz, 4H, H11), 1.29 (d, $J_3^{\text{HH}} = 6.8$ Hz, 12H, H6 or H7), 1.26 (d, $J_3^{\text{HH}} = 6.8$ Hz, 12H, H6 or H7), 0.61 (t, $J_3^{\text{HH}} = 7.4$ Hz, 6H,

H10). ^{19}F NMR (400 MHz, CD_2Cl_2 , 298 K): δ (ppm) -62.84 (s, CF_3). $^{13}\text{C}\{^1\text{H}\}$ -NMR (400 MHz, CD_2Cl_2 , 298 K): δ (ppm) 178.60 (s, C2), 162.5 (m, C13), 146.49 (s, C4), 135.50 (s, C14), 133.61 (s, C3), 132.22 (s, C9), 129.44 (m, C15), 126.65 (s, C17), 125.33 (bs, C1 and C8), 118.15 (s, C16), 87.92 (s, C12), 29.58 (s, C5), 24.98 (d, C6-7), 24.36 (d, C6-7), 15.34 (s, C11), 13.65 (s, C10). Anal. Calcd. for $\text{C}_{65}\text{H}_{58}\text{AuBF}_4\text{N}_2$ (1530.91): C, 51.00; H, 3.82; Au, 12.87; B, 0.71; F, 29.78; N, 1.83. Found: C, 51.02; H, 3.84; N, 1.82.

Synthesis of sNHC imidazolium chloride (5Cl). sNHC imidazolium chloride 227.2 mg (0.41 mmol), 168.9 mg of KHCO_3 (1.69 mmol) and 131.3 mg of $[(\text{THT})\text{AuCl}]$ (0.41 mmol) were added in a Schlenk tube with a 5:1 solution of $\text{CH}_2\text{Cl}_2/\text{MeOH}$. The reaction mixture was stirred at room temperature for 3 days. The reaction mixture was filtered on celite pad, dried under vacuum and then 2 mL of pure CH_2Cl_2 was added. Subsequently the addition of 8 mL of pentene resulted in the formation of a precipitate. The resulting solid was filtered off and washed with 3x3 mL of pentane. Then dried under vacuum to afford the product as a yellow-green powder 305 mg (99%).

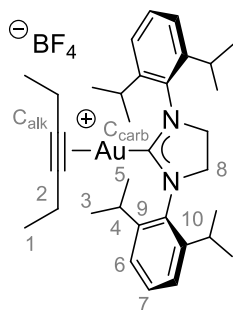


^1H NMR (400 MHz, CD_2Cl_2 , 298 K): δ (ppm) 7.43 (t, 2H, $^3J_{\text{HH}} = 7.8$ Hz, CH_{arom}), 7.25 (d, 4H, $^3J_{\text{HH}} = 7.8$ Hz, CH_{arom}), 4.06 (s, 4H, CH_2 imid), 3.07 (sept, 4H, $^3J_{\text{HH}} = 6.8$ Hz, - $\text{CH}(\text{CH}_3)_2$), 1.43 (d, 12H, $^3J_{\text{HH}} = 6.8$ Hz, - $\text{CH}(\text{CH}_3)_2$), 1.36 (d, 12H, $^3J_{\text{HH}} = 6.8$ Hz, - $\text{CH}(\text{CH}_3)_2$). $^{13}\text{C}\{^1\text{H}\}$ NMR (100.5 MHz, CD_2Cl_2 , 297 K): δ (ppm) 196.07 (s), 146.55 (s), 134.06 (s), 130.06 (s), 124.65 (s), 53.47 (s), 28.97 (s), 25.14 (s), 24.13 (s). Anal.

Calcd for $\text{C}_{27}\text{H}_{38}\text{AuClN}_2$ (623.02) C, 52.05; H, 6.15; Au, 31.61; Cl, 5.69; N, 4.50. Found: C, 52.06; H, 6.11; N, 4.51.

Synthesis of sNHC imidazolium tetrafluoroborate (5BF₄). 5Cl 100 mg (0.16 mmol) and AgBF_4 39 mg (0.20 mmol) were charged in a Schlenk flask. The Schlenk flask was interfaced to the high-vacuum line and about 5 mL of CH_2Cl_2 and 2.0 equivalent of 3-hexyne (36.2 μL) were added by micrometric syringes at RT. The mixture was stirred and a light grey solid (AgCl) formed in a few minutes. The suspension was filtered

through a Celite® pad. The solution was concentrated to minimum volume and 3 mL of *n*-pentane were added. The formed solid was filtered, washed with *n*-pentane and dried under vacuum obtaining 97 mg of the product (80%).

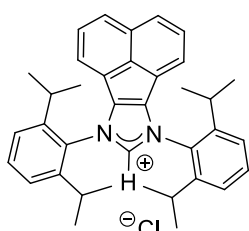


5BF₄

¹H NMR (400 MHz, CD₂Cl₂, 298 K): δ (ppm) 7.46 (t, 2H, ³J_{HH} = 7.8 Hz, H₇), 7.29 (d, 4H, ³J_{HH} = 7.6 Hz, H₆), 4.28 (s, 4H, H₈), 3.07 (sept, 4H, ³J_{HH} = 6.9 Hz, H₄), 2.04 (m, 4H, H₂), 1.33 (d, 12H, ³J_{HH} = 7.0 Hz, H₃), 1.28 (d, 12H, ³J_{HH} = 7.1 Hz, H₅), 0.47 (t, 6H, ³J_{HH} = 7.5 Hz, H₁). ¹³C-¹H} NMR (100.5 MHz, CD₂Cl₂, 297 K): δ (ppm) 199.2 (s, C_{carb}), 147.50 (s, C₉), 133.45 (s, C₁₀), 131.28 (s, C₇), 125.37 (s, C₆), 125.00 (s, C₈), 87.68 (s, C_{alk}), 29.54 (s, C₄), 25.61 (s, C₃), 24.44 (s, C₅), 15.14 (s, C₂), 13.42 (s, C₁). Anal. Calcd for C₃₃H₄₈AuBF₄N₂ (756.52) C, 52.39; H, 6.40; Au, 26.04; B, 1.43; F, 10.05; N, 3.70. Found:

52.31; H, 6.48; N, 3.64.

Synthesis of NHC(BIAN) imidazolium chloride (P6). NHC(BIAN) imidazolium chloride was prepared according to a literature procedure. ¹²⁰ NHC(BIAN) 484 mg (0.97 mmol) and 1.5 mL of methoxy(methyl)chloride (19.4 mmol) were added in a argon flushed Schlenk tube; the reaction mixture was stirred at reflux (70 °C) overnight. Cooling the reaction mixture to ambient temperature and the subsequent addition of 10 mL of diethyl ether resulted in the formation of a yellow precipitate. The resulting solid was filtered off and washed with 3x3 mL of Et₂O and with 2x2 mL of *n*-pentane. Then dried under vacuum to afford the product as a yellow powder 493 mg (92.5%).



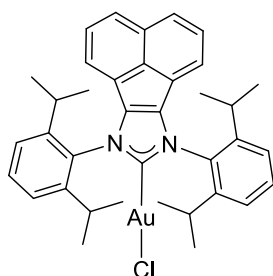
P6

¹H NMR (200 MHz, CDCl₃, 298 K): δ (ppm) 12.11 (bs, 1H), 8.02 (d, ³J_{HH} = 8.3 Hz, 2H), 7.68 (t, ³J_{HH} = 8.3 Hz, 2H), 7.62 (t, ³J_{HH} = 8.3 Hz, 2H), 7.58 (d, ³J_{HH} = 7.7 Hz, 2H), 7.21 (d, ³J_{HH} = 7.1 Hz, 2H), 2.27 (sept, ³J_{HH} = 6.9 Hz, 4H), 1.40 (d, ³J_{HH} = 6.8 Hz, 12H), 1.16 (d, ³J_{HH} = 6.8 Hz, 12H). ¹³C-¹H} NMR (50 MHz, CDCl₃, 298 K): δ (ppm) 145.44 (s), 142.55(s), 138.08(s), 132.68(s), 130.87(s), 130.40(s), 129.43(s), 128.74(s), 125.46(s), 123.46(s), 123.37(s), 29.75(s), 24.84(s), 23.51(d). Anal. Calcd for C₃₇H₄₂ClN₂ (550.20) C, 80.77; H, 7.69; Cl, 6.44; N, 5.09. Found: C, 80.75; H, 7.75; N, 5.15.

C₃₇H₄₂ClN₂ (550.20) C, 80.77; H, 7.69; Cl, 6.44; N, 5.09. Found: C, 80.75; H, 7.75; N, 5.15.

Synthesis of NHC(BIAN)[AuCl] (6Cl). NHC(BIAN) imidazolium chloride 227.2 mg (0.41 mmol), 168.9 mg of KHCO₃ (1.69 mmol) and 131.3 mg of [(THT)AuCl] (0.41 mmol) were added in a Schlenk tube with a 5:1 solution of CH₂Cl₂/MeOH. The reaction mixture was stirred at room temperature for 3 days. The reaction

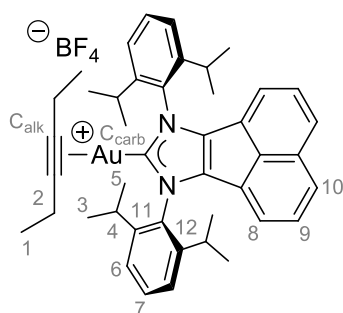
mixture was filtered on celite pad, dried under vacuum and then 2 mL of pure CH₂Cl₂ was added. Subsequently the addition of 8 mL of penetene resulted in the formation of a precipitate. The resulting solid was filtered off and washed with 3x3 mL of *n*-pentane. Then dried under vacuum to afford the product as a yellow-green powder 305 mg (99%).



6Cl

¹H NMR (400.3 MHz, CD₂Cl₂, 298 K): δ (ppm) 7.84 (d, 2H, ³J_{HH} = 8.4 Hz, H10), 7.68 (t, 2H, ³J_{HH} = 7.8 Hz, H7), 7.46 (dd, 2H, ³J_{HH} = 8.4 Hz, ³J_{HH} = 7.0 Hz, H9), 7.45 (d, 4H, ³J_{HH} = 7.9 Hz, H6), 7.03 (d, 2H, ³J_{HH} = 7.1 Hz, H8), 2.83 (*sept*, 4H, ³J_{HH} = 7.2 Hz, H4), 1.38 (d, 12H, ³J_{HH} = 6.9 Hz, H3), 1.21 (d, 12H, ³J_{HH} = 6.9 Hz, H5). ¹³C-¹H NMR (100.5 MHz, CD₂Cl₂, 297 K): δ (ppm) 175.6 (s), 146.11 (s), 138.41 (s), 133.12 (s), 131.33 (s), 130.56 (s), 128.96 (s), 128.26 (s), 125.62 (s), 125.00 (s), 121.70 (s), 29.35 (s), 24.59 (s), 23.91 (s). Anal. Calcd for C₃₇H₄₀AuClN₂ (745.15) C, 59.64; H, 5.41; Au, 26.43; Cl, 4.76; N, 3.76. Found: C, 59.68; H, 5.47; N, 3.72.

Synthesis of NHC(BIAN)[AuCl](3-hexyne) BF₄ (6BF₄). In a Schlenk tube with a 3 mL of CH₂Cl₂ were added 128.6 mg (0.17 mmol) of NHC(BIAN)[AuCl], 40 μL (0.35 mmol) of 3-hexyne and finally 52.6 mg (0.27 mmol) of AgBF₄. The reaction mixture was stirred at room temperature for 1-2 h. The reaction mixture was filtered on celite pad then the volume was reduced to minimum. Subsequently the addition of 8 mL of penetene resulted in the formation of a precipitate. The resulting solid was filtered off and washed with 3x3 mL of pentane. Then dried under vacuum to afford the product as a yellow powder 130 mg (85.7%).

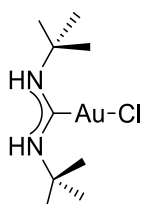


6BF₄

¹H NMR (400.13 MHz, CD₂Cl₂, 297 K): δ (ppm) 8.01 (d, 2H, ³J_{HH} = 8.4 Hz, H10), 7.75 (t, 2H, ³J_{HH} = 7.8 Hz, H7), 7.59 (dd, 2H, ³J_{HH} = 8.4 Hz, ³J_{HH} = 7.0 Hz, H9), 7.54 (d, 4H, ³J_{HH} = 7.9 Hz, H6), 7.26 (d, 2H, ³J_{HH} = 7.1 Hz, H8), 2.83 (*sept*, 4H, ³J_{HH} = 7.2 Hz, H4), 2.34 (*mult*, 4H, H2), 1.38 (d, 12H, ³J_{HH} = 6.9 Hz, H3), 1.21 (d, 12H, ³J_{HH} = 6.9 Hz, H5), 0.73 (t, 6H, ³J_{HH} = 7.5 Hz, H1). ¹⁹F NMR (376.42 MHz, CD₂Cl₂, 297 K): δ (ppm) -153.97 (br, ¹¹BF₄), -153.92 (br, ¹⁰BF₄). ¹³C-¹H NMR (100.5 MHz, CD₂Cl₂, 297 K): δ (ppm) 181.54 (s, C_{carb}), 146.22 (s, C11), 139.36 (s), 132.25 (s, C7), 132.16 (s), 131.09 (s), 130.42 (s), 130.01

(s, C10), 128.58 (s, C9), 125.46 (s, C6), 124.55 (s), 122.56 (s, C8), 87.92 (s, C_{alk}), 29.49 (s, C4), 24.87 (s, C3), 24.10 (s, C5), 15.28 (s, C2), 13.59 (s, C1). Anal. Calcd for C₄₃H₅₀AuBF₄N₂ (787.64) C, 58.78; H, 5.74; Au, 22.42; B, 1.23; F, 8.65; N, 3.19. Found: C, 58.79; H, 5.69; N, 3.17.

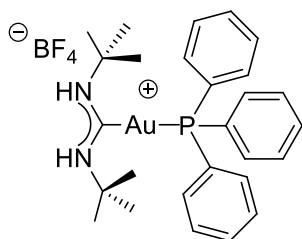
Synthesis of [(tert-Butylamino)₂methylidene]gold(I) Chloride (7Cl). 7Cl was prepared according to a literature procedure.^{133f} First 1.2 equivalents of tertbutylamine were added to a solution of [tert-Butylisocyano]-gold(I) Chloride 173 mg (0.55 mmol) in 4 mL of dichloromethane. The mixture was stirred at room temperature and protect from the light for 3 days. Dichloromethane was added to the mixture (that result milky) until it became limpid, then was filtered on a Silica pad, concentrated to minimum volume and precipitated with pentane. We obtained the product as a white solid; yield: 154 mg (72.6%).



¹H NMR (400.13 MHz, CD₂Cl₂, 297 K): δ (ppm) rotamer A: 6.77 (bs, 2H), 1.59 (s, 18H), rotamer B: 6.37 (bs, 2H), 6.13 (bs, 2H), 1.60 (s, 9H), 1.40 (s, 9H). ¹³C-¹H NMR (100.5 MHz, CD₂Cl₂, 297 K): δ (ppm) 189.31, 53.24, 31.48. Anal. Calcd for C₉H₂₀AuClN₂ (389.7): C, 27.81; H, 5.19; Au, 50.67; Cl, 9.12; N, 7.21. Found: C, 27.79; H, 5.22; N, 7.18.

7Cl

Synthesis of [(Bis(tert-butylamino)methylidene)](Triphenylphosphine)gold(I) tetrafluoroborate (7(PPh₃)BF₄). 7Cl 46.6 mg (0.12 mmol) and PPh₃ 34.62 mg (0.13 mmol) were added in a Schlenk in 2 mL of dichloromethane, then 26 mg of AgBF₄ (0.13 mmol) were added. The reaction proceeds at room temperature with the concomitant precipitation of AgCl. After 30 min the reaction mixture was filtered through Celite and the solvent evaporated under reduced pressure. Then pentane was added to the crude product, which was filtered off and washed with other pentane (3x1 mL). The resulting solid was dried under vacuum. We obtained the product as a white solid; yield: 84 mg (99.9%).

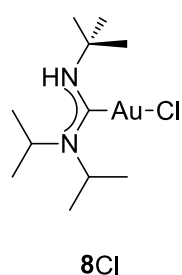


7(PPh₃)BF₄

¹H NMR (400.13 MHz, CD₃OD, 297 K): δ = 7.6 (m, 15H, PPh₃), 1.58 (s, 18H, Bu^t). ¹⁹F NMR (376.42 MHz, CD₃OD, 297 K): δ = -154.78 (br, ¹¹BF₄), -154.83 (br, ¹⁰BF₄). ³¹P{¹H} NMR (161.97 MHz, CD₃OD, 298K): δ = 39.06. ¹³C{¹H} NMR (100.5 MHz, CD₃OD, 298K): δ = 205.1 (d, ²J_{CP} = 108.9 Hz, C_{carb}), 134.0, 133.6 (d, ²J_{CP} = 11.1 Hz), 132.2, 129.6, 129.5, 52.3 (s, C(CH₃)₃), 30.6 (s, C(CH₃)₃). Anal. Calcd. for C₂₇H₃₅AuBF₄N₂P (702.33): C, 46.17; H, 5.02; Au, 28.04; B, 1.54; F, 10.82; N, 3.99; P, 4.41. Found: C, 46.16; H, 5.05; N, 3.98.

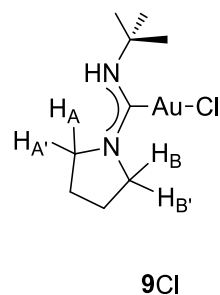
Synthesis of [(tert-Butylamino)(di-iso-propyl-amino)methylidene]-gold(I) Chloride (8Cl). Two equivalents of diisopropylamine were added to a solution of [tert-Butylisocyano]-gold(I) Chloride 221 mg (0.7 mmol) in 3 mL of acetonitrile.²¹³ The mixture was stirred at 60°C overnight. Then the mixture was purified by washing with Et₂O and the supernatant was removed by decantation. The crude product was washed with

pentane and then all volatiles was removed under vacuum. The product was recrystallized from dichloromethane/pentane. We obtained the product as a white-yellow solid; yield: 245 mg (91.3%).



^1H NMR (400.13 MHz, CD_2Cl_2 , 297K): δ (ppm) 6.20 (br s, 1H, NH), 5.36 (m, 1H, CHMe₂), 3.86 (m, 1H, CHMe₂), 1.63 (s, 9H, ^tBu), 1.40 (d, $J = 6.9$ Hz, 6H, CHMe), 1.25 (d, $J = 5.5$ Hz, 6H, CHMe). $^{13}\text{C}\{^1\text{H}\}$ NMR (100.5 MHz, CD_2Cl_2 , 297K): δ (ppm) 190.45 (s, C_{carbene}), 54.46 (s, CMe₃), 45.38 (s, CHMe₂), 31.73 (s, CMe₃), 29.88 (s, CHMe₂), 21.00 (s, CHMe₂), 20.72 (s, CHMe₂). Anal. Calcd. for C₁₁H₂₄AuClN₂ (416.74): C, 31.70; H, 5.80; Au, 47.26; Cl, 8.51; N, 6.72. Found: C, 31.65; H, 5.84; N, 6.62.

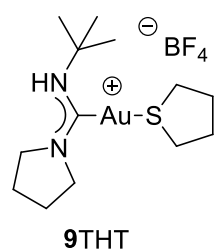
Synthesis of [(tert-Butylamino)(pyrrolidin-1-yl)methylidene]-gold(I) Chloride (9Cl). In a Schlenk 113.6 mg (0.35 mmol) of [(THT)AuCl] was dissolved in a solution of dichloromethane 2 mL and 1.1 equivalent of t-butyl isocyanide 44 μL (3.54 mmol) in 1 mL of CH_2Cl_2 was added at room temperature. The mixture was stirred for 30 min then without any purification, 2 equivalents of pyrrolidine 58 μL (0.70 mmol) were added to the mixture. The mixture was stirred at room temperature and protect from the light for 3 h. The mixture was purified by filtration through silica, then concentrated and precipitated with pentane. We obtained the product as a white solid; yield: 108 mg (78.8%).



^1H NMR (400.13 MHz, CD_3OD , 298K): $\delta = 5.51$ (bs, NH), 3.95 (t, $^3J_{\text{HH}} = 6.9$ Hz, 2H, B), 3.26 (t, $^3J_{\text{HH}} = 7.1$ Hz, 2H, A), 2.09 (m, 2H, A'), 1.92 (m, 2H, B'), 1.62 (s, 9H, NBU^t). $^{13}\text{C}\{^1\text{H}\}$ NMR (100.5 MHz, CD_3OD , 298K): $\delta = 186.7$ (s, C_{carb}), 57.2 (s, B), 53.6 (s, C(CH₃)₃), 45.1 (s, a), 30.9 (s, C(CH₃)₃), 25.2 (s, A'), 24.3 (s, B'). Anal. Calcd for C₉H₁₈AuClN₂ (387.68): C, 27.88; H, 4.94; Au, 50.81; Cl, 9.14; N, 7.23. Found: C, 27.84; H, 4.98; N, 7.21. Anal. Calcd. for C₉H₁₈AuClN₂ (386.67): C, 27.96; H, 4.69; Au, 50.94; Cl, 9.17; N, 7.24. Found:

C, 27.98; H, 4.72; N, 7.23.

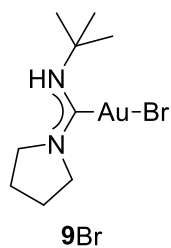
Synthesis of [(tert-Butylamino)(pyrrolidin-1-yl)methylidene][tetrahydrothiophene]-gold(I) tetrafluoroborate (9THT). Complex 9Cl (200 mg, 5.16×10^{-4} mol) was dissolved in dichloromethane (10 mL) in presence of an excess of tetrahydrothiophene (100 μL , 1.13×10^{-3} mol) and 1.1 equivalents of AgBF_4



(110 mg, 5.68×10^{-4} mol), under nitrogen atmosphere. After 1 hour, the white-grey solid (AgCl and the excess of AgBF_4) was filtered off and the volume of the solution was reduced to about 2 mL. Adding 5 mL of *n*-pentane caused the precipitation of a white solid, which was filtered, washed with *n*-pentane and dried under vacuum, giving the desired compound (244 mg, yield 90%).

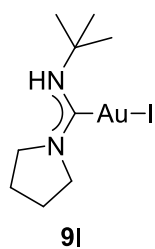
^1H NMR (400.13 MHz, CD_3OD , 298K): δ = 5.51 (bs, NH), 3.96 (t, $^3J_{\text{HH}}$ = 6.7 Hz, 2H, B), 3.42 (bs, 4H, SCH_2CH_2), 2.2 (bs, 4H, SCH_2CH_2), 2.10 (m, 2H, A'), 1.96 (m, 2H, B'), 1.62 (s, 9H, NBu^t). $^{13}\text{C}\{^1\text{H}\}$ NMR (100.5 MHz, CD_3OD , 298K): 190.7 (s, C_{carb}), 58.3 (s, B), 49.7 (s, $\text{C}(\text{CH}_3)_3$), 46.8 (s, a), 39.7 (br, SCH_2CH_2), 32.1 (s, $\text{C}(\text{CH}_3)_3$), 31.9 (s, SCH_2CH_2), 26.1 (s, A'), 25.5 (s, B').

Synthesis of [(tert-Butylamino)(pyrrolidin-1-yl)methylidene]-gold(I) Bromide (9Br). Complex **9THT** (30 mg, 5.7×10^{-5} mol) was dissolved in methanol (5 mL) with an excess of KBr (20 mg, 0.17 mmol) and stirred for 3 hours. The white solid was filtered and the solution was dried under vacuum, giving a white powder. The powder was treated with dichloromethane, and the resulting heterogeneous mixture was stirred for 1 hour and filtered. The addition of pentane caused the precipitation of the desired compound as a white powder (17 mg, yield 70%).



^1H NMR (400.13 MHz, CD_3OD , 298K): δ = 6.51 (bs, NH), 3.96 (t, $^3J_{\text{HH}}$ = 6.8 Hz, 2H, B), 3.23 (t, $^3J_{\text{HH}}$ = 7.1 Hz, 2H, A), 2.08 (m, 2H, A'), 1.92 (m, 2H, B'), 1.62 (s, 9H, NBu^t). $^{13}\text{C}\{^1\text{H}\}$ NMR (100.5 MHz, CD_3OD , 298K): δ = 190.3 (s, C_{carb}), 57.0 (s, B), 53.7 (s, $\text{C}(\text{CH}_3)_3$), 45.1 (s, A), 30.8 (s, $\text{C}(\text{CH}_3)_3$), 25.2 (s, A'), 24.3 (s, B'). Anal. Calcd for $\text{C}_9\text{H}_{18}\text{AuBrN}_2$ (431,12): C, 25.01; H, 4.43; Au, 45.58; Br, 18.49; N, 6.48. Found: C, 25.07; H, 4.49; N, 6.51.

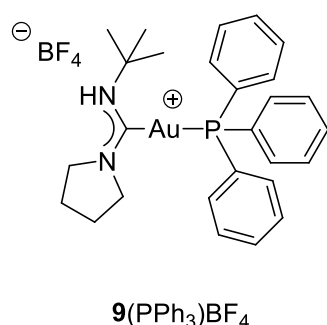
Synthesis of [(tert-Butylamino)(pyrrolidin-1-yl)methylidene]-gold(I) Iodide (9I). The compound was synthesized as **9Br**, using KI instead of KBr.



^1H NMR (400.13 MHz, CD_3OD , 298K): δ = 6.52 (bs, NH), 3.97 (t, $^3J_{\text{HH}}$ = 6.9 Hz, 2H, B), 3.24 (t, $^3J_{\text{HH}}$ = 7.1 Hz, 2H, A), 2.09 (m, 2H, A'), 1.92 (m, 2H, B'), 1.62 (s, 9H, NBu^t). $^{13}\text{C}\{^1\text{H}\}$ NMR (100.5 MHz, CD_3OD , 298K): δ = 196.8 (s, C_{carb}), 56.5 (s, B), 53.8 (s, $\text{C}(\text{CH}_3)_3$), 45.1 (s, A), 30.8 (s, $\text{C}(\text{CH}_3)_3$), 25.2 (s, A'), 24.4 (s, B'). Anal. Calcd for $\text{C}_9\text{H}_{18}\text{AuIN}_2$ (478,12): C, 22.56; H, 4.00; Au, 41.11; I, 26.49; N, 5.85. Found: C, 22.55; H, 4.12; N, 5.87.

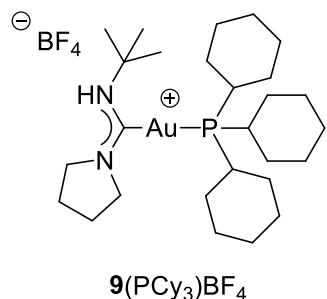
Synthesis of [(tert-Butylamino)(pyrrolidin-1-yl)methylidene][triphenylphosphine]-gold(I) tetrafluoroborate (9(PPh₃)BF₄). Synthesized by **Procedure A**: complex **9Cl** (mg, 7.8×10^{-5} mol) was stirred in dichloromethane (5 mL) with 1 equivalent of the appropriate ligand L and 1.1 equivalents of AgBF_4 , under nitrogen atmosphere. After 1 hour, the white-grey solid (AgCl and the excess of AgBF_4) was filtered off and the volume of the solution was reduced to about 2 mL. Adding 5 mL of *n*-pentane caused the precipitation of

a white solid, which was filtered, washed with *n*-pentane and dried under vacuum, giving the desired compound.



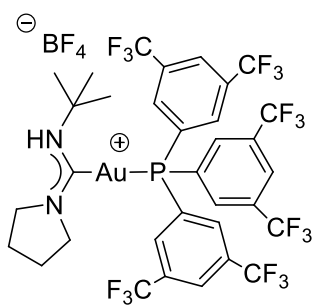
¹H NMR (400.13 MHz, CD₃OD, 298K): δ = 7.60 (m, 15H, PPh₃), 7.00 (br s, 1H, NH), 4.07 (t, ³J_{HH} = 6.9 Hz, 2H, B), 3.35 (t, ³J_{HH} = 7.0 Hz, 2H, A), 2.10 (m, 2H, A'), 1.99 (m, 2H, B'), 1.63 (s, 9H, NBU^t). ³¹P{¹H} NMR (161.97 MHz, CD₃OD, 298K): δ = 40.22 (s). ¹⁹F NMR (100.5 MHz, CD₃OD, 298K): δ = -155.30 (br, ¹⁰BF₄), -155.35 (br, ¹¹BF₄). ¹³C{¹H} NMR (100.5 MHz, CD₃OD, 298K): δ = 202.32 (d, ²J_{CP} = 119.1 Hz, C_{carb}), 134.2 (d, ²J_{CP} = 13.2 Hz, *ortho*-C), 132.5 (d, ³J_{CP} = 11.1 Hz, *meta*-C), 129.8 (d, ⁴J_{CP} = 2.0 Hz, *para*-C), 128.9 (d, ¹J_{CP} = 57.2 Hz, *ipso*-C), 56.7 (s, B), 53.8 (s, C(CH₃)₃), 45.9 (s, A), 31.4 (s, C(CH₃)₃), 25.0 (s, A'), 24.8 (s, B'). Anal. Calcd for C₂₇H₃₃AuBF₄N₂P (700.31): C, 46.31; H, 4.75; Au, 28.13; B, 1.54; F, 10.85; N, 4.00; P, 4.42 Found: C, 46.36; H, 4.77; N, 3.97.

Synthesis of [(tert-Butylamino)(pyrrolidin-1-yl)methylidene][tri-cyclohexylphosphine]-gold(I) tetrafluoroborate (9(PCy₃)BF₄). Synthesized by Procedure A.



¹H NMR (400.13 MHz, CD₃OD, 298K): δ = 6.90 (br d, ⁴J_{PH} = 7.0 Hz, 8.4 Hz, 1H, NH), 3.96 (t, ³J_{HH} = 6.7 Hz, 2H, B), 3.30 (t, ³J_{HH} = 7.0 Hz, 2H, A), 2.26 (m, 3H), 2.12-2.07 (m, 16H), 1.63 (s, 9H, NBU^t), 1.59-1.23 (m, 18H). ³¹P{¹H} NMR (161.97 MHz, CD₃OD, 298K): δ = 56.74 (s). ¹⁹F NMR (100.5 MHz, CD₃OD, 298K): δ = -154.52 (br, ¹⁰BF₄), -154.57 (br, ¹¹BF₄). ¹³C{¹H} NMR (100.5 MHz, CD₃OD, 298K): δ = 207.1 (d, ²J_{CP} = 108.5 Hz, C_{carb}), 57.1 (s, B), 54.9 (s, C(CH₃)₃), 46.7 (d, ⁴J_{CP} = 2.4 Hz, A), 34.1 (d, J_{CP} = 28.1 Hz), 32.3, 31.9 (s, C(CH₃)₃), 27.9 (d, J_{CP} = 11.9 Hz), 27.0 (d, J_{CP} = 1.2 Hz), 25.8 (d, J_{CP} = 6.8 Hz). Anal. Calcd for C₂₇H₅₁Au BF₄N₂P (718.45): C, 45.14; H, 7.15; Au, 27.42; B, 1.50; F, 10.58; N, 3.90; P, 4.31. Found: C, 45.12; H, 7.20; N, 3.89.

Synthesis of [(tert-Butylamino)(pyrrolidin-1-yl)methylidene][tris(3,5-bis(trifluoromethyl)phenyl)-phosphine]-gold(I) tetrafluoroborate (9(PAr^F)BF₄). Synthesized by Procedure A.

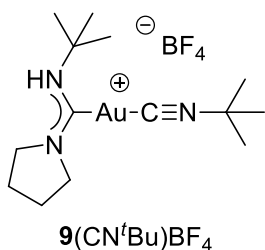


9(PAr^F)BF₄

¹H NMR (400.13 MHz, CD₃OD, 298K): 8.39 (m, 9H, *ortho* and *meta*-H), 4.11 (t, ³J_{HH} = 6.8 Hz, 2H, *B*), 3.38 (t, ³J_{HH} = 6.9 Hz, 2H, *A*), 2.12 (m, 2H, *A'*), 1.99 (m, 2H, *B'*), 1.63 (s, 9H, C_{carb}NBu^t). ³¹P{¹H} NMR (161.97 MHz, CD₃OD, 298K): δ = 45.6 (s). ¹⁹F NMR (100.5 MHz, CD₃OD, 298K): δ = -64.9 (s, CF₃), -155.06 (br, ¹⁰BF₄), -155.11 (br, ¹¹BF₄). ¹³C{¹H} NMR (100.5 MHz, CD₃OD, 298K): δ = 200.71 (d, ²J_{CP} = 122.0 Hz, C_{carb}), 136.0 (br d, ²J_{CP} = 13.8 Hz, *ortho*-C), 134.4 (qd, ²J_{CP} = 34.0 Hz, ³J_{CP} = 11.6 Hz, *meta*-C), 131.50 (d, ¹J_{CP} = 55.4 Hz, *ipso*-C), 128.4 (br s, *para*-C) 124.11 (q, ²J_{CP} = 271.3 Hz, CF₃), 57.7 (s, *B*), 54.9 (s, C(CH₃)₃), 47.2 (s,

A), 32.3 (s, C(CH₃)₃), 26.0 (s, *A'*), 25.7 (s, *B'*). Anal. Calcd for C₃₃H₂₇AuF₂₂N₂P (1108.30): C, 35.76; H, 2.46; Au, 17.77; B, 0.98; F, 37.71; N, 2.53; P, 2.79. Found: C, 35.78; H, 2.47; N, 2.53.

Synthesis of [(*tert*-Butylamino)(pyrrolidin-1-yl)methylidene][*tert*-butyl isocyanide]-gold(I) tetrafluoroborate (9(CN^tBu)BF₄). Synthesized by Procedure A.

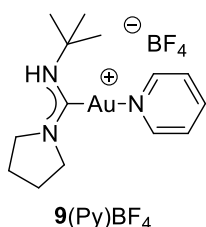


9(CN^tBu)BF₄

¹H NMR (400.13 MHz, CD₃OD, 298K): δ = 6.90 (br s, 1H, NH), 3.96 (t, ³J_{HH} = 6.8 Hz, 2H, *B*), 3.31 (t, ³J_{HH} = 6.9 Hz, 2H, *A*), 2.08 (m, 2H, *A'*), 1.96 (m, 2H, *B'*), 1.63 (s, 9H, C_{carb}NBu^t), 1.60 (s, 9H, C_{isocyanate}NBu^t). ¹⁹F NMR (100.5 MHz, CD₃OD, 298K): δ = -154.60 (br, ¹⁰BF₄), -154.65 (br, ¹¹BF₄). ¹³C{¹H} NMR (100.5 MHz, CD₃OD, 298K): δ = 194.8 (s, C_{carb}), 57.9 (s, *B*), 55.0 (s, C_{carb}NC(CH₃)₃), 46.9 (s, *A*), 32.3 (s, C_{isocyanate}NC(CH₃)₃), 29.7 (s, C_{carb}NC(CH₃)₃), 25.9 (s, *A'*), 25.6 (s, *B'*).²¹⁴ Anal. Calcd for

C₁₄H₂₇AuBF₄N₃ (521.16): C, 32.26; H, 5.22; Au, 37.79; B, 2.07; F, 14.58; N, 8.06. Found: C, 32.29; H, 5.25; N, 8.08.

Synthesis of [(*tert*-Butylamino)(pyrrolidin-1-yl)methylidene][pyridine]-gold(I) tetrafluoroborate (9(Py)BF₄). Synthesized by Procedure A.



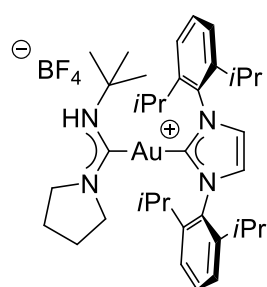
9(Py)BF₄

¹H NMR (400.13 MHz, CD₃OD, 298K): δ = 8.44-8.32 (m, 3H, *o*-H and *p*-H), 4.11 (t, ³J_{HH} = 6.8 Hz, 2H, *B*), 3.38 (t, ³J_{HH} = 7.0 Hz, 2H, *A*), 2.12 (m, 2H, *A'*), 1.99 (m, 2H, *B'*), 1.63 (s, 9H, NBu^t). ¹⁹F NMR (100.5 MHz, CD₃OD, 298K): δ = -155.15 (br, ¹⁰BF₄), -155.20 (br, ¹¹BF₄). ¹³C{¹H} NMR (100.5 MHz, CD₃OD, 298K): δ = 182.7 (s, C_{carb}), 151.9 (s, *ortho*-C), 141.7 (s, *para*-C), 127.2 (s, *meta*-C), 57.6 (s, *B*), 53.9 (s, C(CH₃)₃), 45.7 (s, *A*), 31.2 (s,

C(CH₃)₃), 25.1 (s, *A'*), 24.5 (s, *B'*). Anal. Calcd for C₉H₁₈AuBF₄N₂ (438.02): C, 24.68; H, 4.14; Au, 44.97; B, 2.47; F, 17.35; N, 6.40. Found: C, 24.63; H, 4.17; N, 6.37.

Synthesis of [(tert-Butylamino)(pyrrolidin-1-yl)methylidene][NHC]-gold(I) tetrafluoroborate (9(NHC)BF₄).

To a stirring solution of complex [(NHC)AuCl] (99.4 mg, 0.16 mmol) and *tert*-butyl isocyanide (21.7 μ L, 0.19 mmol) in dichloromethane (2 mL), AgBF₄ (34.3 mg, 0.18 mmol) was added. After 15 min the reaction mixture was treated with activated charcoal and filtered through a pad of Celite®. Subsequently, 19.7 μ L (0.24 mmol) of pyrrolidine were added to the solution. After 30 min the solution was treated with activated charcoal and filtered, and the volume reduced under reduced pressure. Addition of *n*-pentane caused the precipitation of the product as a white solid, which was filtered off and washed with other pentane (3x2 mL). The resulting solid was dried under vacuum (Yield 105 mg, 78.9%).

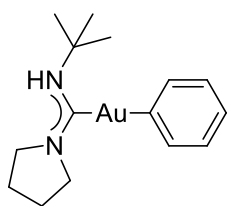


9(NHC)BF₄

¹H NMR (400.13 MHz, CD₃OD, 298K): δ = 7.86 (s, 1H, CH_{backbone,NHC}), 7.85 (s, 1H, CH_{backbone,NHC}), 7.59 (m, 2H, *para*-H), 7.44 (d, ³J_{HH} = 8.0 Hz, 4H, *meta*-H), 3.05 (t, ³J_{HH} = 7.2 Hz, 2H, B), 2.81 (t, ³J_{HH} = 6.8 Hz, 2H, A), 2.64 (sept, ³J_{HH} = 7.2 Hz, 4H, CH(CH₃)₂), 1.87 (m, 2H, A'), 1.56 (m, 2H, B'), 1.55 (d, ³J_{HH} = 7.2 Hz, 12H, CH(CH₃)₂), 1.34 (d, ³J_{HH} = 7.2 Hz, 12H, CH(CH₃)₂), 1.05 (s, 9H, NBu^t). ¹⁹F NMR (100.5 MHz, CD₃OD, 298K): δ = -155.25 (br, ¹⁰BF₄), -155.30 (br, ¹¹BF₄). ¹³C{¹H} NMR (100.5 MHz, CD₃OD, 298K): δ = 199.2 (s, C_{carb,NAC}), 186.8 (s, C_{carb,NHC}), 145.8 (s, *ortho*-C), 134.5 (s, *ipso*-C), 130.5 (s, *para*-C), 124.7 (s, C_{backbone,NHC}), 124.1 (s, *meta*-C), 54.8 (s, B), 52.7 (s, C(CH₃)₃), 44.6 (s, A), 30.6 (s, C(CH₃)₃), 28.7 (s, CH(CH₃)₂), 24.2 (s, A'), 23.8 (s, B'), 23.2 (s, CH(CH₃)₂), 23.1 (s, CH(CH₃)₂). Anal. Calcd for C₃₆H₅₄AuBF₄N₄ (826.61): C, 52.31; H, 6.58; Au, 23.83; B, 1.31; F, 9.19; N, 6.78. Found: C, 52.33; H, 6.61; N, 6.76.

*Synthesis of [(tert-Butylamino)(pyrrolidin-1-yl)methylidene][phenyl]-gold(I) tetrafluoroborate (9(Ph)BF₄).*²¹⁵

60.9 mg (0.16 mmol) of complex 9Cl, 106.00 mg of Cs₂CO₃ (0.33 mmol) and 40.0 mg of PhB(OH)₂ (0.33 mmol) were added in a Schlenk tube with 5 mL of anhydrous isopropanol. The reaction mixture was stirred at 40 °C for 4 h. The reaction mixture was taken to dryness and the resulting solid was extracted with toluene and filtered through Celite. The solution was concentrated in vacuum to dryness, washed twice with 1 mL of pentane and dried. The solid was re-dissolved in toluene and precipitated with pentane. The resulting precipitate was filtered, washed with pentane and dried under vacuum. We obtain the product as a white powder: yield 28 mg (41.5 %).



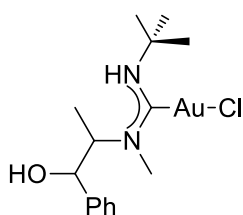
9Ph

^1H NMR (400.13 MHz, CD_3OD , 298K): δ = 7.36 (dd, $^3J_{\text{HH}} = 7.8$ Hz, $^4J_{\text{HH}} = 1.5$ Hz, 2H, *ortho*-H), 7.10 (t, $^3J_{\text{HH}} = 7.7$ Hz, 2H, 2H, *meta*-H), 6.90 (tt, $^3J_{\text{HH}} = 7.4$ Hz, $^4J_{\text{HH}} = 1.4$ Hz, 1H, *para*-H), 6.39 (br s, 1H, NH), 4.08 (t, $^3J_{\text{HH}} = 6.7$ Hz, 2H, B), 3.19 (t, $^3J_{\text{HH}} = 7.2$ Hz, 2H, A), 2.05 (m, 2H, A'), 1.92 (m, 2H, B'), 1.69 (s, 9H, NBU^t). $^{13}\text{C}\{^1\text{H}\}$ NMR (100.5 MHz, CD_3OD , 298K): δ = 210.2 (s, C_{carb}), 168.6 (s, *ipso*-C), 141.1 (s, *ortho*-C), 126.8 (s, *meta*-C), 124.4 (s, *para*-C), 55.8 (s, B), 53.3 (s, $\text{C}(\text{CH}_3)_3$), 44.2 (s, A), 31.1 (s, $\text{C}(\text{CH}_3)_3$), 25.0

(s, A'), 24.6 (s, B'). Anal. Calcd for $\text{C}_{15}\text{H}_{23}\text{AuN}_2$ (428.32): C, 41.96; H, 5.63; Au, 45.88; N, 6.52. Found: C, 41.97; H, 5.65; N, 6.55.

Dissolving complex **10** in methanol leads to a slow decomposition, giving Au(0), biphenyl and other unidentified products. Anyway, the NMR signals of the decomposition products do not overlap with those of **10** and, consequently, do not interfere with EXSY NMR measurements. In fact, the rate of an intramolecular rotation does not depend on the concentration of the species.

Synthesis of [((1R,2S)-1-phenyl-1-propanol-2-amino)(tert-Butylamino)methylidene]-gold(I) Chloride (10Cl). Two equivalents of (1R,2S)-(-)-Ephedrine were added to a solution of [tert-Butylisocyano]-gold(I) Chloride complex 56.8 mg (0.18 mmol) in 2 mL of CH_2Cl_2 . The mixture was stirred at room temperature and protected from the light for 3 days. The mixture was concentrated and precipitate with pentane. We obtained the product as a white solid; yield: 80 mg (92.3%).



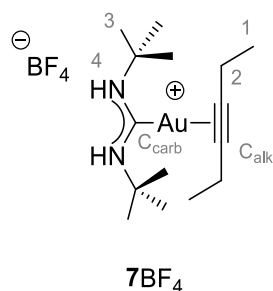
10Cl

^1H NMR (400.13 MHz, CD_2Cl_2 , 297 K): δ = 7.53 (d, 2H, $J_3^{\text{HH}} = 7.4$ Hz, *o*-Ph), 7.41 (t, 2H, $J_3^{\text{HH}} = 7.4$ Hz, *m*-Ph), 7.33 (t, 1H, $J_3^{\text{HH}} = 7.4$ Hz, *p*-Ph), 5.83 (br s, 1H, NH), 5.38 (m, 1H, CHMe), 5.05 (t, 1H, $J_3^{\text{HH}} = 4.0$ Hz, CHO), 2.88 (s, 3H, NMe), 2.21 (d, 1H, $J_3^{\text{HH}} = 3.6$ Hz, OH), 1.61 (s, 9H, CMe_3), 1.31 (d, 3H, $J_3^{\text{HH}} = 6.9$ Hz, CHMe) ppm. $^{13}\text{C}\{^1\text{H}\}$ NMR (100.5 MHz, CD_2Cl_2 , 297 K): δ = 191.15 (s, $\text{C}_{\text{carbene}}$), 140.96 (s, C_{ipso}), 128.60 (s, C_{Ph}), 128.08 (s, $\text{C}_{p\text{-Ph}}$), 125.93 (s, C_{Ph}), 70.34 (s, COH), 59.46 (s, CMe), 54.29 (s, CMe_3),

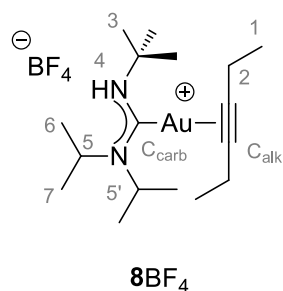
38.10 (s, NMe), 30.85 (s, CMe_3), 12.12 (s, CMe) ppm. Anal. Calcd. for $\text{C}_{15}\text{H}_{24}\text{AuClN}_2\text{O}$ (480.78): C, 37.47; H, 5.03; Au, 40.97; Cl, 7.37; N, 5.83; O, 3.33. Found: C, 37.53; H, 5.12; N, 5.69.

Synthetic procedure for the in-situ generation of 7- BF_4 and 10 BF_4 ion pairs: 1.2 equivalents of AgBF_4 were loaded into a screw-cap NMR tube under nitrogen atmosphere. A solution containing 1 equivalent of a Gold(I) Chloride precursor (**7Cl-10Cl**) and 1.1 equivalents of 3-hexyne dissolved in 0.6 mL of dry CD_2Cl_2 was

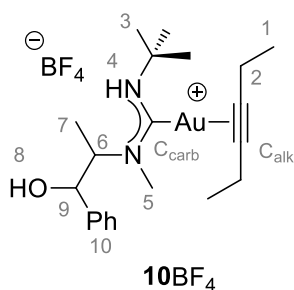
added. The resulting mixture was strongly shaken and after some minutes a white-grey solid (AgCl and the excess of AgBF₄) deposited at the bottom of the tube.



7BF₄. ¹H NMR (400.13 MHz, CD₂Cl₂, 297 K): δ= 7.58 (br s, 2H, H4), 2.77 (br quartet, 4H, $J_3^{\text{HH}} = 7.4$ Hz, H2), 1.54 (s, 18H, H3), 1.34 (br t, 6H, $J_3^{\text{HH}} = 7.4$ Hz, H1). ¹⁹F NMR (376.42 MHz, CD₂Cl₂, 297 K): δ= -149.59 (br, ¹¹BF₄), -149.54 (br, ¹⁰BF₄). ¹³C{¹H} NMR (100.5 MHz, CD₂Cl₂, 297 K): δ= 192.90 (s, C_{carb}), 87.68 (s, C_{alk}), 53.23 (s, C5), 31.66 (s, C3), 16.36 (s, C2), 14.46 (s, C1).



8BF₄. ¹H NMR (400.13 MHz, CD₂Cl₂, 297 K): δ= 6.53 (br s, 1H, H4), 4.84 (br, 1H, H5), 4.00 (br quintet, 1H, $J_3^{\text{HH}} = 7.5$ Hz, H5'), 2.79 (br quartet, 4H, $J_3^{\text{HH}} = 7.7$ Hz, H2), 1.66 (s, 9H, H3), 1.48 (br d, 6H, $J_3^{\text{HH}} = 7.1$ Hz, H6/H7), 1.41 (br d, 6H, $J_3^{\text{HH}} = 6.6$ Hz, H6/H7), 1.36 (br t, 6H, $J_3^{\text{HH}} = 7.7$ Hz, H1). ¹⁹F NMR (376.42 MHz, CD₂Cl₂, 297 K): δ= -153.26 (br, ¹¹BF₄), -153.20 (br, ¹⁰BF₄). ¹³C{¹H} NMR (100.5 MHz, CD₂Cl₂, 297 K): δ= 192.68 (s, C_{carb}), 88.14 (s, C_{alk}), 48.96 (s), 47.17 (s), 31.83 (s), 21.15 (s), 20.71 (s), 18.88 (s), 16.02 (s, C2), 14.30 (s, C1).

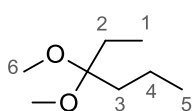


10BF₄. ¹H NMR (400.13 MHz, CD₂Cl₂, 297 K): δ= 7.45 (m, 5H, H10), 6.29 (br s, 1H, H4), 4.90 (d, 1H, $J_3^{\text{HH}} = 7.7$ Hz, H9), 4.79 (quintet, 1H, $J_3^{\text{HH}} = 7.5$ Hz, H6), 3.86 (br, 1H, H8), 2.95 (s, 3H, H5), 2.74 (br quartet, $J_3^{\text{HH}} = 7.4$ Hz, H2), 1.56 (d, 3H, $J_3^{\text{HH}} = 6.6$ Hz, H7), 1.46 (s, 9H, H3), 1.33 (br t, $J_3^{\text{HH}} = 7.1$ Hz, H1). ¹⁹F NMR (376.42 MHz, CD₂Cl₂, 297 K): δ= -152.22 (br, ¹¹BF₄), -152.17 (br, ¹⁰BF₄). ¹³C{¹H} NMR (100.5 MHz, CD₂Cl₂, 297 K): δ= 194.07 (s, C_{carb}), 142.91 (s, Ph_{ipso}), 128.55 (s, Ph), 128.05 (s, *p*-Ph), 125.78 (s, Ph), 87.90 (s, C_{alk}), 75.93 (s, C9), 73.12 (s, C6), 54.56 (s, CMe₃), 31.83 (s), 31.71 (s, C3), 30.71 (s), 16.00 (s, C2), 14.97 (s, C7), 14.36 (s, C1).

4.3 Catalysis

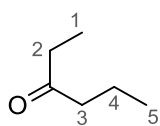
4.3.1 Methoxylation of 3-hexyne catalysed by 4X

All experiments were followed by *in situ* ^1H NMR. 3-hexyne (100 μL , 0.88 mmol), CH_3OH or CH_3OD (143 μL , 3.52 mmol), TMS (5 μL) and CDCl_3 (400 μL) were added by syringe in a NMR tube. The content of the latter was transferred into the vial with the catalyst loading it was briefly shaken for a moment and quickly relocated again into NMR tube and the time count was started. The reaction mixture was further monitored by NMR at 30 $^\circ\text{C}$. Conversion was calculated from the integral intensities of the corresponding signals ($\text{conversion [\%]} = (n_{\text{acetal}} + n_{\text{vinylether}} + n_{\text{ketone}}) / (n_{\text{3-hexyne}}) \times 100$). In the presence of 4OTs the catalysis was carried out by changing the catalyst loading (entries 1-4, Table S1) from 0.5 to 2 mol% observing a pseudo-linear correlation between the average rate $[\text{3-hexyne}]_0/t$ versus [4OTs]. This trend suggests a 1st order dependence on catalyst as recently reported in the literature^{105a} for non-coordinating anions.



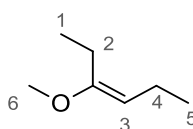
3,3-dimethoxyhexane - ^1H NMR (CDCl_3 , 400 MHz, 298 K): δ (ppm) 3.15 (s, 6H, H6), 1.54 (m, 4H, H2 and H3), 1.25 (m, 2H, H4), 0.92 (t, $^3J_{\text{HH}} = 7.3$ Hz, 3H, H1), 0.82 (t, $^3J_{\text{HH}} = 7.4$ Hz, 3H, H5).

3,3-dimethoxyhexane D2 - ^1H NMR (CDCl_3 , 400 MHz, 298 K): δ (ppm) 3.15 (s, 6H, H6), 1.59 (q, $^3J_{\text{HH}} = 7.6$ Hz, 2H, H2), 1.33 – 1.15 (m, 2H, H4), 0.93 (t, $^3J_{\text{HH}} = 7.3$ Hz, 3H, H1), 0.82 (t, $^3J_{\text{HH}} = 7.5$ Hz, 3H, H5).



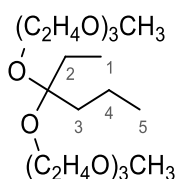
3-hexanone - ^1H NMR (CDCl_3 , 400 MHz, 298 K): δ (ppm) 2.36 – 2.39 (tq, $^3J_{\text{HH}} = 7.4$ Hz, $^3J_{\text{HH}} = 7.3$ Hz, 4H, H2 and H3), 1.58 (m, 2H, H4), 1.03 (t, $^3J_{\text{HH}} = 7.4$ Hz, 3H, H1), 0.89 (t, $^3J_{\text{HH}} = 7.4$ Hz, 3H, H5).

3-hexanone D2 - ^1H NMR (CDCl_3 , 400 MHz, 298 K): δ (ppm) 2.37 (q, $^3J_{\text{HH}} = 7.5$ Hz, 2H), 1.61-1.57 (m, 2H, H4), 1.04 (t, $^3J_{\text{HH}} = 7.4$ Hz, 3H, H1), 0.87 (t, $^3J_{\text{HH}} = 7.3$ Hz, 3H, H5).

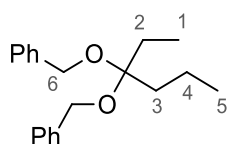


3-methoxy-3-hexene - ^1H NMR (CDCl_3 , 400 MHz, 298 K): δ (ppm) 4.35 (t, $^3J_{\text{HH}} = 7.3$, 1H, H3), 3.53 (s, 3H, H6), 2.00 (m, 4H, H2 and H4), 1.06 (t, $^3J_{\text{HH}} = 7.2$, 6H, H1 and H5).

3-methoxy-3-hexene D1 - ^1H NMR (CDCl_3 , 400 MHz, 298 K): δ (ppm) 3.52 (s, 3H, H6), 2.05-2.01 (m, 4H, H2 and H4), 1.09 (t, $^3J_{\text{HH}} = 7.4$ Hz, 6H, H1 and H5).



12-ethyl-12-propyl-2,5,8,11,16,19,22-heptaacosane - ^1H NMR (CDCl_3 , 400 MHz, 298 K): δ (ppm) 3.78 - 3.26 (m, 30H, Gly-OMe), 1.58 (m, 4H, H2 and H3), 1.27 (m, 2H, H4), 0.91 (t, 3H, $^3J_{\text{HH}} = 7.2$ Hz, H1), 0.82 (t, 3H, $^3J_{\text{HH}} = 7.6$ Hz, H5).



((hexane-3,3-diylbis(oxy))bis(methylene))dibenzene - ^1H NMR (CDCl_3 , 400 MHz, 298 K): δ (ppm) 7.35-7.15 (m, 10H, Ar), 4.48 (s, 4H, H6) 1.76 (m, 4H, H2 and H3), 1.35 (m, 2H, H4), 0.92 (t, 3H, $^3J_{\text{HH}} = 7.2$ Hz, H1), 0.85 (t, 3H, $^3J_{\text{HH}} = 7.2$ Hz, H5).

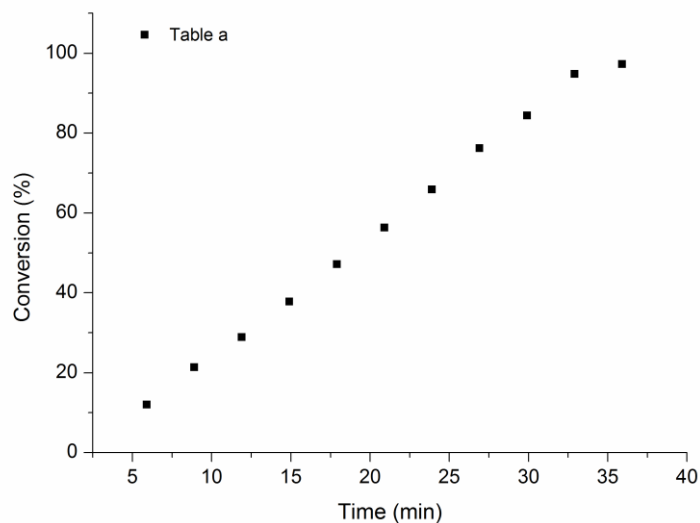
Table 16. Methoxylation of 3-hexyne catalysed by 4X						
Entry	Anion	Au [mol%]	Conv. [%]	t [min] ^[e]	TOF ^[f] [min ⁻¹]	
[a]	1	OTs ⁻	0.5	97	33	5.8
	2	OTs ⁻	1	99	17	5.6
	3	OTs ⁻	1.5	98	11	5.8
	4	OTs ⁻	2	99	7	6.8
	5 ^[c]	OTs ⁻	1	99	20	4.8
	6 ^[d]	OTs ⁻	1	99	22	4.3
	7	OTf ⁻	1	99	33	2.9
	8	BF ₄ ⁻	1	99	40	2.4
	9	BAr ^{F-}	1	99	48	2.0
	10	TFA ⁻	1	96	266	0.4
	11	OAc ⁻	1	0	0	0
[b]	12	OTs ⁻	1	99	18	5.3
	13	OTf ⁻	1	99	47	2.0
	14	BF ₄ ⁻	1	99	64	1.5
	15	BAr ^{F-}	1	99	89	1.1
[g]	16	OTs ⁻	1	0	-	-
[g]	17	BAr ^{F-}	1	0	-	-
[h]	18	OTs ⁻	1	98	345	0.28
[h]	19	BAr ^{F-}	1	98	476	0.20
[i]	20	OTs ⁻	1	99	78	1.20
[i]	21	BAr ^{F-}	1	99	1619	0.06
[k]	22	OTs ⁻	1	18	5430	0.0034
[k]	23	BAr ^{F-}	1	0	-	-

Catalysis conditions: 30 °C, 3-hexyne (100 μL), 4X (mol%), [a] methanol (143 μL) or [b] deuterated methanol (143 μL) in CDCl_3 (400 μL). [c] With 5% N(Bu)₄OTs as additive. [d] With 15% pTsOH as additive. Conversions were determined by ^1H NMR spectroscopy, using TMS as internal standard, as average of three runs. [e] time for 95% conversion. [f] TOF= (n acetal /n NHC-Au-X)/t [min] at 95% of conversion. [g] 2,2,2-trifluoroethanol (3.52 mmol, 256 μL). [h] Triethylene glycol monomethyl ether (1.16 mmol, 186 μL), 3-hexyne (0.29 mmol, 33 μL). [i] Benzyl alcohol (1.16 mmol, 120 μL), 3-hexyne (0.29 mmol, 33 μL). [k] 2,6-dimethoxyphenol (0.88 mmol, 136 mg), 3-hexyne (0.22 mmol, 25 μL), TOF calculated at 18 min.

(Entry 1 – Table 16)

Table a. 4OTs 0.5 mol% (6.8 mM)

t [min]	Conversion [%]
5.9	12.04
8.9	21.40
11.9	28.91
14.9	37.84
17.9	47.18
20.9	56.35
23.9	65.92
26.9	76.24
29.9	84.45
32.9	94.83
35.9	97.31

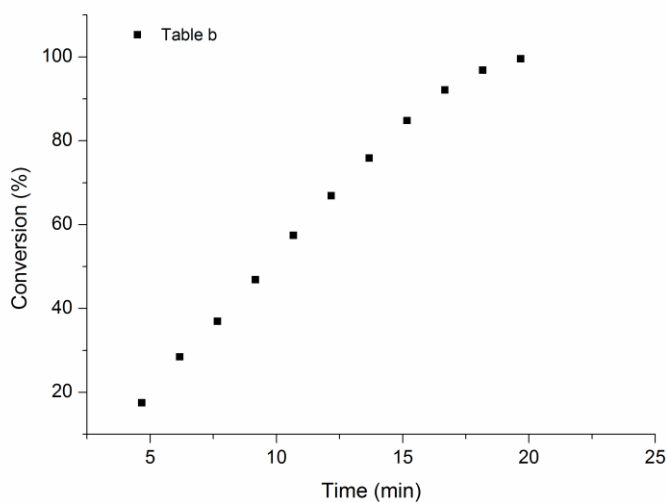


Plot 1. Plot of conversion (%) vs time (min) entry 1 – Table 16.

(Entry 2 – Table 16)

Table b. 4OTs 1 mol% (13.7 mM)

t [min]	Conversion [%]
4.67	17.53
6.17	28.46
7.67	36.95
9.17	46.86
10.67	57.43
12.17	66.90
13.67	75.88
15.17	84.82
16.67	92.12
18.17	96.87
19.67	99.54

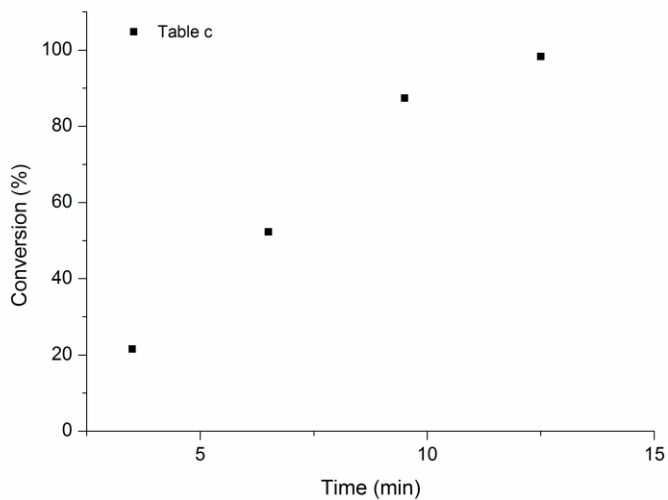


Plot 2. Plot of conversion (%) vs time (min) entry 2 – Table 16

(Entry 3 – Table 16)

Table c. 4OTs 1.5 mol%
(20.5 mM)

t [min]	Conversion [%]
3.5	21.58
6.5	52.34
9.5	87.39
12.5	98.32

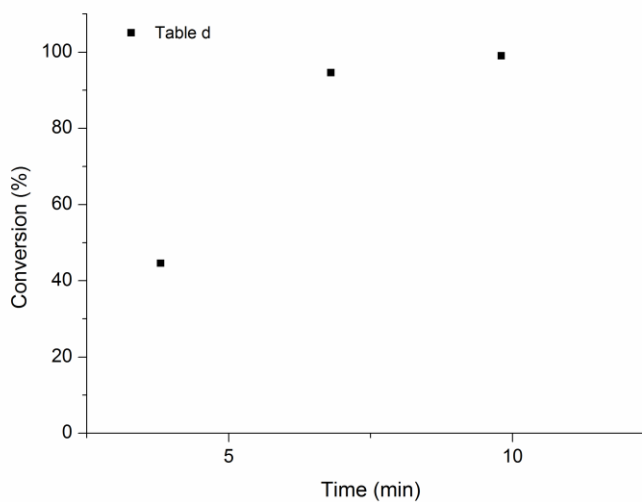


Plot 3. Plot of conversion (%) vs time (min) entry 3 – Table 16

(Entry 4 – Table 16)

Table d. 10Ts 2 mol% (27.4 mM)

t [min]	Conversion [%]
3.8	44.62
6.8	94.61
9.8	99.04

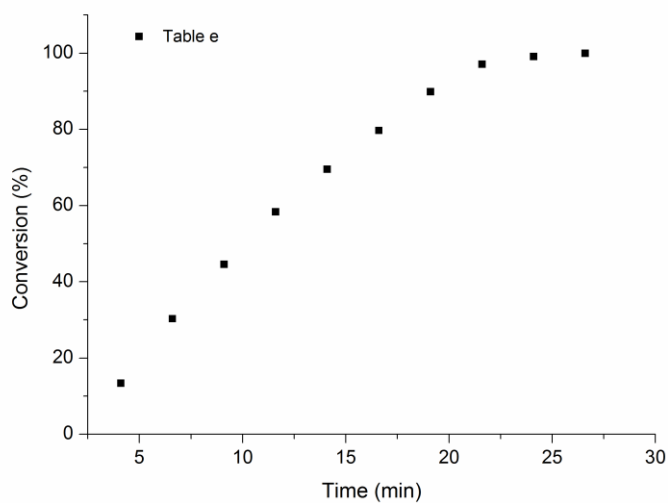


Plot 4. Plot of conversion (%) vs time (min) entry 4 – Table 16

(Entry 5 – Table 16)

Table e. 4OTs + NBU₄OTs

t [min]	Conversion [%]
4.1	13.38
6.6	30.34
9.1	44.60
11.6	58.37
14.1	69.58
16.6	79.70
19.1	89.89
21.6	97.10
24.1	99.11
26.6	99.96

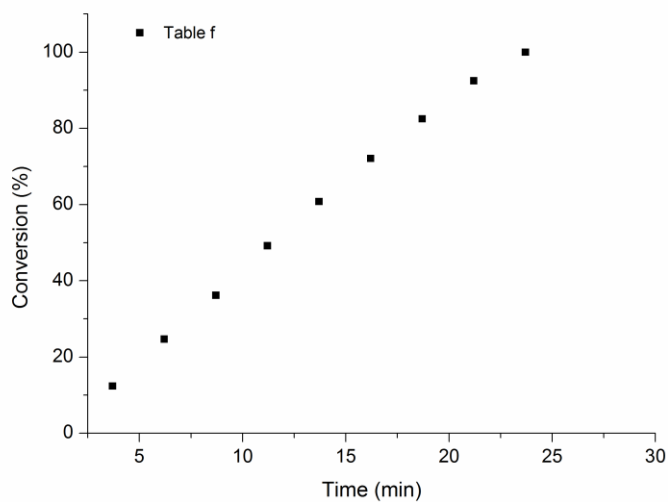


Plot 5. Plot of conversion (%) vs time (min) entry 5 – Table 16

(Entry 6 – Table 16)

Table f. 4OTs + pTsOH

t [min]	Conversion [%]
3.7	12.40
6.2	24.70
8.7	36.20
11.2	49.20
13.7	60.80
16.2	72.10
18.7	82.50
21.2	92.50
23.7	100.00

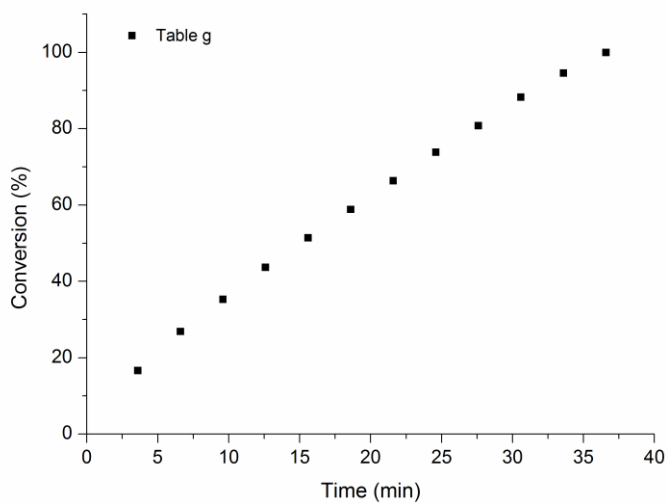


Plot 6. Plot of conversion (%) vs time (min) entry 6 – Table 16

(Entry 7 – Table 16)

Table g. 4OTf

t [min]	Conversion [%]
3.59	16.64
6.59	26.87
9.59	35.29
12.59	43.67
15.59	51.42
18.59	58.84
21.59	66.35
24.59	73.85
27.59	80.81
30.59	88.28
33.59	94.59
36.59	99.96

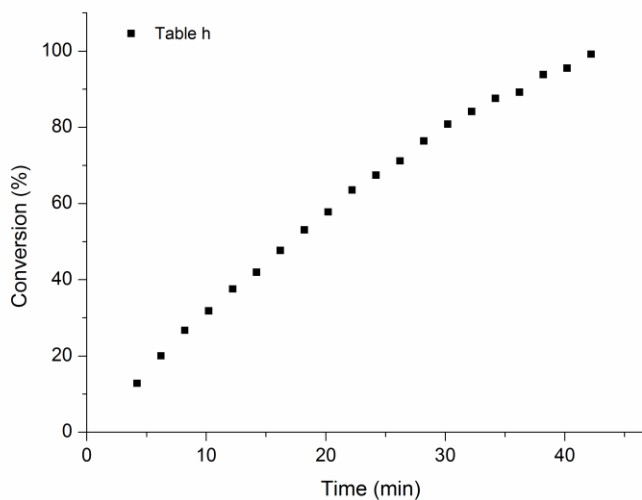


Plot 7. Plot of conversion (%) vs time (min) entry 7 – Table 16

(Entry 8 – Table 16)

Table h. 4BF₄

t [min]	Conversion [%]
4.2	12.83
6.2	20.04
8.2	26.75
10.2	31.87
12.2	37.61
14.2	41.97
16.2	47.71
18.2	53.08
20.2	57.83
22.2	63.55
24.2	67.46
26.2	71.22
28.2	76.46
30.2	80.87
32.2	84.18
34.2	87.6
36.2	89.25
38.2	93.87
40.2	95.53
42.2	99.21

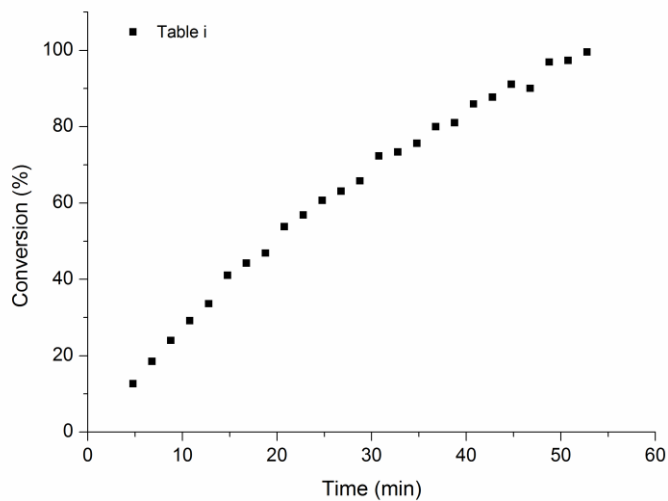


Plot 8. Plot of conversion (%) vs time (min) entry 8 – Table 16

(Entry 9 – Table 16)

Table i. 4BAr^F

t [min]	Conversion [%]
4.8	12.67
6.8	18.50
8.8	24.00
10.8	29.20
12.8	33.63
14.8	41.07
16.8	44.25
18.8	46.90
20.8	53.81
22.8	56.89
24.8	60.71
26.8	63.11
28.8	65.79
30.8	72.32
32.8	73.36
34.8	75.65
36.8	80.00
38.8	81.03
40.8	85.96
42.8	87.72
44.8	91.15
46.8	90.04
48.8	96.92
50.8	97.37
52.8	99.56

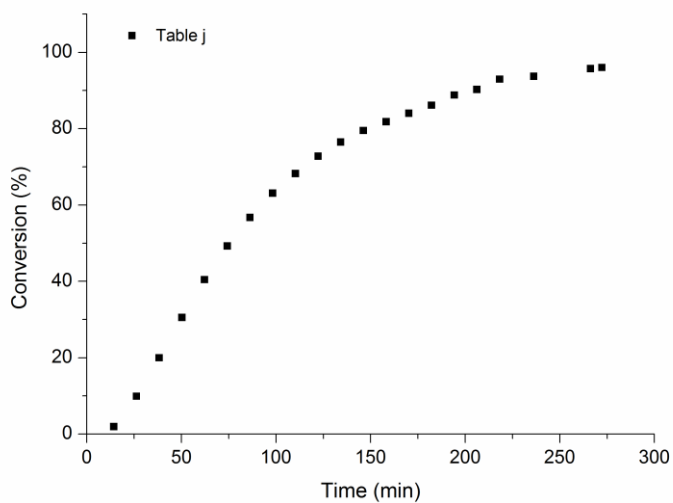


Plot 9. Plot of conversion (%) vs time (min) entry 9 – Table 16

(Entry 10 – Table 16)

Table j. 4TFA

t [min]	Conversion [%]
14.2	1.96
26.2	9.91
38.2	20.00
50.2	30.56
62.2	40.48
74.2	49.24
86.2	56.71
98.2	63.10
110.2	68.25
122.2	72.79
134.2	76.50
146.2	79.53
158.2	81.82
170.2	84.04
182.2	86.15
194.2	88.83
206.2	90.26
218.2	92.97
236.2	93.75
266.2	95.73
272.2	96.04

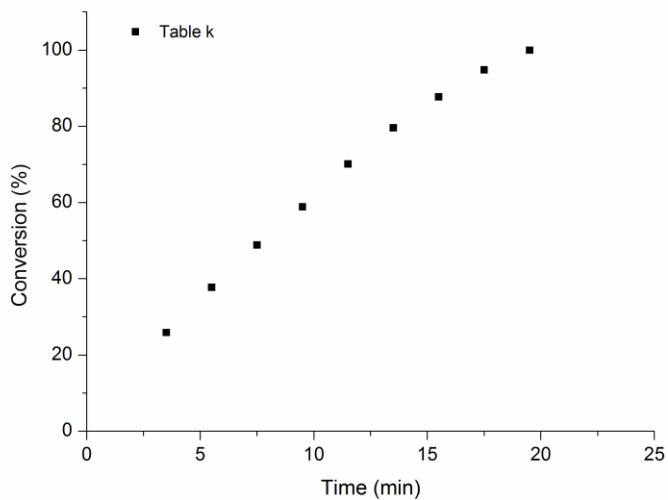


Plot 10. Plot of conversion (%) vs time (min) entry 10 – Table 16

(Entry 12 – Table 16)

Table k. 4OTs + CD₃OD

t [min]	Conversion [%]
3.5	25.91
5.5	37.75
7.5	48.86
9.5	58.90
11.5	70.16
13.5	79.61
15.5	87.74
17.5	94.84
19.5	100.00

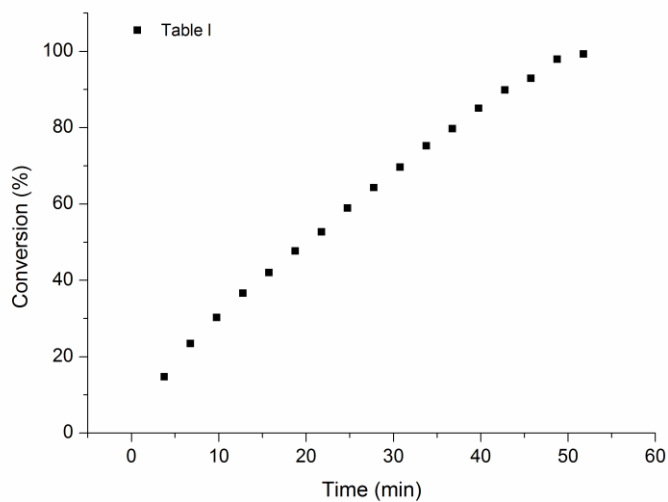


Plot 11. Plot of conversion (%) vs time (min) entry 12 – Table 16

(Entry 13 – Table 16)

Table I. 4OTf + CD₃OD

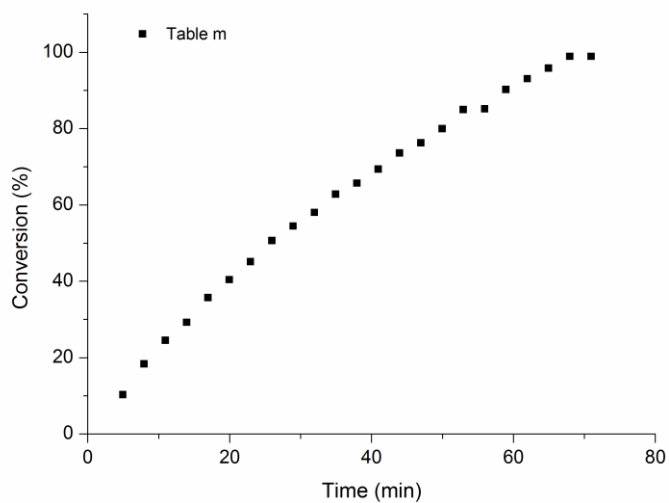
t [min]	Conversion [%]
3.75	14.77
6.75	23.48
9.75	30.30
12.75	36.66
15.75	42.07
18.75	47.70
21.75	52.70
24.75	58.99
27.75	64.31
30.75	69.71
33.75	75.27
36.75	79.74
39.75	85.13
42.75	89.89
45.75	92.93
48.75	97.94
51.75	99.30



(Entry 14 – Table 16)

Table m. $4\text{BF}_4 + \text{CD}_3\text{OD}$

t [min]	Conversion [%]
4.93	10.38
7.93	18.40
10.93	24.57
13.93	29.31
16.93	35.76
19.93	40.48
22.93	45.17
25.93	50.69
28.93	54.51
31.93	58.08
34.93	62.85
37.93	65.74
40.93	69.44
43.93	73.61
46.93	76.29
49.93	80.00
52.93	85.02
55.93	85.22
58.93	90.28
61.93	93.10
64.93	95.86
67.93	98.97
70.93	98.97

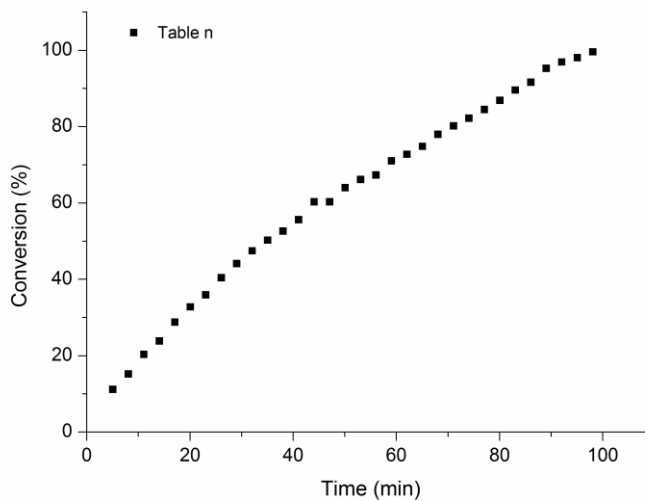


Plot 12. Plot of conversion (%) vs time (min) entry 14 – Table 16

(Entry 15 – Table 16)

Table n. 4BAr^F + CD₃OD

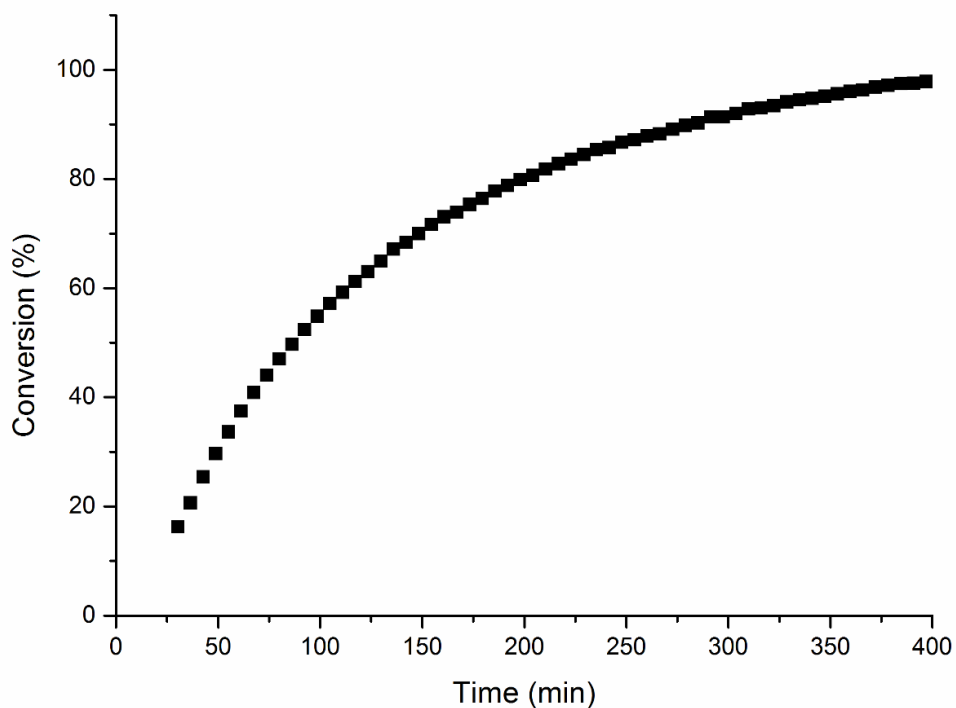
t [min]	Conversion [%]
5.05	11.21
8.05	15.21
11.05	20.33
14.05	23.86
17.05	28.81
20.05	32.79
23.05	35.96
26.05	40.44
29.05	44.14
32.05	47.48
35.05	50.29
38.05	52.64
41.05	55.65
44.05	60.31
47.05	60.31
50.05	64.04
53.05	66.20
56.05	67.31
59.05	71.05
62.05	72.76
65.05	74.86
68.05	78.01
71.05	80.19
74.05	82.22
77.05	84.49
80.05	86.88
83.05	89.59
86.05	91.64
89.05	95.24
92.05	96.92
95.05	98.08
98.05	99.59



Plot 13. Plot of conversion (%) vs time (min) entry 15 – Table 16

(Entry 18 – Table 16)

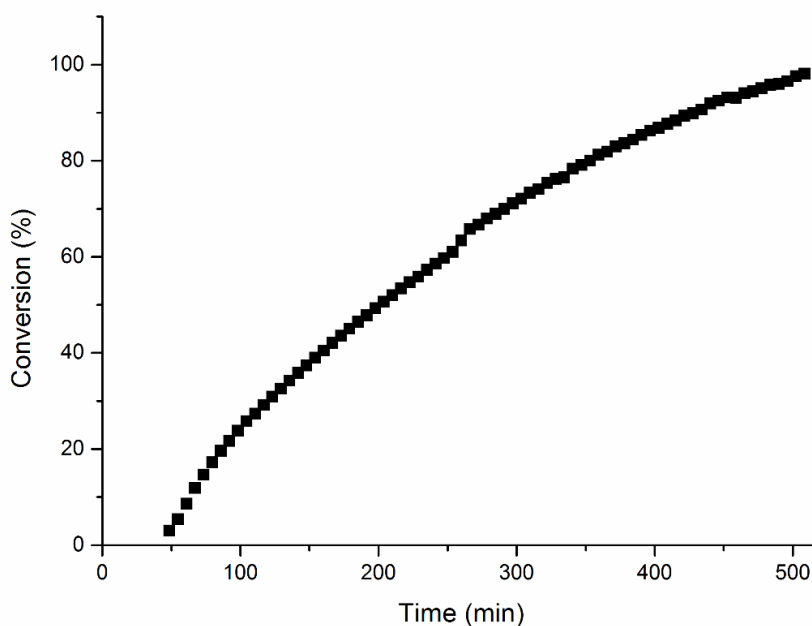
Table o. 4OTs + Gly-OMe					
t [min]	Conversion [%]				
		148.3	69.96	278.9	89.78
		154.6	71.66	285.1	90.27
30.2	16.28	160.8	73.05	291.3	91.35
36.4	20.62	167.0	73.92	297.5	91.34
42.7	25.41	173.2	75.34	303.8	91.98
48.9	29.67	179.4	76.40	310.0	92.84
55.1	33.68	185.6	77.76	316.2	93.05
61.3	37.46	191.9	78.80	322.4	93.39
67.5	40.86	198.1	79.91	328.6	94.12
73.7	44.04	204.3	80.68	334.8	94.54
80.0	47.00	210.5	81.81	341.1	94.76
86.2	49.73	216.7	82.80	347.3	95.15
92.4	52.40	222.9	83.63	353.5	95.58
98.6	54.84	229.2	84.43	359.7	96.08
104.8	57.15	235.4	85.36	365.9	96.33
111.0	59.23	241.6	85.75	372.1	96.80
117.3	61.25	247.8	86.74	378.4	97.17
123.5	63.02	254.0	87.14	384.6	97.45
129.7	64.96	260.2	87.87	390.8	97.52
135.9	67.17	266.5	88.28	397.0	97.88
142.1	68.39	272.7	89.12		



Plot 14. Plot of conversion (%) vs time (min) entry 18 – Table 16.

(Entry 19 – Table 16)

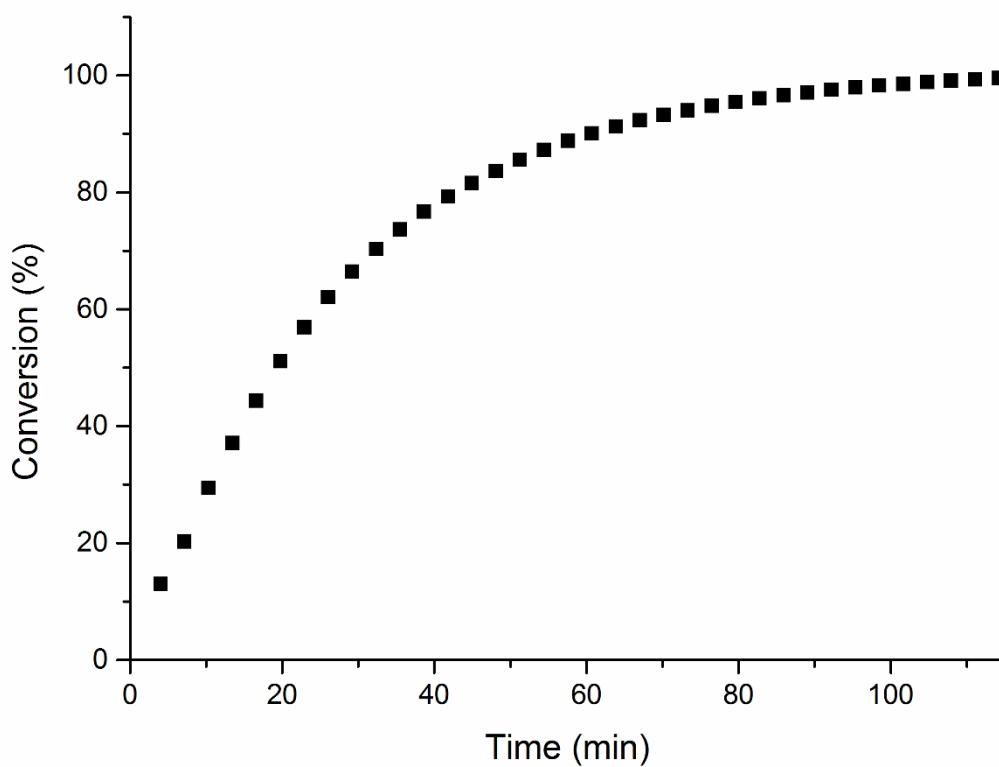
Table p. 4BAr ^F + Gly-OMe					
t [min]	Conversion [%]				
48.5	3.01	197.7	49.29	359.4	81.25
54.7	5.38	203.9	50.70	365.6	81.86
61.0	8.62	210.2	52.00	371.8	82.98
67.2	11.92	216.4	53.42	378.0	83.62
73.4	14.68	222.6	54.72	384.2	84.38
79.6	17.25	228.8	55.88	390.4	85.36
85.8	19.63	235.0	57.30	396.7	86.28
92.0	21.67	241.2	58.60	402.9	86.84
98.3	23.82	247.5	59.77	409.1	87.67
104.5	25.78	253.7	61.02	415.3	88.36
110.7	27.35	259.9	63.41	421.5	89.38
116.9	29.14	266.1	65.78	427.7	89.89
123.1	30.91	272.3	66.71	434.0	90.62
129.3	32.53	278.5	68.01	440.2	91.90
135.6	34.25	284.8	68.98	446.4	92.48
141.8	35.80	291.0	69.99	452.6	93.16
148.0	37.38	297.2	71.13	458.8	93.12
154.2	38.97	303.4	72.13	465.0	94.05
160.4	40.49	309.6	73.32	471.3	94.45
166.6	42.05	315.8	74.08	477.5	95.11
172.9	43.54	322.1	75.39	483.7	95.79
179.1	45.03	328.3	76.24	489.9	95.95
185.3	46.47	334.5	76.56	496.1	96.53
191.5	47.84	340.7	78.33	502.3	97.58
		346.9	79.14	508.6	98.10
		353.1	80.00		



Plot 15. Plot of conversion (%) vs time (min) entry 19 – Table 16.

(Entry 20 – Table 16)

Table q. 4OTs + BnOH			
t [min]	Conversion [%]		
4.0	13.04	60.7	90.10
7.2	20.23	63.9	91.25
10.3	29.44	67.0	92.34
13.5	37.12	70.2	93.25
16.6	44.33	73.3	94.00
19.8	51.10	76.5	94.76
22.9	56.90	79.6	95.44
26.1	62.10	82.8	96.07
29.2	66.48	85.9	96.59
32.4	70.30	89.1	97.05
35.5	73.66	92.2	97.56
38.7	76.67	95.4	97.92
41.8	79.27	98.5	98.28
45.0	81.56	101.7	98.55
48.1	83.66	104.8	98.84
51.3	85.58	108.0	99.11
54.4	87.24	111.1	99.32
57.6	88.81	114.3	99.54

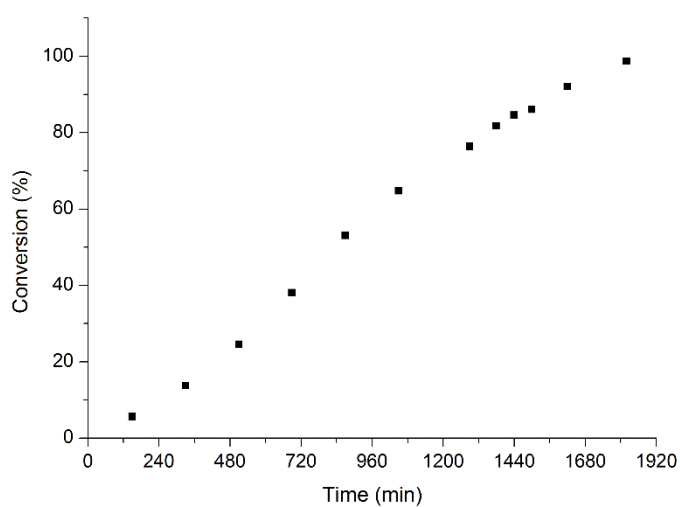


Plot 16. Plot of conversion (%) vs time (min) entry 20 – Table 16

(Entry 21 – Table 16)

Table r. 4BAr^F + BnOH

t [min]	Conversion [%]
149	5.66
329	13.79
509	24.62
689	38.14
869	53.11
1049	64.83
1289	76.47
1379	81.78
1439	84.59
1499	86.07
1619	92.06
1819	98.72

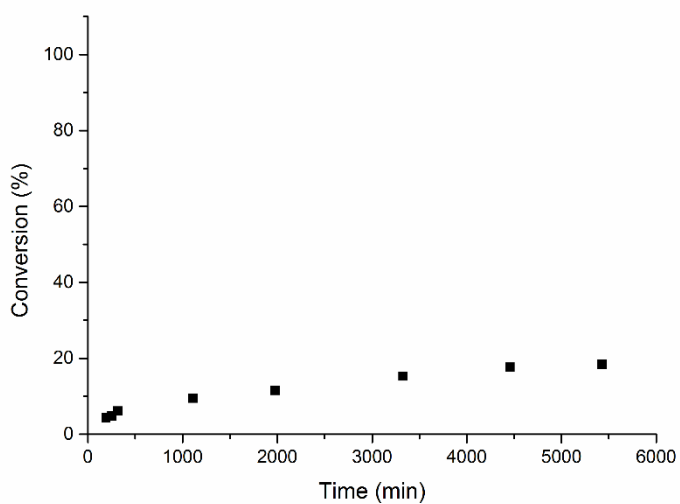


Plot 17. Plot of conversion (%) vs time (min) entry 21 – Table 16.

(Entry 22 – Table 16)

Table s. 4OTs + 2,6-DMP

t [min]	Conversion [%]
190.5	4.31
252.7	4.76
314.8	6.10
1110	9.50
1977	11.56
3326	15.29
4458	17.64
5430	18.37

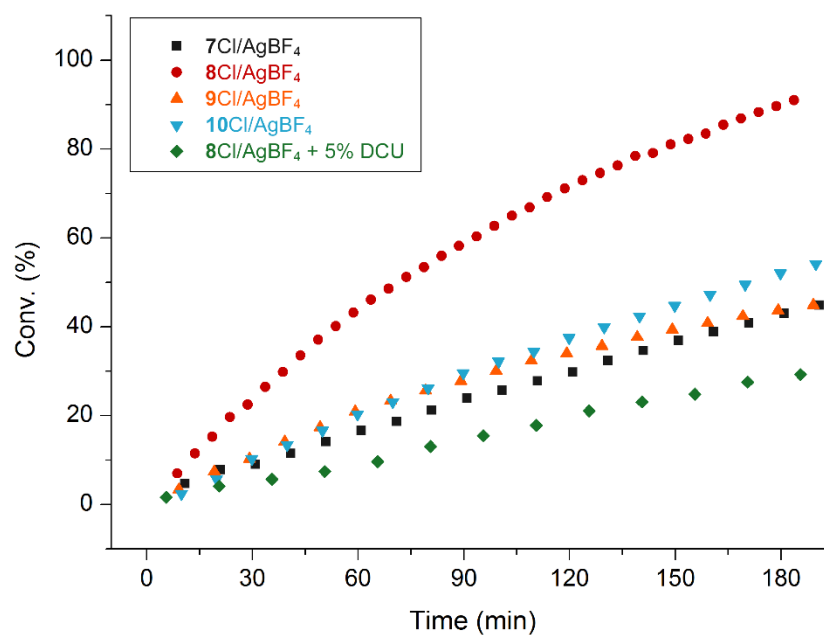


Plot 18. Plot of conversion (%) vs time (min) entry 22 – Table 16

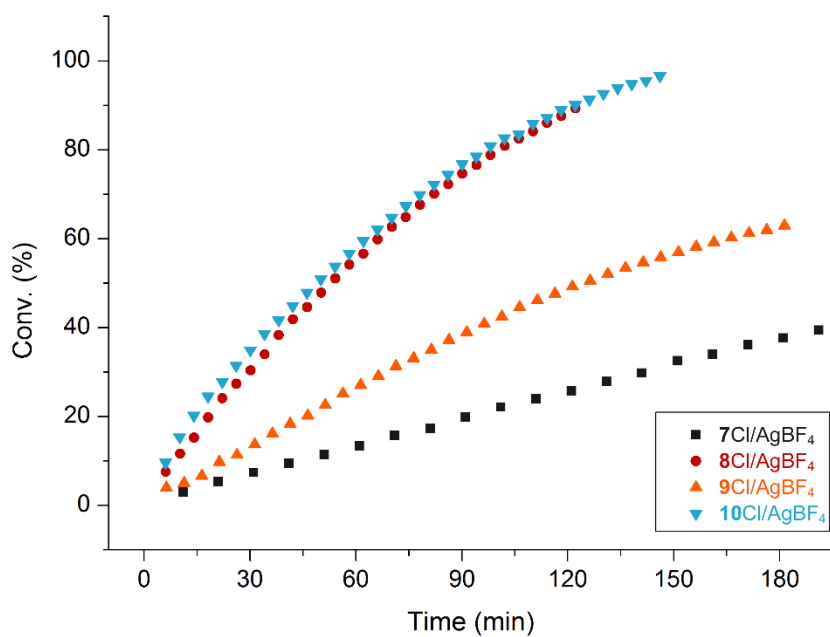
4.3.2 Methoxylation of 3-hexyne catalysed by 7-10X

Table 17. Methoxylation of 3-hexyne catalysed by 7-10X					
Entry	Cat.	AgX	Conv. (Yield) [%] ^[c]		TOF ₃₀ [min ⁻¹] ^[d]
			90 min	180 min	
1	7Cl	BF ₄ ⁻	24 (21)	43 (34)	0.30
2	8Cl	BF ₄ ⁻	59 (55)	91 (87)	0.83
3 ^[a]	8Cl	BF ₄ ⁻	33(26)	54(48)	0.35
4	9Cl	BF ₄ ⁻	28 (23)	44 (37)	0.43
5	10Cl	BF ₄ ⁻	30 (20)	52 (42)	0.36
6	7Cl	OTf ⁻	50 (47)	77 (73)	0.73
7	8Cl	OTf ⁻	83 (79)	99 (96)*	1.60
8	9Cl	OTf ⁻	58 (44)	84 (69)	0.88
9	10Cl	OTf ⁻	57 (54)	91 (88)	0.66
10 ^[b]	7Cl	BF ₄ ⁻	20 (11)	37 (24)	0.26
11 ^[b]	8Cl	BF ₄ ⁻	75 (68)	99 (94)*	1.06
12 ^[b]	9Cl	BF ₄ ⁻	39 (34)	62 (56)	0.43
13 ^[b]	10Cl	BF ₄ ⁻	77 (71)	97 (90)*	1.23

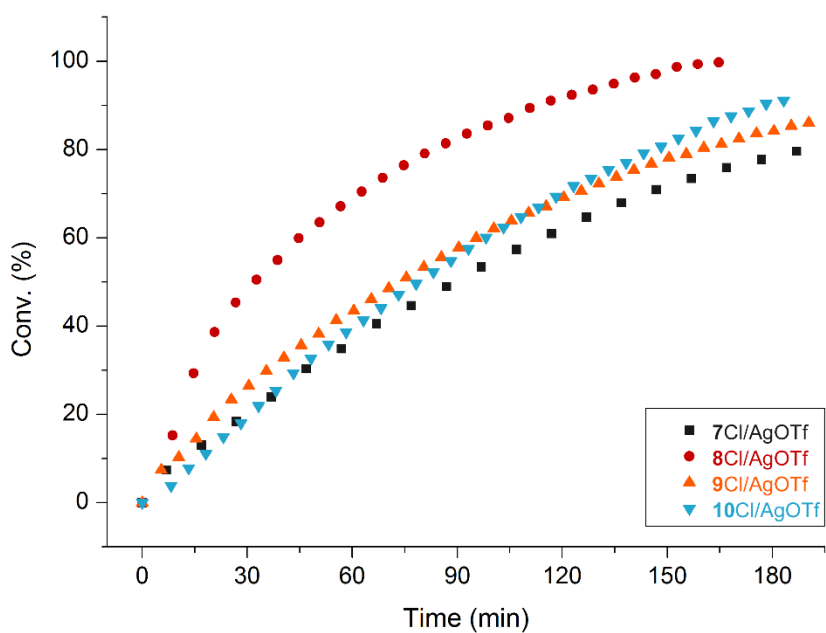
Catalysis conditions: 30 °C, 3-hexyne (100 μL), Cat/AgX (1 mol%), CH₃OH (143 μL), CDCl₃ (400 μL), [a] performed with 5 mol% of N,N'-Dicyclohexylurea as additive, [b] CD₃OD (543 μL). [c] Conversions and TOF₃₀ were determined by ¹H NMR spectroscopy, using TMS as internal standard, as average of three runs. [d] TOF₃₀= (n product /n catalyst)/(30 min). * the catalysis reached full conversion before 180 min.



Plot 19. Methoxylation of 3-hexyne catalysed by 7Cl-10Cl complexes activated with AgBF₄ in CDCl₃ (entry 1-5).



Plot 20. Methoxylation of 3-hexyne catalysed by 7Cl-10Cl complexes activated with AgOTf in CDCl₃ (entry 6-9).



Plot 21. Methoxylation of 3-hexyne catalysed by 7Cl-10Cl complexes activated with AgBF₄ in CD₃OD (entry 10-13).

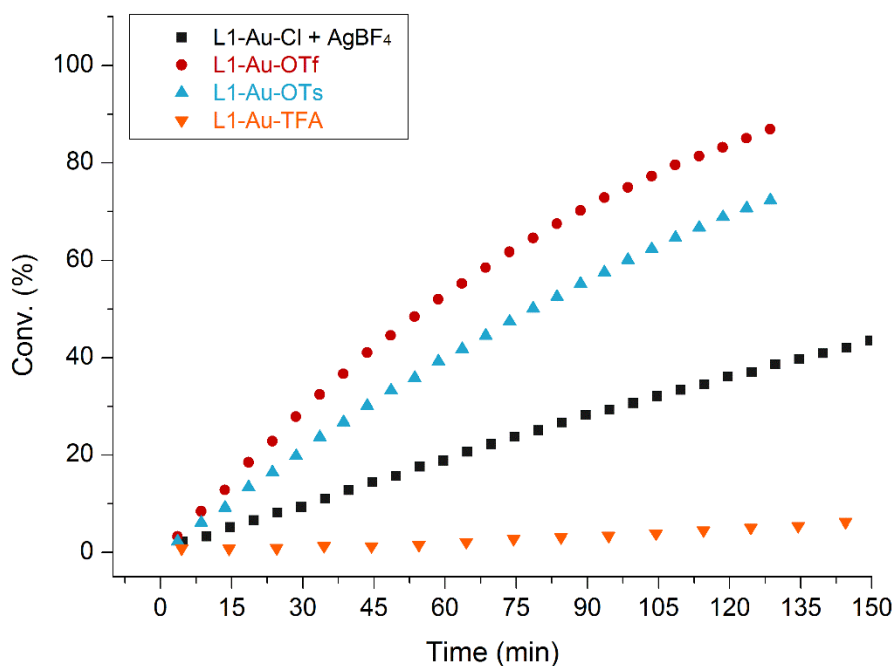
4.3.3 Methoxylation of 3-hexyne catalysed by 1-4X

Table 18. Methoxylation of 3-hexyne catalysed by 1-4X				
Entry	Catalyst	Time (min)	Conversion^[a] (%)	TOF_i^[b] [min⁻¹]
1	1BF₄	120	36	0.31
2	2BF₄	118	>98	2.72
3	3BF₄	120	>98	1.43
4	4BF₄	42	>98	2.86*
5	1OTf	120	84	0.97
6	2OTf	61	>98	5.84
7	3OTf	52	>98	3.45
8	4OTf	33	>98	3.46*
9	1OTs	120	70	0.69
10	2OTs	120	82	2.43
11	3OTs	120	94	2.37
12	4OTs	18	>98	5.06*
13	1TFA	120	5	0.05 ^[c]
14	2TFA	120	4	0.04 ^[c]
15	3TFA	120	1	0.03 ^[c]
16	4TFA	120	72	0.60*

Catalysis conditions: 30 °C, 3-hexyne (100 μL, 0.88 mmol), catalyst 1 mol% (or 1:1 L-Au-Cl/AgX), CH₃OH (143 μL, 4 eq), in CDCl₃ (400 μL). [a] Conversions and TOF_i were determined by ¹H NMR spectroscopy as average of three runs. [b] TOF_i = (n_{product}/n_{catalyst})time (at 30% conversion). [c] In order to calculate the TOF_i value, the catalytic process was followed until 30% conversion was reached.

Methoxylation promoted by 1X (Table 18)

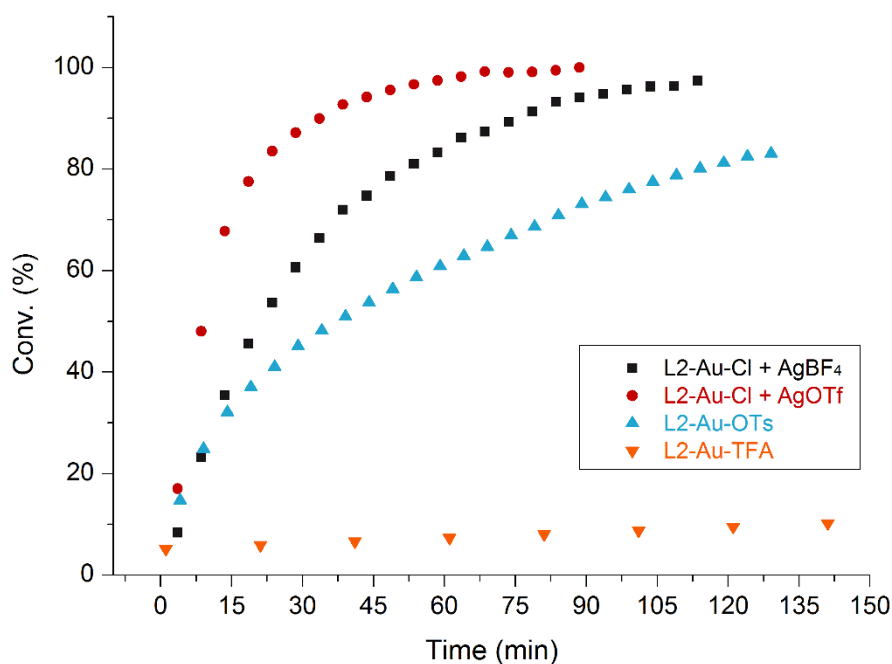
Entry 1, Table 18		...	Entry 5, Table 18		...	Entry 9, Table 18		...	Entry 13, Table 18	
time [min]	Conv. [%]		time[min]	Conv. [%]		time [min]	Conv. [%]		time [min]	Conv. [%]
4.67	2.32		3.55	3.30		3.59	2.29		4.47	0.85
9.67	3.28		8.55	8.46		8.59	6.15		14.47	0.85
14.67	5.20		13.55	12.84		13.59	9.24		24.47	0.94
19.67	6.60		18.55	18.54		18.59	13.41		34.47	1.37
24.67	8.18		23.55	22.86		23.59	16.47		44.47	1.31
29.67	9.37		28.55	27.91		28.59	19.85		54.47	1.58
34.67	11.04		33.55	32.45		33.59	23.68		64.47	2.18
39.67	12.82		38.55	36.69		38.59	26.74		74.47	2.83
44.67	14.44		43.55	41.04		43.59	30.13		84.47	3.18
49.67	15.76		48.55	44.59		48.59	33.30		94.47	3.44
54.67	17.62		53.55	48.43		53.59	35.82		104.47	3.94
59.67	18.86		58.55	52.02		58.59	39.24		114.47	4.55
64.67	20.71		63.55	55.24		63.59	41.75		124.47	5.09
69.67	22.25		68.55	58.52		68.59	44.54		134.47	5.43
74.67	23.73		73.55	61.75		73.59	47.45		144.47	6.31
79.67	25.08		78.55	64.56		78.59	50.10		154.47	7.19
84.67	26.72		83.55	67.51		83.59	52.52		164.47	7.57
89.67	28.24		88.55	70.22		88.59	55.20		174.47	8.03
94.67	29.34		93.55	72.89		93.59	57.54		184.47	8.26
99.67	30.66		98.55	74.98		98.59	60.08		194.47	9.47
104.67	32.09		103.55	77.28		103.59	62.31		204.47	10.12
109.67	33.40		108.55	79.57		108.59	64.64		214.47	10.09
114.67	34.52		113.55	81.38		113.59	66.72		224.47	10.81
119.67	36.10		118.55	83.20		118.59	68.90		234.47	11.35
124.67	37.05		123.55	85.05		123.59	70.68		244.47	11.93
129.67	38.65		128.55	86.96		128.59	72.32		254.47	12.23



Plot 22. Plot (time vs conversion) of entries 1, 5, 9 and 13 of Table 18.

Methoxylation promoted by 2X (Table 18)

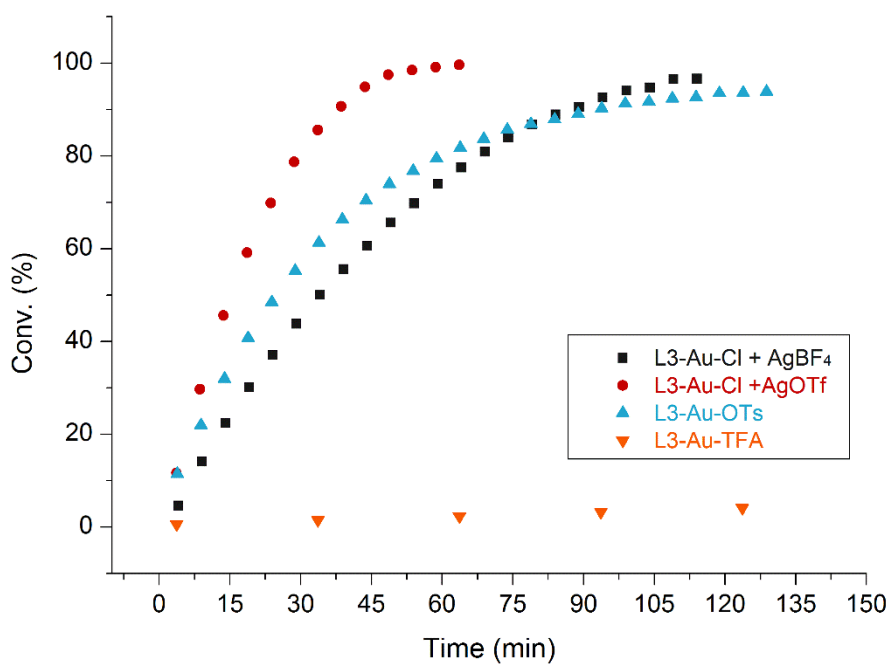
Entry 2, Table 18		...	Entry 6, Table 18		...	Entry 10, Table 18		...	Entry 14, Table 18	
time [min]	Conv. [%]		time [min]	Conv. [%]		time [min]	Conv. [%]		time [min]	Conv. [%]
3.55	8.41		3.55	17.04		4.07	14.76		1.07	5.20
8.55	23.24		8.55	48.04		9.07	24.92		21.07	5.92
13.55	35.40		13.55	67.75		14.07	32.11		41.07	6.64
18.55	45.60		18.55	77.56		19.07	37.03		61.07	7.36
23.55	53.74		23.55	83.54		24.07	41.03		81.07	8.08
28.55	60.64		28.55	87.15		29.07	45.12		101.07	8.80
33.55	66.45		33.55	89.95		34.07	48.20		121.07	9.52
38.55	71.99		38.55	92.70		39.07	50.95		141.07	10.24
43.55	74.76		43.55	94.15		44.07	53.72		161.07	10.96
48.55	78.65		48.55	95.57		49.07	56.37		181.07	11.68
53.55	81.04		53.55	96.67		54.07	58.70		201.07	12.40
58.55	83.28		58.55	97.42		59.07	60.87		221.07	13.12
63.55	86.19		63.55	98.23		64.07	62.93		241.07	13.84
68.55	87.34		68.55	99.21		69.07	64.68		261.07	14.56
73.55	89.30		73.55	99.07		74.07	66.95		281.07	15.28
78.55	91.34		78.55	99.11		79.07	68.66		301.07	16.00
83.55	93.26		83.55	99.43		84.07	70.89		321.07	16.72
88.55	94.14		88.55	100.00		89.07	73.11		341.07	17.44
93.55	94.77		-	-		94.07	74.46		361.07	18.16
98.55	95.72		-	-		99.07	76.02		381.07	18.88
103.55	96.24		-	-		104.07	77.50		401.07	19.60
108.55	96.28		-	-		109.07	78.77		421.07	20.32
113.55	97.42		-	-		114.07	80.14		441.07	21.04
118.55	99.11		-	-		119.07	81.23		461.07	21.76
-	-		-	-		124.07	82.48		481.07	22.48
-	-		-	-		129.07	83.06		501.07	23.20



Plot 23. Plot (time vs conversion) of entries 2, 6, 10 and 14 of Table 18.

Methoxylation B promoted by 3X (Table 18)

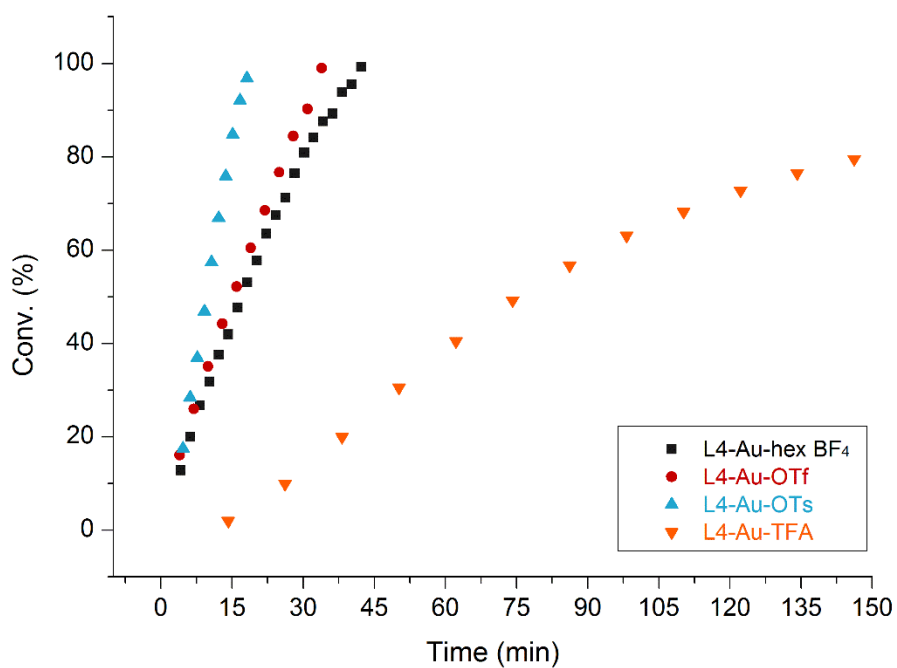
Entry 3, Table 18		...	Entry 7, Table 18		...	Entry 11, Table 18		...	Entry 15, Table 18	
time [min]	Conv. [%]		time[min]	Conv. [%]		time [min]	Conv. [%]		time [min]	Conv. [%]
4.05	4.60		3.63	11.67		3.83	11.50		3.67	0.60
9.05	14.13		8.63	29.72		8.83	21.96		33.67	1.48
14.05	22.39		13.63	45.61		13.83	31.95		63.67	2.36
19.05	30.16		18.63	59.12		18.83	40.73		93.67	3.24
24.05	37.12		23.63	69.84		23.83	48.48		123.67	4.12
29.05	43.82		28.63	78.66		28.83	55.20		153.67	5.00
34.05	50.03		33.63	85.60		33.83	61.29		183.67	5.88
39.05	55.61		38.63	90.70		38.83	66.27		213.67	6.76
44.05	60.60		43.63	94.87		43.83	70.40		243.67	7.64
49.05	65.62		48.63	97.48		48.83	73.94		273.67	8.52
54.05	69.78		53.63	98.48		53.83	76.78		303.67	9.40
59.05	73.92		58.63	99.13		58.83	79.43		333.67	10.28
64.05	77.53		63.63	99.60		63.83	81.78		363.67	11.16
69.05	80.87		68.63	99.10		68.83	83.66		393.67	12.04
74.05	83.89		73.63	99.67		73.83	85.66		423.67	12.92
79.05	86.79		78.63	99.42		78.83	86.89		453.67	13.80
84.05	88.89		-	-		83.83	87.88		483.67	14.68
89.05	90.59		-	-		88.83	89.06		513.67	15.56
94.05	92.59		-	-		93.83	90.28		543.67	16.44
99.05	94.07		-	-		98.83	91.28		573.67	17.32
104.05	94.74		-	-		103.83	91.66		603.67	18.20
109.05	96.58		-	-		108.83	92.39		633.67	19.08
114.05	96.64		-	-		113.83	92.70		663.67	19.96
-	-		-	-		118.83	93.56		693.67	20.84
-	-		-	-		123.83	93.64		723.67	21.72
-	-		-	-		128.83	93.87		753.67	22.60



Plot 24. Plot (time vs conversion) of entries 3, 7, 11 and 15 of Table 18.

Methoxylation promoted by 4X (Table 18)

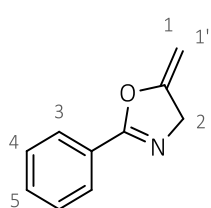
Entry 4, Table 18		...	Entry 8, Table 18		...	Entry 12, Table 18		...	Entry 16, Table 18	
time [min]	Conv. [%]		time [min]	Conv. [%]		time [min]	Conv. [%]		time [min]	Conv. [%]
4.2	12.83		3.94	16.09		4.67	17.53		14.2	1.96
6.2	20.04		6.94	26.01		6.17	28.46		26.2	9.91
8.2	26.75		9.94	35.10		7.67	36.95		38.2	20.00
10.2	31.87		12.94	44.24		9.17	46.86		50.2	30.56
12.2	37.61		15.94	52.18		10.67	57.43		62.2	40.48
14.2	41.97		18.94	60.47		12.17	66.90		74.2	49.24
16.2	47.71		21.94	68.54		13.67	75.88		86.2	56.71
18.2	53.08		24.94	76.66		15.17	84.82		98.2	63.10
20.2	57.83		27.94	84.44		16.67	92.12		110.2	68.25
22.2	63.55		30.94	90.25		18.17	96.87		122.2	72.79
24.2	67.46		33.94	99.00		-	-		134.2	76.50
26.2	71.22		-	-		-	-		146.2	79.53
28.2	76.46		-	-		-	-		158.2	81.82
30.2	80.87		-	-		-	-		170.2	84.04
32.2	84.18		-	-		-	-		182.2	86.15
34.2	87.60		-	-		-	-		194.2	88.83
36.2	89.25		-	-		-	-		206.2	90.26
38.2	93.87		-	-		-	-		218.2	92.97
40.2	95.53		-	-		-	-		236.2	93.75
42.2	99.21		-	-		-	-		266.2	95.73
-	-		-	-		-	-		272.2	96.04
-	-		-	-		-	-		-	-
-	-		-	-		-	-		-	-
-	-		-	-		-	-		-	-
-	-		-	-		-	-		-	-
-	-		-	-		-	-		-	-
-	-		-	-		-	-		-	-
-	-		-	-		-	-		-	-
-	-		-	-		-	-		-	-



Plot 25. Plot (time vs conversion) of entries 4, 8, 12 and 16 of Table 18.

4.3.4 Cyclization of *N*-(prop-2-yn-yl)benzamide to 2-phenyl-5-vinylidene-2-oxazoline.

N-(prop-2-yn-1-yl)benzamide (80 mg, 0.5 mmol) was dissolved in CDCl₃ (500 μL) containing 5 μL of TMS. The solution was then transferred into a 5 mm NMR tube, previously charged with 1 mol% of the catalyst (or 1:1 L-Au-Cl/AgX), and the mixture was vigorously shaken. The time count was started simultaneously. The progress of the reaction was monitored by ¹H NMR at 30 °C. Conversion was calculated from the integral intensities of the vinylidene signals (conversion[%] = (n_{oxazole}) / (n_{propagylamide}) × 100).



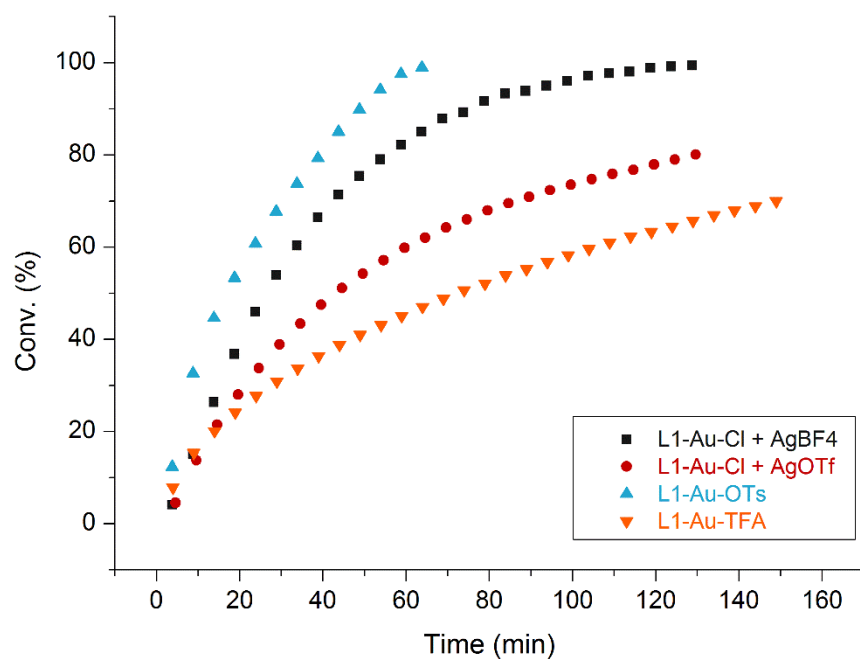
2-phenyl-5-vinylidene-2-oxazoline^{181a} – ¹H NMR (CDCl₃, 200 MHz, 298 K): δ (ppm) 8.04 - 7.91 (m, 2H, H₃), 7.57 - 7.32 (m, 3H, H_{4,5}), 4.80 (dt, 1H, ¹J_{HH} = 2.9 Hz, ⁴J_{HH} = 3.0 Hz, H₁), 4.63 (t, 2H, ⁴J_{HH} = 2.9 Hz, H₂), 4.34 (dt, 1H, ¹J_{HH} = 2.9 Hz, ⁴J_{HH} = 3.0 Hz, H_{1'}).

Table 19. Propargylamide cyclization catalyzed by 1-4X				
Entry	Catalyst	Time (min)	Conversion ^[a] (%)	TOF _i ^[b] [min ⁻¹]
18	1BF ₄	114	>98	1.88
19	2BF ₄	84	>98	1.94
20	3BF ₄	120	55	1.25
21	4BF ₄	99	>98	1.86
22	1OTf	120	78	1.40
5*	1OTf	120	85	1.31
23	2OTf	120	83	0.92
24	3OTf	120	50	0.74
25	4OTf	120	89	1.29
26	1OTs	63	>98	4.16
27	2OTs	40	>98	3.67
28	3OTs	120	53	0.76
29	4OTs	120	65	0.84
30	1TFA	120	63	1.07
31	2TFA	73	>98	3.89
32	3TFA	120	22	0.13 ^[c]
33	4TFA	120	56	0.54

Catalysis A conditions: 30 °C, *N*-(prop-2-yn-yl)benzamide (80 mg, 0.5 mmol), 1 mol% catalyst (or 1:1 L-Au-Cl/AgX) in CDCl₃ (500 μL). [a] Conversions and TOF_i were determined by ¹H NMR spectroscopy as average of three runs. [b] TOF_i = (n_{product}/n_{catalyst})/time (at 30% conversion). [c] In order to calculate the TOF_i value, the catalytic process was followed until 30% conversion was reached. *using isolated L1-Au-OTf as catalyst.

Cyclization promoted by 1X (Table 19)

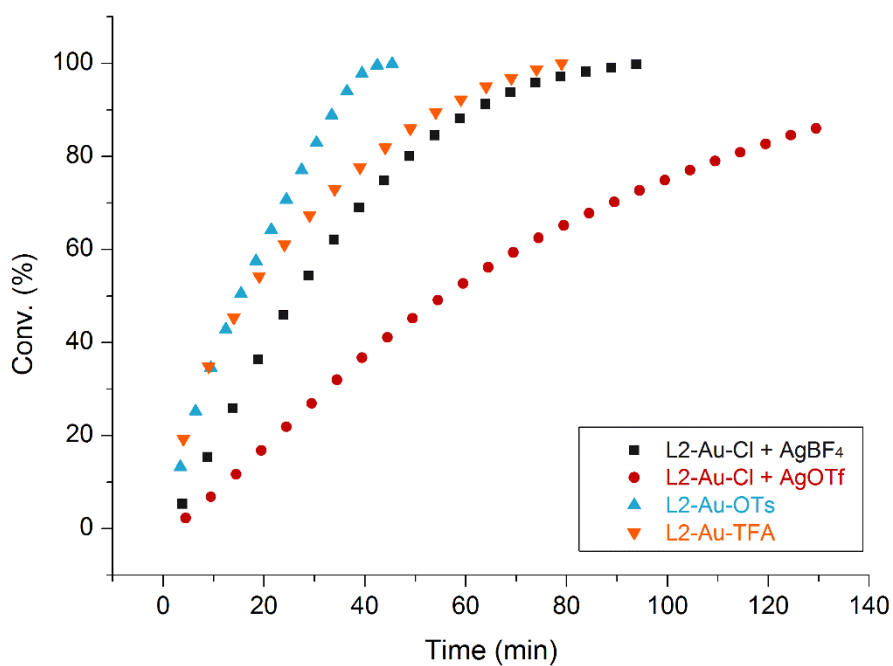
Entry 1, Table 19		...	Entry 5, Table 19		...	Entry 9, Table 19		...	Entry 13, Table 19	
time [min]	Conv. [%]		time [min]	Conv. [%]		time [min]	Conv. [%]		time [min]	Conv. [%]
3.73	4.14		4.59	4.55		3.77	12.34		3.94	7.88
8.73	15.02		9.59	13.78		8.77	32.62		8.94	15.39
13.73	26.39		14.59	21.49		13.77	44.65		13.94	20.08
18.73	36.83		19.59	28.02		18.77	53.33		18.94	24.13
23.73	45.93		24.59	33.75		23.77	60.78		23.94	27.73
28.73	53.91		29.59	38.89		28.77	67.71		28.94	30.89
33.73	60.33		34.59	43.41		33.77	73.74		33.94	33.68
38.73	66.43		39.59	47.49		38.77	79.31		38.94	36.36
43.73	71.42		44.59	51.15		43.77	85.04		43.94	38.82
48.73	75.44		49.59	54.23		48.77	89.85		48.94	40.96
53.73	79.05		54.59	57.14		53.77	94.11		53.94	43.09
58.73	82.19		59.59	59.85		58.77	97.58		58.94	45.08
63.73	85.01		64.59	62.07		63.77	98.94		63.94	47.02
68.73	87.89		69.59	64.23		-	-		68.94	48.87
73.73	89.27		74.59	66.02		-	-		73.94	50.64
78.73	91.64		79.59	67.95		-	-		78.94	52.09
83.73	93.31		84.59	69.50		-	-		83.94	53.87
88.73	93.86		89.59	70.93		-	-		88.94	55.25
93.73	95.02		94.59	72.37		-	-		93.94	56.81
98.73	96.06		99.59	73.54		-	-		98.94	58.23
103.73	97.21		104.59	74.71		-	-		103.94	59.59
108.73	97.69		109.59	75.88		-	-		108.94	61.01
113.73	98.05		114.59	76.74		-	-		113.94	62.31
118.73	98.91		119.59	77.91		-	-		118.94	63.34
123.73	99.19		124.59	78.99		-	-		123.94	64.50
128.73	99.39		129.59	80.08		-	-		128.94	65.72



Plot 26. Plot (time vs conversion) of entries 1, 5, 9 and 13 of Table 19.

Cyclization promoted by 2X (Table 19)

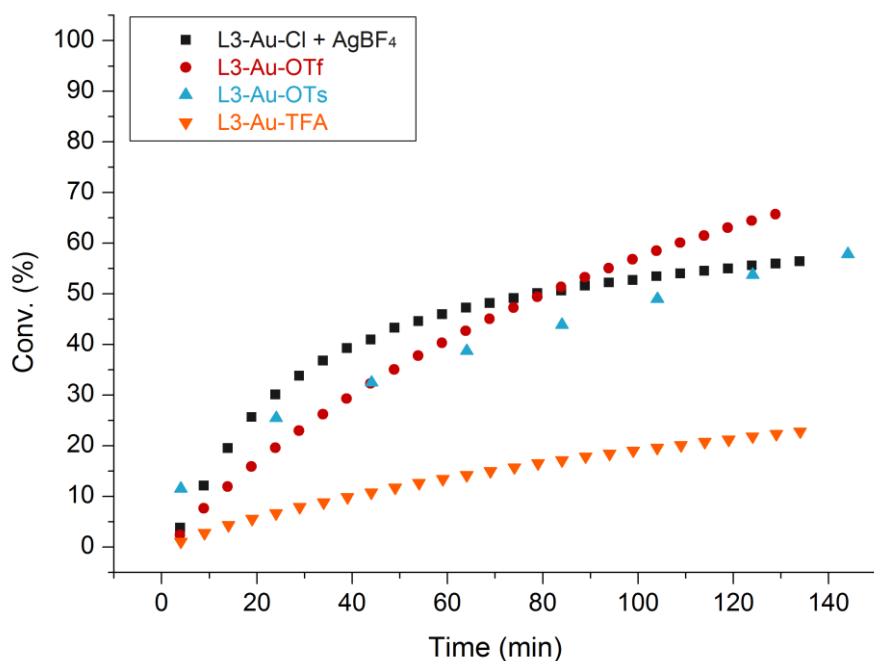
Entry 2. Table 19		...	Entry 6. Table 19		...	Entry 10. Table 19		...	Entry 14. Table 19	
time [min]	Conv. [%]		time[min]	Conv. [%]		time [min]	Conv. [%]		time [min]	Conv. [%]
3.82	5.33		4.45	2.29		3.42	13.24		4.02	19.30
8.82	15.40		9.45	6.84		6.42	25.23		9.02	34.82
13.82	25.94		14.45	11.67		9.42	34.58		14.02	45.39
18.82	36.36		19.45	16.78		12.42	42.84		19.02	54.24
23.82	45.93		24.45	21.90		15.42	50.51		24.02	61.03
28.82	54.42		29.45	26.92		18.42	57.49		29.02	67.38
33.82	62.09		34.45	31.95		21.42	64.20		34.02	72.95
38.82	68.93		39.45	36.72		24.42	70.70		39.02	77.64
43.82	74.81		44.45	41.11		27.42	77.05		44.02	81.89
48.82	80.05		49.45	45.22		30.42	82.91		49.02	86.03
53.82	84.50		54.45	49.11		33.42	88.85		54.02	89.45
58.82	88.13		59.45	52.68		36.42	93.99		59.02	92.21
63.82	91.23		64.45	56.16		39.42	97.86		64.02	95.00
68.82	93.76		69.45	59.36		42.42	99.55		69.02	96.88
73.82	95.81		74.45	62.44		45.42	99.87		74.02	98.72
78.82	97.10		79.45	65.17		48.42	100.00		79.02	99.96
83.82	98.19		84.45	67.80		-	-		84.02	100.00
88.82	99.06		89.45	70.22		-	-		-	-
93.82	99.75		94.45	72.68		-	-		-	-
-	-		99.45	74.86		-	-		-	-
-	-		104.45	77.03		-	-		-	-
-	-		109.45	78.99		-	-		-	-
-	-		114.45	80.84		-	-		-	-
-	-		119.45	82.67		-	-		-	-
-	-		124.45	84.54		-	-		-	-
-	-		129.45	85.99		-	-		-	-



Plot 27. Plot (time vs conversion) of entries 2, 6, 10 and 14 of Table 19.

Cyclization promoted by 3X (Table 19)

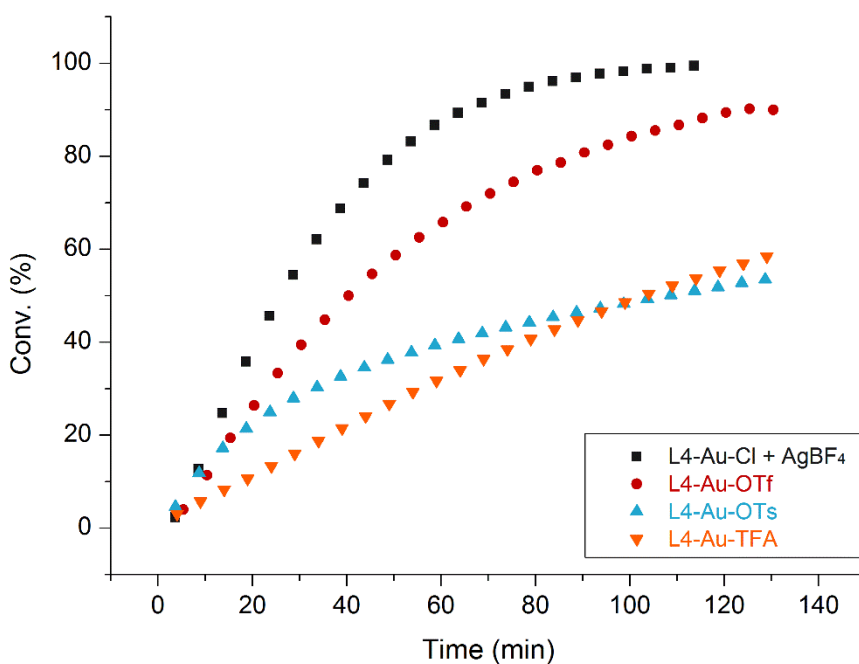
Entry 3, Table 19		...	Entry 7, Table 19		...	Entry 11, Table 19		...	Entry 15, Table 19	
time [min]	Conv. [%]		time [min]	Conv. [%]		time [min]	Conv. [%]		time [min]	Conv. [%]
3.87	3.82		3.83	2.38		3.67	0.93		4.00	1.05
8.87	12.13		8.83	7.64		8.67	4.46		9.00	2.79
13.87	19.57		13.83	11.93		13.67	7.64		14.00	4.32
18.87	25.68		18.83	15.89		18.67	11.02		19.00	5.55
23.87	30.14		23.83	19.58		23.67	14.19		24.00	6.65
28.87	33.80		28.83	22.99		28.67	17.24		29.00	7.89
33.87	36.79		33.83	26.24		33.67	20.34		34.00	8.80
38.87	39.28		38.83	29.31		38.67	23.14		39.00	9.88
43.87	40.98		43.83	32.3		43.67	25.92		44.00	10.77
48.87	43.31		48.83	35.08		48.67	28.55		49.00	11.72
53.87	44.64		53.83	37.77		53.67	31.15		54.00	12.67
58.87	45.99		58.83	40.35		58.67	33.69		59.00	13.41
63.87	47.27		63.83	42.71		63.67	35.98		64.00	14.20
68.87	48.16		68.83	45.09		68.67	38.31		69.00	15.00
73.87	49.15		73.83	47.27		73.67	40.49		74.00	15.73
78.87	50.15		78.83	49.42		78.67	42.67		79.00	16.53
83.87	50.68		83.83	51.35		83.67	44.60		84.00	17.15
88.87	51.61		88.83	53.28		88.67	46.55		89.00	17.87
93.87	52.25		93.83	55.09		93.67	48.27		94.00	18.42
98.87	52.73		98.83	56.83		98.67	50.13		99.00	19.03
103.87	53.46		103.83	58.51		103.67	51.79		104.00	19.60
108.87	54.02		108.83	60.09		108.67	53.47		109.00	20.15
113.87	54.58		113.83	61.51		113.67	54.97		114.00	20.74
118.87	55.00		118.83	63.06		118.67	56.49		119.00	21.23
123.87	55.64		123.83	64.46		123.67	57.94		124.00	21.83
128.87	55.98		128.83	65.73		128.67	59.27		129.00	22.33



Plot 28. Plot (time vs conversion) of entries 3, 7, 11 and 15 of Table 19.

Cyclization promoted by 4X (Table 19)

Entry 4, Table 19		...	Entry 8, Table 19		...	Entry 12, Table 19		...	Entry 16, Table 19	
time [min]	Conv. [%]		time [min]	Conv. [%]		time [min]	Conv. [%]		time [min]	Conv. [%]
3.57	2.33		5.37	3.98		3.70	4.62		4.67	3.04
8.57	12.70		10.37	11.40		8.70	11.83		9.67	5.75
13.57	24.76		15.37	19.40		13.70	17.20		14.67	8.29
18.57	35.81		20.37	26.38		18.70	21.42		19.67	10.64
23.57	45.64		25.37	33.33		23.70	24.96		24.67	13.32
28.57	54.46		30.37	39.44		28.70	27.93		29.67	16.02
33.57	62.13		35.37	44.83		33.70	30.33		34.67	18.79
38.57	68.81		40.37	50.00		38.70	32.59		39.67	21.48
43.57	74.22		45.37	54.65		43.70	34.55		44.67	24.06
48.57	79.19		50.37	58.69		48.70	36.24		49.67	26.78
53.57	83.16		55.37	62.55		53.70	37.81		54.67	29.27
58.57	86.73		60.37	65.77		58.70	39.38		59.67	31.68
63.57	89.35		65.37	69.14		63.70	40.70		64.67	34.02
68.57	91.49		70.37	71.98		68.70	41.95		69.67	36.40
73.57	93.36		75.37	74.42		73.70	43.22		74.67	38.47
78.57	94.94		80.37	76.95		78.70	44.27		79.67	40.70
83.57	96.12		85.37	78.60		83.70	45.43		84.67	42.76
88.57	96.93		90.37	80.78		88.70	46.38		89.67	44.76
93.57	97.73		95.37	82.42		93.70	47.27		94.67	46.64
98.57	98.30		100.37	84.31		98.70	48.26		99.67	48.54
103.57	98.86		105.37	85.49		103.70	49.27		104.67	50.44
108.57	99.02		110.37	86.72		108.70	50.12		109.67	52.15
113.57	99.48		115.37	88.19		113.70	51.05		114.67	53.72
-	-		120.37	89.37		118.70	51.84		119.67	55.41
-	-		125.37	90.20		123.70	52.74		124.67	56.91
-	-		130.37	89.96		128.70	53.48		129.67	58.42



Plot 29. Plot (time vs conversion) of entries 4, 8, 12 and 16 of Table 19.

4.4 4. NMR studies

4.4.1 4.1 Pre-equilibrium studies

NHC gold complex bearing OTs. The treatment of a 1 mM solution of **4OTs** in CDCl_3 with 3.3, 9, 18 and 100 equivalents of 3-hexyne did not cause any variation in the ^1H NMR spectra of the cation, whereas the NMR signal of the anion (Figure 47) become progressively broader and slightly shifted to higher frequencies. Such broadening indicates that the anion and the 3-hexyne are involved in a dynamic equilibrium, which likely is the substitution of the anion by the 3-hexyne (ISIP/OSIP equilibrium). The fact that the frequency of the tosylate anion is only slightly influenced by the excess of 3-hexyne demonstrates that the OSIP is thermodynamically less favoured than the ISIP, but kinetically accessible.

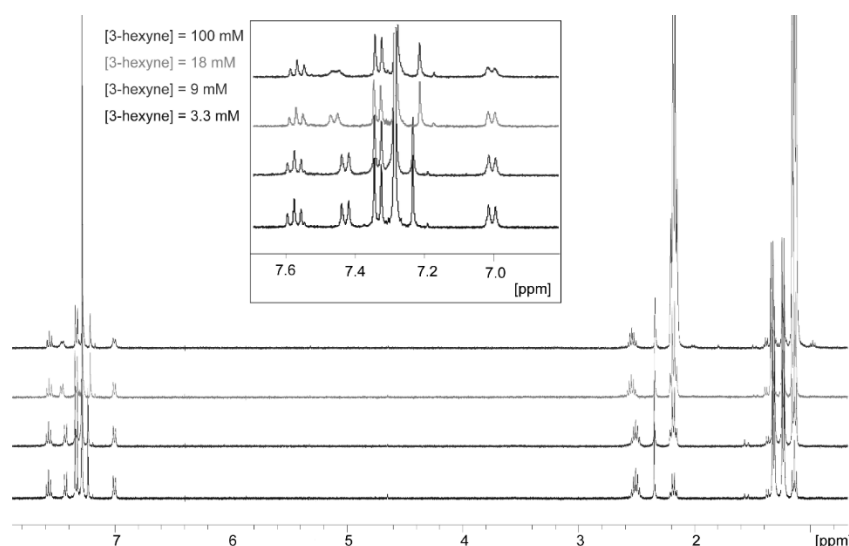


Figure 47. ^1H NMR spectra of **4OTs** (CDCl_3 , 1 mM) in presence of an increasing concentration of 3-hexyne. The insert shows an enlargement of the aromatic section, showing more clearly the broadening of the tosylate anion.

Analysing the aromatic region of the NMR spectra recorded during the addition of MeOH to 3-hexyne catalysed by **4OTs**, it is evident that the anion resonances changes during the course of the catalysis. In particular, the doublet due to the *ortho*-protons of the tosylate shifts from 7.14 ppm at $t = 6$ minutes to 7.08 ppm at $t = 18$ minutes (Figure 20, chapter 2.1). The NMR signal of a non-coordinated tosylate anion can be estimated by the NMR shift of the salt NBu_4OTs , which is 7.17 ppm in $\text{CDCl}_3/\text{CD}_3\text{OD}$ (same concentration of methanol as in the catalytic conditions) and 7.05 ppm in pure CDCl_3 . Therefore, the anion can be considered always not-coordinated to the metal.

NHC gold complex bearing OTf. The treatment of a 1 mM solution of **4OTf** in CDCl_3 with 0.8, 1.3 and 27 equivalents of 3-hexyne caused a variation of the isopropyl signals in the ^1H NMR (Figure 48). This means that the anion substitution by 3-hexyne is accessible.

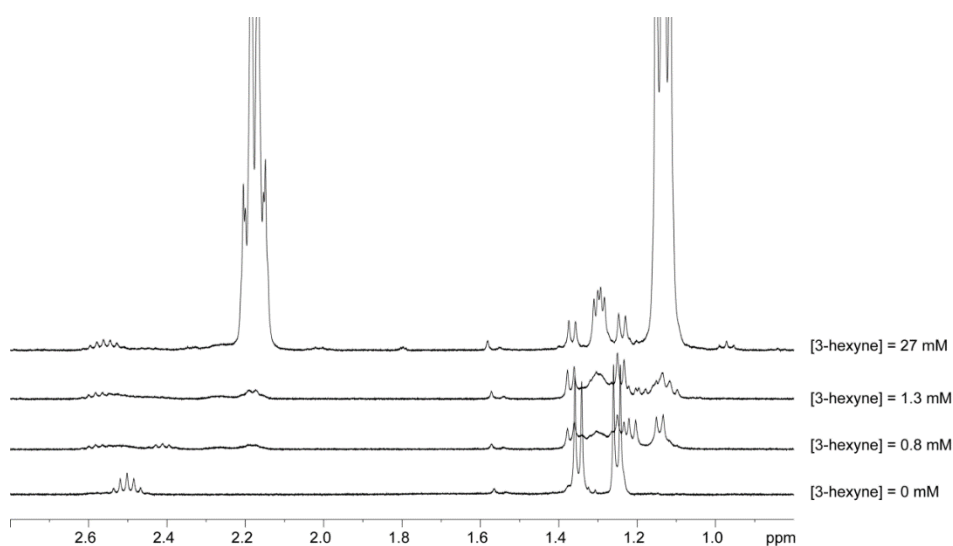


Figure 48. ^1H NMR spectra of 4OTf (1 mM) in presence of an increasing concentration of 3-hexyne.

NHC gold complex bearing TFA. The treatment of a 1 mM solution of 4TFA in CDCl_3 with 0.6, 1.6, 4 and 43 equivalents of 3-hexyne did not cause any variation in the ^1H NMR spectra and a small variation on the broad NMR signal of the anion (Figure 49 left). In particular, when the concentration ratio between the gold complex and the 3-hexyne is larger than 40, the NMR signal of the anion becomes broader and shifts to lower frequencies. As in the case of OTs^- , this means that the anion substitution by 3-hexyne is unfavored, but kinetically accessible.

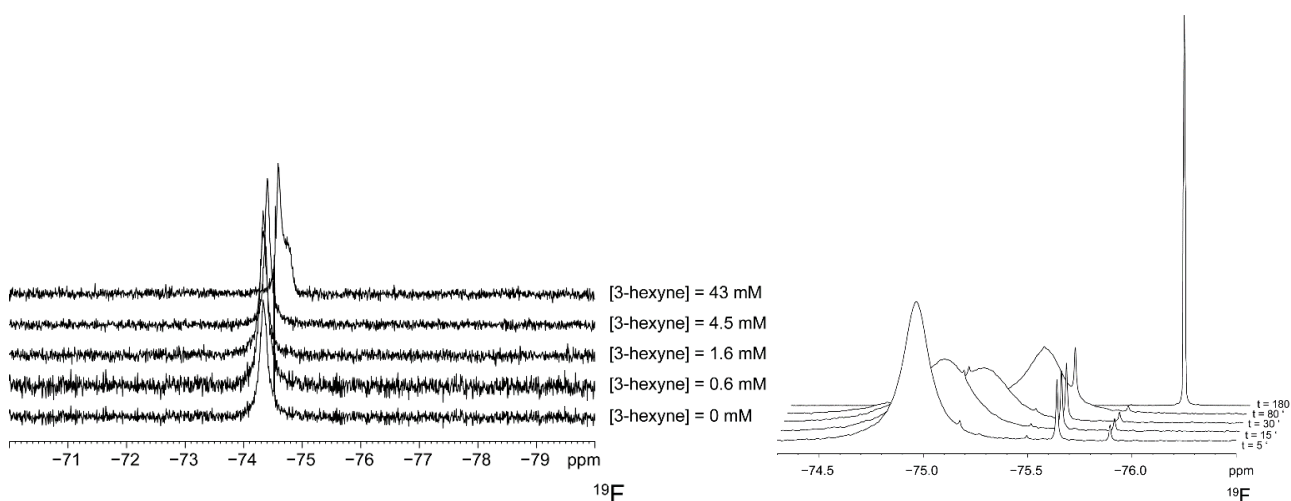


Figure 49. (Left panel) ^{19}F NMR spectra of 4TFA (CDCl_3 , 1 mM) in presence of an increasing concentration of 3-hexyne. (Right panel) ^{19}F NMR spectra of 4TFA in catalytic condition, recorded at different times.

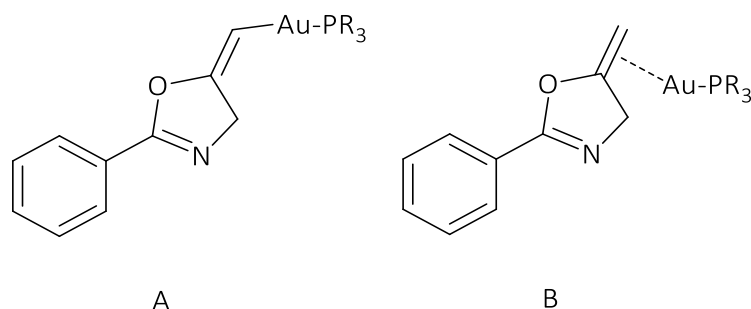
Treating a 1 mM solution of 4TFA in CDCl_3 with MeOH (400 eq), the broad ^{19}F NMR signal relative to the coordinated TFA^- at -73.8 ppm becomes broader, shifts to lower frequencies and, finally, disappears within one hour. At the same time, a different sharp signal rises at -76.3 ppm (Figure 18, chapter 2.1). The

latter was assigned to trifluoroacetic acid by comparison with pure sample. The same trend was observed in catalytic conditions (Figure 49 left). Likely, trifluoroacetate anion reacts with the excess of methanol, giving trifluoroacetic acid and methoxide, which coordinates to the gold center.

NHC complex bearing OAc. Treating a 1 mM solution of **4OAc** in CDCl_3 with 100, 200, 300 and 400 equivalents of methanol, the sharp ^1H NMR signal relative to the coordinated OAc^- at 1.78 ppm becomes broader and shifts to lower frequencies. At the same time, a different sharp signal rises at 2.18 ppm (Figure 19, chapter 2.1). The latter was assigned to trifluoroacetic acid by comparison with pure sample. Differently from TFA^- , OAc^- anion react slowly with the excess of methanol, giving acetic acid (less than 30% in 48 hours) and methoxide, which coordinates to the gold center.

4.4.2 ^{31}P NMR of **1-3X** for cyclization

In the cyclization reactions of propargylamides to oxazoles, it is well known that the RDS is the protodeauration, and that the formation of the σ coordinated species **A** is instantaneous even at -78°C .^{52,181c,d} In order to better understand which catalytic species are present in solution during the catalysis we recorded the ^{31}P -NMR spectra for each run after 130 minutes.



Scheme 29. Species present in solution during the catalysis (σ and π coordination of gold on the vinyl bond).

In the case of **L1** complexes, only two species were clearly dominant: the σ -vinyl species (**A**, Scheme 29) around 43 ppm as reported by Fürstner *et al.*,^[216] and the π species (**B**, Scheme 29) whose resonance is between 34 and 33 ppm, as reported by Widenhoefer *et al.*^[217] For **1TFA** we observed also the presence of the σ -alkyne derivative at about 42 ppm as reported by Hashmi *et al.*^[218] and the $\text{Ph}_3\text{P-Au-TFA}^{210}$ or -OMe around 30 ppm.^[219]

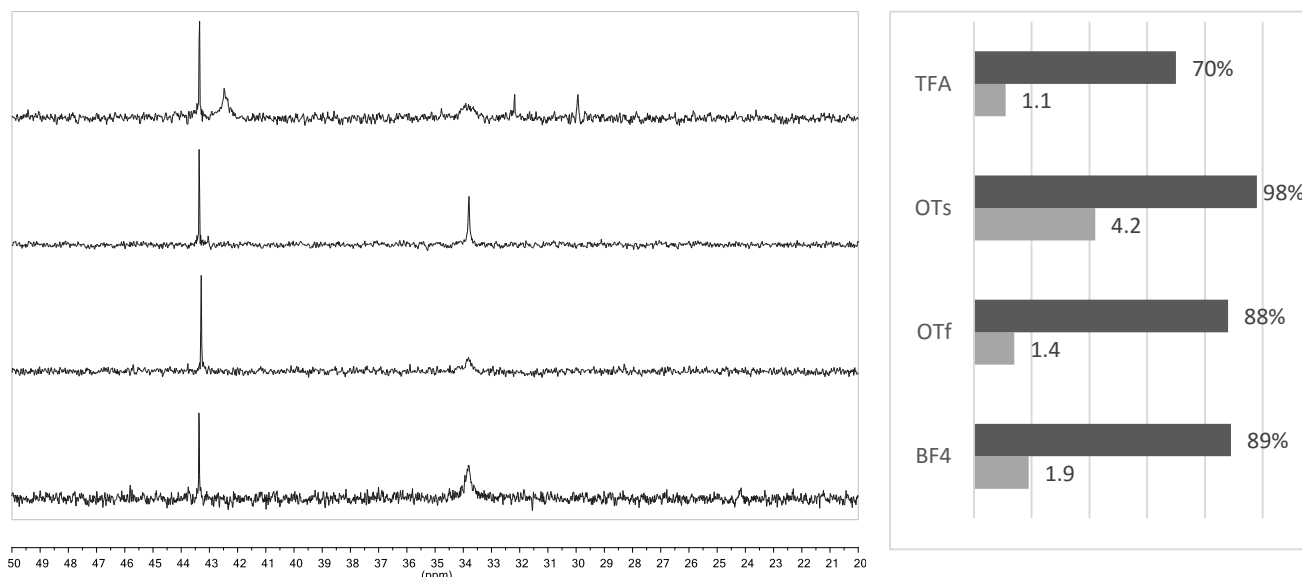


Figure 50. ^{31}P NMR spectra of $\text{Ph}_3\text{P-Au-X}$ in catalysis A, ■ Conversion reached when the phosphorous was recorded, ■ TOF_i.

Concerning **L2** complexes, in the case of the most coordinating anions (TFA^- and OTs^-) the main species detectable is **A** around 93 ppm,^[220] whereas species **B** is hardly observable.²²⁰ Both species **A** and **B** are observable for OTf^- and BF_4^- , but other P-containing unidentified complexes are clearly present.

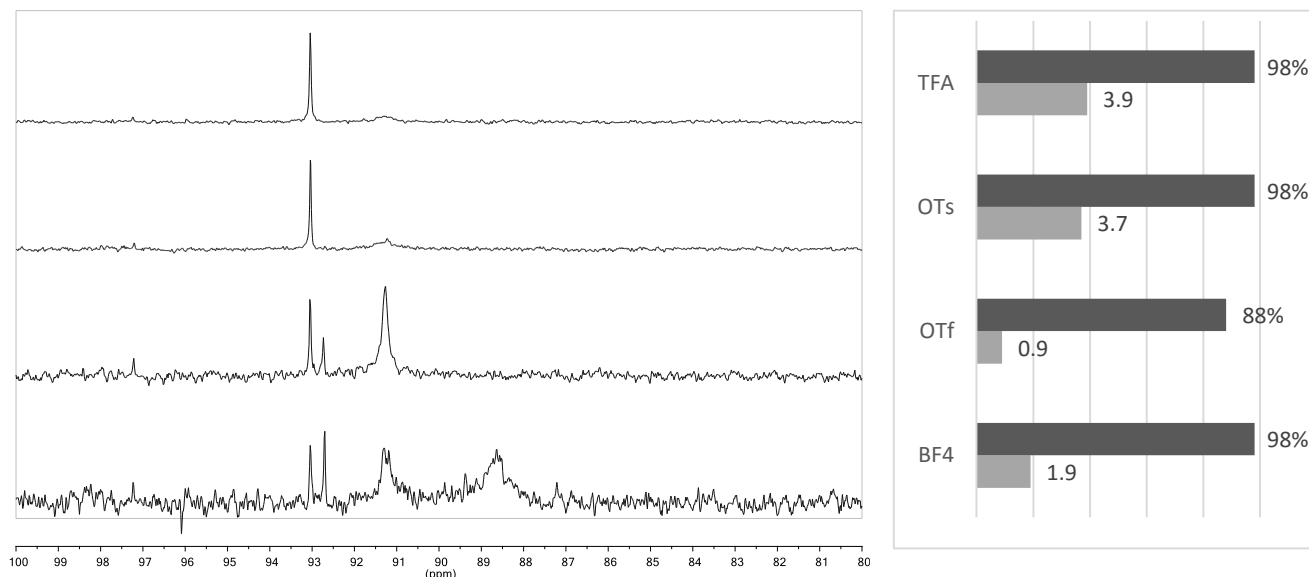


Figure 51. ^{31}P NMR spectra of $^t\text{Bu}_3\text{P-Au-X}$ in catalysis A, ■ Conversion reached when the phosphorous was recorded, ■ TOF_i .

As far as **L3** ligand is concerned, to the best of our knowledge no ^{31}P NMR characterization of complexes type **A** and **B** is present in the literature. We can safely suggest that the prevailing species should be **A** (around 46 ppm, similar to **L1**) and a second one containing the product (2-phenyl-5-vinylidene-2-oxazoline) coordinated to gold through the nitrogen atom (around 22 ppm).²¹⁹

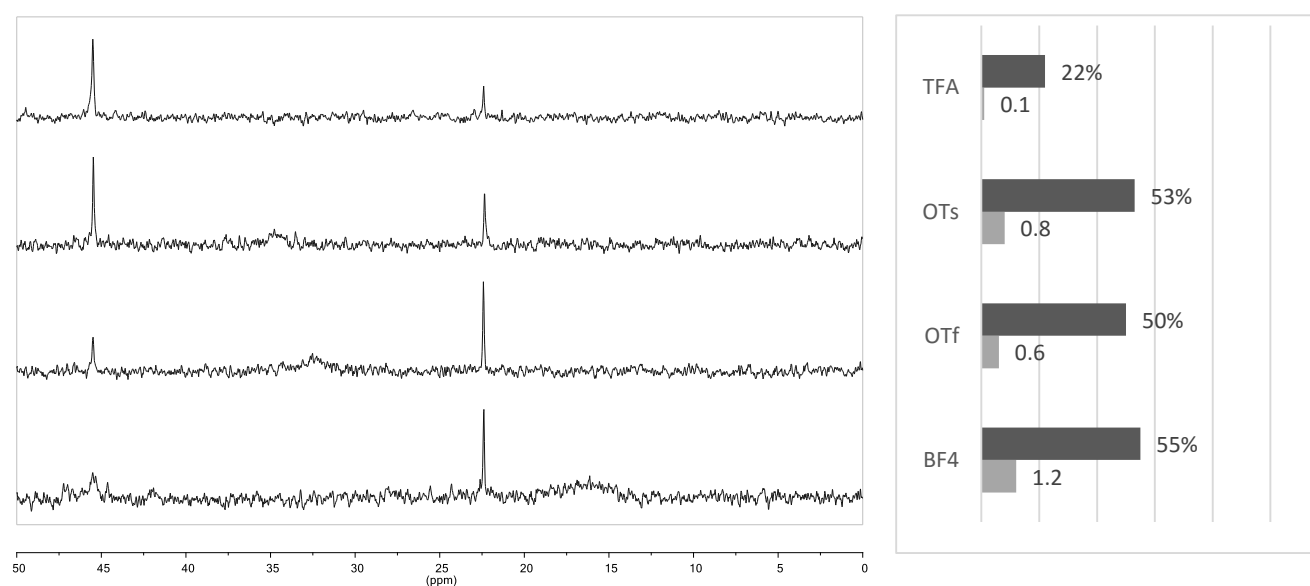
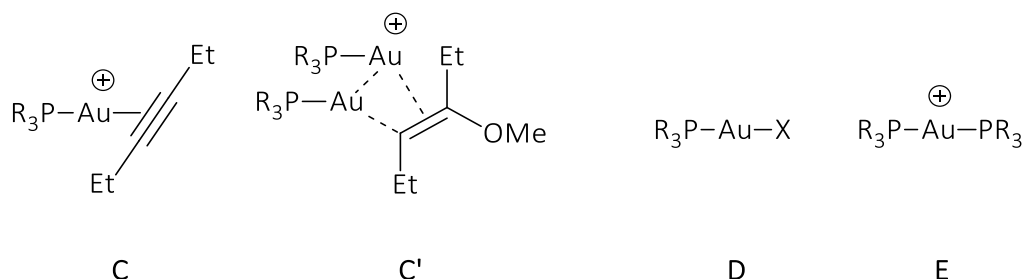


Figure 52. ^{31}P NMR spectra of PARF-Au-X in catalysis A, ■ Conversion reached when the phosphorous was recorded, ■ TOF_i .

4.4.3 ^{31}P NMR of **1-3X** for methoxylation

In order to better understand which catalytic species are present during the catalysis **B** we recorded the ^{31}P -NMR spectra for each run after 130 minutes (Scheme 30).



Scheme 30. Species present in solution during the catalysis.

In the case of **L1** complexes, it is possible to identify the following species: the $[\text{L1-Au-L1}]^+$ derivate **E** around 45 ppm,^[221] the π species **C**²¹⁷ (or **C'**, as suggested by Zhdanko and Mayer^[222]) at about 37 ppm and the ISIP species **D** below 30 ppm.^{[209],[97a],[210]} As we can be clearly noted in Figure S12, their relative abundance depends on the anion: for weak coordinating anions (BF_4^- and OTf^-) the predominant species is the π coordinated (**C** and/or **C'**) and is also possible to observe the formation of small amounts of **E**. For the most coordinating anions (OTs^- and TFA^-) also the ISIP species (**D**) is significantly present in solution.

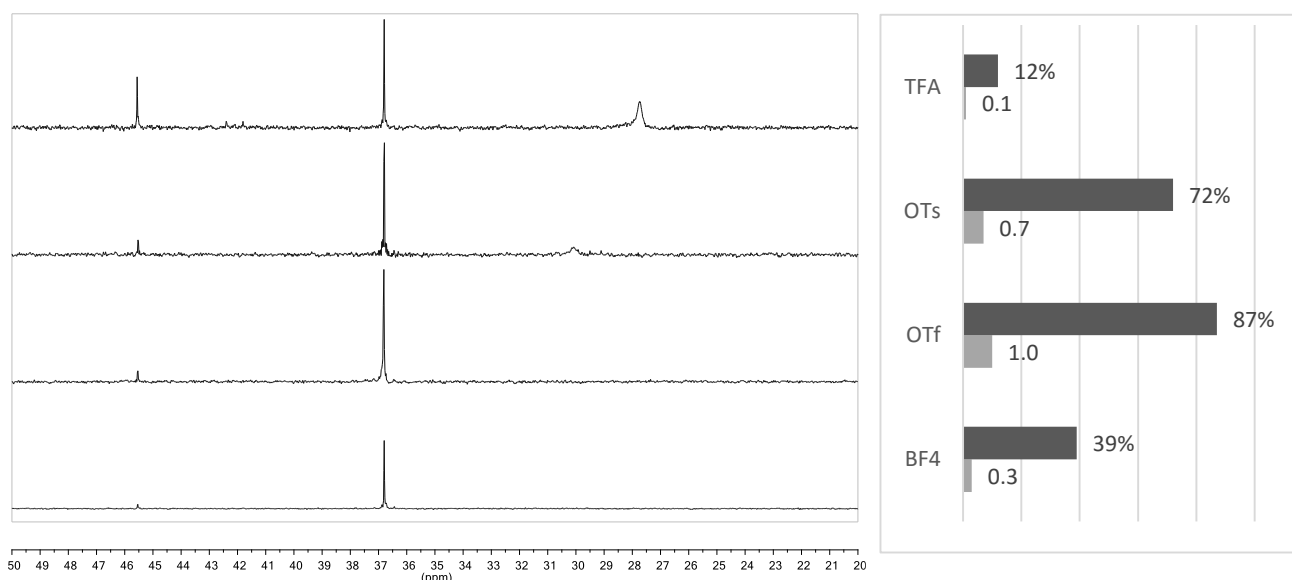


Figure 53. ^{31}P NMR spectra of $\text{Ph}_3\text{P-Au-X}$ in catalysis **B**, ■ Conversion reached when the phosphorous was recorded, ■ TOF_i.

For **L2** complexes, two species are predominant: **C** (and/or **C'**) around 93 ppm and the ISIP complex **D** whose signal appears below 91 ppm.^[220] In-depth study of the behavior of **2OTs** during the outcome of the catalysis shows that the anion tends to re-coordinate to the $[\text{L2-Au}]^+$ fragment (**Figure 39**).

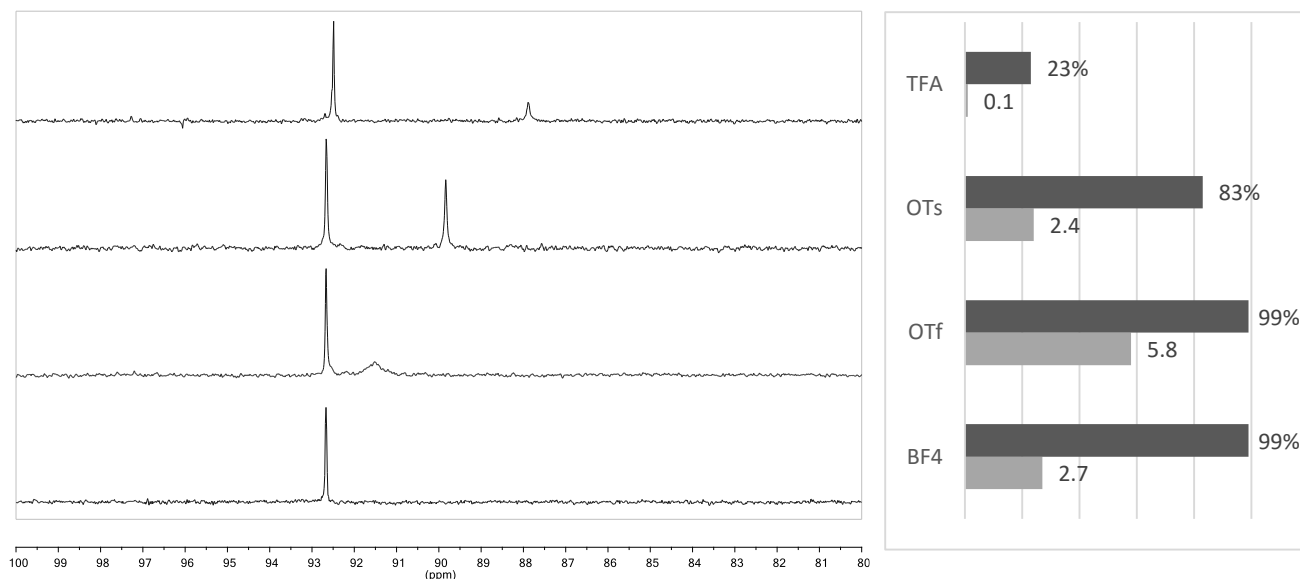


Figure 54. ^{31}P NMR spectra of $^t\text{Bu}_3\text{P-Au-X}$ in catalysis B, ■ Conversion reached when the phosphorous was recorded, ■ TOFi.

Concerning **L3** ligand ^{31}P NMR characterization of type **C** and **E** species is described in literature, their resonances being detectable at about 41 and 47 ppm, respectively.^{70b} By contrast, no ^{31}P NMR characterization can be found for **C'**. When the anion is BF_4^- , we can see that type **C** (and/or **C'**) complex is present in solution. In the case of OTf^- , the prevalent species is **E**, most probably because the ^{31}P NMR spectrum was recorded about one hour after the complete conversion of the substrate. For OTs^- , as observed for other phosphines complexes, the prevalent species at the end of the catalysis is **D**. Finally, species **E** is present together with a second not characterized species in the case of TFA^- .

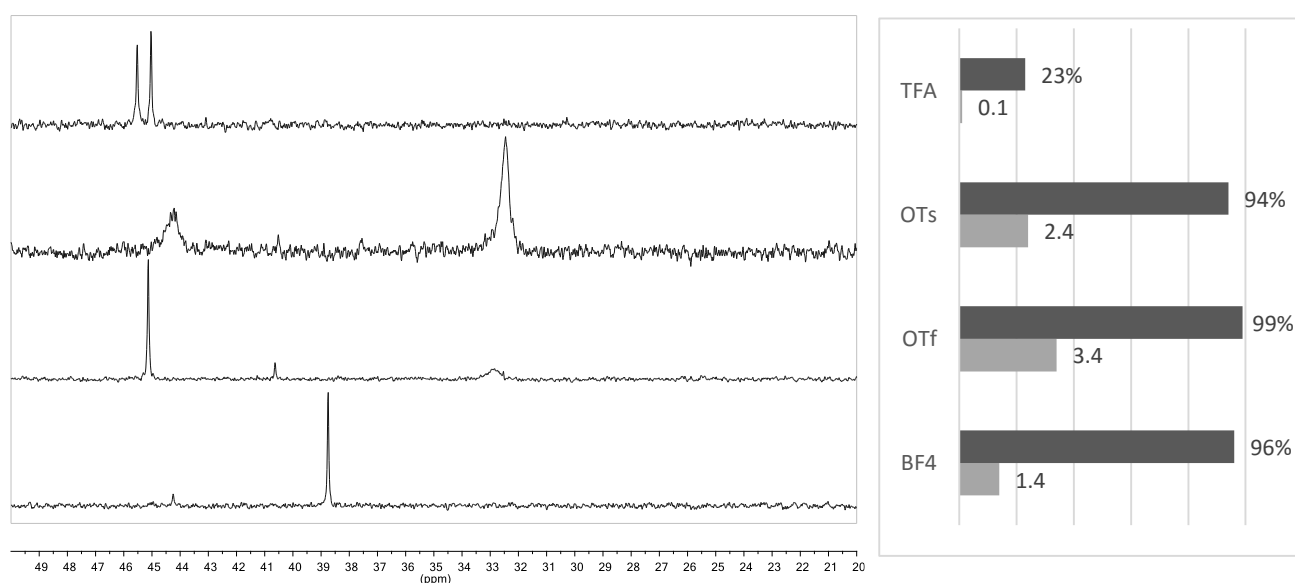


Figure 55. ^{31}P NMR spectra of PARf-Au-X in catalysis B, ■ Conversion reached when the phosphorous was recorded, ■ TOF₃₀.

4.4.4 Intramolecular and Interionic Characterization.

4-8BF₄ and **10BF₄** were characterized in solution by ^1H , ^{13}C , ^{19}F NMR spectroscopies (Chapter 2.2). Proton and carbon resonances belonging to the ligand and alkyne were assigned by combining the information coming from ^1H , ^{13}C , ^1H -COSY, ^1H -NOESY, ^1H , ^{13}C HMQC NMR, and ^1H , ^{13}C HMBC NMR techniques. The ^1H -NOESY²²³ NMR experiments were acquired by the standard three-pulse sequence or by the PFG version.²²⁴ Two-dimensional ^{19}F , ^1H -HOESY NMR experiments were acquired using the standard four-pulse sequence or the modified version.²²⁵ The number of transients and the number of data points was chosen according to the sample concentration and to the desired final digital resolution. Semi-quantitative spectra were acquired using a 1s relaxation delay and 800 ms mixing times.

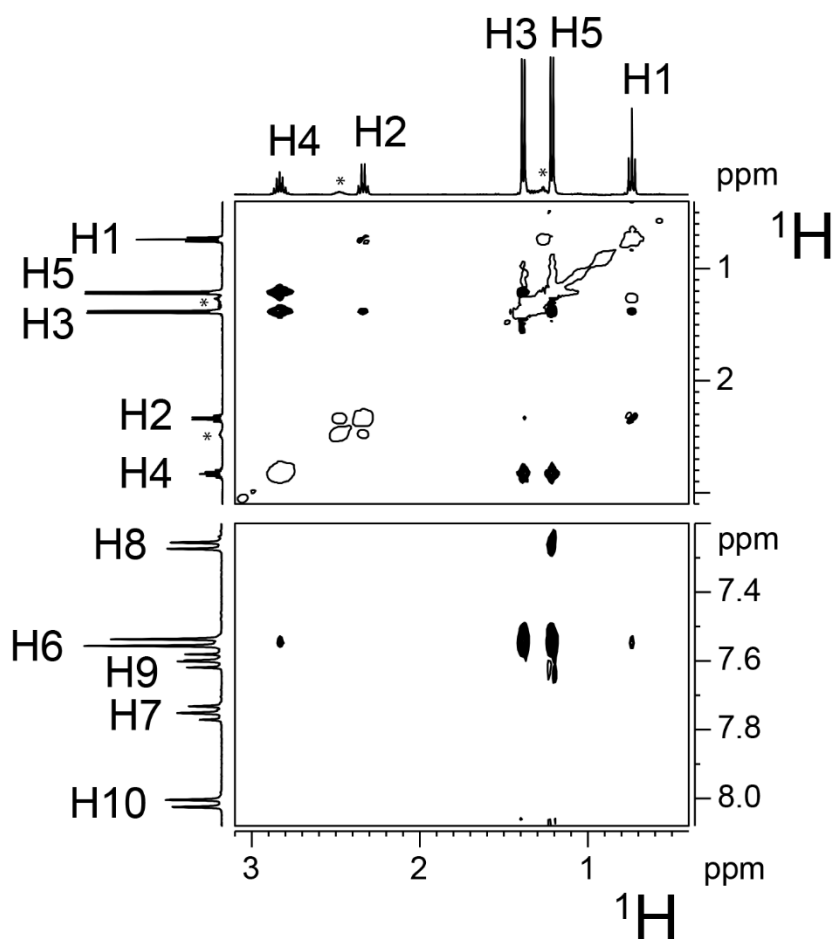


Figure 56. A section of ^1H -NOESY NMR spectrum (400.13 MHz, 297 K, CD_2Cl_2) of the complex **6BF₄** showing dipolar correlations between H3 with H2 and between H5 with H8. From these dipolar interactions the orientation of the methyl of isopropyl groups and the assignment of H8 of acenaphthene moiety are elucidated. *denotes the resonances of free 3-hexyne

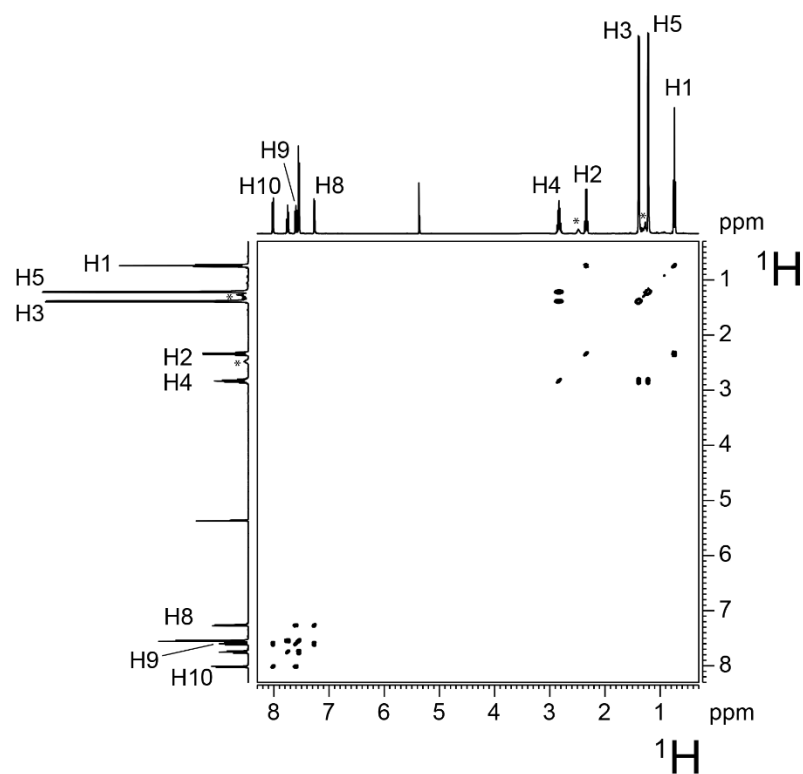


Figure 57. ^1H -COSY NMR spectrum (400.13 MHz, 297 K, CD_2Cl_2) of the complex 6BF_4 showing scalar correlations between H8 with H9 and between H9 with H10 of the acenaphthene moiety. *denotes the resonances of free 3-hexyne, when it was activated *in situ*.

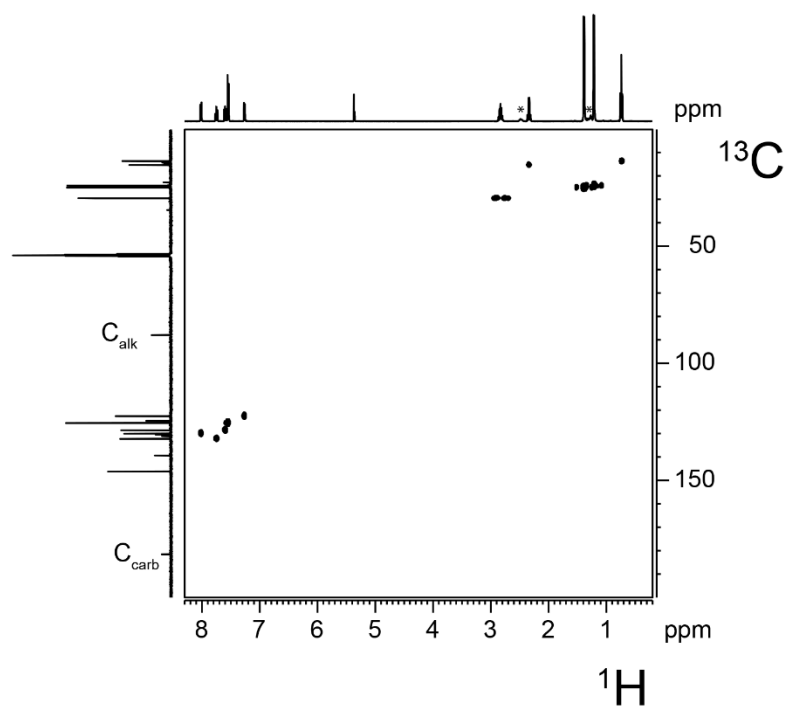


Figure 58. ^1H , ^{13}C HMQC NMR spectrum (400.13 MHz, 253 K, CD_2Cl_2) of the complex 6BF_4 . *denotes the resonances of free 3-hexyne, when it was activated *in situ*.

The anion-cation relative orientation in solution⁶⁵ for complexes **4-6**BF₄ was determined by detecting dipolar interionic interactions in the ¹⁹F,¹H-HOESY NMR spectra (Figure 24, Figure 25 and Figure 26, Chapter 2.1.1). Two-dimensional ¹⁹F,¹H-HOESY NMR experiments were acquired using the standard four-pulse sequence or the modified version.²²⁵ The number of transients and the number of data points was chosen according to the sample concentration and to the desired final digital resolution. Semi-quantitative spectra were acquired using a 1s relaxation delay and 800 ms mixing times.

Complexes **7-10**BF₄ are not stable in methanol since they react with the solvent, undergoing the nucleophilic attack of the methanol itself on the 3-hexyne. For this reason, we synthesized **7**(PPh₃)BF₄, in which the 3-hexyne has been substituted with the triphenylphosphine. The -NH moiety is not visible in the spectrum, probably because a H/D exchange with the solvent occurs. Remarkably, the two *tert*-butyl groups are magnetically equivalent (*syn-syn* isomer). The relative anion/cation orientation in solution of **7**(PPh₃)BF₄ complex has been investigated by ¹⁹F, ¹H-HOESY NMR spectroscopy (Figure 28, Chapter 2.2.2) in methanol-d₄ at room temperature. A weak NOE contact is visible between BF₄⁻ and the two *tert*-butyl groups of the carbene (Figure 29, Chapter 2.2.2). A very small contact is visible at 4.70 ppm, but it does not correspond with any signal. The contact could be due to the -NH moiety, which is almost completely deuterated by H/D exchange with the solvent, but the remaining traces of NH are expected to give an intense NOE contact (Figure 29, Chapter 2.2.2).

4.4.5 4.5 EXSY NMR measurements and Eyring plots.

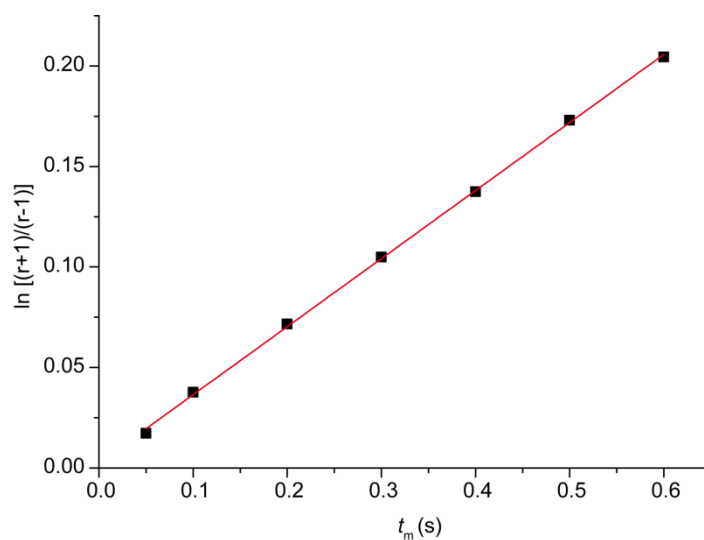
In the EXSY NMR spectrum, the integration of diagonal (AA and BB) and off-diagonal (AB and BA) peaks allows the rotation rate (k_r) to be obtained through Eq. 1.^{66e}

$$k_r = \frac{1}{t_m} \times \ln \left(\frac{r+1}{r-1} \right) \quad \text{Eq. 1}$$

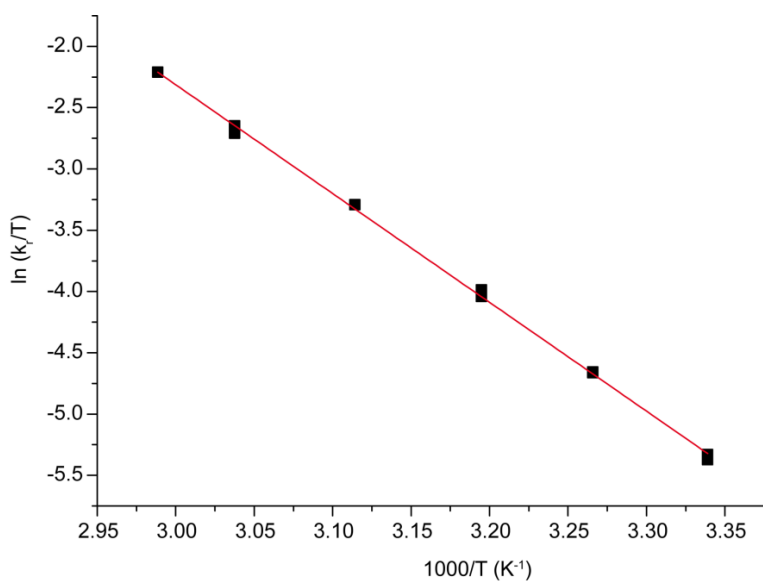
where t_m is the mixing time, and

$$r = \frac{(AA+BB)}{(AB+BA)} \quad \text{Eq. 2}$$

The T_1 relaxation time is 1.5 and 1.8 s for protons A and B, respectively, for the smallest complex (**9Cl**) and 0.8 and 0.7 s for the largest one (**9NHC**). All the EXSY NMR experiment have been performed with a $t_m < T_1$, and, specifically, always smaller or equal to 0.4 s. At 0.4 s the value of $\ln [(r+1)/(r-1)]$ is still directly proportional to t_m .

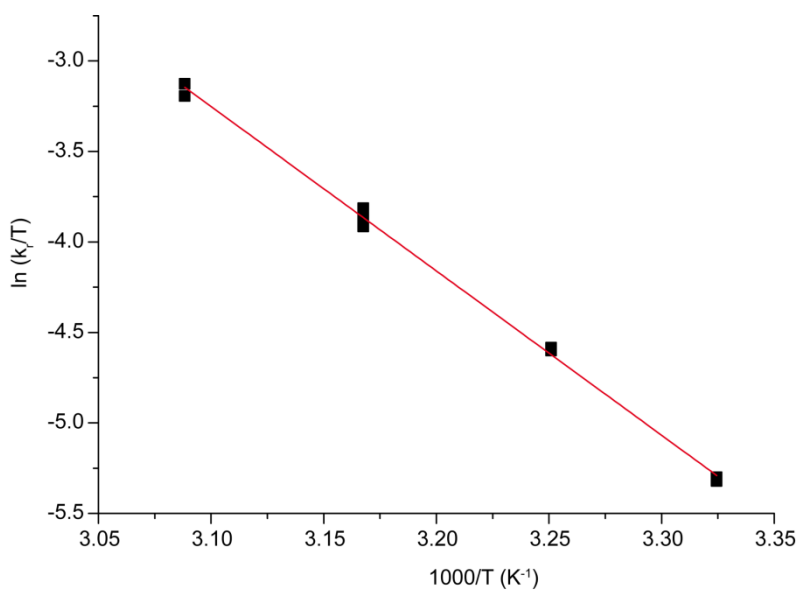


Plot 30. Trend of $\ln [(r+1)/(r-1)]$ vs. t_m for complex **9NHC** at 298K. The best linear fit (red line) equation is $y = (0.339 \pm 0.003)x + (0.002 \pm 0.001)$, $r^2 = 0.9995$.



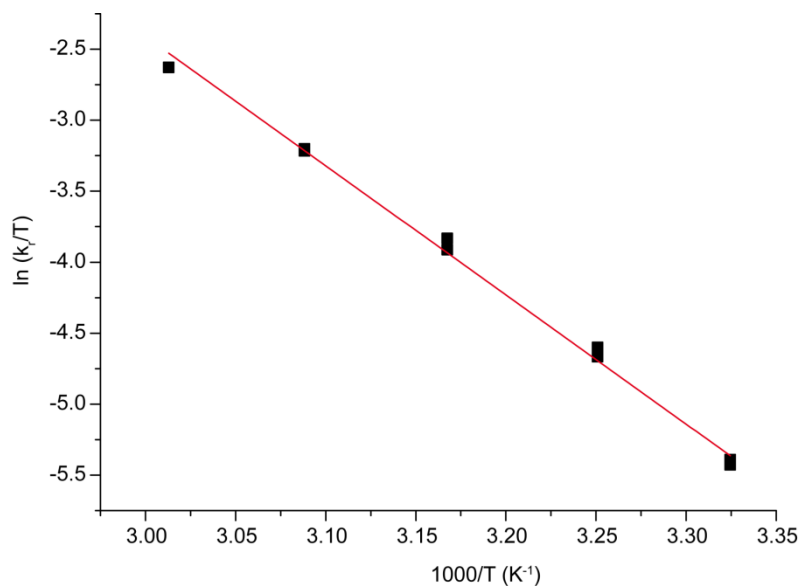
9Cl		
T (K)	t _m (s)	k _r (s ⁻¹)
299.5	0.25	1.39
299.5	0.125	1.45
306.2	0.25	2.91
306.2	0.125	2.89
313.0	0.125	5.81
313.0	0.09	5.50
321.1	0.09	11.94
329.2	0.075	23.3
329.2	0.05	21.9
334.6	0.035	36.7

Plot 31. Eyring plot for complex **9Cl**. $r^2 = 0.9988$.



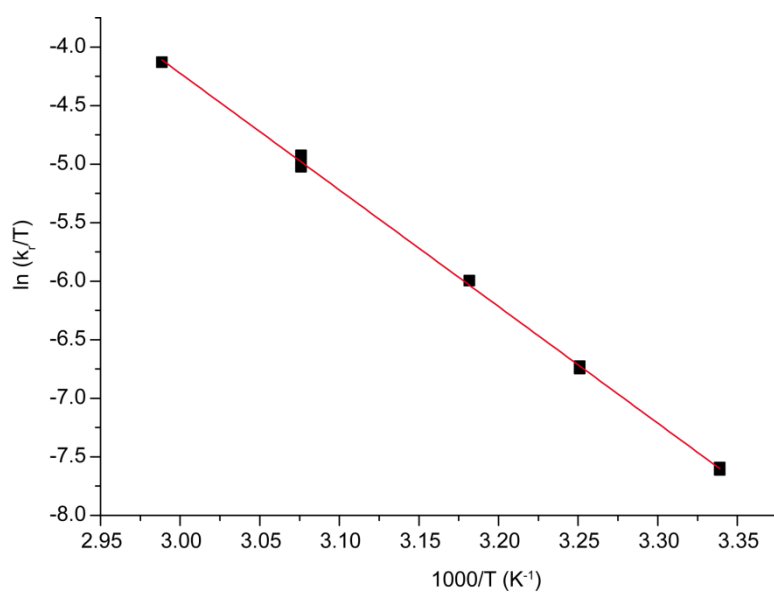
9Br		
T (K)	t _m (s)	k _r (s ⁻¹)
300.8	0.3	1.50
300.8	0.2	1.47
300.8	0.4	1.48
307.6	0.3	3.13
307.6	0.2	3.09
307.6	0.1	3.14
315.7	0.1	6.97
315.7	0.2	6.58
315.7	0.075	6.30
323.8	0.07	13.28
323.8	0.09	14.21

Plot 32. Eyring plot for complex **9Br**. $r^2 = 0.9978$.



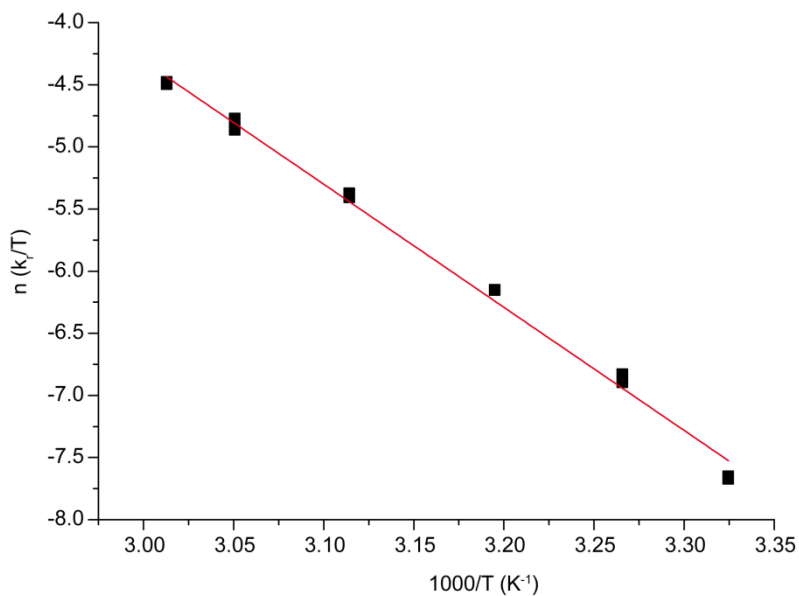
9I		
T (K)	t _m (s)	k _r (s ⁻¹)
300.8	0.3	1.32
300.8	0.15	1.32
300.8	0.4	1.37
307.6	0.3	3.09
307.6	0.15	2.89
315.7	0.2	6.83
315.7	0.1	6.31
323.8	0.1	13.18
323.8	0.05	12.97
331.9	0.08	23.93

Plot 33. Eyring plot for complex 9I. $r^2 = 0.9952$.



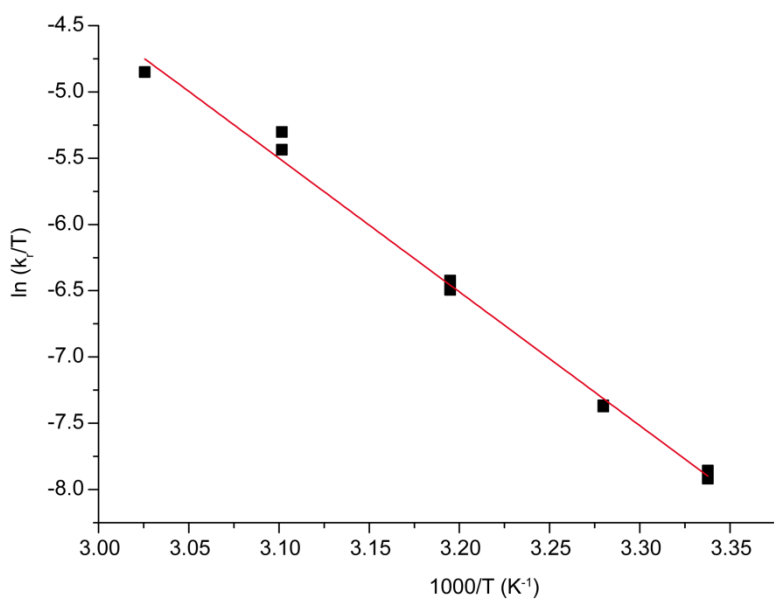
9(PPh ₃)BF ₄		
T (K)	t _m (s)	k _r (s ⁻¹)
299.5	0.25	0.151
299.5	0.18	0.148
307.6	0.25	0.361
307.6	0.18	0.369
314.3	0.2	0.782
325.1	0.125	2.358
325.1	0.075	2.138
334.6	0.075	5.380

Plot 34. Eyring plot for complex 9(PPh₃)BF₄. $r^2 = 0.9992$.



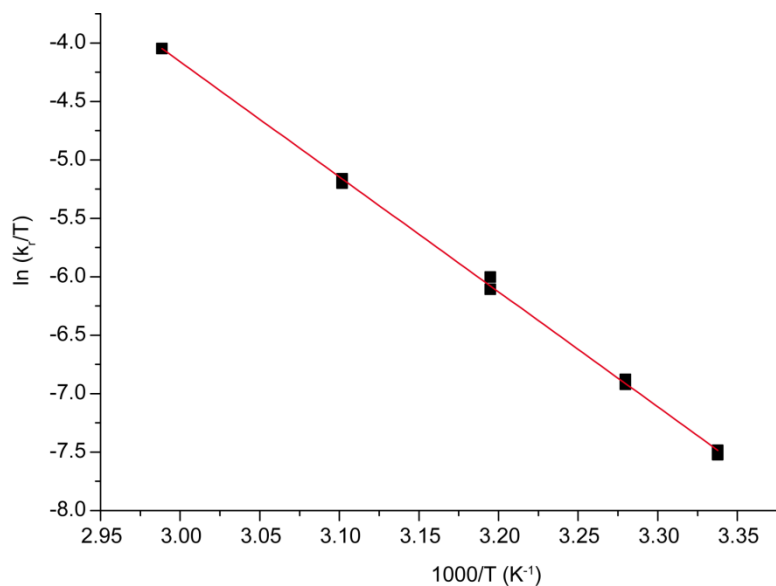
9(PCy₃)BF₄		
T (K)	t_m (s)	k_r (s⁻¹)
300.8	0.2	0.140
300.8	0.35	0.143
306.2	0.25	0.331
306.2	0.35	0.310
313.0	0.35	0.665
313.0	0.2	0.667
321.1	0.12	1.489
321.1	0.22	1.457
321.1	0.32	1.441
327.8	0.2	2.771
327.8	0.1	2.531
327.8	0.3	2.554
331.9	0.25	3.774
331.9	0.15	3.699
331.9	0.075	3.705

Plot 35. Eyring plot for complex **9(PCy₃)BF₄**. $r^2 = 0.9945$.



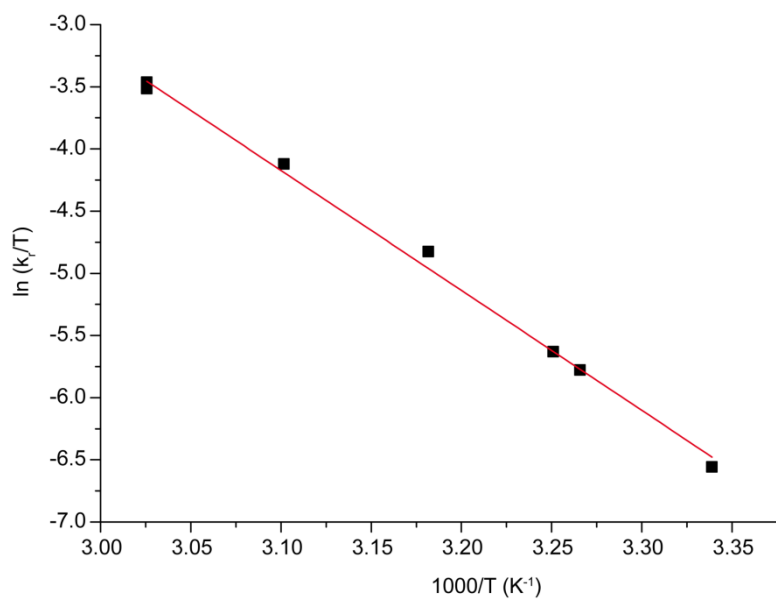
9(PAr^F)BF₄		
T (K)	t_m (s)	k_r (s⁻¹)
299.6	0.4	0.109
299.6	0.25	0.116
304.9	0.25	0.193
304.9	0.15	0.191
313.0	0.15	0.507
313.0	0.25	0.473
322.4	0.2	1.604
322.4	0.1	1.404
330.5	0.08	2.583
330.5	0.15	2.582

Plot 36. Eyring plot for complex **9(PAr^F)BF₄**. $r^2 = 0.9929$.



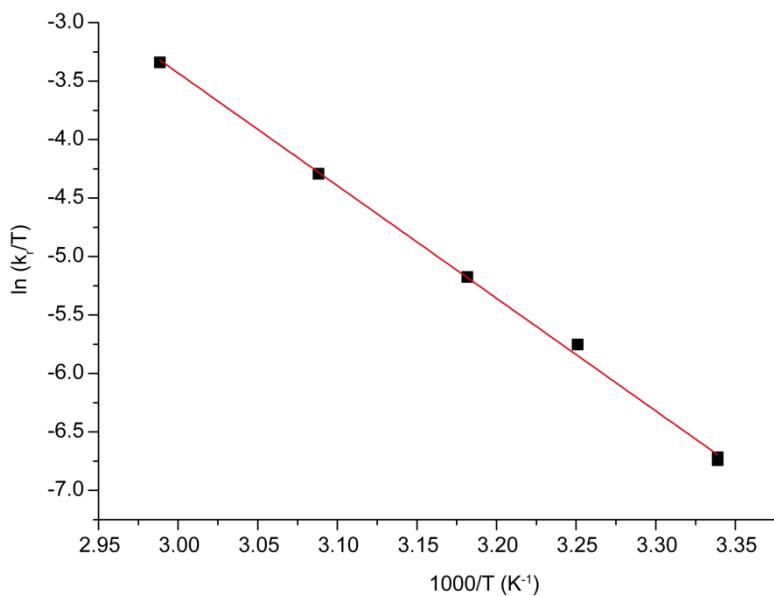
9(CN^tBu)BF₄		
T (K)	t_m (s)	k_r (s⁻¹)
299.6	0.3	0.168
299.6	0.4	0.162
304.9	0.35	0.314
304.9	0.25	0.301
313.0	0.225	0.774
313.0	0.3	0.697
322.4	0.25	1.845
322.4	0.25	1.778
334.6	0.1	5.843

Plot 37. Eyring plot for complex **9(CN^tBu)BF₄**. $r^2 = 0.9989$.



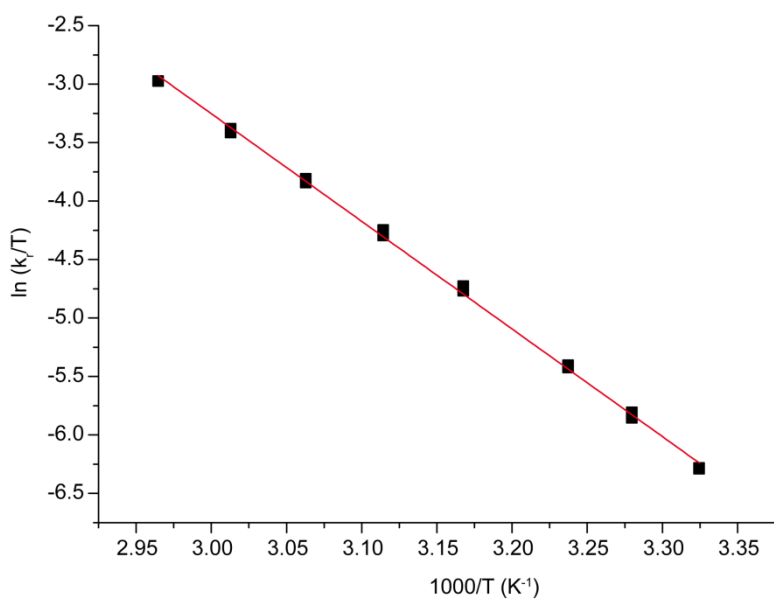
9(Py)BF₄		
T (K)	t_m (s)	k_r (s⁻¹)
299.5	0.3	0.425
306.2	0.25	0.948
307.6	0.25	1.104
314.3	0.2	2.524
322.4	0.15	5.231
330.5	0.09	10.346
330.5	0.07	9.824
330.5	0.05	9.916

Plot 38. Eyring plot for complex **9(Py)BF₄**. $r^2 = 0.9959$.



9(NHC)BF ₄		
T (K)	t _m (s)	k _r (s ⁻¹)
299.5	0.3	0.353
299.5	0.2	0.362
307.6	0.2	0.976
314.3	0.17	1.776
323.8	0.12	4.427
334.6	0.075	11.844

Plot 39. Eyring plot for complex 9(NHC)BF₄. r²= 0.9983.



9Ph		
T (K)	t _m (s)	k _r (s ⁻¹)
300.8	0.25	0.558
300.8	0.35	0.562
304.9	0.3	0.916
304.9	0.25	0.890
304.9	0.2	0.875
308.9	0.25	1.39
308.9	0.3	1.36
315.7	0.25	2.79
315.7	0.3	2.68
321.1	0.25	4.59
321.1	0.2	4.38
326.5	0.2	7.23
326.5	0.125	6.99
331.9	0.09	11.26
331.9	0.125	10.91
337.3	0.08	17.20

Plot 40. Eyring plot for complex 9Ph. r²= 0.9988.

4.5 Computational Studies

All optimizations were performed with ADF2013.01 program package^{127,226} to identify the structures of the reaction intermediates and transition states. For geometry optimizations, calculations were carried out at the DFT level of theory using the GGA functional BP86. All atoms were described with a Slater-type TZ2P triple- ξ quality basis set, using the frozen core approximation (1s for C, N, O, F; 2p for S; 4d for Au). Frequency calculations at the same BP86 level of theory have been also performed to identify all stationary points as minima (zero imaginary frequencies) or transition states (one imaginary frequency). Final energies have been calculated by single point B2PLYP functional calculations (with Gaussian program package^[227]) on the optimized BP86 gas phase structures, with def2-TZVPP basis set and relativistic effective core potential (RECP). This combined BP86 geometry optimization and B2PLYP energy calculation approach has been shown to be accurate enough to describe gold species along reaction paths in a benchmark study performed by us.¹¹⁷ Relativistic effects were treated with the scalar zero-order regular approximation, ZORA mode^{127,228} Due to the fact that the investigated reactions involve four molecules ($[(\text{NHC})\text{Au}]^+$, butyne, methanol and the counterion X^-), the reference energy has been set to the most stable adduct involving the four molecules. All calculations were performed for the closed shell singlet state.

Compound	E (B2PLYP)	E (B2PLYP)/ COSMO(CHCl_3)	E (B2PLYP-D3) ^[229]	E (M06)
IC _{OTs}	0.0	0.0	0.0	0.0
RC _{OTs}	2.7	1.1	-0.7	0.4
TSI _{OTs}	18.3	17.7	15.4	15.3
I _{OTs}	1.2	2.3	1.3	0.6
TSII _{OTs}	5.9	5.6	3.5	2.3
PC _{OTs}	-14.3	-18.0	-18.8	-20.4
$[(\text{NHC}')\text{AuOTs}] \cdot (2\text{-butyne})$	0.0	0.0	0.0	0.0
$[(\text{NHC}')\text{Au}(\eta^2\text{-}2\text{-butyne})]\text{OTs}$	3.5	1.8	0.8	1.9
$[(\text{NHC}')\text{AuOTs}] \cdot (\text{MeOH})$	0.0	0.0	0.0	0.0
$[(\text{NHC}')\text{Au}(\text{MeOH})]\text{OTs}$	3.6	2.9	1.8	2.8

In order to estimate the entropic contribution to the path in Figure S8, we computed it for the two most different adducts (**RC_{OTs}** and **PC_{OTs}**) and they resulted identical in terms of translational contribution, very similar for the rotational one (difference of 0.04 entropic units) and only with a small difference for the vibrational one (13 entropic units).

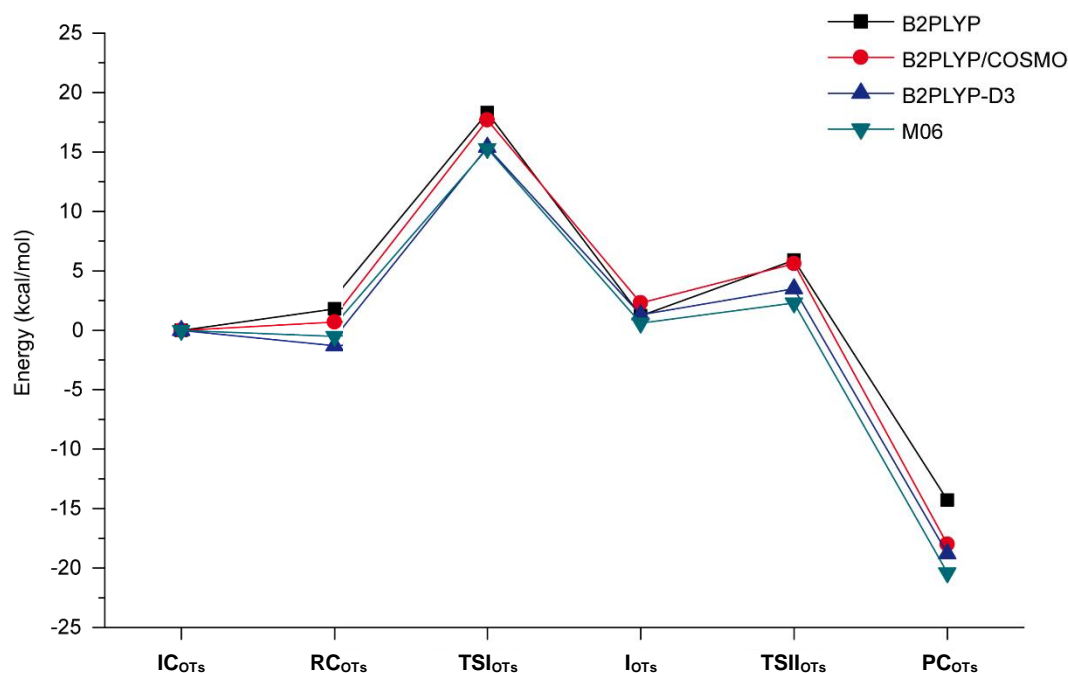


Figure 59. Energies of the studied complexes (in kcal/mol) calculated with various density functionals using def2-TZVP basis set.

4.5.1 Computational details for 4-10X complexes.

All calculations here reported have been performed using density functional theory (DFT) with the ADF (Amsterdam Density Functional) package.^{127, 226} The BLYP GGA²³⁰ Functional was used. An all-electron triple-zeta basis set with two polarization functions was used on all atoms (TZ2P).^{127, 226} Relativistic effects were included with the zeroth-order regular approximation (ZORA) Hamiltonian²²⁸ as implemented in ADF, with a small frozen core. The satisfactory accuracy of this approach was verified by both coupled-cluster and all-electron four-component Dirac–Kohn–Sham calculations on closely related systems.¹³⁹ A fine integration grid has been used both in the SCF iterations and in the optimization procedure in order to converge properly the geometrical parameters. Geometrical optimization and the SCF iterations have been performed including explicitly the solvent (CH₂Cl₂), using a conductor like screening model (COSMO, with $\epsilon = 8.93$) as implemented in ADF.¹²⁸

The charge displacements occurring upon the formation of the bond were analysed through the Charge Displacement Function (CDF),^{70b,129} defined in the following equation:

$$\Delta q = \int_{-\infty}^{\infty} dx \int_{-\infty}^{\infty} dy \int_{-\infty}^z dz' \Delta \rho(x, y, z') \quad (\text{Eq. 3})$$

where $\Delta\rho$ is the difference between the electron density of the complex and the ones of its constituting fragments placed in the same position they occupy in the complex. In the present case, the fragments are the gold-ligand moiety and the hexyne. The CDF defines, at each point z along a chosen axis, the amount of electron charge that moves across a plane perpendicular to the z axis upon the formation of the bond. A positive (negative) value corresponds to electrons flowing in the direction of decreasing (increasing) z . Charge accumulates (decreases) where the slope is positive (negative), the difference between the Δq values computed at two points gives the amount of the charge that has flowed into (away from) the region of space delimited by the two corresponding planes. The systems **4-10**BF₄ will be thoroughly characterized by means of DFT calculations. The optimized structures, of all systems (including different ion-pair configuration) presented in the work, have been reported in the following section as Cartesian coordinates.

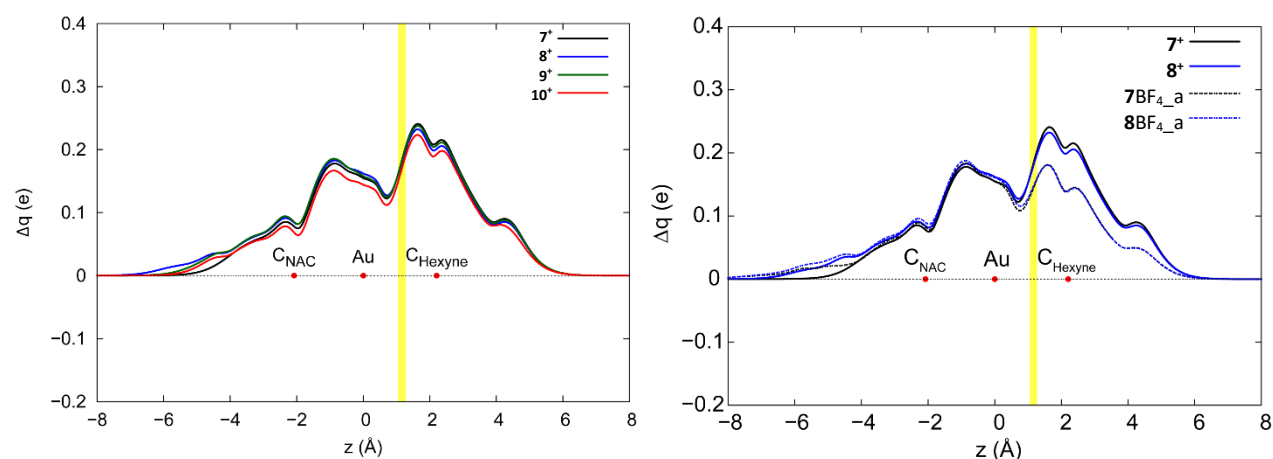


Figure 60. (Left panel) Charge displacement curves for the complexes **7⁺-10⁺**. The red dots represent approximate positions of the atoms. The vertical band identifies a suitable boundary between the metallic and the 3-hexyne fragments. (Right panel) Charge displacement curves for the complex **7⁺, 8⁺, 7BF₄_a, 8BF₄_a**. The red dots represent the approximate position of the atoms. The vertical band identifies a suitable boundary between the metallic and the 3-hexyne fragments.

The interaction energies and the selected geometrical parameters for the cations **7⁺-10⁺**, in which the gold fragment is coordinated to 3-hexyne and to the corresponding NAC ligand are given in Table 7. All the systems show very similar interaction energies, around 40 kcal/mol with variations of only 2.8 kcal/mol. Also the most important geometrical parameters are very similar in all the systems. The N-Ĉ-N angles are between 116° and 119°, and the small variation well correlate with the steric hindrance of the substituents on the nitrogen. In fact, the N-Ĉ-N angle increases according to the series **1⁺ < 4⁺ = 3⁺ < 2⁺**. Also the hexyne bending ($180^\circ - \text{C}-\hat{\text{C}}\equiv\text{C}$) is an important parameter. In fact, we previously shown that, in the case of acetylene, the bending occurring upon coordination to a metallic fragment is strongly related with the

DCD bonding components and, in particular, with the amount of back-donation to its π^* orbitals.¹³⁹ Our systems present very similar values for the hexyne bending, around 13°.

XYZ Coordinates.

4 ⁺ .xyz (82)			
Au	0.041048	-0.017047	0.088604
C	0.006579	-0.023241	2.125457
N	1.078825	0.012071	2.973609
C	0.649526	-0.006976	4.297992
C	-0.711553	-0.055824	4.274244
N	-1.094479	-0.064607	2.935612
H	-1.431700	-0.083925	5.076996
H	1.340889	0.016063	5.125881
H	1.749201	4.438574	1.530691
H	1.305092	2.424069	2.878552
H	1.894246	2.989249	0.512607
C	2.336968	3.528279	1.358828
H	3.351264	3.832753	1.073425
C	2.930491	3.441678	3.839465
H	2.905786	2.845774	4.759996
H	2.346721	4.355426	4.007979
H	3.970958	3.735730	3.652959
C	2.347764	2.653158	2.637821
H	1.465761	-2.375884	2.802708
H	2.631786	-4.256401	3.897679
C	2.523291	-2.527366	2.565505
C	3.151209	-3.300440	3.754483
H	4.211088	-3.516722	3.570603
H	3.078515	-2.728827	4.687800
C	2.581197	-3.372092	1.267471
H	2.111884	-2.844260	0.428460
H	2.053349	-4.322662	1.413873
H	3.615708	-3.603155	0.985682
C	3.175690	-1.152311	2.381232
C	2.482673	0.064893	2.569398
C	4.530186	-1.068404	2.016289
H	5.098664	-1.981914	1.860998
C	5.160683	0.165792	1.852180

H	6.209814	0.205224	1.570477
C	4.448706	1.349420	2.051486
H	4.954052	2.303399	1.923559
C	3.091837	1.330958	2.416953
H	-1.473270	2.324665	2.756566
H	-2.022522	4.281524	1.365903
C	-2.544730	3.331579	1.197048
H	-3.570954	3.563511	0.887150
C	-2.523607	2.477362	2.489971
H	-3.139556	2.663508	4.596943
C	-3.186311	3.241453	3.665848
H	-2.672509	4.197039	3.830142
H	-4.240798	3.457634	3.453075
C	-3.169453	1.103399	2.276884
H	-5.073564	1.936087	1.696031
C	-4.510911	1.021596	1.866121
C	-5.135468	-0.211663	1.674521
H	-6.174556	-0.249515	1.357651
C	-4.430479	-1.396455	1.891197
H	-4.931219	-2.349597	1.740879
C	-3.086752	-1.380066	2.302294
C	-2.483343	-0.114879	2.482372
H	-1.314160	-2.475300	2.810702
C	-2.350222	-2.703200	2.541873
H	-2.964894	-2.895944	4.648396
C	-2.965994	-3.491343	3.727217
H	-4.001724	-3.783367	3.513054
H	-2.388623	-4.406234	3.910851
C	-2.305590	-3.577787	1.263350
H	-1.722475	-4.488088	1.450392
H	-3.311852	-3.882314	0.950900
H	-1.840555	-3.038401	0.429382
H	-2.050516	2.810346	0.368232
C	0.143870	0.605208	-2.088295

C	0.010794	-0.628134	-2.093504
C	-0.141617	-2.058000	-2.441708
H	0.660512	-2.632689	-1.962705
H	-1.086089	-2.429080	-2.025255
C	0.306524	2.036921	-2.424197
H	1.231455	2.409434	-1.967191
H	-0.516872	2.607215	-1.977056
C	-0.114686	-2.292915	-3.972802
H	-0.233405	-3.363470	-4.170352
H	0.836291	-1.962604	-4.403774
H	-0.931100	-1.755201	-4.466246
C	0.343208	2.277738	-3.954209
H	-0.587486	1.945686	-4.426140
H	1.181714	1.744896	-4.414760
H	0.466045	3.349456	-4.142823

5 ⁺ .xyz (84)			
Au	0.040837	-0.018147	0.153268
C	0.005727	-0.022716	2.199720
N	1.089453	0.095962	2.983927
C	0.734938	0.058674	4.440528
C	-0.803145	-0.109369	4.412948
N	-1.105210	-0.144292	2.944530
H	-1.136568	-1.038016	4.884618
H	-1.329337	0.726794	4.882007
H	1.051173	0.986865	4.924820
H	1.244140	-0.778008	4.927160
H	1.367047	4.532884	1.464766
H	1.142463	2.514295	2.867661
H	1.553804	3.074527	0.467352
C	2.005743	3.660715	1.276540
H	2.979661	4.026716	0.928732
C	2.732805	3.678215	3.721532
H	2.810479	3.103830	4.652899
H	2.086631	4.545488	3.907615
H	3.733470	4.051607	3.470114
C	2.150785	2.818106	2.569543
H	1.657198	-2.252775	2.860503

H	3.013198	-4.041041	3.890569
C	2.706525	-2.334072	2.560233
C	3.459760	-3.055333	3.708223
H	4.516636	-3.206428	3.454997
H	3.414574	-2.481646	4.642211
C	2.741423	-3.183243	1.263877
H	2.173992	-2.703057	0.457535
H	2.302702	-4.171788	1.449039
H	3.770126	-3.333142	0.913513
C	3.245303	-0.917041	2.331074
C	2.460496	0.245346	2.529855
C	4.573211	-0.741560	1.906824
H	5.200870	-1.613646	1.739490
C	5.103510	0.532350	1.697609
H	6.133974	0.644241	1.369401
C	4.313972	1.662971	1.912548
H	4.740463	2.649763	1.748841
C	2.979102	1.549234	2.335998
H	-1.674823	2.204584	2.815263
H	-2.271896	4.128671	1.388470
C	-2.699911	3.139505	1.182575
H	-3.714922	3.287750	0.793759
C	-2.712192	2.284866	2.475701
H	-3.500377	2.420482	4.529339
C	-3.510604	2.998971	3.597287
H	-3.073376	3.984489	3.801866
H	-4.557170	3.149229	3.303982
C	-3.238763	0.867840	2.220132
H	-5.173765	1.563572	1.563596
C	-4.550363	0.691851	1.748114
C	-5.070061	-0.582144	1.514147
H	-6.088184	-0.694654	1.149655
C	-4.286091	-1.712146	1.751587
H	-4.704835	-2.698864	1.568398
C	-2.967497	-1.597830	2.223124
C	-2.458895	-0.293828	2.441158
H	-1.148626	-2.560750	2.815400
C	-2.145108	-2.865831	2.481099

H	-2.876566	-3.159616	4.539122
C	-2.764810	-3.730970	3.609361
H	-3.754943	-4.106583	3.322126
H	-2.123117	-4.597048	3.815387
C	-1.952781	-3.703766	1.191249
H	-1.318705	-4.574920	1.398815
H	-2.912877	-4.071321	0.808415
H	-1.474521	-3.113658	0.400246
H	-2.100435	2.664580	0.396576
C	0.690866	0.055636	-2.019602
C	-0.541614	-0.080653	-2.038766
C	-1.968087	-0.237307	-2.396705
H	-2.351711	-1.160695	-1.946108
H	-2.540790	0.587262	-1.955064
C	2.127250	0.214860	-2.334549
H	2.686383	-0.615783	-1.886876
H	2.498938	1.132027	-1.861853
C	-2.184436	-0.268471	-3.930630
H	-3.253725	-0.384654	-4.136831
H	-1.649326	-1.108589	-4.385713
H	-1.839896	0.661644	-4.394765
C	2.387525	0.264964	-3.861152
H	1.866507	1.111466	-4.320791
H	2.055567	-0.658763	-4.346757
H	3.462343	0.382388	-4.035155

6+.xyz (96)			
Au	0.041115	-0.158127	0.105597
C	0.038126	0.169519	2.115716
N	1.138938	0.372667	2.921305
C	0.725613	0.561281	4.228803
C	-0.658037	0.472265	4.240485
N	-1.065911	0.232377	2.939798
H	-0.179551	2.461331	-4.646425
H	0.804217	0.980875	-4.669602
H	1.520936	4.400383	0.628597
H	1.302955	2.747182	2.451505
H	1.632613	2.752351	-0.028781

C	2.129688	3.487765	0.615439
H	3.098588	3.734369	0.163909
C	2.955757	4.009251	2.971945
H	3.055546	3.647053	4.002088
H	2.337621	4.915572	2.987232
H	3.953130	4.289755	2.611645
C	2.304746	2.941640	2.056047
H	1.610998	-1.993456	3.196635
H	2.898370	-3.693917	4.433077
C	2.648610	-2.165349	2.893975
C	3.388009	-2.763939	4.118090
H	4.431862	-2.999089	3.876051
H	3.383633	-2.071230	4.968064
C	2.620410	-3.179918	1.721992
H	2.069120	-2.778985	0.863060
H	2.132423	-4.109616	2.039921
H	3.634680	-3.429634	1.387044
C	3.252315	-0.823591	2.462431
C	2.527288	0.389667	2.461944
C	4.589641	-0.770268	2.034172
H	5.181066	-1.682211	2.017401
C	5.173115	0.430876	1.629362
H	6.209251	0.446612	1.301260
C	4.429865	1.611779	1.644034
H	4.897233	2.539700	1.324383
C	3.088608	1.623883	2.062759
H	-1.535504	2.563479	2.447892
H	-2.053128	4.205746	0.680823
C	-2.541252	3.223280	0.671918
H	-3.554664	3.354532	0.273081
C	-2.572396	2.630889	2.104318
H	-3.311583	3.196665	4.100377
C	-3.313630	3.585595	3.075177
H	-2.823628	4.567249	3.081801
H	-4.356791	3.732685	2.769126
C	-3.176142	1.221486	2.117680
H	-5.102345	1.894801	1.416284
C	-4.512146	1.035299	1.723886

C	-5.095887	-0.232082	1.719127
H	-6.131032	-0.350868	1.409576
C	-4.354231	-1.347467	2.110307
H	-4.821914	-2.328685	2.100056
C	-3.014295	-1.226410	2.515699
C	-2.452646	0.070526	2.504465
H	-1.230950	-2.168603	3.246026
C	-2.231990	-2.478297	2.930080
H	-2.988870	-2.528473	4.997294
C	-2.886561	-3.199295	4.135962
H	-3.883220	-3.579807	3.880719
H	-2.269421	-4.053833	4.440326
C	-2.054065	-3.454010	1.738199
H	-1.447380	-4.315872	2.042708
H	-3.022200	-3.830236	1.385133
H	-1.553592	-2.961948	0.895391
H	-1.988641	2.571501	-0.015272
C	0.003509	0.104064	-2.142666
C	0.083540	-1.118406	-1.944270
C	0.175448	-2.590340	-2.066681
H	1.083785	-2.937582	-1.559454
H	-0.671705	-3.048142	-1.541772
C	-0.089669	1.461831	-2.724093
H	0.759158	2.061690	-2.373857

H	-0.996004	1.952353	-2.348820
C	0.188817	-3.053560	-3.544723
H	0.256624	-4.146121	-3.573855
H	1.049082	-2.636741	-4.079029
H	-0.727973	-2.747748	-4.059671
C	-0.110335	1.434145	-4.272923
H	-0.972731	0.870356	-4.643865
C	1.223175	0.818705	5.580837
C	0.028842	0.870378	6.371002
C	-1.161754	0.663164	5.601132
C	0.025415	1.100666	7.756434
C	-1.253630	1.121427	8.395884
C	-2.410328	0.920069	7.654592
C	-2.386526	0.687696	6.248154
C	1.301392	1.289472	8.373968
C	2.461653	1.240830	7.612838
C	2.444924	1.005157	6.206874
H	-3.321347	0.535877	5.716197
H	-1.316911	1.295262	9.467034
H	-3.373357	0.937886	8.156128
H	1.359458	1.471763	9.443908
H	3.422082	1.386969	8.097830
H	3.382622	0.977596	5.659080

7 ⁺ .xyz (48)			
C	0.598139	2.263982	-3.870643
C	0.545410	2.001224	-2.344562
C	0.215543	0.593632	-2.032307
C	-0.064201	-0.613408	-2.041718
C	-0.388199	-2.017131	-2.376406
C	-0.404103	-2.262904	-3.906195
Au	0.041162	-0.017948	0.165105
C	0.005109	-0.024036	2.236194
N	-1.140556	-0.090062	2.929576
N	1.125214	0.039524	2.970342
C	-2.576381	-0.153692	2.466576
C	2.576863	0.103335	2.559650
H	1.004290	0.037448	3.984431
H	-1.055898	-0.091973	3.947532
H	0.344721	-2.679979	-1.900331
H	-1.365316	-2.272892	-1.948497

H	1.511281	2.254085	-1.890101
H	-0.200145	2.657417	-1.879179
H	-0.647529	-3.313832	-4.094213
H	0.574190	-2.047826	-4.348949
H	-1.157650	-1.637693	-4.396652
H	-0.368612	2.052156	-4.339480
H	1.364560	1.645507	-4.349603
H	0.844216	3.317354	-4.040849
C	3.364103	0.158170	3.887998
C	2.974896	-1.165792	1.773207
C	2.852627	1.384812	1.741994
C	-3.411289	-0.213205	3.765234
C	-2.946757	1.117607	1.670215
C	-2.821229	-1.432676	1.635392
H	-3.880815	-1.494896	1.360285
H	-2.231027	-1.427686	0.711422
H	-2.557012	-2.327389	2.211390

H	-4.008719	1.084158	1.398953
H	-2.768926	2.017198	2.271428
H	-2.362889	1.195737	0.745729
H	-4.476503	-0.262990	3.517086
H	-3.155531	-1.101768	4.356207
H	-3.244726	0.680406	4.379904
H	4.045949	-1.132167	1.540472
H	2.775104	-2.067085	2.364913
H	2.424618	-1.240886	0.828100
H	4.437701	0.207581	3.678856
H	3.087803	1.045273	4.471880
H	3.174230	-0.736857	4.493776
H	3.921427	1.446955	1.505017
H	2.295896	1.383351	0.797468
H	2.568651	2.277881	2.311100

8 ⁺ .xyz (54)			
C	0.484477	2.256166	-3.886850
C	0.440868	2.027025	-2.354923
C	0.174251	0.613526	-2.011677
Au	0.055737	0.008435	0.196121
C	-0.007353	-0.057938	2.278448
N	1.105271	-0.055758	3.043904
C	2.502808	-0.088430	2.454978
C	2.862361	1.222065	1.727986
C	-0.060120	-0.602943	-2.006600
C	-0.335851	-2.021510	-2.321743
C	-0.367743	-2.287613	-3.847852
N	-1.207614	-0.133961	2.883912
C	-2.613541	-0.095462	2.322862
C	-2.883291	-1.348897	1.460752
C	-3.531736	-0.118671	3.566107
C	-2.863545	1.206241	1.530551
H	3.148448	-0.148292	3.329606
C	2.796219	-1.352792	1.622696
C	1.009605	-0.125118	4.558232
H	-1.217725	-0.223833	3.894845
H	0.428569	-2.651071	-1.850106
H	-1.295588	-2.309601	-1.875051
H	1.392931	2.334188	-1.905073
H	-0.334899	2.659126	-1.905400
H	-0.575415	-3.349171	-4.018533
H	0.594452	-2.042694	-4.309902
H	-1.151806	-1.697181	-4.333703
H	-0.470573	1.988662	-4.351472
H	1.279058	1.661864	-4.350422
H	0.682374	3.315200	-4.083117
H	-3.920870	-1.337623	1.106317
H	-2.224422	-1.377899	0.585031

H	-2.724254	-2.263127	2.044922
H	-3.908718	1.235711	1.199941
H	-2.670841	2.085360	2.156896
H	-2.225829	1.266124	0.641006
H	-4.580300	-0.107924	3.251414
H	-3.366930	-1.025662	4.162065
H	-3.357291	0.759897	4.199967
H	3.865969	-1.374148	1.380346
H	2.553794	-2.261519	2.184846
H	2.237876	-1.367743	0.679456
H	3.922703	1.202723	1.448576
H	2.273600	1.351980	0.811482
H	2.690535	2.090420	2.373581
C	2.119180	0.650004	5.295640
H	0.086971	0.400032	4.823882
C	0.919293	-1.591417	5.033032
H	0.748385	-1.621250	6.115813
H	0.101245	-2.131444	4.542569
H	1.854596	-2.123210	4.820713
H	1.812620	0.750741	6.343270
H	3.081382	0.126756	5.288346
H	2.254710	1.656861	4.886974

9 ⁺ .xyz (46)			
Au	0.196514	0.054848	2.333547
C	0.019646	-0.010118	4.401300
N	0.651210	-0.921310	5.159961
H	0.491935	-0.882192	6.163942
N	-0.765148	0.879077	5.023287
C	1.609309	-2.026397	4.766309
C	0.906798	-3.041141	3.837754
H	0.606129	-2.572119	2.893091
H	0.014316	-3.459795	4.317614
H	1.592982	-3.863612	3.603930
C	1.992687	-2.715656	6.094496
H	2.486052	-2.012627	6.778206
H	2.690548	-3.536302	5.899340
H	1.109958	-3.137950	6.592129
C	2.872245	-1.433888	4.102929
H	3.366340	-0.718913	4.771361
H	2.627712	-0.921871	3.164866
H	3.580123	-2.239335	3.874355
C	-1.534593	1.962860	4.336609
H	-0.930731	2.400200	3.538295
H	-2.446772	1.538949	3.896871
C	-1.866397	2.945203	5.471488
H	-1.022663	3.625708	5.640270
H	-2.750313	3.548126	5.244682
C	-2.065857	2.018024	6.691371

H	-3.063517	1.564066	6.664804
H	-1.956358	2.534929	7.648784
C	-0.988973	0.929673	6.502752
H	-0.046759	1.197381	7.002614
H	-1.317326	-0.050039	6.873670
C	0.003431	-0.346726	0.085830
C	0.730791	0.650916	0.186213
C	1.605972	1.824047	-0.027902
H	1.129696	2.712220	0.407214
H	2.546539	1.676095	0.518123
C	-0.816134	-1.492972	-0.364477
H	-1.835265	-1.382712	0.027796
H	-0.413044	-2.416344	0.071238
C	1.901447	2.066971	-1.530869
H	2.550068	2.943664	-1.631033
H	0.977821	2.253686	-2.088118
H	2.411575	1.206164	-1.975022
C	-0.855091	-1.613182	-1.910082
H	-1.289567	-0.716317	-2.363198
H	-1.472102	-2.474664	-2.186700
H	0.149788	-1.761342	-2.318483

10⁺.xyz (59)

C	0.281125	1.458424	-3.950542
C	0.126003	1.484072	-2.409262
C	0.253258	0.136418	-1.813269
C	0.376257	-1.073161	-1.574784
C	0.541643	-2.542377	-1.607396
C	0.943560	-3.057410	-3.012193
Au	0.171903	-0.059406	0.462967
C	0.065303	0.344718	2.498601
N	-1.061669	0.149410	3.200631
C	-2.413418	-0.363143	2.753383
C	-3.037272	0.590891	1.710792
N	1.139261	0.824207	3.162701
C	1.036041	1.170963	4.603277
C	2.432964	1.098145	2.467231
H	2.245155	0.847473	1.418096
C	2.813218	2.589476	2.540152
C	-2.293001	-1.801390	2.202907
C	-3.280783	-0.370609	4.031518
C	3.610601	0.164897	2.890624
H	-1.036625	0.352716	4.196791
H	1.299181	-2.835599	-0.870154
H	-0.398309	-3.012428	-1.291932
H	0.881977	2.146622	-1.970372
H	-0.850950	1.903679	-2.138949
H	1.045599	-4.147313	-2.977176
H	1.899887	-2.627922	-3.329577

H	0.181103	-2.804418	-3.756263
H	-0.487888	0.830100	-4.412297
H	1.266531	1.077904	-4.239846
H	0.175221	2.478017	-4.335619
H	-3.288257	-2.176955	1.936908
H	-1.666209	-1.832998	1.303694
H	-1.856040	-2.470269	2.953595
H	-4.038076	0.233569	1.440232
H	-3.127462	1.605210	2.117478
H	-2.433764	0.634209	0.796503
H	-4.285857	-0.733768	3.792974
H	-2.852284	-1.032598	4.794699
H	-3.375051	0.639512	4.449970
H	3.709284	2.764444	1.934036
H	2.000546	3.206426	2.140595
H	3.032947	2.914418	3.560980
H	1.993454	1.544192	4.954635
H	0.269930	1.941478	4.759331
H	0.781343	0.282739	5.194929
H	4.429594	0.443219	2.210359
O	3.995947	0.492064	4.249114
C	3.337395	-1.325740	2.698461
C	2.732021	-2.106144	3.698566
C	2.495288	-3.470900	3.491436
C	2.863120	-4.076046	2.282814
C	3.475478	-3.308885	1.283592
C	3.711330	-1.944662	1.492514
H	2.461940	-1.651693	4.648643
H	2.028991	-4.061808	4.276401
H	2.685945	-5.137516	2.126028
H	3.785660	-3.773886	0.350872
H	4.204328	-1.359907	0.716913
H	4.759411	-0.069314	4.478082

7BF₄_a⁺.xyz (53)

C	1.007770	2.108342	-3.828213
C	0.894886	1.848257	-2.304955
C	0.324333	0.519028	-1.997750
C	-0.159486	-0.619522	-2.012183
C	-0.717177	-1.945486	-2.354647
C	-0.738867	-2.203554	-3.882344
Au	0.039689	-0.058763	0.207202
C	0.007812	-0.055575	2.280261
N	-1.127982	-0.213893	2.973157
N	1.123481	0.111580	3.007081
C	-2.553675	-0.271199	2.498346
C	2.558189	0.201733	2.568989
H	-1.030386	-0.321306	3.998223
H	-0.127150	-2.722995	-1.852609

H	-1.734136	-2.020638	-1.948300
H	1.885041	1.928437	-1.838057
H	0.271407	2.621825	-1.838373
H	-1.160819	-3.195799	-4.077139
H	0.272580	-2.169772	-4.301078
H	-1.354181	-1.458783	-4.398284
H	0.023948	2.069770	-4.307896
H	1.657582	1.367710	-4.306527
H	1.435350	3.103144	-3.995744
C	3.388543	0.268962	3.871964
C	2.975588	-1.056267	1.771965
C	2.794287	1.491473	1.745773
C	-3.412728	-0.378803	3.779663
C	-2.931512	1.023427	1.740504
C	-2.787579	-1.523079	1.619203
H	-3.843898	-1.581939	1.328010
H	-2.183859	-1.487634	0.703331
H	-2.526481	-2.434309	2.169984
H	-3.993645	0.994534	1.465931
H	-2.760406	1.900989	2.374527
H	-2.345489	1.139879	0.820660
H	-4.473446	-0.411398	3.505474
H	-3.169595	-1.287531	4.342177
H	-3.245551	0.479525	4.440213
H	4.045780	-1.003701	1.535300
H	2.794826	-1.961566	2.363343
H	2.423416	-1.143997	0.828695
H	4.453025	0.347098	3.622994
H	3.104695	1.134539	4.480136
H	3.239087	-0.632791	4.477336
H	3.853925	1.574615	1.472690
H	2.202725	1.485706	0.821482
H	2.513408	2.375770	2.329447
H	0.993253	0.284036	4.018321
B	-0.318738	0.476134	6.451086
F	0.773975	1.032183	5.678805
F	-0.738861	-0.712872	5.724553
F	-1.379614	1.390071	6.469357
F	0.117445	0.127202	7.719424

7BF ₄ _b.xyz (54)			
C	0.19594004	1.93376007	-3.96466472
C	0.23205173	1.74939159	-2.42680543
C	-0.38841712	0.47568428	-2.00482713
C	-0.96415134	-0.61955661	-1.91992461
C	-1.67814233	-1.89023722	-2.17736406
C	-1.99373049	-2.08981295	-3.68036425
Au	-0.39320388	-0.07455032	0.21116846
C	-0.11546303	-0.06127839	2.26235316

N	-0.63501661	-1.00364917	3.06480544
N	0.59884628	0.89247929	2.87726988
C	-1.48550228	-2.20554265	2.74144813
C	1.32894296	2.08758056	2.31337860
H	-0.43332989	-0.91591353	4.06190729
H	-1.06812327	-2.72509246	-1.81164240
H	-2.60914115	-1.90290080	-1.59766486
H	1.26924656	1.79070668	-2.07452242
H	-0.29150588	2.58177281	-1.94113106
H	-2.51919139	-3.04187814	-3.81126469
H	-1.07405334	-2.11597742	-4.27428926
H	-2.63345606	-1.28492660	-4.05746512
H	-0.83398446	1.94642918	-4.33692699
H	0.74364803	1.13105764	-4.46981920
H	0.66931485	2.88890999	-4.21475490
C	1.96349367	2.78608160	3.53595808
C	2.43957018	1.63023652	1.34231532
C	0.33349289	3.04829840	1.62599489
C	-1.76234080	-2.88261800	4.10180291
C	-2.82124470	-1.76572703	2.10135620
C	-0.71334798	-3.18084125	1.82499021
H	-1.32755347	-4.06744438	1.62715343
H	-0.46670561	-2.71440848	0.86363704
H	0.22114917	-3.50183385	2.30034782
H	-3.44655438	-2.64608493	1.91056312
H	-3.36629182	-1.08813308	2.76930891
H	-2.65731751	-1.24950002	1.14776041
H	-2.38129484	-3.77332197	3.95168785
H	-0.82629342	-3.19293873	4.58286354
H	-2.29783414	-2.20263627	4.77621017
H	2.97473662	2.50332103	0.95138255
H	3.15652921	0.97719261	1.85423831
H	2.02355494	1.08170667	0.48882679
H	2.51697174	3.67223665	3.20842426
H	1.19288765	3.10777535	4.24793851
H	2.66383711	2.11629156	4.05076138
H	0.86910591	3.92356742	1.24035700
H	-0.17231726	2.56329800	0.78268411
H	-0.43030294	3.38795953	2.33574788
H	0.67603411	0.82250762	3.89313370
B	3.14665921	4.74514967	-2.25516301
F	3.89749710	5.50773249	-1.31963962
F	3.44369284	3.36809386	-2.08942876
F	3.49575816	5.14624518	-3.57531558
F	1.76265679	4.96966970	-2.04637586

8BF ₄ _a.xyz (59)			
Au	0.03978583	0.04924710	0.15396877
C	0.11309675	0.14444539	-1.93113494

N	1.28191142	0.25935037	-2.59810172
C	2.63246101	0.17917546	-1.91268476
C	2.91686762	1.37381173	-0.98147519
N	-1.03995880	0.07190153	-2.62333457
C	-2.47526547	0.09796054	-2.13893042
C	-2.80423328	-1.18866827	-1.34861923
C	-3.33732778	0.14502171	-3.42059989
C	-2.75555478	1.36777824	-1.30388046
H	3.33986941	0.25796102	-2.73913923
C	2.89454460	-1.18791176	-1.24984711
C	1.36600592	0.46435578	-4.09830671
H	-0.98664731	-0.05038450	-3.63349693
H	-3.85637655	-1.17561999	-1.03938493
H	-2.18521674	-1.27007296	-0.44724961
H	-2.63294517	-2.07790827	-1.96672530
H	-3.81998654	1.40034921	-1.04145240
H	-2.51174389	2.26907632	-1.87893071
H	-2.17713409	1.38332302	-0.37313982
H	-4.39726915	0.15569837	-3.14514457
H	-3.15361010	-0.72822342	-4.05632983
H	-3.12604310	1.05047060	-4.00284357
H	3.94234081	-1.23312761	-0.92765444
H	2.71562657	-2.00757033	-1.95449973
H	2.26213104	-1.34504434	-0.36816139
H	3.95850431	1.32307648	-0.64131419
H	2.27261479	1.36072790	-0.09394339
H	2.76848154	2.32642320	-1.50094650
C	2.08634830	1.78496770	-4.44617026
H	0.34925952	0.57667717	-4.47180297
C	1.97868204	-0.76000860	-4.80648759
H	1.92677418	-0.60866889	-5.89074315
H	1.42390646	-1.67313493	-4.56625024
H	3.03165455	-0.90497909	-4.53741860
H	2.01464195	1.94670004	-5.52816584
H	3.15034742	1.76699887	-4.18487206
H	1.61460710	2.63587039	-3.94195160
C	0.75656443	1.87817928	4.40424949
C	0.80346318	1.73268674	2.86250241
C	0.18312065	0.47108802	2.40285056
C	-0.37486946	-0.63064214	2.30245227
C	-1.04977573	-1.92817431	2.52382081
C	-1.25808679	-2.23024634	4.02955550
H	-0.45767572	-2.72680653	2.06023723
H	-2.01868614	-1.92187185	2.00967397
H	1.84416175	1.76877450	2.51755310
H	0.28894676	2.57986060	2.39281264
H	-1.76264915	-3.19673746	4.13342109
H	-0.29981951	-2.27996237	4.55750742
H	-1.87936464	-1.46187883	4.50201353

H	-0.27688034	1.88350357	4.76683135
H	1.29607185	1.05981170	4.89292580
H	1.22952984	2.82440954	4.68761001
B	-1.49283166	-0.59569575	-7.00099899
F	-0.58178226	-1.10572884	-7.96246678
F	-2.82092465	-0.89398300	-7.40332480
F	-1.33318000	0.81034862	-6.89480037
F	-1.23456355	-1.19792324	-5.73813540

8BF ₄ _b.xyz (59)			
Au	0.25491911	0.01408833	-0.00755096
C	0.02341220	-0.28040667	-2.05898015
N	0.36008777	0.66215133	-2.96639427
C	1.19016239	1.88095065	-2.60981430
C	0.39817362	2.92648859	-1.80154274
N	-0.51079009	-1.43678781	-2.49871071
C	-1.06719357	-2.62281644	-1.74567428
C	0.03699982	-3.30327231	-0.90614799
C	-1.54871096	-3.59933830	-2.84271870
C	-2.27056624	-2.19894620	-0.87494522
H	1.41268506	2.33076580	-3.57852961
C	2.55181354	1.52285636	-1.98308049
C	0.03281522	0.52513815	-4.43857337
H	-0.57675412	-1.56933798	-3.50297913
H	-0.37548783	-4.18387826	-0.39936221
H	0.43732312	-2.62574486	-0.14290246
H	0.86647669	-3.62564389	-1.54668685
H	-2.68894074	-3.07793719	-0.37005253
H	-3.05462742	-1.74525813	-1.49295006
H	-1.97476955	-1.47223949	-0.10947525
H	-1.96843883	-4.49811379	-2.37915563
H	-0.71654889	-3.90826694	-3.48831150
H	-2.32896909	-3.14106221	-3.46370145
H	3.15643902	2.43384294	-1.90041299
H	3.09541860	0.80347756	-2.60588062
H	2.44805892	1.09723267	-0.97812179
H	1.01494072	3.82317024	-1.66773875
H	0.12787436	2.55094103	-0.80725998
H	-0.52277779	3.21344299	-2.31992828
C	-0.60728995	1.80346920	-5.02005666
H	-0.74996053	-0.23206678	-4.51717302
C	1.25755461	0.04947647	-5.24568026
H	0.96833544	-0.11633733	-6.29038261
H	1.66012913	-0.88900239	-4.84702156
H	2.05701452	0.79990361	-5.23275533
H	-0.96378983	1.57676258	-6.03174750
H	0.09881348	2.63652865	-5.09984830
H	-1.46638528	2.12346211	-4.42074542
C	1.71135036	2.49937645	3.68067314

C	1.48265725	2.10803177	2.19899530
C	0.75592278	0.82713395	2.07088884
C	0.15291786	-0.24034136	2.25640289
C	-0.51067145	-1.43288584	2.82848803
C	-0.50001306	-1.42236564	4.37723581
H	-0.00813660	-2.33559714	2.46050803
H	-1.54470372	-1.47787741	2.46561432
H	2.44758146	2.03681682	1.68299224
H	0.91601761	2.89718229	1.69041487
H	-1.00104924	-2.32498931	4.74338401
H	0.52476507	-1.41341044	4.76304578
H	-1.03062631	-0.54768869	4.76804460
H	0.75895574	2.63068543	4.20559008
H	2.29839885	1.73591366	4.20243324
H	2.26287944	3.44458499	3.71129480
B	4.80464370	4.60368444	1.52575985
F	4.86085372	3.20961880	1.27088293
F	3.45453365	5.02013954	1.63748433
F	5.42957487	5.30477945	0.45758064
F	5.49003400	4.88835277	2.73916253

10BF₄_a.xyz (64)			
C	0.40887809	1.42162087	-4.06326278
C	0.28396112	1.45997052	-2.51943945
C	0.31606977	0.10683461	-1.92347485
C	0.35617775	-1.10779391	-1.68330006
C	0.42006046	-2.58482828	-1.71851134
C	0.73357795	-3.12644251	-3.13582690
Au	0.25354875	-0.08249958	0.35674976
C	0.21858381	0.32434324	2.39725590
N	-0.88257760	0.13285180	3.13995897
C	-2.25458705	-0.34754023	2.71395794
C	-2.87712098	0.62646844	1.68814041
N	1.32625560	0.79092520	3.01458570
C	1.29089581	1.13469329	4.45997584
C	2.58444246	1.06659491	2.25907520
H	2.34196122	0.83865004	1.21577080
C	2.98297605	2.55339182	2.33766267
C	-2.17349676	-1.78447118	2.15128978
C	-3.10801887	-0.34731474	4.00072016
C	3.77628146	0.11796155	2.60043512
H	-0.82623865	0.31317165	4.14229543
H	1.18374664	-2.92751216	-1.00931460
H	-0.53640377	-2.99136261	-1.36647567
H	1.09766617	2.06114791	-2.09543129
H	-0.65174085	1.95566136	-2.23283457
H	0.76229499	-4.22086225	-3.10208459
H	1.70481726	-2.76358712	-3.48932619
H	-0.03625801	-2.82168719	-3.85251200

H	-0.41535057	0.85546805	-4.50993208
H	1.35582254	0.96419476	-4.36953699
H	0.37688537	2.44602297	-4.44889819
H	-3.18061186	-2.13714956	1.89823163
H	-1.56089473	-1.82444397	1.24232285
H	-1.73993440	-2.46715979	2.89139227
H	-3.89109424	0.29230232	1.43711334
H	-2.93730276	1.63958463	2.10312290
H	-2.29314575	0.66405589	0.76088920
H	-4.12273055	-0.68479908	3.76415790
H	-2.68700871	-1.02225542	4.75520960
H	-3.17130852	0.65868187	4.43271921
H	3.85015629	2.73032840	1.69121607
H	2.15764566	3.18405724	1.98864013
H	3.25459264	2.85995303	3.35152779
H	2.26648335	1.49995135	4.76727193
H	0.53619833	1.90784022	4.65246830
H	1.05085796	0.25058067	5.06201701
H	4.56189745	0.40836786	1.88626798
O	4.23173805	0.41032443	3.94522450
C	3.48770112	-1.36642854	2.38665659
C	2.91581853	-2.16546337	3.39187299
C	2.66481411	-3.52450116	3.16466704
C	2.98408780	-4.10518141	1.93040007
C	3.56226629	-3.31933629	0.92511380
C	3.81327446	-1.96107387	1.15453939
H	2.68088074	-1.72956126	4.35976634
H	2.22318336	-4.12928362	3.95329343
H	2.79450482	-5.16211442	1.75763314
H	3.83253748	-3.76451636	-0.02956101
H	4.27812268	-1.36130810	0.37294835
H	4.98352831	-0.18120064	4.13300087
F	-0.58290456	1.59346194	8.35713397
B	-1.51376327	1.13854080	7.38628643
F	-2.73118082	0.78628638	8.02436194
F	-0.98149972	0.00091224	6.71929936
F	-1.75338952	2.17070645	6.44120308

10BF₄_b.xyz (64)			
C	-3.95976756	-1.79633616	-2.08134622
C	-3.16677672	-1.22034872	-0.88143529
C	-1.71080722	-1.16424867	-1.14400662
C	-0.56987488	-1.22307985	-1.62570935
C	0.65076785	-1.40586260	-2.44059924
C	0.33567884	-1.94224571	-3.86058637
Au	-0.31225384	-0.36035314	0.47011893
C	0.58137746	0.45770467	2.15537211
N	-0.01975364	1.40004675	2.90139437
C	-1.37487329	2.05010145	2.74410283

C	-1.45700136	2.82491043	1.40910298
N	1.82238361	0.07314370	2.52034040
C	2.50347406	0.72093935	3.66979036
C	2.59569635	-0.92964640	1.72426211
H	1.90964946	-1.24549244	0.93143186
C	3.83404379	-0.29557103	1.06216947
C	-2.49625884	0.99359638	2.85172478
C	-1.48198211	3.04280611	3.92329140
C	2.94374912	-2.24613338	2.48615221
H	0.48746464	1.75187184	3.70908666
H	1.17444491	-0.44513277	-2.51693890
H	1.32964173	-2.09602520	-1.92475520
H	-3.52868542	-0.21150891	-0.64869148
H	-3.34826551	-1.83071984	0.01151484
H	1.27521095	-2.05438060	-4.41204954
H	-0.31006790	-1.24997451	-4.41118408
H	-0.15613259	-2.91951010	-3.81266021
H	-3.63941157	-2.81817139	-2.31027193
H	-3.82412250	-1.17807234	-2.97493395
H	-5.02534325	-1.81425347	-1.82896764
H	-3.47475601	1.48365138	2.78416647
H	-2.42722354	0.25810929	2.04151438
H	-2.43740190	0.46013563	3.80740197
H	-2.42574662	3.33402164	1.33934294
H	-0.66260514	3.57823740	1.34807038
H	-1.36204537	2.15183413	0.54903712
H	-2.44389940	3.56409503	3.88151192
H	-1.41920037	2.51978203	4.88594105
H	-0.68493064	3.79569517	3.87627932
H	4.33047844	-1.04210217	0.43243327
H	3.53367938	0.54816634	0.43087776
H	4.55980060	0.05766963	1.80003997
H	3.49010283	0.28345406	3.79385249
H	2.60624459	1.80077769	3.49957884
H	1.93915693	0.55272576	4.59540561
H	3.34389065	-2.90454421	1.70204064
O	3.99580725	-1.96284149	3.44510322
C	1.73846388	-2.94350078	3.11839109
C	1.38680458	-2.74975180	4.46516791
C	0.27075871	-3.39902914	5.01042461
C	-0.50764727	-4.25045468	4.21621360
C	-0.15903682	-4.45625075	2.87446724
C	0.95798504	-3.81045640	2.33172268
H	1.99372502	-2.10174019	5.09270926
H	0.01230354	-3.24108275	6.05511592
H	-1.37175223	-4.75663526	4.64089941
H	-0.74951907	-5.12631497	2.25381471
H	1.23445302	-3.98583001	1.29298510
H	4.28040806	-2.81488262	3.82355733

F	4.97780063	-3.74227798	-0.35590958
B	4.02311284	-3.78688591	-1.40639803
F	2.71392968	-3.73347698	-0.85803058
F	4.17802527	-4.99793013	-2.13437830
F	4.22293736	-2.68458584	-2.27441051

10BF₄_c.xyz (64)			
C	-0.71946359	-3.44428639	-2.44342984
C	-0.17991332	-2.17291571	-1.74176633
C	-0.80323449	-1.95730929	-0.41772006
C	-1.47640939	-2.01284435	0.62165272
C	-2.41494924	-2.35948252	1.71065688
C	-3.22466595	-3.64226359	1.39690240
Au	-0.13348813	-0.18065813	0.83628767
C	0.83544156	1.53200050	1.50164084
N	0.40943324	2.23060490	2.56487082
C	-0.76531461	1.98421992	3.48262046
C	-2.09064162	2.02876317	2.69034778
N	1.92277715	1.99499433	0.84845884
C	2.55062928	3.28379401	1.23741077
C	2.48663836	1.29328847	-0.34364763
H	1.89570044	0.37628164	-0.44454481
C	2.31489343	2.14105815	-1.61856821
C	-0.59460476	0.64346264	4.23172698
C	-0.73467758	3.15074220	4.49505029
C	3.96081729	0.83362645	-0.07222000
H	0.99925717	2.99338472	2.88978599
H	-1.85116720	-2.49404104	2.64159182
H	-3.09972930	-1.51863051	1.87527233
H	0.90733865	-2.25012766	-1.61801556
H	-0.36272926	-1.29364501	-2.37124695
H	-3.90158121	-3.84942713	2.23249965
H	-2.56062676	-4.50321868	1.26596797
H	-3.82252171	-3.51713959	0.48787037
H	-1.79949708	-3.37197714	-2.60882545
H	-0.51403275	-4.33953368	-1.84701095
H	-0.22649681	-3.55262819	-3.41550514
H	-1.42959477	0.50093756	4.92823639
H	-0.58142095	-0.20481772	3.53695190
H	0.34174408	0.63499612	4.80133673
H	-2.93339505	1.90733878	3.38138921
H	-2.19988966	2.98880276	2.17200364
H	-2.14522315	1.22730127	1.94407076
H	-1.55824441	3.04089470	5.20834954
H	0.20706611	3.15772670	5.05794658
H	-0.85075653	4.11511384	3.98458473
H	2.61050323	1.56193632	-2.49903505
H	1.26459896	2.43244142	-1.73362585
H	2.92546014	3.05134345	-1.59719743

H	3.36299937	3.51383426	0.54996840
H	1.81657202	4.09722360	1.18268279
H	2.96029639	3.23145190	2.25228710
H	4.59013610	1.72175557	0.07648875
O	4.01856400	-0.01007191	1.10074251
C	4.52960534	0.04054059	-1.24279208
C	4.13132748	-1.28898362	-1.46951896
C	4.64793355	-2.01239686	-2.55106791
C	5.56848876	-1.41503751	-3.42316488
C	5.97561884	-0.09383997	-3.20071411
C	5.46121912	0.62627068	-2.11452227
H	3.43309148	-1.76664287	-0.78572895
H	4.33665860	-3.04225642	-2.71019299
H	5.97037338	-1.97747723	-4.26271847
H	6.69782678	0.37450590	-3.86501873
H	5.79094083	1.64938723	-1.94207960
H	3.91096855	0.53277076	1.90906228
F	3.11774321	3.05321299	4.70953696
B	4.10641723	2.03981848	4.80105066
F	3.90781548	1.09257093	3.74579589
F	3.99882514	1.37463315	6.04393153
F	5.39202673	2.61742949	4.66884552

4.5.2 Computational details for **9L**, **9'L** and **C₂H₂L** systems.

All calculations here reported have been performed using density functional theory (DFT) with the ADF (Amsterdam Density Functional) package.²²⁶ The BP86 GGA^{230a,231} Functional was used. The TZ2P triple zeta basis set with two polarization functions was used for all atoms. Relativistic effects were included with the zeroth-order regular approximation (ZORA) Hamiltonian^{228b} as implemented in ADF, with a small frozen core. A fine integration grid has been used both in the SCF iterations and in the optimization procedure in order to converge properly the geometrical parameters. Several series of complexes were fully optimized. The optimized geometries are available for **9L** ([LAu(NAC)]⁺⁰), **9'L** ([LAu(**NAC^{sym}**)]⁺⁰ systems) and **C₂H₂L** ([LAu(C₂H₂)]⁺⁰ systems) in xyz format and are reported at the end of this Supporting Information.

The Au-C bond in **9'L** has been analyzed using the charge-displacement function (CDF): numeriamo?

$$\Delta q(z) = \int_{-\infty}^z dz' \iint_{-\infty}^{\infty} \Delta \rho(x, y, z') dx dy \quad (\text{Eq. 4})$$

where $\Delta \rho$ is the difference between the electronic density of a complex and that of its non-interacting fragments [LAu] metal substrate and NAC, and z is any suitable axis joining them. Here we consider the axis joining the gold nuclei position and carbonic carbon of NAC moiety. The CDF gives the exact definition of the amount of electronic charge which, upon formation of the complex, is displaced from left to the right (the direction of decreasing z) across the plane perpendicular to the axis at point z . As previously shown by some of us^{36,129,232}, for suitable symmetric complexes and fragments, $\Delta \rho$, and consequently $\Delta q(z)$, can be decomposed into additive symmetry components which can be readily identified with the DCD components of the bond. In all the cases, the fragments used are [LAu]⁺⁰ and [**NAC^{sym}**], with the aim to analyze the charge displacement between the metal fragment and the carbene. The use of symmetry permits the separation of the total $\Delta \rho$ function into components according to the following equations:

$$\Delta \rho = \sum_p \Delta \rho_p \quad (\text{Eq. 5})$$

$$\Delta \rho_p = \sum_{i \in p} |\phi_i^{(AB)}|^2 - \sum_{i \in p} |\phi_i^{(A)}|^2 - \sum_{i \in p} |\phi_i^{(B)}|^2 \quad (\text{Eq. 6})$$

Here p labels the symmetry irreducible representations of a complex AB and its fragments A and B (the symmetry is the same in the cases studied here), while ϕ_i are the Kohn-Sham orbitals.

All the complexes except the one bearing phosphine ligands, present a C_s symmetry with the symmetry plane passing through the N-C_{carbenic}-N atoms of **NAC^{sym}** and the gold atom. The z -axis is that passing

through gold and C_{carbenic} of NAC^{sym} . The separation of the Δq function in the two irreducible representations A' and A'' thus provides a rigorous definition of the components of the DCD bond model.

In the case of systems $[\text{LAu}(\text{C}_2\text{H}_2)]^{+/0} (\text{C}_2\text{H}_2\text{L})$ we analyze the DCD components using a simple method based on the demonstration¹³⁹ that the distortion $\Delta\vartheta$ of ethyne from linearity upon its coordination to a metal center depends on the metal $\rightarrow (\text{C}_2\text{H}_2)$ π back-donation ($CT_{\text{back}}^{\text{eth}}$), with only a small contribution of the $(\text{C}_2\text{H}_2) \rightarrow \text{M}$ σ donation ($CT_{\text{don}}^{\text{eth}}$), and an even smaller influence of an electrostatic term ($\Delta\vartheta_{\text{elect}}$). By evaluating the total CT between ethyne and the metal fragment ($CT_{\text{tot}}^{\text{eth}}$), $\Delta\vartheta$ and $\Delta\vartheta_{\text{elect}}$, we can easily evaluate the DCD components, and in particular the Au $\rightarrow (\text{C}_2\text{H}_2)$ π back-donation ($CT_{\text{back}}^{\text{eth}}$) through (Eq. 7) and (Eq. 8).

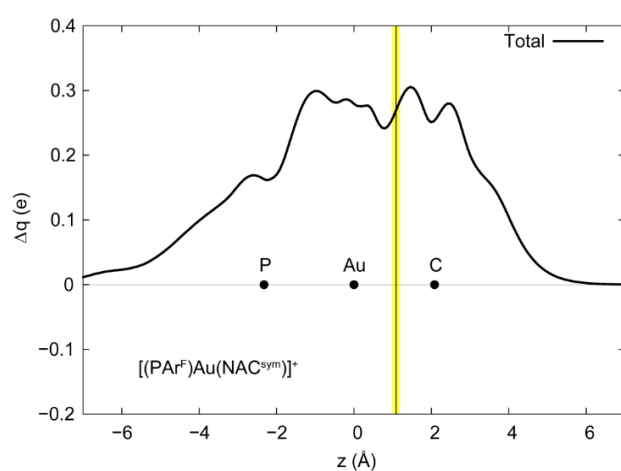
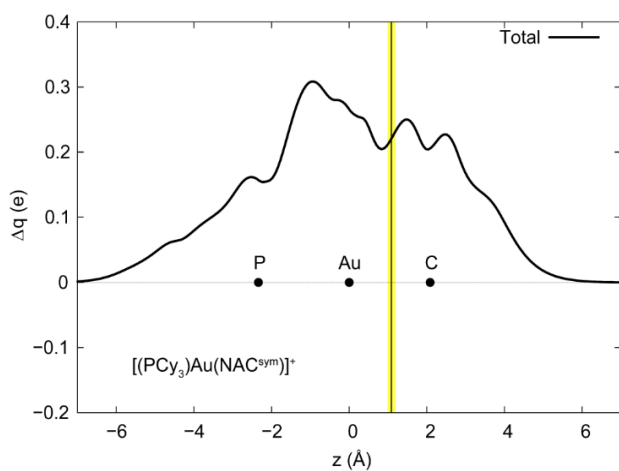
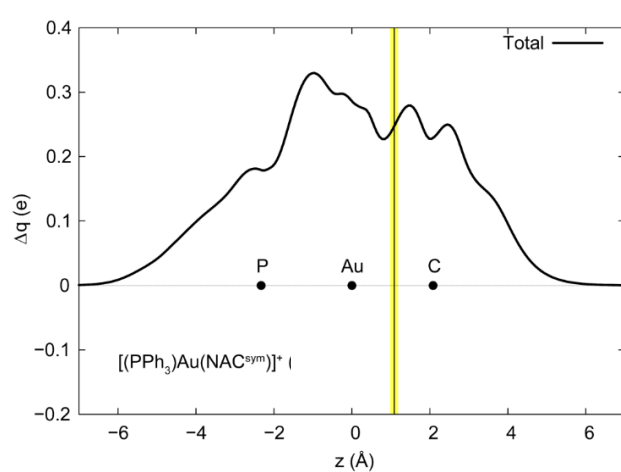
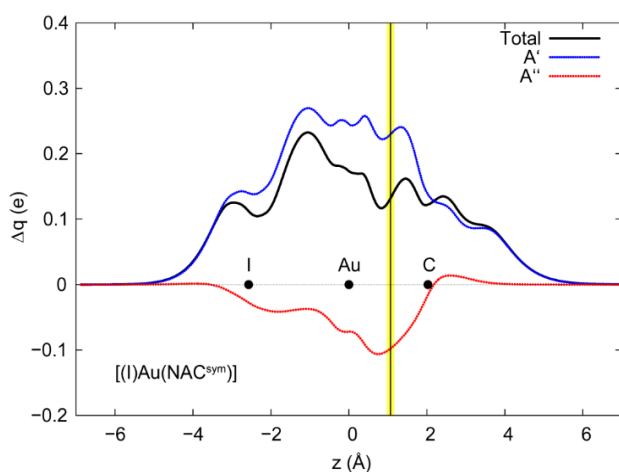
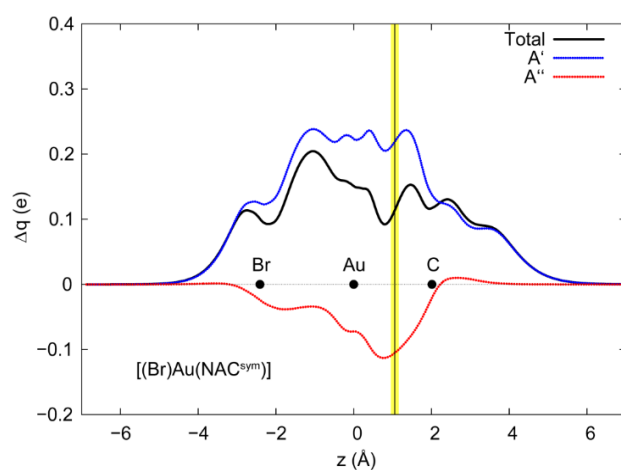
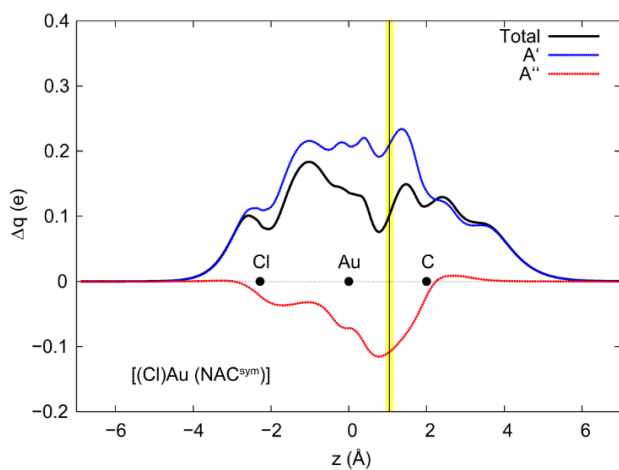
$$\Delta\vartheta = 7.9 |CT_{\text{don}}^{\text{eth}}| + 57.5 |CT_{\text{back}}^{\text{eth}}| + \Delta\vartheta_{\text{elect}} \quad (\text{Eq. 7})$$

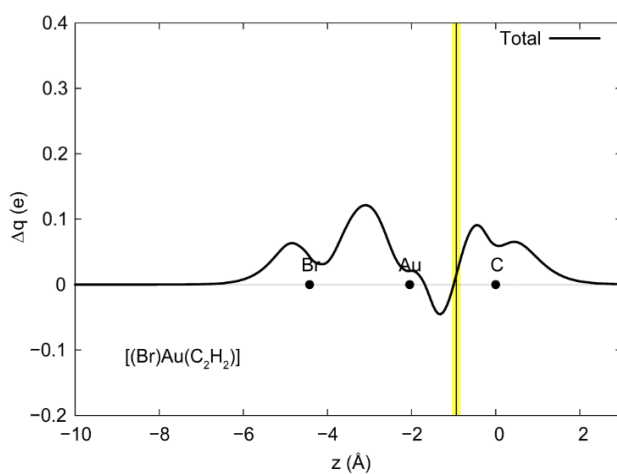
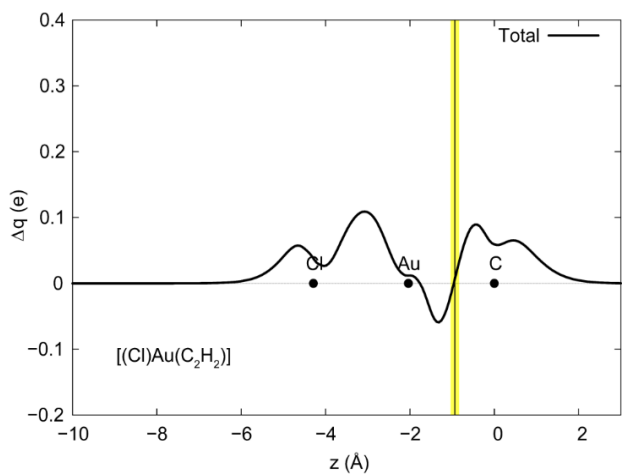
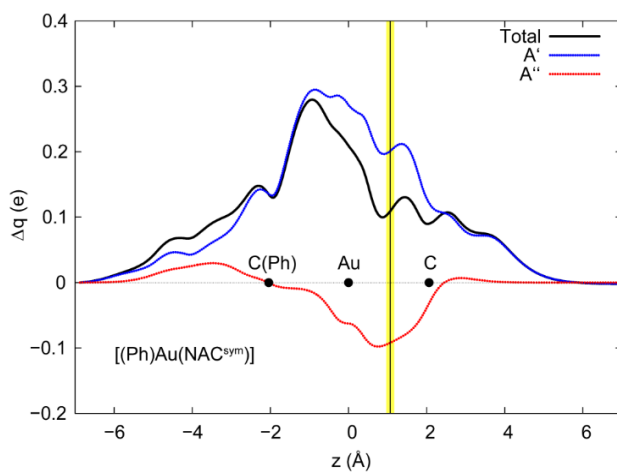
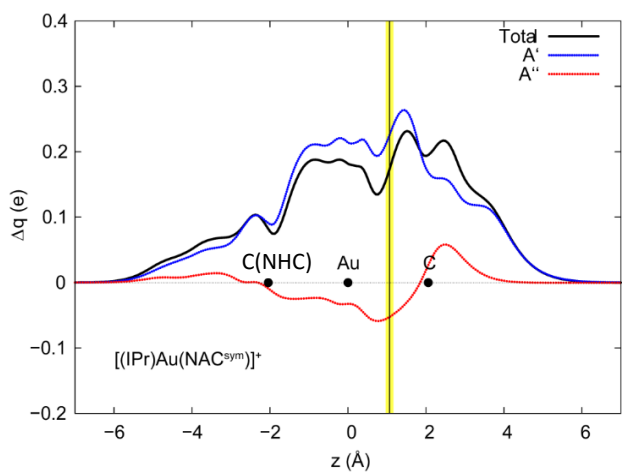
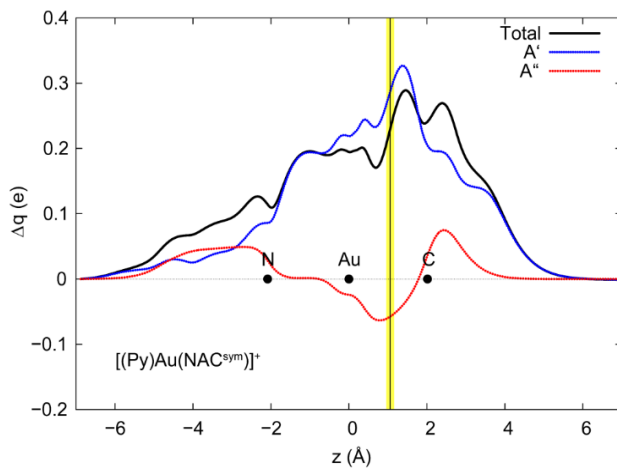
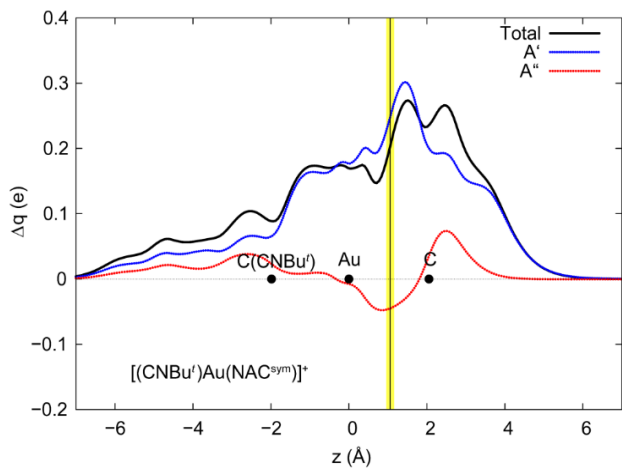
$$CT_{\text{tot}}^{\text{eth}} = CT_{\text{don}}^{\text{eth}} + CT_{\text{back}}^{\text{eth}} (\text{Eq. 8})$$

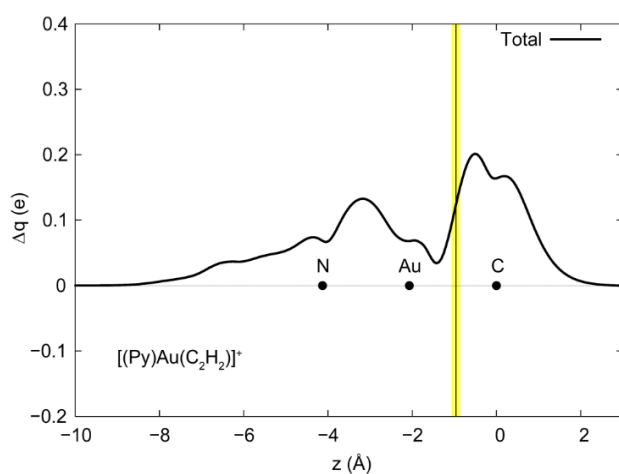
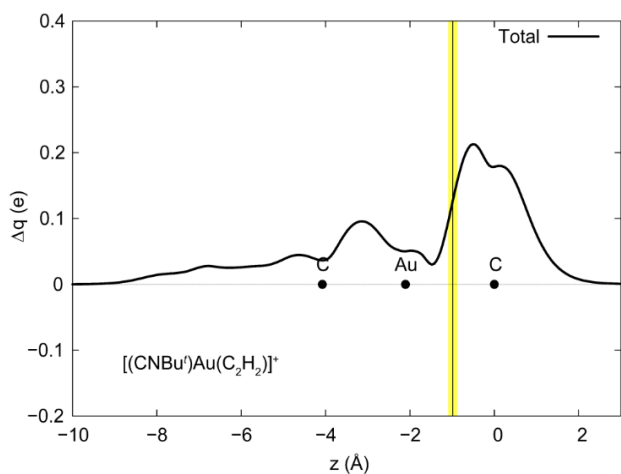
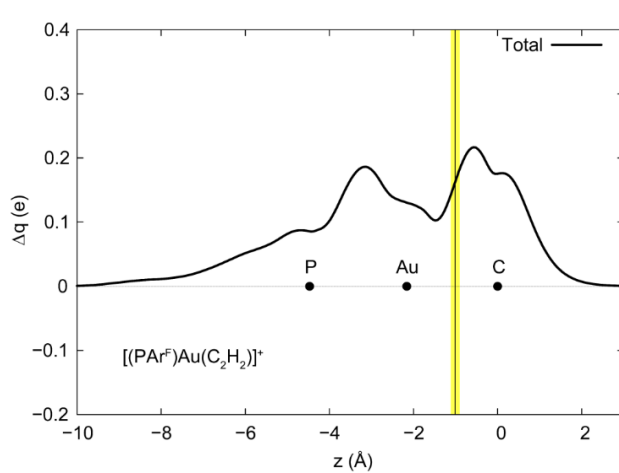
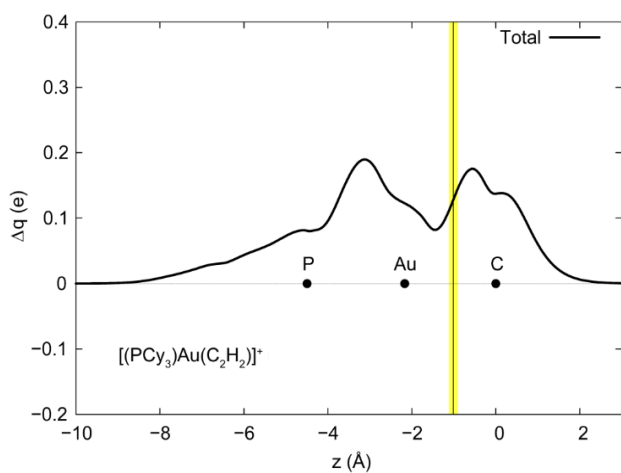
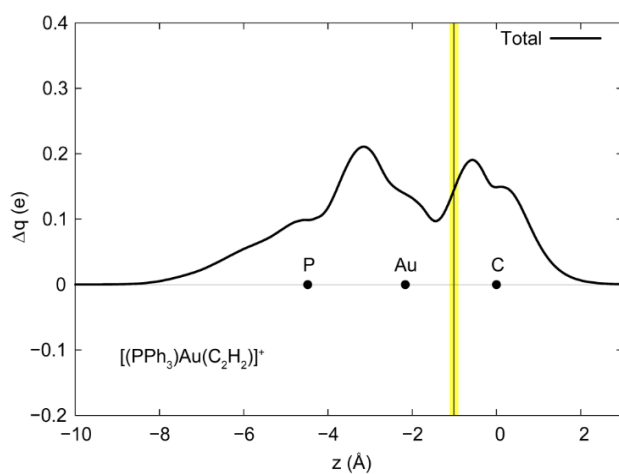
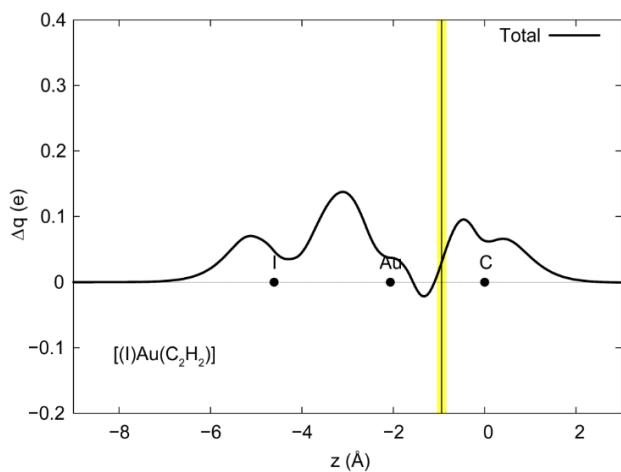
The electrostatic contributions to ethyne distortion $\Delta\vartheta_{\text{elect}}$, were determined by computing the distortion of the ethyne placed in the field of three point charges replacing the Au atoms. The charges were derived by an atomic charge analysis in the adduct. In particular we used Hirshfeld charges but, as we showed,¹³⁹ the results are negligibly affected by the particular method used for evaluating these partial charges. For the geometry optimizations in presence of point charges we set the value of the “qpnear” keywords to 20 in ADF program. The results of this analysis is reported in Table S2.

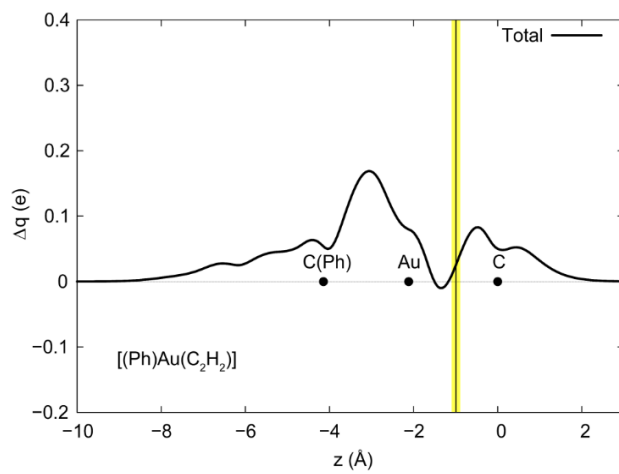
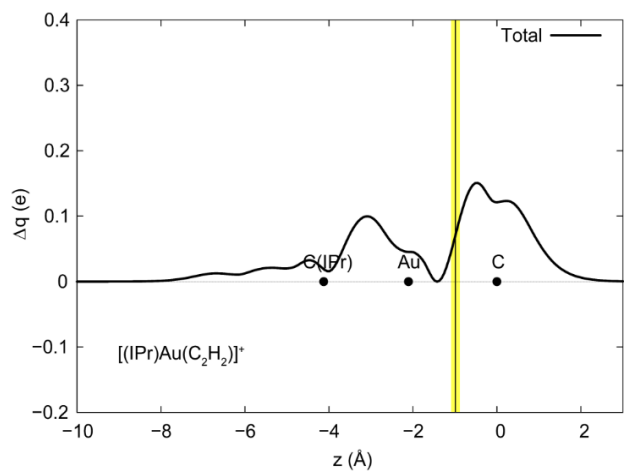
Table 21. $CT_{\text{tot}}^{\text{eth}}$, $\Delta\vartheta$, $\Delta\vartheta_{\text{elect}}$ and $CT_{\text{back}}^{\text{eth}}$ values for $[\text{LAu}(\text{C}_2\text{H}_2)]^{+/0}$ model systems.				
L	$CT_{\text{tot}}^{\text{eth}}$ (e)	$\Delta\vartheta$ (°)	$\Delta\vartheta_{\text{elect}}$ (°)	$CT_{\text{back}}^{\text{eth}}$ (e)
Cl	0.007	18.35	0.41	-0.273
Br	0.015	18.25	0.39	-0.271
I	0.030	17.44	0.33	-0.258
PPh ₃	0.144	11.95	2.71	-0.124
PCy ₃	0.128	11.75	2.82	-0.121
PAr ^F	0.163	11.58	2.85	-0.114
CN ^t Bu	0.125	12.61	2.86	-0.134
Py	0.112	14.99	3.22	-0.166
NHC	0.071	14.03	2.66	-0.165
Ph	0.026	14.59	0.33	-0.215

Charge Displacement Curves.

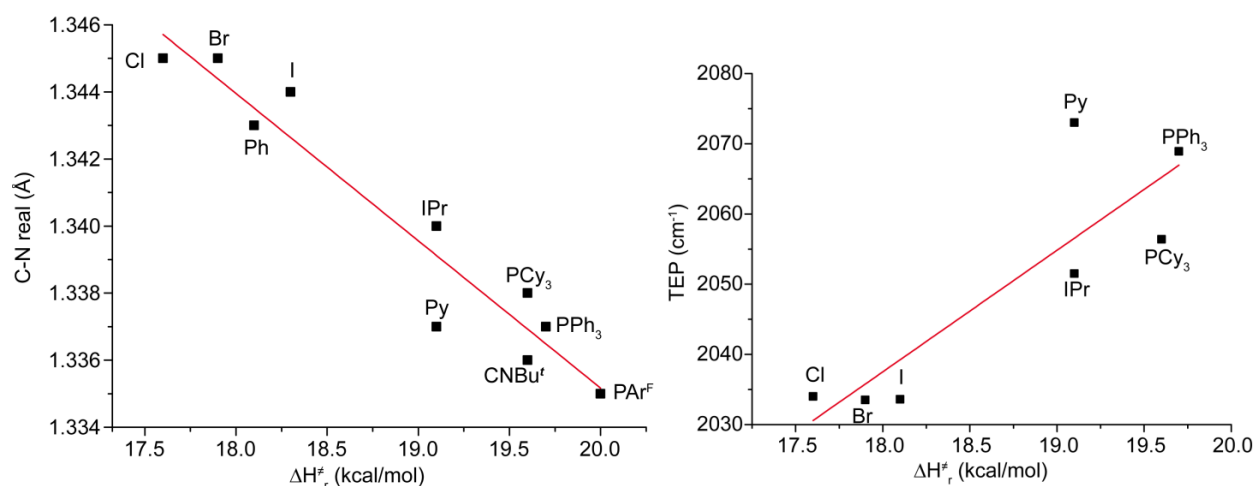




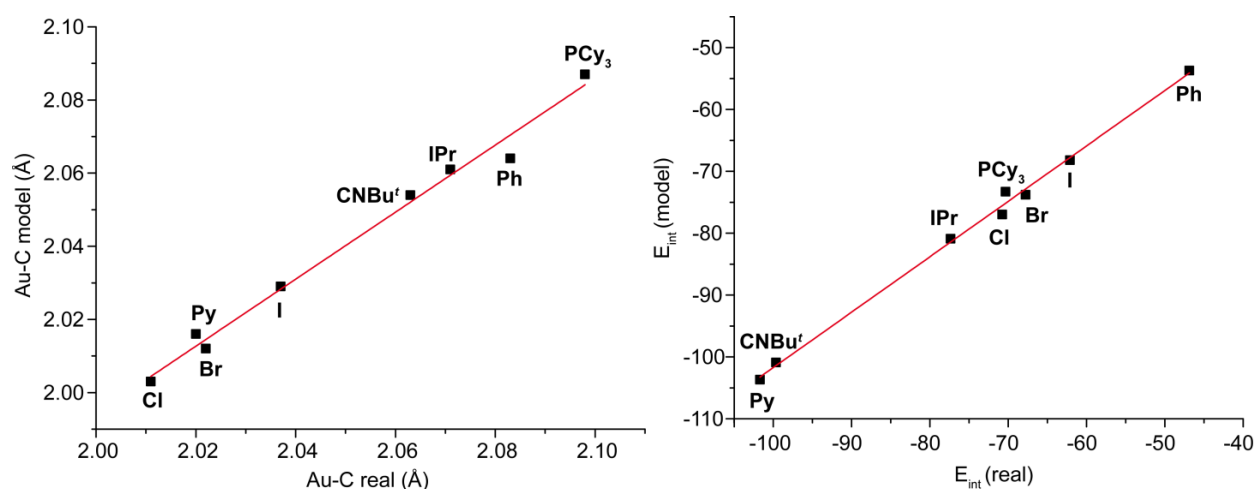




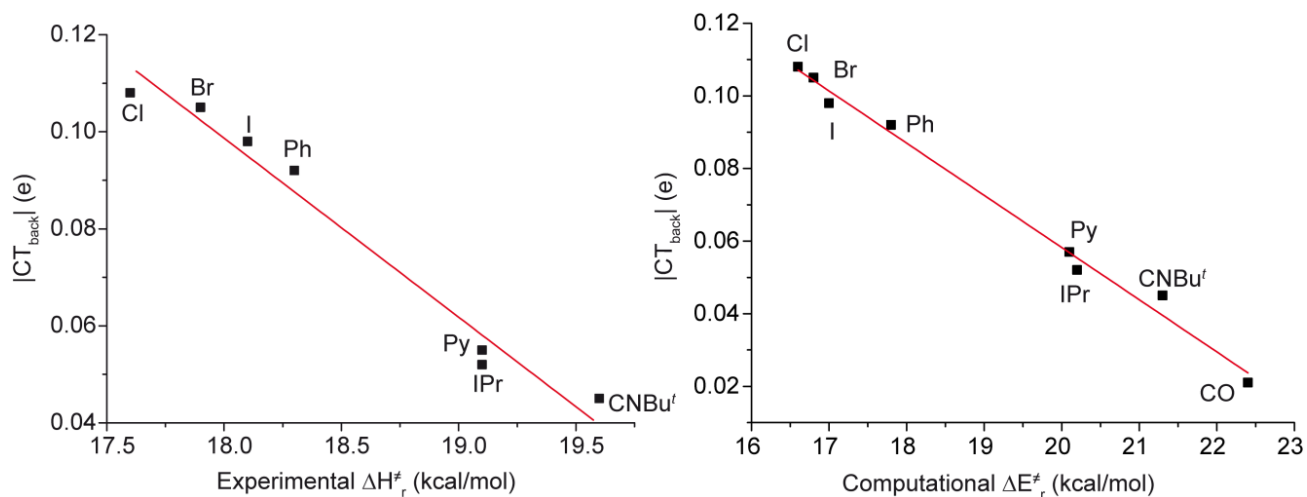
Supplementary figures



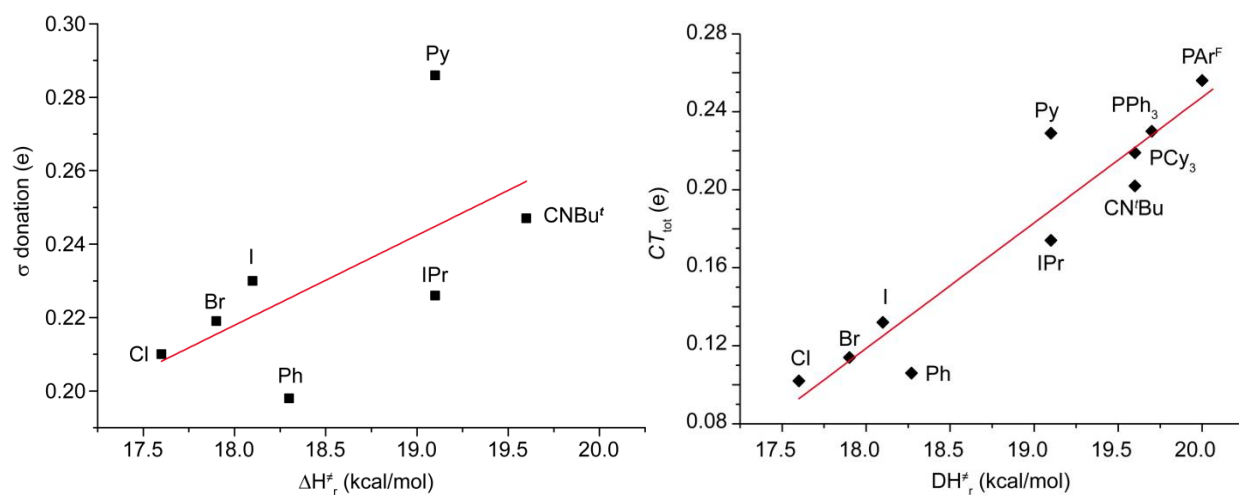
Plot 41. (Left panel) Correlation between the computed C-N bond distance in complexes **9L** and the experimental rotational barrier. The best linear fit (red line) equation is $y = (4.4 \pm 0.4) \cdot 10^{-3} x + (1.42 \pm 0.01)$, $r^2 = 0.923$. (Right panel) Correlation between the Tolman Electronic Parameter (TEP) and the rotational barrier. The best linear fit (red line) equation is $y = (17 \pm 4)x + (1730 \pm 80)$, $r^2 = 0.753$.



Plot 42. (Left panel) Correlation between the Au-C_{NAC} bond distances for complexes **9L** (real) and **9'L** (symmetric model). The best linear fit (red line) equation is $y = (0.92 \pm 0.04)x - (0.0 \pm 0.2)$, $r^2 = 0.9880$. (Right panel) Correlation between the [(L)Au]⁺-NAC interaction energies (E_{int}) for **9L** (real) and **9'L** (symmetric model). The best linear fit (red line) equation is $y = (0.90 \pm 0.02)x - (12 \pm 2)$, $r^2 = 0.9961$ (right). numerazione?



Plot 43. (Left panel) Linear correlation between the experimental C-N rotational barrier (ΔH_r^\ddagger) and $|CT_{\text{back}}|$. (Right panel) Linear correlation (R^2 is 0.991), between the C-N rotational barrier evaluated by DFT calculations and $|CT_{\text{back}}|$. In this case the carbonyl complex $[\text{COAu}(\text{NAC})]^+$ is also included.



Plot 44. (Left panel) Correlation between the C-N rotational barrier (ΔH_r^\ddagger) and the σ donation component. The equation for the best linear fit (red line) is $y = (0.02 \pm 0.01)x - (0.2 \pm 0.3)$, with a correlation $r^2 = 0.397$. (Right panel) Correlation between the C-N rotational barrier (ΔH_r^\ddagger) and CT_{tot} . The equation for the best linear fit (red line) is $y = (0.064 \pm 0.008)x - (1.0 \pm 0.1)$, with a correlation $r^2 = 0.8890$.

List of Cartesian coordinates (Å) for all 9L, 9'L and (C₂H₂)L DFT-optimized structures

9Cl.xyz (31)			
Au	0.017143	0.034913	2.305968
Cl	0.006065	0.111674	0.019277
C	0.002382	-0.009600	4.316068
N	0.635918	-0.933673	5.063576
H	0.556028	-0.865440	6.076313
N	-0.686311	0.919671	5.003009
C	1.490853	-2.071815	4.612376
C	0.675126	-3.052640	3.756269
H	0.311660	-2.561111	2.843155
H	-0.190612	-3.432675	4.316551
H	1.305167	-3.904531	3.464291
C	1.951088	-2.769366	5.901859
H	2.534895	-2.086015	6.537185
H	2.590555	-3.626107	5.655266
H	1.092410	-3.145806	6.478419
C	2.712706	-1.553151	3.838876
H	3.303350	-0.864360	4.459218
H	2.399233	-1.022799	2.928950
H	3.353078	-2.396677	3.545042
C	-1.437331	2.018670	4.361281
H	-0.875082	2.397481	3.501231
H	-2.407538	1.645688	3.997549
C	-1.618718	3.032755	5.493260
H	-0.718907	3.658032	5.587431
H	-2.476785	3.693908	5.325079
C	-1.780596	2.136943	6.732359
H	-2.805424	1.742349	6.781367
H	-1.574321	2.653141	7.677392
C	-0.793249	0.988388	6.475851
H	0.197354	1.200141	6.915055
H	-1.155043	0.031912	6.886997

9'Cl.xyz (15)			
H	0.00000	-1.07351	3.74262

N	0.00000	-1.13491	2.72437
C	0.00000	-2.48339	2.17398
C	0.00000	0.00000	2.00336
N	0.00000	1.13491	2.72437
C	0.00000	2.48339	2.17398
Au	0.00000	0.00000	0.00000
Cl	0.00000	0.00000	-2.28167
H	0.00000	1.07351	3.74262
H	0.00000	-2.40157	1.08073
H	-0.89553	-3.03313	2.49402
H	0.89553	-3.03313	2.49402
H	-0.89553	3.03313	2.49402
H	0.00000	2.40157	1.08073
H	0.89553	3.03313	2.49402

(C ₂ H ₂)Cl.xyz (6)			
Cl	0.0000	0.0000	-2.2523
Au	0.0000	0.0000	0.0000
C	0.6227	0.0000	2.0369
C	-0.6229	0.0000	2.0368
H	-1.6448	0.0000	2.3757
H	1.6445	0.0000	2.3759

9Br.xyz (31)			
Au	0.015450	0.031538	2.327150
Br	0.011469	0.120155	-0.108138
C	-0.004259	-0.011634	4.348980
N	0.635550	-0.930165	5.096530
H	0.552109	-0.864875	6.108958
N	-0.694804	0.913851	5.038869
C	1.490557	-2.069713	4.648108
C	0.671916	-3.052481	3.798585
H	0.303325	-2.561293	2.887132
H	-0.190136	-3.432471	4.364723
H	1.301014	-3.903974	3.503995
C	1.952746	-2.759385	5.940177

H	2.536551	-2.071700	6.570479
H	2.592619	-3.616848	5.697571
H	1.094978	-3.133271	6.519435
C	2.708878	-1.551289	3.870617
H	3.300888	-0.861727	4.488753
H	2.390831	-1.021939	2.961540
H	3.348504	-2.394631	3.575332
C	-1.453713	2.012359	4.404627
H	-0.906607	2.382884	3.531253
H	-2.432537	1.640966	4.063024
C	-1.609551	3.030646	5.535899
H	-0.700784	3.644335	5.617774
H	-2.461633	3.701720	5.378301
C	-1.765401	2.138376	6.777833
H	-2.791679	1.749577	6.836380
H	-1.547318	2.654476	7.720112
C	-0.787183	0.984248	6.512915
H	0.209061	1.191451	6.940762
H	-1.149012	0.030808	6.930335

9'Br.xyz (15)			
H	0.00000	-1.07498	3.75093
N	0.00000	-1.13549	2.73246
C	0.00000	-2.48417	2.18086
C	0.00000	0.00000	2.01214
N	0.00000	1.13549	2.73246
C	0.00000	2.48417	2.18086
Au	0.00000	0.00000	0.00000
Br	0.00000	0.00000	-2.41080
H	0.00000	1.07498	3.75093
H	0.00000	-2.40267	1.08824
H	-0.89536	-3.03356	2.50128
H	0.89536	-3.03356	2.50128
H	-0.89536	3.03356	2.50128
H	0.00000	2.40267	1.08824
H	0.89536	3.03356	2.50128

(C ₂ H ₂)Br.xyz (6)			
--	--	--	--

Br	0.0000	0.0000	2.3803
Au	0.0000	0.0000	0.0000
C	0.6225	0.0000	-2.0463
C	-0.6226	0.0000	-2.0462
H	-1.6450	0.0000	-2.3834
H	1.6449	0.0000	-2.3835

9I.xyz (31)			
Au	0.015874	0.024639	2.381036
I	0.006323	0.130076	-0.215071
C	-0.002657	-0.018206	4.417842
N	0.637850	-0.935625	5.163650
H	0.558336	-0.871195	6.176822
N	-0.693238	0.909677	5.101300
C	1.493483	-2.073221	4.708838
C	0.672369	-3.053662	3.858962
H	0.299959	-2.560498	2.949972
H	-0.187266	-3.436722	4.426679
H	1.301324	-3.903311	3.558764
C	1.961346	-2.766529	5.996671
H	2.547342	-2.080430	6.626632
H	2.600812	-3.622704	5.748471
H	1.106164	-3.142845	6.578092
C	2.708426	-1.551379	3.928146
H	3.302217	-0.862754	4.545579
H	2.387258	-1.020347	3.020970
H	3.347712	-2.393296	3.628044
C	-1.451285	2.004646	4.458737
H	-0.902804	2.369778	3.583900
H	-2.429346	1.630797	4.117713
C	-1.608970	3.030047	5.582920
H	-0.700992	3.645352	5.661116
H	-2.461699	3.699026	5.419800
C	-1.765137	2.145886	6.830778
H	-2.791213	1.756795	6.890670
H	-1.548487	2.668694	7.769684
C	-0.785844	0.990534	6.575036
H	0.210423	1.201726	7.000708

H	-1.146517	0.039515	6.998740
---	-----------	----------	----------

9 ^l .xyz (15)			
H	0.00000000	1.07852800	3.76459800
N	0.00000000	1.13593900	2.74556900
C	0.00000000	2.48301900	2.18966100
C	0.00000000	0.00000000	2.02861600
N	0.00000000	-1.13593900	2.74556900
C	0.00000000	-2.48301900	2.18966100
H	0.00000000	-1.07852800	3.76459800
H	0.00000000	-2.39843000	1.09719100
H	-0.89534700	-3.03299700	2.50850100
H	0.89534700	-3.03299700	2.50850100
H	0.00000000	2.39843000	1.09719100
H	0.89534700	3.03299700	2.50850100
H	-0.89534700	3.03299700	2.50850100
Au	0.00000000	0.00000000	-0.00000000
I	-0.00000000	0.00000000	-2.57333100

(C ₂ H ₂)Cl.xyz (6)			
I	0.0000	0.0000	2.5437
Au	0.0000	0.0000	0.0000
C	0.6216	0.0000	-2.0656
C	-0.6217	0.0000	-2.0656
H	-1.6485	0.0000	-2.3881
H	1.6483	0.0000	-2.3883

9PPh ₃ .xyz (64)			
P	0.003311	-0.021844	2.258601
Au	0.005167	-0.045228	-0.071934
C	-1.251519	-1.118506	3.014178
C	-1.405040	-2.418907	2.503670
C	-2.048689	-0.696761	4.087981
C	-2.342255	-3.284700	3.064832
C	-3.138014	-2.858700	4.132834
C	-2.989480	-1.567737	4.642483

C	1.614197	-0.532276	2.955414
C	2.784692	-0.290585	2.216722
C	4.026357	-0.665122	2.730107
C	4.107650	-1.287076	3.978940
C	2.946461	-1.531241	4.716068
C	1.701088	-1.156819	4.209150
C	-0.347314	1.660235	2.887577
C	-1.444627	2.356885	2.350897
C	-1.741544	3.643596	2.796945
C	-0.940537	4.249889	3.770167
C	0.152706	3.563686	4.300916
C	0.450895	2.270167	3.864726
H	-2.068068	1.888155	1.587972
H	-2.596355	4.176372	2.382382
H	-1.168590	5.259016	4.111629
H	0.779702	4.033246	5.057524
H	1.307062	1.740698	4.281675
H	2.719861	0.184414	1.236409
H	4.930090	-0.479049	2.151405
H	5.076899	-1.588208	4.375135
H	3.007195	-2.020418	5.687221
H	0.797728	-1.360265	4.783761
H	-0.788553	-2.753951	1.668810
H	-2.456865	-4.291418	2.665206
H	-3.876457	-3.533435	4.564640
H	-3.607854	-1.231989	5.473715
H	-1.940558	0.310694	4.488592
C	0.040032	0.045904	-2.160413
N	0.146613	-1.029748	-2.952268
H	0.151451	-0.880001	-3.960088
N	-0.039100	1.232647	-2.771175
C	0.258520	-2.471985	-2.569204
C	-1.005699	-2.916453	-1.820248
H	-1.131080	-2.343144	-0.889758
H	-1.901555	-2.768960	-2.438360
H	-0.932415	-3.981553	-1.562037
C	0.376992	-3.236980	-3.894892
H	1.272744	-2.927879	-4.452983

H	0.459849	-4.313032	-3.699645
H	-0.509942	-3.078892	-4.525786
C	1.517741	-2.701057	-1.721829
H	2.418605	-2.384550	-2.264676
H	1.465904	-2.139171	-0.777292
H	1.615147	-3.767630	-1.478567
C	-0.149810	2.532060	-2.068756
H	0.456894	2.517241	-1.156689
H	-1.199312	2.710654	-1.788355
C	0.317912	3.541408	-3.118336
H	1.415986	3.588055	-3.133824
H	-0.063286	4.549652	-2.923027
C	-0.213507	2.938950	-4.428792
H	-1.284728	3.155714	-4.539674
H	0.298864	3.315354	-5.320911
C	-0.002953	1.429723	-4.241470
H	0.976644	1.103428	-4.628980
H	-0.787720	0.833764	-4.732606

9'PPh ₃ .xyz (48)			
H	-0.329108	-0.410324	-2.197071
N	-0.011175	-0.144720	-1.263594
C	-0.170673	1.268775	-0.934269
C	0.508761	-1.083243	-0.466902
N	0.577286	-2.322687	-0.962278
C	1.101965	-3.494333	-0.268201
Au	1.179846	-0.626104	1.450691
P	1.934947	-0.056719	3.577940
C	1.452279	1.655938	3.999300
C	0.116106	2.042891	3.791674
C	-0.286907	3.344875	4.082839
C	0.639684	4.271912	4.571293
C	1.966764	3.891716	4.776263
C	2.376670	2.586304	4.492956
C	1.251658	-1.131684	4.887602
C	1.108386	-2.505551	4.629082
C	0.596674	-3.352775	5.610602
C	0.218300	-2.835065	6.852858

C	0.357990	-1.470589	7.113906
C	0.873578	-0.616960	6.136256
C	3.755275	-0.155728	3.694642
C	4.525278	0.205550	2.575505
C	5.916676	0.136574	2.632897
C	6.547267	-0.301995	3.800800
C	5.785711	-0.664123	4.913845
C	4.392215	-0.592763	4.865305
H	-0.608177	1.323254	3.406546
H	-1.323426	3.639139	3.923294
H	0.325490	5.292141	4.789028
H	2.690702	4.611636	5.155150
H	3.415257	2.296453	4.650314
H	4.033734	0.535104	1.658673
H	6.508896	0.415817	1.762596
H	7.634099	-0.367068	3.840454
H	6.275005	-1.010425	5.822992
H	3.802760	-0.886308	5.733522
H	1.395910	-2.909995	3.657749
H	0.485353	-4.416462	5.404383
H	-0.191602	-3.496372	7.615519
H	0.060755	-1.064434	8.079602
H	0.973036	0.448357	6.342754
H	0.232152	-2.497367	-1.907477
H	0.201196	1.435837	0.082337
H	0.403162	1.891229	-1.632214
H	-1.228721	1.555121	-0.981889
H	1.916247	-3.946814	-0.847458
H	1.490615	-3.175491	0.704556
H	0.310339	-4.238726	-0.114703

(C ₂ H ₂)PPh ₃ .xyz (39)			
Au	0.0000	0.0000	0.0000
C	-0.0228	-0.5929	2.1660
C	0.0232	0.6356	2.1517
H	0.0638	1.6913	2.3572
H	-0.0629	-1.6423	2.4010
P	0.0000	0.0000	-2.3155

C	-1.2747	-1.1178	-2.9813
C	-1.4409	-2.3842	-2.3942
C	-2.0740	-0.7391	-4.0696
C	-2.4000	-3.2621	-2.8952
C	-3.1992	-2.8810	-3.9776
C	-3.0346	-1.6246	-4.5632
C	1.6140	-0.5163	-2.9805
C	2.7876	-0.1767	-2.2859
C	4.0299	-0.5530	-2.7941
C	4.1066	-1.2748	-3.9888
C	2.9417	-1.6156	-4.6795
C	1.6937	-1.2392	-4.1807
C	-0.3606	1.6874	-2.9042
C	-1.4972	2.3491	-2.4046
C	-1.7837	3.6464	-2.8238
C	-0.9369	4.2926	-3.7307
C	0.1927	3.6383	-4.2240
C	0.4862	2.3355	-3.8140
H	-2.1590	1.8485	-1.6962
H	-2.6653	4.1564	-2.4384
H	-1.1583	5.3105	-4.0496
H	0.8531	4.1402	-4.9294
H	1.3719	1.8301	-4.1979
H	2.7286	0.3770	-1.3476
H	4.9375	-0.2923	-2.2520
H	5.0776	-1.5792	-4.3778
H	3.0005	-2.1826	-5.6073
H	0.7870	-1.5165	-4.7177
H	-0.8206	-2.6832	-1.5476
H	-2.5296	-4.2413	-2.4367
H	-3.9554	-3.5649	-4.3616
H	-3.6574	-1.3263	-5.4052
H	-1.9545	0.2435	-4.5251

9PCy ₃ .xyz (82)			
Au	-0.009289	-0.094563	2.096900
N	0.632018	-0.815355	4.997187
C	-0.041825	0.016817	4.191531

H	0.550006	-0.677562	6.003407
N	-0.759736	0.971336	4.794356
C	1.517934	-1.962952	4.630274
C	0.710824	-3.031043	3.879463
H	0.311571	-2.625392	2.938167
H	-0.131207	-3.386921	4.488500
H	1.354867	-3.888064	3.640269
C	2.023332	-2.530761	5.963911
H	2.597197	-1.778097	6.523924
H	2.684363	-3.386372	5.779875
H	1.188431	-2.881150	6.588287
C	2.704837	-1.470687	3.790411
H	3.282061	-0.711027	4.334649
H	2.357703	-1.031751	2.843141
H	3.370404	-2.312271	3.555481
C	-1.554971	1.995074	4.079830
H	-1.024446	2.311164	3.175050
H	-2.527064	1.570311	3.785644
C	-1.728500	3.101522	5.121672
H	-0.836594	3.743711	5.142128
H	-2.599314	3.733627	4.915744
C	-1.852962	2.313575	6.435325
H	-2.868055	1.906601	6.538958
H	-1.640088	2.914995	7.325852
C	-0.845972	1.167791	6.262597
H	0.148920	1.437425	6.654727
H	-1.176890	0.242733	6.759422
P	-0.008030	-0.089265	-0.244888
C	-0.279644	-1.771790	-1.012656
C	0.874759	-2.750043	-0.706609
C	0.623534	-4.128400	-1.341691
C	-0.723554	-4.719522	-0.907821
C	-1.872218	-3.749777	-1.212240
C	-1.635192	-2.370217	-0.575541
C	-1.449074	0.955347	-0.835869
C	-1.365581	2.418757	-0.351645
C	-2.684438	3.158806	-0.628589
C	-3.062115	3.092611	-2.115137

C	-3.110544	1.642349	-2.615129
C	-1.792337	0.896188	-2.338650
C	1.660754	0.482548	-0.870458
C	2.179296	1.755927	-0.165717
C	3.645274	2.023795	-0.545469
C	3.827224	2.117894	-2.066984
C	3.286865	0.866736	-2.772926
C	1.818353	0.593453	-2.400409
H	-0.307672	-1.600473	-2.103136
H	0.970510	-2.861905	0.387402
H	1.831882	-2.350480	-1.070908
H	1.447616	-4.807455	-1.078923
H	0.640785	-4.027050	-2.439865
H	-0.699330	-4.927372	0.175501
H	-0.895346	-5.683353	-1.407669
H	-1.970240	-3.631489	-2.304489
H	-2.828811	-4.158122	-0.855648
H	-1.642783	-2.466726	0.524363
H	-2.462499	-1.695641	-0.838787
H	-2.284643	0.481960	-0.284647
H	-1.120440	2.452375	0.721648
H	-0.547584	2.933433	-0.880857
H	-2.599337	4.204971	-0.299985
H	-3.488065	2.702332	-0.025801
H	-2.317254	3.655099	-2.703009
H	-4.030001	3.585634	-2.284315
H	-3.936490	1.109976	-2.113501
H	-3.329647	1.614151	-3.692114
H	-0.982388	1.360787	-2.922653
H	-1.878130	-0.144075	-2.684516
H	2.302962	-0.351061	-0.525999
H	1.565979	2.621307	-0.462818
H	2.077124	1.653275	0.926433
H	4.274367	1.207371	-0.151665
H	3.990447	2.947624	-0.058904
H	3.291607	3.006304	-2.442395
H	4.888022	2.265683	-2.314776
H	3.376299	0.971097	-3.863787

H	3.898965	-0.006511	-2.490278
H	1.468310	-0.321000	-2.901976
H	1.193637	1.421706	-2.772140

9'PCy3.xyz (66)			
Au	-0.020765	-0.077100	2.078124
N	0.661079	-0.962422	4.878659
C	-0.028257	-0.065638	4.166233
H	0.633606	-0.913292	5.898557
N	-0.717611	0.844515	4.861858
C	1.485477	-2.034730	4.331527
C	-1.535655	1.911846	4.295850
H	-1.492200	1.837757	3.204103
H	-2.578597	1.810788	4.621608
P	-0.010033	-0.060525	-0.259799
C	-0.272676	-1.766724	-0.974249
C	0.866987	-2.732548	-0.581705
C	0.627422	-4.144962	-1.140763
C	-0.734194	-4.703667	-0.709766
C	-1.868212	-3.750966	-1.107416
C	-1.644604	-2.336269	-0.548180
C	-1.447179	0.973173	-0.871173
C	-1.382231	2.438754	-0.389409
C	-2.701845	3.167738	-0.692236
C	-3.054355	3.092003	-2.184548
C	-3.083588	1.639543	-2.679904
C	-1.763916	0.905498	-2.379359
C	1.666745	0.505543	-0.864609
C	2.164639	1.791670	-0.167407
C	3.635493	2.064064	-0.523885
C	3.845162	2.135660	-2.043025
C	3.325849	0.870521	-2.739905
C	1.851614	0.594738	-2.392696
H	-0.265308	-1.645100	-2.071625
H	0.927724	-2.781701	0.520118
H	1.837031	-2.357192	-0.937671
H	1.440654	-4.809255	-0.814303
H	0.676023	-4.109554	-2.241940

H	-0.742125	-4.843318	0.384902
H	-0.896474	-5.696287	-1.152921
H	-1.933140	-3.699278	-2.207169
H	-2.837056	-4.133253	-0.755147
H	-1.688486	-2.367257	0.555068
H	-2.459670	-1.676612	-0.878384
H	-2.288211	0.494871	-0.332572
H	-1.156089	2.479631	0.688117
H	-0.558895	2.957990	-0.905653
H	-2.628928	4.215929	-0.367485
H	-3.512281	2.709187	-0.100213
H	-2.304852	3.658336	-2.762742
H	-4.023317	3.576481	-2.370948
H	-3.913271	1.102321	-2.189756
H	-3.284727	1.605766	-3.760177
H	-0.948121	1.376146	-2.950110
H	-1.832989	-0.137010	-2.722589
H	2.306074	-0.320047	-0.496099
H	1.551220	2.649006	-0.486699
H	2.043889	1.702552	0.924276
H	4.262939	1.259003	-0.104937
H	3.964099	2.998209	-0.045712
H	3.311781	3.015030	-2.442087
H	4.909611	2.285915	-2.272771
H	3.436332	0.958392	-3.830203
H	3.936663	0.005179	-2.431321
H	1.515636	-0.329122	-2.886728
H	1.230049	1.414230	-2.788113
H	-0.687309	0.816499	5.882450
H	-1.154569	2.893387	4.605124
H	2.530971	-1.913247	4.642178
H	1.428230	-1.990000	3.238761
H	1.119159	-3.011475	4.671740

(C₂H₂)PCy₃.xyz (57)			
P	0.0000	0.0000	2.3251
Au	0.0000	0.0000	0.0000
C	1.6923	-1.0350	4.4324

C	1.5863	-0.7937	2.9110
C	2.8583	-0.1080	2.3658
C	4.1030	-0.9507	2.6919
C	4.2199	-1.2239	4.1978
C	2.9439	-1.8739	4.7494
C	-0.2953	1.7552	2.8941
C	0.6829	2.7807	2.2797
C	0.2347	4.2141	2.6113
C	0.0870	4.4224	4.1250
C	-0.8598	3.3846	4.7426
C	-0.4164	1.9455	4.4211
C	-1.4025	-1.0319	2.9882
C	-1.2623	-2.5089	2.5567
C	-2.4274	-3.3617	3.0862
C	-3.7866	-2.7916	2.6630
C	-3.9289	-1.3293	3.1022
C	-2.7760	-0.4598	2.5723
H	-1.3140	-0.9749	4.0878
H	-1.2483	-2.5567	1.4527
H	-0.3087	-2.9293	2.9066
H	-2.3111	-4.3951	2.7297
H	-2.3733	-3.4024	4.1868
H	-3.8854	-2.8556	1.5660
H	-4.6006	-3.3966	3.0859
H	-3.9442	-1.2769	4.2035
H	-4.8851	-0.9114	2.7564
H	-2.8268	-0.4187	1.4696
H	-2.8961	0.5704	2.9364
H	-1.2901	1.9515	2.4502
H	0.7499	2.6419	1.1882
H	1.6941	2.6160	2.6829
H	0.9564	4.9298	2.1926
H	-0.7309	4.4146	2.1171
H	1.0783	4.3405	4.6019
H	-0.2763	5.4383	4.3338
H	-1.8809	3.5422	4.3564
H	-0.9147	3.5129	5.8329
H	0.5604	1.7540	4.8929

H	-1.1293	1.2285	4.8545
H	1.5159	-1.7835	2.4196
H	2.9666	0.8863	2.8273
H	4.0437	-1.9083	2.1474
H	5.0011	-0.4354	2.3226
H	4.4022	-0.2734	4.7268
H	5.0893	-1.8649	4.4003
H	3.0214	-2.0145	5.8368
H	2.8243	-2.8791	4.3111
H	0.7954	-1.5427	4.8169
H	1.7627	-0.0674	4.9541
H	2.7760	0.0505	1.2786
C	0.1601	-0.5956	-2.1702
C	-0.1149	0.6016	-2.1682
H	0.3936	-1.6222	-2.3910
H	-0.3464	1.6293	-2.3848

9PAr ^F .xyz (82)			
Au	0.117369	0.008459	-0.037710
C	0.204170	0.157501	-2.121046
N	0.907081	-0.679733	-2.893534
H	0.876040	-0.527956	-3.900651
N	-0.477470	1.124278	-2.740328
C	1.775570	-1.834664	-2.498954
C	0.936899	-2.904088	-1.786990
H	0.504407	-2.502716	-0.857917
H	0.116251	-3.254030	-2.426980
H	1.568011	-3.763578	-1.525485
C	2.328211	-2.395404	-3.816776
H	2.926528	-1.641731	-4.348915
H	2.978501	-3.254772	-3.613538
H	1.516265	-2.738376	-4.474295
C	2.930414	-1.349679	-1.612902
H	3.524544	-0.581415	-2.125267
H	2.551513	-0.926199	-0.670442
H	3.589455	-2.191862	-1.364123
C	-1.295070	2.153558	-2.055674
H	-0.798077	2.470247	-1.131913

H	-2.280739	1.732650	-1.805102
C	-1.420340	3.261461	-3.103086
H	-0.526346	3.900322	-3.084729
H	-2.296512	3.895580	-2.930925
C	-1.494351	2.475800	-4.421663
H	-2.505036	2.071278	-4.568105
H	-1.243024	3.078164	-5.301270
C	-0.497715	1.327844	-4.211329
H	0.514755	1.597883	-4.554604
H	-0.806964	0.404168	-4.724032
P	-0.033114	-0.065594	2.284418
C	0.014804	2.119625	4.096393
C	-0.588623	1.538660	2.977069
C	-1.639244	2.205928	2.327024
C	-2.075846	3.441336	2.799515
C	-1.472731	4.028024	3.917180
C	-0.431168	3.361968	4.559536
C	-3.226788	4.146983	2.116442
F	-3.335276	3.775220	0.808710
C	0.269574	3.994424	5.744412
F	1.463927	4.527485	5.374196
C	-1.227580	-1.310254	2.902319
C	-2.046543	-1.062724	4.009615
C	-2.949264	-2.040452	4.437850
C	-3.041629	-3.262078	3.772665
C	-2.220216	-3.505896	2.667646
C	-1.319394	-2.537917	2.228302
C	-2.297930	-4.844242	1.964614
F	-1.843643	-4.765339	0.684668
C	-3.865109	-1.736413	5.605666
F	-3.225771	-1.011834	6.559100
C	1.561059	-0.443228	3.104430
C	2.735555	0.092354	2.549036
C	3.967542	-0.183767	3.134989
C	4.048052	-0.995624	4.272708
C	2.881873	-1.524436	4.819523
C	1.636860	-1.253454	4.240938
C	5.244108	0.387134	2.555745

F	5.029717	1.002544	1.363466
C	2.939410	-2.434633	6.029187
F	4.141080	-2.385375	6.645459
F	-4.410735	3.856485	2.709665
F	-3.078819	5.491803	2.143675
F	-0.464366	4.985577	6.297649
F	0.525963	3.077055	6.711477
F	1.990710	-2.098736	6.940881
F	2.711543	-3.727216	5.676535
F	5.800084	1.300069	3.389278
F	6.168939	-0.584421	2.350968
F	-4.939626	-1.007593	5.204072
F	-4.333535	-2.863631	6.186893
F	-1.543264	-5.777776	2.598549
F	-3.566480	-5.313301	1.920075
H	-2.111544	1.766217	1.448605
H	-1.808445	4.998772	4.278195
H	0.833872	1.618444	4.611774
H	2.690435	0.717870	1.657779
H	5.014102	-1.216786	4.724505
H	0.737248	-1.682824	4.681529
H	-0.697900	-2.737429	1.355901
H	-3.752055	-4.016546	4.107260
H	-1.993653	-0.113387	4.541952

9 ^F Par ^F .xyz (66)			
C	0.028420	0.065186	-0.019912
C	0.043850	0.023700	1.383504
C	1.247913	-0.194028	2.059588
C	2.429312	-0.369077	1.331471
C	2.418616	-0.332462	-0.061520
C	1.211357	-0.112694	-0.733150
P	-1.554999	0.200037	2.258689
Au	-3.226041	-1.119743	1.328249
C	-4.730205	-2.313253	0.522778
N	-5.823079	-2.617347	1.226399
C	-6.119605	-2.192770	2.592072
C	3.714748	-0.650850	2.082363

F	4.806746	-0.438188	1.315488
C	1.192065	-0.047332	-2.245521
F	1.408873	1.214534	-2.690857
C	-1.250858	-0.252111	4.006296
C	-1.026005	0.706202	4.999546
C	-0.846000	0.300072	6.325612
C	-0.889611	-1.050257	6.668093
C	-1.114397	-2.005117	5.671117
C	-1.296789	-1.614033	4.346848
C	-1.142008	-3.474627	6.035280
F	0.108250	-3.999229	6.065673
C	-0.657637	1.356011	7.395871
F	0.149802	2.357188	6.962594
C	-1.962995	1.982469	2.223579
C	-0.972958	2.966723	2.120396
C	-1.339392	4.314641	2.078665
C	-2.681973	4.688945	2.134421
C	-3.667017	3.702597	2.236135
C	-3.314684	2.355248	2.279810
C	-0.261206	5.366998	1.915989
F	0.099992	5.494493	0.612763
C	-5.124003	4.105740	2.321390
F	-5.475462	4.414361	3.595536
F	-0.672919	6.580779	2.345100
F	0.857486	5.037144	2.610547
F	-5.389688	5.187669	1.554900
F	-5.945335	3.100095	1.913270
F	-1.696101	-3.676551	7.253472
F	-1.858884	-4.198396	5.133057
F	-1.846941	1.920355	7.734071
F	-0.115192	0.843324	8.522378
N	-4.643716	-2.802310	-0.715868
C	-3.542051	-2.595646	-1.652187
F	2.138740	-0.841302	-2.794784
F	-0.014212	-0.443284	-2.743427
F	3.821223	0.132987	3.185555
F	3.755924	-1.941908	2.505235
H	-6.540904	-3.198889	0.791020

H	-0.905567	0.226998	-0.558523
H	3.340434	-0.481358	-0.621283
H	1.277533	-0.234219	3.148275
H	-1.487369	-2.369091	3.583718
H	-0.759543	-1.357355	7.704641
H	-0.998138	1.767926	4.755823
H	-4.093861	1.595499	2.339886
H	-2.959525	5.741065	2.089994
H	0.081051	2.695346	2.064240
H	-6.274912	-3.067297	3.235383
H	-5.270211	-1.616608	2.974009
H	-7.018773	-1.564536	2.612196
H	-5.409484	-3.376799	-1.071732
H	-3.134306	-3.561022	-1.975221
H	-3.883634	-2.034529	-2.530841
H	-2.753313	-2.028474	-1.147153

(C₂H₂)PAr^F.xyz (57)			
P	0.0000	0.0000	-2.3131
Au	0.0000	0.0000	0.0000
C	0.0522	-0.6125	2.1577
C	-0.0031	0.6157	2.1556
H	-0.0485	1.6706	2.3694
H	0.1027	-1.6661	2.3757
C	-1.7928	-1.0604	-4.2061
C	-1.6492	-0.3642	-2.9999
C	-2.7855	0.0539	-2.2894
C	-4.0551	-0.2240	-2.7901
C	-4.2052	-0.9200	-3.9937
C	-3.0730	-1.3325	-4.6957
C	-5.2836	0.2479	-2.0385
F	-5.0191	0.4251	-0.7167
C	-3.2133	-2.1302	-5.9779
F	-3.0338	-3.4556	-5.7434
C	0.5298	1.6348	-2.9299
C	-0.1754	2.2989	-3.9388
C	0.2432	3.5678	-4.3504
C	1.3516	4.1762	-3.7635

C	2.0526	3.5059	-2.7552
C	1.6485	2.2414	-2.3347
C	3.2731	4.1517	-2.1304
F	3.4798	3.6968	-0.8653
C	-0.5606	4.2970	-5.4096
F	-0.9795	3.4459	-6.3793
C	1.1573	-1.2496	-2.9689
C	1.1399	-2.5329	-2.3957
C	2.0248	-3.5040	-2.8520
C	2.9328	-3.2118	-3.8774
C	2.9424	-1.9397	-4.4436
C	2.0586	-0.9517	-3.9945
C	2.0123	-4.8951	-2.2513
F	1.3056	-4.9324	-1.0902
C	3.9388	-1.5830	-5.5295
F	4.5213	-2.6781	-6.0617
F	-5.7254	1.4353	-2.5224
F	-6.2996	-0.6374	-2.1405
F	-4.4324	-1.9739	-6.5369
F	-2.2825	-1.7550	-6.8913
F	3.3381	-0.8975	-6.5353
F	4.9241	-0.7882	-5.0371
F	1.4489	-5.7899	-3.0976
F	3.2668	-5.3252	-1.9811
F	-1.6692	4.8641	-4.8670
F	0.1556	5.2791	-5.9977
F	4.3920	3.8757	-2.8441
F	3.1485	5.4961	-2.0690
H	-2.6852	0.5831	-1.3416
H	-5.1992	-1.1467	-4.3766
H	-0.9206	-1.3991	-4.7652
H	0.4433	-2.7769	-1.5936
H	3.6316	-3.9711	-4.2260
H	2.0858	0.0397	-4.4466
H	2.1999	1.7381	-1.5400
H	1.6645	5.1693	-4.0825
H	-1.0489	1.8439	-4.4050

9CN ^t Bu.xyz (45)			
C	-0.006215	-0.007552	4.452058
N	0.632489	-0.929466	5.183539
H	0.547463	-0.870595	6.196841
N	-0.701266	0.921504	5.113717
C	1.483674	-2.074866	4.725489
C	0.654066	-3.045707	3.873013
H	0.291770	-2.558232	2.955565
H	-0.214259	-3.418209	4.432829
H	1.272762	-3.903800	3.578135
C	1.943971	-2.774687	6.011907
H	2.533875	-2.095538	6.644404
H	2.578062	-3.634093	5.762726
H	1.086155	-3.148509	6.589691
C	2.703828	-1.556040	3.951472
H	3.296337	-0.866048	4.567036
H	2.399307	-1.028987	3.034961
H	3.343692	-2.399299	3.658996
C	-1.458098	2.021114	4.468442
H	-0.898970	2.404762	3.607747
H	-2.430008	1.642209	4.117310
C	-1.635615	3.037919	5.597557
H	-0.734854	3.660919	5.689203
H	-2.491898	3.699342	5.427037
C	-1.801136	2.145260	6.837724
H	-2.824143	1.747962	6.886346
H	-1.597863	2.666226	7.779514
C	-0.808594	1.000541	6.590654
H	0.183914	1.221344	7.017525
H	-1.161626	0.043490	7.004542
Au	0.037561	0.021178	2.390039
C	0.063860	0.072598	0.407533
N	0.088848	0.099927	-0.755700
C	0.125912	0.131035	-2.209821
C	-0.595749	-1.130104	-2.715646
H	-0.093106	-2.039473	-2.363255
H	-0.579797	-1.126520	-3.813076
H	-1.641012	-1.146295	-2.382581

C	-0.595358	1.411886	-2.662962
H	-0.094251	2.305755	-2.270911
H	-1.641569	1.412746	-2.332528
H	-0.576441	1.454918	-3.759495
C	1.605323	0.139543	-2.631809
H	2.120632	-0.762784	-2.279619
H	2.122201	1.024120	-2.239208
H	1.656293	0.164125	-3.727880

9'CN ^t Bu.xyz (29)			
H	3.77262	-0.01710	-1.08790
N	2.75298	-0.01793	-1.14055
C	2.20326	-0.03921	-2.49382
C	2.05353	-0.00007	-0.00463
N	2.73954	0.01794	1.14096
C	2.13972	0.03896	2.47791
H	3.75844	0.01748	1.11175
H	2.94806	0.05054	3.21487
H	1.52721	-0.85466	2.64590
H	1.52721	0.93742	2.61772
H	1.11018	-0.03821	-2.43039
H	2.53098	-0.94224	-3.02347
H	2.53098	0.84673	-3.05159
Au	0.00000	0.00000	0.00000
C	-1.98121	0.00008	0.00492
N	-3.14392	-0.00000	0.00000
C	-4.59824	-0.00014	-0.00915
C	-5.06187	1.28290	0.70180
H	-4.70780	-1.25305	1.78023
H	-6.15917	-1.27878	0.74826
H	-4.70122	-2.16997	0.24575
H	-4.68557	0.86233	-2.01715
H	-4.68557	-0.92532	-1.98905
H	-6.14488	-0.02374	-1.51019
H	-4.70780	1.30839	1.73996
H	-4.70122	2.17662	0.17741
C	-5.06187	-1.26020	0.74178

C	-5.04783	-0.02327	-1.48022
H	-6.15917	1.30167	0.70769

(C₂H₂)CN^tBu.xyz (20)			
Au	0.0000	0.0000	0.0000
C	0.2383	-0.5679	2.1066
C	-0.2377	0.5687	2.1064
C	0.0000	0.0000	-1.9719
C	0.0012	-0.0006	-4.5911
C	-0.7359	-1.2725	-5.0458
C	1.4709	0.0009	-5.0465
C	-0.7350	1.2742	-5.0419
H	-0.6443	1.5388	2.3426
H	0.6450	-1.5378	2.3431
H	-0.2241	-2.1754	-4.6901
H	-0.7466	-1.2886	-6.1430
H	-1.7726	-1.2794	-4.6873
H	1.9966	-0.8938	-4.6906
H	1.9958	0.8951	-4.6883
H	1.4902	0.0020	-6.1437
H	-0.2222	2.1755	-4.6840
H	-1.7719	1.2807	-4.6837
H	-0.7454	1.2921	-6.1391
N	0.0002	0.0000	-3.1322

9Py.xyz (41)			
C	0.001803	-0.009121	2.010460
Au	0.005321	-0.003637	-0.009468
N	1.092198	-0.282762	2.740828
H	0.991161	-0.266425	3.754335
N	-1.127823	0.258757	2.673686
C	2.485632	-0.604118	2.291369
C	2.495905	-1.896877	1.461922
H	1.910233	-1.778351	0.538671
H	2.077137	-2.735363	2.034492
H	3.527095	-2.148610	1.179664
C	3.287986	-0.811761	3.584720
H	3.290116	0.098409	4.202234

H	4.330145	-1.052800	3.342477
H	2.880690	-1.644847	4.176134
C	3.076388	0.570776	1.497590
H	3.074041	1.491353	2.096576
H	2.503830	0.752652	0.576526
H	4.112607	0.343023	1.213477
C	-2.420117	0.593603	2.029040
H	-2.247999	1.241602	1.162825
H	-2.909838	-0.330009	1.684556
C	-3.217331	1.258174	3.153783
H	-2.948681	2.321305	3.229895
H	-4.298196	1.191412	2.987870
C	-2.751469	0.494229	4.403563
H	-3.266565	-0.473747	4.472592
H	-2.931676	1.037777	5.337446
C	-1.252926	0.271803	4.151680
H	-0.643862	1.093955	4.563342
H	-0.894025	-0.677681	4.578182
N	-0.014738	0.004556	-2.099776
C	-0.016173	0.005992	-4.889212
C	-0.341323	-1.113145	-2.789664
C	0.310159	1.123230	-2.788826
C	0.319407	1.158950	-4.178046
C	-0.352109	-1.147366	-4.178937
H	-0.595649	-1.988091	-2.196162
H	0.565494	1.997515	-2.194758
H	0.587925	2.081980	-4.687684
H	-0.620998	-2.069948	-4.689243
H	-0.015931	0.006299	-5.978438

9'Py.xyz (25)			
H	0.00000	1.08519	3.73523
N	0.00000	1.13935	2.71630
C	0.00000	2.49317	2.17032
C	0.00000	0.00000	2.01605
N	0.00000	-1.13935	2.71630
C	0.00000	-2.49317	2.17032
H	0.00000	-1.08519	3.73523

H	0.00000	2.42920	1.07790
H	-0.89451	3.03681	2.49811
H	0.89451	3.03681	2.49811
H	0.89451	-3.03681	2.49811
H	-0.89451	-3.03681	2.49811
H	0.00000	-2.42920	1.07790
Au	0.00000	0.00000	-0.00000
N	0.00000	0.00000	-2.08511
C	0.00000	0.00000	-4.87313
C	0.00000	-1.16499	-2.77491
C	0.00000	1.16499	-2.77491
C	0.00000	1.20094	-4.16317
C	0.00000	-1.20094	-4.16317
H	0.00000	-2.07658	-2.18252
H	0.00000	2.07658	-2.18252
H	0.00000	2.16207	-4.67358
H	0.00000	-2.16207	-4.67358
H	0.00000	0.00000	-5.96254

(C₂H₂)py.xyz (16)			
N	0.0000	0.0000	-2.0628
Au	0.0000	0.0000	0.0000
C	0.0012	-0.6185	2.0686
C	-0.0013	0.6178	2.0689
H	-0.0044	1.6615	2.3383
H	0.0041	-1.6622	2.3378
C	-0.0023	-0.0004	-4.8460
C	-0.0002	1.1696	-2.7490
C	-0.0008	-1.1698	-2.7487
C	-0.0020	-1.2014	-4.1361
C	-0.0014	1.2008	-4.1364
H	0.0004	2.0839	-2.1606
H	-0.0008	-2.0839	-2.1599
H	-0.0029	-2.1632	-4.6463
H	-0.0018	2.1623	-4.6470
H	-0.0034	-0.0006	-5.9357

9NHC.xyz (95)			
----------------------	--	--	--

C	0.050040	-0.009643	2.014521
Au	0.050529	-0.013893	-0.033782
N	1.089518	0.019947	2.899757
C	0.626851	0.013326	4.207486
C	-0.730544	-0.023428	4.145231
N	-1.067485	-0.034655	2.800649
H	-1.479890	-0.042254	4.925115
H	1.300979	0.035769	5.053096
H	1.722426	4.341876	1.232111
H	1.305490	2.405241	2.724264
H	1.772905	2.815108	0.318260
C	2.275906	3.402076	1.098319
H	3.282477	3.657068	0.738067
C	2.954030	3.503407	3.538371
H	2.984707	2.974439	4.500591
H	2.363398	4.420730	3.670231
H	3.981638	3.801751	3.287874
C	2.338383	2.629681	2.427486
H	1.539736	-2.330440	3.147578
H	2.771818	-3.985344	4.494784
C	2.599587	-2.494773	2.912533
C	3.268850	-3.056342	4.182790
H	4.328441	-3.287461	4.005033
H	3.219484	-2.344263	5.017946
C	2.658199	-3.521468	1.767735
H	2.081708	-3.184442	0.897272
H	2.245623	-4.483646	2.101784
H	3.692099	-3.699416	1.440893
C	3.213686	-1.153886	2.523111
C	2.495379	0.058035	2.546562
C	4.567623	-1.085781	2.168731
H	5.157007	-2.002118	2.139552
C	5.175430	0.130460	1.869338
H	6.230474	0.158577	1.599604
C	4.445222	1.313448	1.940052
H	4.939050	2.262625	1.732532
C	3.088775	1.309906	2.290870
H	-1.472472	2.327710	2.899907

H	-1.921060	4.390822	1.601129
C	-2.386237	3.437071	1.315937
H	-3.377623	3.662359	0.898237
C	-2.493605	2.510111	2.540391
H	-3.330366	2.558657	4.572261
C	-3.266803	3.198384	3.681614
H	-2.767968	4.134736	3.967408
H	-4.292573	3.447104	3.375590
C	-3.115891	1.166550	2.178156
H	-4.996945	2.041138	1.594448
C	-4.433753	1.114485	1.704934
C	-5.038120	-0.098480	1.385087
H	-6.066037	-0.115167	1.024866
C	-4.337753	-1.291539	1.541151
H	-4.825850	-2.236409	1.302533
C	-3.018288	-1.303267	2.012994
C	-2.430740	-0.057597	2.307882
H	-1.302612	-2.417785	2.626713
C	-2.287986	-2.628462	2.190865
H	-3.188530	-3.084382	4.142605
C	-3.031177	-3.561016	3.165654
H	-4.015096	-3.851474	2.772024
H	-2.452353	-4.481685	3.322857
C	-2.049916	-3.322997	0.837381
H	-1.492746	-4.258954	0.982109
H	-3.001883	-3.572258	0.347144
H	-1.472704	-2.678734	0.158668
H	-1.774577	2.983383	0.524097
C	-0.098932	-0.008281	-2.099151
N	0.918398	-0.228289	-2.945812
H	0.716427	-0.206245	-3.943721
N	-1.291570	0.217990	-2.666601
C	2.356088	-0.503009	-2.644747
C	2.485877	-1.788007	-1.817722
H	1.968513	-1.676753	-0.853940
H	2.053912	-2.645586	-2.351569
H	3.544582	-1.997666	-1.614386
C	3.030300	-0.689016	-4.011207

H	2.942106	0.219894	-4.624434
H	4.098461	-0.897593	-3.874916
H	2.590334	-1.534588	-4.559946
C	2.981350	0.689963	-1.910747
H	2.886235	1.608711	-2.505632
H	2.493427	0.847481	-0.938733
H	4.047556	0.499760	-1.728077
C	-2.538749	0.486143	-1.914946
H	-2.323749	1.112111	-1.042623
H	-2.970341	-0.462319	-1.560259
C	-3.442604	1.149916	-2.954501
H	-3.206599	2.220830	-3.032991
H	-4.504493	1.052244	-2.703249
C	-3.061157	0.419879	-4.251648
H	-3.550163	-0.563242	-4.290188
H	-3.336340	0.967483	-5.159780
C	-1.541511	0.241311	-4.127099
H	-0.994750	1.085253	-4.580882
H	-1.191923	-0.691156	-4.597542

9'NHC.xyz (79)			
Au	0.00000000	0.00000000	0.00000000
C	-2.03855997	-0.00129832	0.00000000
N	-2.87068798	-0.00155468	-1.08143000
C	-4.19817470	-0.00214826	-0.67984000
H	-5.01154170	-0.00262649	-1.39274000
H	-1.39284059	-4.39177954	-1.91969000
H	-2.70523571	-2.38574829	-1.36246000
H	-0.36713909	-2.93971676	-2.06516000
C	-1.23681011	-3.46268759	-2.48538000
H	-0.99352681	-3.74180243	-3.51989000
C	-3.71427490	-3.32831117	-3.00334000
H	-4.63184748	-2.72918194	-2.92786000
H	-3.87645358	-4.27199698	-2.46395000
H	-3.55976143	-3.57023704	-4.06432000
C	-2.49763012	-2.58206569	-2.42268000
H	-2.69933902	2.38108349	-1.37199000
H	-3.85001374	4.27350759	-2.48301000

C	-2.48473453	2.57311663	-2.43159000
C	-3.69222092	3.32784928	-3.02022000
H	-3.53003375	3.56727325	-4.08062000
H	-4.61474830	2.73596666	-2.94897000
C	-1.21624173	3.44303282	-2.49024000
H	-0.35366029	2.91439583	-2.06253000
H	-1.36789836	4.37583355	-1.92947000
H	-0.96435639	3.71541699	-3.52451000
C	-2.27677867	1.23183233	-3.12338000
C	-2.45117706	-0.00460433	-2.47165000
C	-1.90833763	1.19653922	-4.47470000
H	-1.76621186	2.13356789	-5.01289000
C	-1.72830946	-0.01112238	-5.14271000
H	-1.44657758	-0.01361815	-6.19479000
C	-1.91424817	-1.21556183	-4.47051000
H	-1.77685005	-2.15512823	-5.00545000
C	-2.28261788	-1.24424345	-3.11903000
C	-2.28261788	-1.24424345	3.11903000
C	-1.91424817	-1.21556183	4.47051000
C	-1.72830946	-0.01112238	5.14271000
C	-1.90833763	1.19653922	4.47470000
C	-2.45117706	-0.00460433	2.47165000
C	-2.27677867	1.23183233	3.12338000
C	-1.21624173	3.44303282	2.49024000
C	-3.69222092	3.32784928	3.02022000
C	-2.48473453	2.57311663	2.43159000
C	-2.49763012	-2.58206569	2.42268000
C	-3.71427490	-3.32831117	3.00334000
C	-1.23681011	-3.46268759	2.48538000
C	-4.19817470	-0.00214826	0.67984000
N	-2.87068798	-0.00155468	1.08143000
H	-1.77685005	-2.15512823	5.00545000
H	-1.44657758	-0.01361815	6.19479000
H	-1.76621186	2.13356789	5.01289000
H	-0.96435639	3.71541699	3.52451000
H	-1.36789836	4.37583355	1.92947000
H	-0.35366029	2.91439583	2.06253000
H	-4.61474830	2.73596666	2.94897000

H	-3.53003375	3.56727325	4.08062000
H	-3.85001374	4.27350759	2.48301000
H	-2.69933902	2.38108349	1.37199000
H	-3.55976143	-3.57023704	4.06432000
H	-3.87645358	-4.27199698	2.46395000
H	-4.63184748	-2.72918194	2.92786000
H	-0.99352681	-3.74180243	3.51989000
H	-0.36713909	-2.93971676	2.06516000
H	-2.70523571	-2.38574829	1.36246000
H	-1.39284059	-4.39177954	1.91969000
H	-5.01154170	-0.00262649	1.39274000
H	1.13142702	2.41396970	0.00000000
H	3.78967414	-1.08090978	0.00000000
N	2.77025992	-1.13512614	0.00000000
N	2.77152287	1.13433706	0.00000000
C	2.22397118	2.48537888	0.00000000
H	3.79086203	1.07892594	0.00000000
H	1.12848202	-2.41252747	0.00000000
H	2.54484150	-3.03268983	-0.89450000
C	2.06087587	-0.00000000	0.00000000
C	2.22096083	-2.48549672	0.00000000
H	2.54861179	3.03216409	-0.89457000
H	2.54861179	3.03216409	0.89457000
H	2.54484150	-3.03268983	0.89450000

(C₂H₂)NHC.xyz (70)

Au	0.0000	0.0000	0.0000
C	0.0046	-0.6162	-2.1050
C	-0.0046	0.6172	-2.1047
H	-0.0122	1.6611	-2.3653
H	0.0121	-1.6599	-2.3661
C	0.0000	0.0000	2.0197
N	1.0847	0.0356	2.8439
C	0.6823	0.0249	4.1660
C	-0.6808	-0.0194	4.1664
N	-1.0840	-0.0342	2.8446
H	-1.3920	-0.0417	4.9814
H	1.3940	0.0492	4.9804

H	1.6967	4.4061	1.3191
H	1.3116	2.4322	2.7553
H	1.7752	2.9135	0.3482
C	2.2654	3.4812	1.1516
H	3.2669	3.7641	0.7991
C	2.9856	3.4816	3.5832
H	3.0218	2.9178	4.5252
H	2.4115	4.4023	3.7566
H	4.0141	3.7728	3.3285
C	2.3425	2.6582	2.4510
H	1.4633	-2.3419	2.7434
H	2.6868	-4.2411	3.7401
C	2.5072	-2.5003	2.4404
C	3.2000	-3.2843	3.5714
H	4.2458	-3.5067	3.3182
H	3.1973	-2.7227	4.5154
C	2.4854	-3.3223	1.1383
H	1.9622	-2.7842	0.3353
H	1.9761	-4.2820	1.3016
H	3.5036	-3.5403	0.7875
C	3.1549	-1.1378	2.2263
C	2.4728	0.0806	2.4112
C	4.4964	-1.0608	1.8295
H	5.0598	-1.9810	1.6760
C	5.1226	0.1668	1.6342
H	6.1675	0.2007	1.3287
C	4.4195	1.3511	1.8343
H	4.9228	2.3059	1.6841
C	3.0758	1.3407	2.2313
H	-1.4656	2.3424	2.7488
H	-1.9812	4.2854	1.3122
C	-2.4891	3.3254	1.1464
H	-3.5076	3.5429	0.7962
C	-2.5097	2.5002	2.4463
H	-3.2002	2.7163	4.5219
C	-3.2033	3.2804	3.5795
H	-2.6912	4.2372	3.7508
H	-4.2494	3.5025	3.3267

C	-3.1557	1.1374	2.2293
H	-5.0612	1.9791	1.6785
C	-4.4970	1.0593	1.8314
C	-5.1216	-0.1687	1.6341
H	-6.1661	-0.2035	1.3275
C	-4.4172	-1.3524	1.8335
H	-4.9194	-2.3077	1.6820
C	-3.0738	-1.3410	2.2312
C	-2.4723	-0.0804	2.4128
H	-1.3098	-2.4309	2.7594
C	-2.3389	-2.6578	2.4496
H	-3.0274	-2.9267	4.5195
C	-2.9851	-3.4871	3.5758
H	-4.0114	-3.7806	3.3152
H	-2.4091	-4.4067	3.7486
C	-2.2546	-3.4755	1.1473
H	-1.6856	-4.4005	1.3137
H	-3.2541	-3.7579	0.7890
H	-1.7612	-2.9039	0.3486
H	-1.9652	2.7903	0.3419

9Ph.xyz (41)			
C	0.011413	-0.022446	2.049766
Au	0.006703	-0.010753	-0.033596
N	1.089591	-0.290915	2.808674
H	0.992406	-0.274970	3.823118
N	-1.116753	0.247279	2.727651
C	2.474950	-0.606839	2.351196
C	2.481213	-1.896316	1.515509
H	1.871238	-1.767639	0.609599
H	2.077151	-2.738717	2.094678
H	3.508788	-2.140356	1.210791
C	3.294608	-0.813687	3.633867
H	3.300738	0.096376	4.252887
H	4.334619	-1.052353	3.378256
H	2.894961	-1.647526	4.230852
C	3.054393	0.566766	1.546210
H	3.061821	1.486718	2.147931

H	2.454899	0.742773	0.641326
H	4.085457	0.338933	1.240759
C	-2.400830	0.569314	2.069288
H	-2.215251	1.172557	1.174325
H	-2.903811	-0.358950	1.755190
C	-3.192859	1.282864	3.166900
H	-2.902168	2.342587	3.213912
H	-4.275210	1.233455	2.999528
C	-2.745942	0.547946	4.441843
H	-3.282675	-0.407022	4.533278
H	-2.919849	1.119638	5.361233
C	-1.251163	0.284330	4.200167
H	-0.625400	1.095331	4.611964
H	-0.920103	-0.665932	4.649749
C	-0.018137	0.008420	-2.078466
C	-0.028740	0.028187	-4.929676
C	-0.295084	-1.154459	-2.829050
C	0.252906	1.181674	-2.814944
C	0.248713	1.196402	-4.214354
C	-0.301556	-1.149684	-4.228522
H	-0.511583	-2.091372	-2.312363
H	0.474798	2.110972	-2.286877
H	0.464038	2.123807	-4.748350
H	-0.519691	-2.069914	-4.773689
H	-0.031838	0.035519	-6.020376

9 ⁺ Ph.xyz (25)			
C	1.20454	0.00000	-4.18670
C	0.00000	0.00000	-4.89417
C	-1.20454	0.00000	-4.18670
C	-1.19961	0.00000	-2.78807
C	0.00000	0.00000	-2.04501
C	1.19961	0.00000	-2.78807
Au	0.00000	0.00000	0.00000
C	0.00000	0.00000	2.06430
N	0.00000	-1.13431	2.77921
C	0.00000	-2.47239	2.18811

N	0.00000	1.13431	2.77921
C	0.00000	2.47239	2.18811
H	0.00000	1.09491	3.79922
H	2.15836	0.00000	-2.26580
H	-2.15836	0.00000	-2.26580
H	-2.15338	0.00000	-4.72616
H	2.15338	0.00000	-4.72616
H	0.00000	0.00000	-5.98478
H	0.00000	-1.09491	3.79922
H	0.00000	3.20739	3.00042
H	0.89004	2.62525	1.56652
H	-0.89004	2.62525	1.56652
H	0.00000	-3.20739	3.00042
H	-0.89004	-2.62525	1.56652
H	0.89004	-2.62525	1.56652

(C ₂ H ₂)Ph.xyz (25)			
Au	1.847316	8.174332	6.189522
C	1.246691	9.045842	8.149691
C	1.243131	9.979232	7.347176
H	1.171425	10.924141	6.841410
H	1.181958	8.404028	9.008544
C	2.418837	6.904633	4.711164
C	3.216451	5.133178	2.648643
C	2.624700	7.362055	3.395447
C	2.623688	5.534724	4.964504
C	3.017357	4.660031	3.947247
C	3.018302	6.488488	2.377173
H	2.477718	8.415036	3.153271
H	2.475867	5.136263	5.968691
H	3.168679	3.603617	4.172707
H	3.170200	6.871016	1.367054
H	3.523246	4.451588	1.855009

5


References




















Science has authority, not because of white coats, or titles, but because of precision and transparency: you explain your theory, set out your evidence, and reference the studies that support your case.

Ben Goldacre



- ¹ N. G. Connelly, T. Damhus, R. M. Hartshorn and A. T. Hutton, *Red Book: IUPAC Nomenclature of Inorganic Chemistry*. Third edition, Blackwell Scientific Publications, Oxford, **1990**. 
- ² D. Seyferth, *Organometallics* **2001**, *20*, 1488–1498. 
- ³ W. C. Zeise, *Ann. der Phys. und Chemie* **1831**, *97*, 497-541. 
- ⁴ M. J. S. Dewar, *Bull. Soc. Chim. Fr.* **1951**, C79.
- ⁵ J. Chatt, L. A. Duncanson, *J. Chem. Soc.* **1953**, 2939–2947. 
- ⁶ M. B. Smith, J. March, *March's Advanced Organic Chemistry*, John Wiley & Sons, Inc., Hoboken, NJ, USA, **2006**.
- ⁷ T. Kamikawa, T. Hayashi, *Synlett* **1997**, *1997*, 163–164. 
- ⁸ a) T. J. Kealy, P. L. Pauson, *Nature* **1951**, *168*, 1039–1040;  b) S. A. Miller, J. A. Tebboth, J. F. Tremaine, *J. Chem. Soc.* **1952**, 632–635. 
- ⁹ a) G. Wilkinson, M. Rosenblum, M. C. Whiting, R. B. Woodward, *J. Am. Chem. Soc.* **1952**, *74*, 2125–2126;  b) J. D. Dunitz, L. E. Orgel, A. Rich, *Acta Crystallogr.* **1956**, *9*, 373–375. 
- ¹⁰ G. W. Coates, *Chem. Rev.* **2000**, *100*, 1223–1252. 
- ¹¹ G. Gasser, I. Ott, N. Metzler-Nolte, *J. Med. Chem.* **2011**, *54*, 3–25. 
- ¹² L. Vaska and J.W. Di Luzio, *J. Am. Chem. Soc.* **1961**, *83*, 2784-2785. 
- ¹³ A. Fredga, in *Nobel Lect. Chem. 1963-1970*, **1972**.
- ¹⁴ P. T. Anastas, J. C. Warner, *Green Chemistry: Theory and Practice*, **1998**, Oxford University Press: New York.
- ¹⁵ a) R. Sheldon, *Chem. Commun.* **2001**, *23*, 2399-2407. ; b) P. Wasserscheid and W. Keim, *Angew. Chem. Int. Ed.* **2000**, *39*, 3772-3789. 
- ¹⁶ W. Leitner, *Acc. Chem. Res.* **2002**, *35*, 746-756. 
- ¹⁷ For Heck reaction see: B. K. Allam and K. N. Singh, *Synthesis*, **2011**, 1125-1131;  for Suzuki reaction see: L. Liu, Y. Zhang, Y. Wang, *J. Org. Chem.*, **2005**, *70*, 6122-6125;  for Negishi reaction see: A. Krasovskiy, C. Duplais and B. H. Lipshutz, *J. Am. Chem. Soc.*, **2009**, *131*, 15592-15593. 
- ¹⁸ B. H. Lipshutz, T. B. Petersen, A. R. Abela, *Org. Lett.*, **2008**, *10*, 1333-1336. 
- ¹⁹ P. T. Anastas, *Handbook of Green Chemistry, Volume 1: Homogeneous Catalysis*, **2010**, WILEY-VCH Verlag GmbH & Co. KGaA, Weinheim, Germany. 
- ²⁰ R. Sherr, K. T. Bainbridge and H. H. Anderson, *Phys. Rev.* **1941**, *60*, 473-479. 
- ²¹ K. Aleklett, D. J. Morrissey, W. Loveland, P. L. McGaughey and G. T. Seaborg, *Phys. Rev. C.* **1981**, *23*, 1044-1046. 
- ²² World Gold Council FAQ. Retrieved on 12 September **2013**, www.gold.org 
- ²³ Le riserve auree della Banca d'Italia, **2013**, 
- ²⁴ World Official Gold Holdings: International Financial Statistics, January **2015**, www.gold.org 
- ²⁵ <http://www.infomine.com/investment/metal-prices/> 
- ²⁶ H. Erdmann and P. Köthner, *Z. Anorg. Chem.* **1898**, *18*, 48.
- ²⁷ G. J. Hutchings, *Chem. Commun.* **2008**, *2008*, 1148-1164. 

- ²⁸ A. Corma and H. Garcia, *Chem. Soc. Rev.* **2008**, *37*, 2096-2126. 
- ²⁹ G. Zhang, Y. Peng, L. Cui and L. Zhang, *Angew. Chem. Int. Ed.* **2009**, *48*, 3112-3115. 
- ³⁰ A. Fürstner and P. W. Davies, *Angew. Chem. Int. Ed.* **2007**, *46*, 3410-3449. 
- ³¹ G. Frenking and N. Fröhlich, *Chem. Rev.* **2000**, *100*, 717-774. 
- ³² Q. Xu, Y. Imamura, M. Fujiwara and Y. Souma, *J. Org. Chem.* **1997**, *62*, 1594-1598. 
- ³³ K. K. Irikura and W. A. Goddard, *J. Am. Chem. Soc.* **1994**, *116*, 8733-8740. 
- ³⁴ M. Barysz and P. Pyykkö, *Chem. Phys. Lett.* **1998**, *285*, 398-403. 
- ³⁵ F. Aguirre, J. Husband, C. J. Thompson and R. B. Metz, *Chem. Phys. Lett.* **2000**, *318*, 466-470. 
- ³⁶ N. Salvi, L. Belpassi and F. Tarantelli, *Chem. Eur. J.* **2010**, *16*, 7231-7240. 
- ³⁷ D. J. Gorin and F. D. Toste, *Nature*, **2007**, *446*, 395-403. 
- ³⁸ A. S. K. Hashmi and F. D. Toste, *Modern Gold Catalyzed Synthesis*, **2012**, WILEY-VCH Verlag GmbH & Co. KGaA, Weinheim, Germany. 
- ³⁹ R. D. Crabtree, *The Organometallic Chemistry of the Transition Metals, 6th Edition*, **2014**, Wiley, Weinheim, Germany. 
- ⁴⁰ F. Scherbaum, A. Grohmann, B. Huber, C. Krüger and H. Schmidbaur, *Angew. Chem. Int. Ed. Engl.* **1988**, *27*, 1544-1546. 
- ⁴¹ L. Y. Cao, M. C. Jennings and R. J. Puddephatt, *Inorg. Chem.* **2007**, *46*, 1361-1368. 
- ⁴² a) A. S. K. Hashmi, *Chem. Rev.* **2007**, *107*, 3180-3211.  b) A. Arcadi, *Chem. Rev.*, **2008**, *108*, 3266-3325. 
- ⁴³ A. S. K. Hashmi, L. Schwarz, J.-H. Choi and T. M. Frost, *Angew. Chem., Int. Ed.* **2000**, *39*, 2285-2288. 
- ⁴⁴ a) R. A. Widenhoefer and X. Han, *Eur. J. Org. Chem.* **2006**, *2006*, 4555-4563.  b) X. Zeng, M. Soleilhavoup and G. Bertrand, *Org. Lett.* **2009**, *11*, 3166-3169.  c) R. L. LaLonde, J. W. E. Brenzovich, D. Benitez, E. Tkatchouk, K. Kelley, W. A. Goddard III and F. D. Toste, *Chem. Sci.* **2010**, *1*, 226-233. 
- ⁴⁵ L-P Liu and G. B. Hammond, *Chem. Soc. Rev.* **2012**, *41*, 3129-3139. 
- ⁴⁶ R. O. C. Norman, W. J. E. Parr and C. B. Thomas, *J. Chem. Soc. Perkin. Trans. 1*, **1976**, 1983-1987. 
- ⁴⁷ Y. Fukuda, K. Utimoto and H. Nozaki, *Heterocycles*. **1987**, *25*, 297-300. 
- ⁴⁸ M-C. Brandys, M. C. Jennings and R. J. Puddephatt, *J. Chem. Soc., Dalton Trans.* **2000**, *2000*, 4601-4606. 
- ⁴⁹ R. Uson, A. Laguna, M. Laguna, D. A. Briggs, H. H. Murray and J. P. Fackler, *Inorg. Synth.* **1989**, *26*, 85-91. 
- ⁵⁰ W. F. Kean, L. Hart and W. W. Buchanan, *Br. J. Rheum.* **1997**, *36*, 560-572. 
- ⁵¹ D. J. Gorin, B. D. Sherry and F. D. Toste, *Chem. Rev.* **2008**, *108*, 3351-3378. 
- ⁵² W. Wang, G. B. Hammond and B. Xu, *J. Am. Chem. Soc.* **2012**, *134*, 5697-5705. 
- ⁵³ A. Zhdanko and M. E. Maier, *ACS Catal.* **2014**, *4*, 2770-2775. 
- ⁵⁴ M. Jia and M. Bandini, *ACS Catal.* **2015**, *5*, 1638-1652. 
- ⁵⁵ C. Brouwer and C. He, *Angew. Chem., Int. Ed.* **2006**, *45*, 1744-1747. 
- ⁵⁶ A. Homs, C. Obradors, D. Lebœuf and Echavarren M., *Adv. Synth. Catal.* **2014**, *356*, 221-228. 
- ⁵⁷ Y. Xia, A. S. Dudnik, V. Gevorgyan and Y. Li, *J. Am. Chem. Soc.* **2008**, *130*, 6940-6941. 

- ⁵⁸ M. Jia, G. Cera, D. Perrotta, M. Monari and M. Bandini, *Chem. Eur. J.* **2014**, *20*, 9875-9878. 
- ⁵⁹ D. Weber, T. D. Jones, L. Adduci and M. R. Gagné, *Angew. Chem., Int. Ed.* **2012**, *51*, 2452-2456. 
- ⁶⁰ G. L. Hamilton, E. J. Kang, M. Mba and F. D. Toste, *Science* **2007**, *317*, 496-499. 
- ⁶¹ K. Aikawa, M. Kojima and K. Mikami, *Angew. Chem., Int. Ed.* **2009**, *48*, 6073-6077. 
- ⁶² a) A. S. K. Hashmi, *Angew. Chem., Int. Ed.*, **2010**, *49*, 5232-5241;  b) C. Obradors and A. M. Echavarren, *Chem. Commun.* **2014**, *50*, 16-28. 
- ⁶³ a) H. Schmidbaur and A. Schier, *Organometallics*, **2010**, *29*, 2-23 and reference therein;  b) R. E. M. Brooner, R. Widenhofer, *Angew. Chem., Int. Ed.* **2013**, *52*, 11714-11724. 
- ⁶⁴ A. Macchioni, *Chem. Rev.* **2005**, *105*, 2039-2074. 
- ⁶⁵ A. Macchioni, *Eur. J. Inorg. Chem.* **2003**, *2003*, 195-205. 
- ⁶⁶ a) C. Zuccaccia, N. G. Stahl, A. Macchioni, M. C. Chen, J. A. Roberts and T. J. Marks, *J. Am. Chem. Soc.* **2004**, *126*, 1448-1464;  b) G. Ciancaleoni, N. Fraldi, P. H. M. Budzelaar, V. Busico and A. Macchioni, *Dalton Trans.* **2009**, *2009*, 8824-8827;  c) L. Rocchigiani, G. Bellachioma, G. Ciancaleoni, A. Macchioni, D. Zuccaccia and C. Zuccaccia, *Organometallics* **2011**, *30*, 100-114;  d) L. Rocchigiani, G. Ciancaleoni, C. Zuccaccia and A. Macchioni, *Angew. Chem., Int. Ed.* **2011**, *50*, 11752-11755;  e) G. Ciancaleoni, N. Fraldi, P. H. M. Budzelaar, V. Busico and A. Macchioni, *Organometallics* **2011**, *30*, 3096-3105. 
- ⁶⁷ B. Binotti, G. Bellachioma, G. Cardaci, C. Carfagna, C. Zuccaccia and A. Macchioni, *Chem. Eur. J.* **2007**, *13*, 1570-1582. 
- ⁶⁸ For the importance of this technique in organometallic chemistry see: G. Bellachioma, G. Ciancaleoni, C. Zuccaccia, D. Zuccaccia and A. Macchioni, *Coord. Chem. Rev.* **2008**, *252*, 2224-2238;  P. S. Pregosin, *Pure Appl. Chem.* **2009**, *81*, 615-633. 
- ⁶⁹ a) D. Zuccaccia, L. Belpassi, F. Tarantelli and A. Macchioni, *J. Am. Chem. Soc.* **2009**, *131*, 3170-3171;  b) N. Salvi, L. Belpassi, D. Zuccaccia, F. Tarantelli and A. Macchioni, *J. Organomet. Chem.* **2010**, *695*, 2679-2686. 
- ⁷⁰ a) G. Ciancaleoni, L. Belpassi, F. Tarantelli, D. Zuccaccia and A. Macchioni, *Dalton Trans.* **2013**, *42*, 4122-4131;  b) D. Zuccaccia, L. Belpassi, L. Rocchigiani, F. Tarantelli and A. Macchioni, *Inorg. Chem.* **2010**, *49*, 3080-3082. 
- ⁷¹ P. S. Nolan, *Nature* **2007**, *445*, 496-497. 
- ⁷² G. Patrick, E. Lingen, C. W. Corti, R. J. Holliday and D. T. Thompson, *Topics in Catalysis*, **2004**, *30*, 273-279. 
- ⁷³ C. Vidal, L. Merza and J. García-Álvarez, *Green Chem.* **2015**, *17*, 3870-3878. 
- ⁷⁴ I. Ott, *Coord. Chem. Rev.* **2009**, *253*, 1670-1681. 
- ⁷⁵ C. W. Corti, R. C. Holliday and D. T. Thompson, *Top. Catal.* **2007**, *44*, 331-343. 
- ⁷⁶ a) F. Alonso, I. P. Beletskaya, M. Yus, *Chem. Rev.* **2004**, *104*, 3079-3160.  b) L. Hintermann, A. Labonne, *Synthesis* **2007**, *8*, 1121-1150.  c) C. Bruneau, P. H. Dixneuf, *Chem. Commun.* **1997**, 507-512. 
- ⁷⁷ M. G. Kutscheroff, *Chem. Ber.* **1884**, *17*, 13-29.  (b) M. G. Kutscheroff, *Chem. Ber.* **1909**, *42*, 2759-2762. 
- ⁷⁸ G. F. Hennion, D. B. Killian, T. H. Vaughn, J. A. Nieuwland, *J. Am. Chem. Soc.* **1934**, *56*, 1130-1132. 

- ⁷⁹ (a) D. B. Killian, G. F. Hennion, J. A. Nieuwland, *J. Am. Chem. Soc.* **1934**, *56*, 1786-1787.  (b) D. B. Killian, G. F. Hennion, J. A. Nieuwland, *J. Am. Chem. Soc.* **1936**, *58*, 80-81. 
- ⁸⁰ Acetaldehyde. In Ullmann's Encyclopedia of Industrial Chemistry, 7th ed.; Wiley-VCH: Weinheim, **2006**.
- ⁸¹ T. W. Clarkson and L. Magos, *Crit. Rev. Toxicol.* **2006**, *36*, 609-662. 
- ⁸² Report of the Social Scientific Study Group on Minamata Disease, In the Hope of Avoiding Repetition of a Tragedy of Minamata Disease, National Institute for Minamata Disease
- ⁸³ Timothy S. George, *Minamata: Pollution and the Struggle for Democracy in Postwar Japan*, Harvard University Press, **2001**.
- ⁸⁴ Minamata Disease The History and Measures - Chapter 2, Ministry of the Environment Government of Japan.
- ⁸⁵ Jane Hightower (**2008**). *Diagnosis Mercury: Money, Politics and Poison*, Island Press, p. 77.
- ⁸⁶ Report of the Intergovernmental Negotiating Committee to Prepare a Global Legally Binding Instrument on Mercury on the Work of Its First Session; United Nations Environment Programme: Stockholm, Sweden, **2010**.
- ⁸⁷ Y. Wu, S. X. Wang, D. G. Streets, J. Hao, M. Chan, J. Jiang, *Environ. Sci. Technol.* **2006**, *40*, 5312-5318. 
- ⁸⁸ China Chloro-Alkali Industry Association. The 12th Five-Year Plan of chloro-alkali industry in China. *China Chem. Ind. News* **2011**, *7*
- ⁸⁹ W. Ren, L. Duan, Z. Zhu, W. Du, Z. An, L. Xu, C. Zhang, Y. Zhuo and C. Chen, *Environ. Sci. Technol.* **2014**, *48*, 2321-2327. 
- ⁹⁰ K. Utimoto, *Pure Appl. Chem.* **1983**, *55*, 1845-1852. 
- ⁹¹ W. Hiscox, P. W. Jennings, *Organometallics* **1990**, *9*, 1997-1999. 
- ⁹² (a) M. Nishizawa, M. Skwarczynski, H. Imagawa, T. Sugihara, *Chem. Lett.* **2002**, *31*, 12-13.  In some cases, thermal heating without acidic promoters can be enough to achieve the hydration, see: (b) H. Chang, S. Datta, A. Das, A. Odedra, R. Liu, *Angew. Chem., Int. Ed.* **2007**, *46*, 4744-4747. 
- ⁹³ Y. Fukuda, K. Utimoto, *J. Org. Chem.* **1991**, *56*, 3729-3731. 
- ⁹⁴ (a) J. H. Teles, S. Brode, M. Chabanas, *Angew. Chem., Int. Ed.* **1998**, *37*, 1415-1418.  (b) J. H. Teles, M. Schulz, *Chem. Abstr.* **1997**, *127*, 121-499; BASF AG, WO-A1 9721648, **1997**.
- ⁹⁵ E. Mizushima, K. Sato, T. Hayashi, M. Tanaka, *Angew. Chem., Int. Ed.* **2002**, *41*, 4563-4565. 
- ⁹⁶ R. Casado, M. Contel, M. Laguna, P. Romero, S. Sanz, *J. Am. Chem. Soc.* **2003**, *125*, 11925-11935. 
- ⁹⁷ (a) P. Roembke, H. Schmidbaur, S. Cronje, H. Raubenheimer, *J. Mol. Catal. A* **2004**, *212*, 35-42.  For a recent report about the formation of cyclic acetals and thioacetals, see: (b) L. L. Santos, V. R. Ruiz, M. J. Sabater, A. Corma, *Tetrahedron* **2008**, *64* (34), 7902-7909. 
- ⁹⁸ a) B. K. Min and C. M. Friend, *Chem. Rev.* **2007**, *107*, 2709-2724;  b) A. Corma and H. Garcia, *Chem. Soc. Rev.* **2008**, *37*, 2096-2126. 
- ⁹⁹ C. Winter and N. Krause, *Green Chem.* **2009**, *11*, 1309-1312. 
- ¹⁰⁰ S. Sanz, L. A. Jones, F. Mohr and M. Laguna, *Organometallics*, **2007**, *26*, 952-957. 
- ¹⁰¹ E. T. Mendivil, P. Y. Toullec, J. Borge, S. Conejero, V. Michelet and V. Cadierno, *ACS Catal.* **2013**, *3*, 3086-3098.



- ¹⁰² E. Mizushima, T. Hayashi and M. Tanaka, *Org. Lett.* **2003**, *5*, 3349-3352. 
- ¹⁰³ J. H. Teles in *Modern Gold catalyzed synthesis* (Eds A. S. K. Hashmi, F. D. Toste) Wiley-VCH, **2012**, pp 201-236.
- ¹⁰⁴ a) E. Mizushima, K. Sato, T. Hayashi, M. Tanaka, *Angew. Chem. Int. Ed.* **2002**, *41*, 4563-4565;  b) N. Marion, R. S. Ramón, S. P. Nolan, *J. Am. Chem. Soc.* **2009**, *131*, 448-449;  c) J. Oliver-Meseguer, J. R. Cabrero-Antonino, I. Domínguez, A. Leyva-Pérez, A. Corma, *Science* **2012**, *338*, 1452-1455. 
- ¹⁰⁵ a) A. Zhdanko, M. M. Maier, *Chem. Eur. J.* **2014**, *20*, 1918-1930;  b) J. Roithová, Š. Janková, L. Jašíková, J. Váňa, S. Hybelbauerová, *Angew. Chem. Int. Ed.* **2012**, *51*, 8378-8382;  c) Y. Oonishi, A. Gómez-Suárez, A. R. Martín, S. P. Nolan, *Angew. Chem. Int. Ed.* **2013**, *52*, 9767-9771. 
- ¹⁰⁶ G. Ciancaleoni, L. Biasiolo, G. Bistoni, A. Macchioni, F. Tarantelli, D. Zuccaccia, L. Belpassi, *Organometallics* **2013**, *32*, 4444-4447. 
- ¹⁰⁷ E. P. Kündig, C. M. Saudan, G. Bernardinelli, *Angew. Chem., Int. Ed.* **1999**, *38*, 1220. 
- ¹⁰⁸ A. Kütt, T. Rodima, J. Saame, E. Raamat, V. Memets, I. Kaljurand, I. A. Koppel, R. Y. Garlyauskayte, Y. L. Yagupolskii, L. M. Yagupolskii, E. Bernhardt, H. Willner, I. Leito, *J. Org. Chem.* **2011**, *76*, 391-395. 
- ¹⁰⁹ T. M. Schmid, G. Consiglio, *Chem. Commun.* **2004**, 2318-2319. 
- ¹¹⁰ M. Raducan, M. Moreno, C. Bour, A. M. Echavarren, *Chem. Commun.* **2012**, *48*, 52-54. 
- ¹¹¹ M. Gómez-Gallego, M. A. Sierra, *Chem. Rev.* **2011**, *111*, 4857-4963. 
- ¹¹² E. M. Simmons, J. F. Hartwig, *Angew. Chem. Int. Ed.* **2012**, *51*, 3066-3072. 
- ¹¹³ S. G. Weber, D. Zahner, F. Rominger, B. F. Straub, *ChemCatChem* **2013**, *5*, 2330-2335. 
- ¹¹⁴ T. J. Brown, D. Weber, M. R. Gagné, R. A. Widenhoefer, *J. Am. Chem. Soc.* **2012**, *134*, 9134-9137. 
- ¹¹⁵ G. Kovács, G. Ujaque, A. Lledós, *J. Am. Chem. Soc.* **2008**, *130*, 853-864. 
- ¹¹⁶ M. Bandini, A. Bottoni, M. Chiarucci, G. Cera, G. P. Miscione, *J. Am. Chem. Soc.* **2012**, *134*, 20690-20700. 
- ¹¹⁷ a) G. Ciancaleoni, S. Rampino, D. Zuccaccia, F. Tarantelli, P. Belanzoni, L. Belpassi, *J. Chem. Theory Comput.* **2014**, *10*, 1021-1034;  b) R. H. Kang, H. Chen, S. Shaik, J. Yao, *J. Chem. Theory Comput.* **2011**, *7*, 4002-4011;  c) R. H. Rang, W. Lai, J. Yao, S. Shaik, H. Chen, *J. Chem. Theory Comput.* **2012**, *8*, 3119-3127. 
- ¹¹⁸ Y. Zhu, C. S. Day, A. C. Jones, *Organometallics* **2012**, *31*, 7332-7335. 
- ¹¹⁹ Functionalized ligands also may direct and promote nucleophilic attack. Y. Wang, Z. Wang, Y. Li, G. Wu, Z. Cao, L. Zhang, L. *Nature Comm.* **2014**, *5*, 3470. 
- ¹²⁰ K. V. Vasudevan, R. R. Butorac, C. D. Abernethy and A. H. Cowley, *Dalton Trans.* **2010**, *39*, 7401-7408. 
- ¹²¹ G. Bellachioma, B. Binotti, G. Cardaci, C. Carfagna, A. Macchioni, S. Sabatini and C. Zuccaccia, *Inorg. Chim. acta* **2002**, *330*, 44-51. 
- ¹²² P. de Frémont, N. M. Scott, E. D. Stevens and S. P. Nolan, *Organometallics* **2005**, *24*, 2411-2418. 
- ¹²³ P. de Frémont, N. Marion and S. P. Nolan, *Coord. Chem. Rev.* **2009**, *253*, 862-892. 
- ¹²⁴ a) H. M. J. Wang and I. J. B. Lin, *Organometallics* **1998**, *17*, 972-975;  b) J. C. Y. Lin, R. T. W. Huang, C. S. Lee, A. Bhattacharyya, W. S. Hwang, I. J. B. Lin, *Chem. Rev.* **2009**, *109*, 3561-3598. 








- ¹²⁵ M. Fèvre, J. Pinaud, A. Leteneur, Y. Gnanou, J. Vignolle, D. Taton, K. Miqueu and J. Sotiropoulos, *J. Am. Chem. Soc.*, **2012**, *134*, 6776-6784. 
- ¹²⁶ In concomitance with the preparation of this Thesis, Nolan and coworkers published a similar procedure. Please, see A. Collado, A. Gómez-Suárez, A. R. Martin, A. M. Z. Slawin and S. P. Nolan, *Chem. Commun.* **2013**, *49*, 5541-5543. 
- ¹²⁷ E. van Lenthe, A. E. Ehlers and E. J. Baerends, *J. Chem. Phys.* **1999**, *110*, 8943-8953. 
- ¹²⁸ C. C. Pye and T. Ziegler, *Theor. Chem. Acc.* **1999**, *101*, 396-408. 
- ¹²⁹ D. Zuccaccia, L. Belpassi, F. Tarantelli and A. Macchioni, *Eur. J. Inorg. Chem.* **2013**, *24*, 4121-4135. 
- ¹³⁰ a) C. Zuccaccia, A. Macchioni, I. Orabona and F. Ruffo, *Organometallics* **1999**, *18*, 4367-4372;  b) A. Macchioni, A. Magistrato, I. Orabona, F. Ruffo, U. Rothlisberger and C. Zuccaccia, *New J. Chem.* **2003**, *27*, 455-458. 
- ¹³¹ S. Macura and R. R. Ernst, *Molecular Physics* **1980**, *41*, 95-117. 
- ¹³² L. M. Slaughter, *ACS Catal.* **2012**, *2*, 1802-1816. 
- ¹³³ a) C. Bartolomé, Z. Ramiro, P. Pérez-Galán, C. Bour, M. Raducan, A.M. Echavarren and P. Espinet, *Inorg. Chem.* **2008**, *47*, 11391-11397.  b) C. Nieto-Oberhuber, S. López and A.M. Echavarren, *J. Am. Chem. Soc.* **2005**, *127*, 6178-6179.  c) C. Bartolomé, Z. Ramiro, D. García-Cuadrado, P. Pérez-Galán, M. Raducan, C. Bour, A. M. Echavarren and P. Espinet, *Organometallics* **2010**, *29*, 951-956.  d) C. Bartolomé, D. García-Cuadrado, Z. Ramiro and P. Espinet, *Organometallics* **2010**, *29*, 3589-3592.  e) C. Bartolomé, D. García-Cuadrado, Z. Ramiro and P. Espinet, *Inorg. Chem.* **2010**, *49*, 9758-9764.  f) A.S.K. Hashmi, T. Hengst, C. Lothschütz and F. Rominger, *Adv. Synth. Catal.* **2010**, *352*, 1315-1337.  g) H. Seo, B. P. Roberts, K. A. Abboud, K. A. Merz Jr. and S. Hong, *Org. Lett.* **2010**, *12*, 4860-4863.  h) H. Seo, D. R. Snead, K. A. Abboud and S. Hong, *Organometallics* **2011**, *30*, 5725-5730.  i) A. S. K. Hashmi, T. Haffner, M. Rudolph and F. Rominger, *Eur. J. Org. Chem.* **2011**, *2011*, 667-671.  l) A. S. K. Hashmi, T. Haffner, M. Rudolph and F. Rominger, *Chem. Eur. J.* **2011**, *17*, 8195-8201.  m) C. F. Bender and R. A. Widenhoefer, *Org. Lett.* **2006**, *8*, 5303-5305.  n) Y.M. Wang, C. N. Kuzniewski, V. Rauniyar, C. Hoong and F. D. Toste, *J. Am. Chem. Soc.* **2011**, *133*, 12972-12975.  o) M. C. Blanco Jaimes, C. R. N. Bçhling, J. M. Serrano-Becerra and A. S. K. Hashmi, *Angew. Chem. Int. Ed.* **2013**, *52*, 7963-7966. 
- ¹³⁴ V. Amendola, L. Fabbrizzi and L. Mosca, *Chem. Soc. Rev.* **2010**, *39*, 3889-3915 and reference therein. 
- ¹³⁵ K. A. Schug, W. Lindner, *Chem. Rev.* **2005**, *105*, 67-113 and references therein. 
- ¹³⁶ E. A. Kataev, C. Müller, G. V. Kolesnikov and V. N. Khrustalev, *Eur. J. Org. Chem.*, **2014**, *2014*, 2747-2753. 
- ¹³⁷ a) R. Romeo, N. Nastasi, L. Mosù Scolaro, M. R. Plutino, A. Albinati and A. Macchioni, *Inorg. Chem.* **1998**, *37*, 5460-5466;  b) D. Zuccaccia and A. Macchioni, *Organometallics* **2005**, *24*, 3476-3486;  c) L. Ion, D. Morales, J. Pérez, L. Riera, V. Riera, R. A. Kowenicki and M. McPartlin, *Chem. Commun.* **2006**, 91-93. 
- ¹³⁸ A. S. K. Hashmi, I. Braun, M. Rudolph and F. Rominger, *ChemCatChem* **2010**, *2*, 1226-1230. 
- ¹³⁹ G. Bistoni, L. Belpassi and F. Tarantelli, *Angew. Chem. Int. Ed.* **2013**, *52*, 11599-11602. 

- ¹⁴⁰ D. Zuccaccia, G. Bellachioma, G. Cardaci, G. Ciancaleoni, C. Zuccaccia, E. Clot and A. Macchioni, *Organometallics*, **2007**, *26*, 3930-3946. 
- ¹⁴¹ M. J. S. Dewar, *Bull. Soc. Chim. Fr.* **1951**, *18*, C71-C79.
- ¹⁴² J. Chatt and L. A. Duncanson, *J. Chem. Soc.*, **1953**, 2939-2942. 
- ¹⁴³ N. Winterton, G. J. Leigh, *Modern Coordination Chemistry. The legacy of Joseph Chatt*, **2002**, RSC, London. 
- ¹⁴⁴ C. A. Tolman, *Chem. Rev.*, **1977**, *77*, 313-348. 
- ¹⁴⁵ A. B. P. Lever, *Inorg. Chem.*, **1990**, *29*, 1271-1285. 
- ¹⁴⁶ A. B. P. Lever, *Inorg. Chem.*, **1991**, *30*, 1980-1985. 
- ¹⁴⁷ M. D. Sason, J. W. Kamplain and C. W. Bielawski, *J. Am. Chem. Soc.*, **2006**, *128*, 16514-16515. 
- ¹⁴⁸ D. M. Khramov, V. M. Lynch and C. W. Bielawski, *Organometallics*, **2007**, *26*, 6042-6049. 
- ¹⁴⁹ D. M. Khramov, E. L. Rosen, V. M. Lynch and C. W. Bielawski, *Angew. Chem. Int. Ed.*, **2008**, *47*, 2267-2270. 
- ¹⁵⁰ O. Back, H.-E. Martin, C. D. Martin, D. Martin, D. and G. Bertrand, *Angew. Chem. Int. Ed.*, **2013**, *52*, 2939-2943. 
- ¹⁵¹ L. Triguero, A. Föhlisch, P. Väterlein, J. Hasselström, M. Weinelt, L. G. M. Pettersson, Y. Luo, H. Agren and A. Nilsson, *J. Am. Chem. Soc.* **2000**, *122*, 12310-12316. 
- ¹⁵² L. Belpassi, I. Infante, F. Tarantelli and L. Visscher, *J. Am. Chem. Soc.* **2008**, *130*, 1048-1060. 
- ¹⁵³ G. Bistoni, S. Rampino, N. Scafuri, G. Ciancaleoni, D. Zuccaccia, L. Belpassi and F. Tarantelli, *Chem. Sci.*, **2016**, Accepted Article. 
- ¹⁵⁴ R. H. Crabtree, *Carbonyls, Phosphine Complexes, and Ligand Substitution Reaction*, in *The Organometallic Chemistry of the Transition Metals*, Fourth Edition, **2005**, John Wiley & Sons, Inc., Hoboken, NJ, USA. 
- ¹⁵⁵ E. O. Fischer and A. Maasböl, *Chem. Ber.* **1967**, *100*, 2445-2456. 
- ¹⁵⁶ G. Seidel, R. Mynott and A. Fürstner, *Angew. Chem. Int. Ed.* **2009**, *48*, 2510-2513. 
- ¹⁵⁷ M. M. Hansmann, F. Rominger, A. S. K. Hashmi, *Chem. Sci.* **2013**, *4*, 1552-1559. 
- ¹⁵⁸ A. S. K. Hashmi, *Angew. Chem. Int. Ed.* **2008**, *47*, 6754-6756. 
- ¹⁵⁹ A. M. Echavarren, *Nature Chem.* **2009**, *1*, 431-433. 
- ¹⁶⁰ G. Seidel, B. Gabor, R. Goddard, B. Heggen, W. Thiel and A. Fürstner, *Angew. Chem. Int. Ed.* **2014**, *53*, 879-882. 
- ¹⁶¹ G. Seidel and A. Fürstner, *Angew. Chem. Int. Ed.* **2014**, *53*, 4807-4811. 
- ¹⁶² R.E. Brooner and R. A. Widenhoefer, *Chem. Comm.* **2014**, *50*, 2420-2423. 
- ¹⁶³ R. J. Harris and R. A. Widenhoefer, *Angew. Chem. Int. Ed.* **2014**, *53*, 9369-9371. 
- ¹⁶⁴ C. Ferrer, C. H. M. Amijs and A. M. Echavarren, *Chem. Eur. J.* **2007**, *13*, 1358-1373. 
- ¹⁶⁵ D. Benitez, N. D. Shapiro, E. Tkatchouk, Y. Wang, W. A. Goddard III and F. D. Toste, *Nat. Chem.* **2009**, *1*, 482-486. 
- ¹⁶⁶ M. Alcarazo, T. Stork, A. Anoop, W. Thiel and A. Fürstner, *Angew. Chem. Int. Ed.* **2010**, *49*, 2542-2546. 

- ¹⁶⁷ Y. Xi, Y. Su, Z. Yu, B. Dong, E. J. McClain, Y. Lan and X. Shi, *Angew. Chem. Int. Ed.* **2014**, *53*, 9817-9821. 
- ¹⁶⁸ NACs are also known as acyclic diaminocarbene (ADCs): L. M. Slaughter, *ACS Catal.* **2012**, *2*, 1802-1816. 
- ¹⁶⁹ C. L. Perrin and T. J. Dwyer, *Chem. Rev.* **1990**, *90*, 935-967. 
- ¹⁷⁰ E. L. Eliel, S. H. Wilen, L. N. Mander, *Stereochemistry of Organic Compounds*, **1994**, Wiley, New York, and references therein. 
- ¹⁷¹ L. Rocchigiani, V. Busico, A. Pastore and A. Macchioni, *Angew. Chem. Int. Ed.* **2014**, *53*, 2157-2161. 
- ¹⁷² H. Xu and W. H. Bernskoetter, *J. Am. Chem. Soc.* **2011**, *133*, 14956-14959. 
- ¹⁷³ R. Dorta E. D. Stevens N. M. Scott, C. Costabile L. Cavallo C. D. Hoff, S. P. Nolan, *J. Am. Chem. Soc.* **2005**, *127*, 2485-2495. 
- ¹⁷⁴ H. Haas and R. K. Sheline, *J. Chem. Phys.* **1967**, *47*, 2996-3021. 
- ¹⁷⁵ C. R. Landis and F. Weinhold, *J. Comput. Chem.* **2007**, *28*, 198-203. 
- ¹⁷⁶ Z. Yu, B. Ma, M. Chen, H.-H. Wu, L. Liu and J. Zhang, *J. Am. Chem. Soc.* **2014**, *136*, 6904-6907. 
- ¹⁷⁷ A. Zhdanko and M. E. Maier, *Organometallics* **2013**, *32*, 2000-2006. 
- ¹⁷⁸ G. Ciancaleoni, L. Belpassi, D. Zuccaccia, F. Tarantelli, P. Belanzoni, *ACS Catal.* **2015**, *5*, 803-814. 
- ¹⁷⁹ a) D. Benitez, E. Tkatchouk, A. Z. Gonzalez, W. A. Goddard III, F. D. Toste, *Org. Lett.* **2009**, *11*, 4798-4801;  b) H. Clavier, S. P. Nolan, *Chem. Commun.* **2010**, *46*, 841-861;  c) P. Klahn, S. F. Kirsch, *ChemCatChem* **2011**, *3*, 649-652.  d) R. Rüttinger, J. Leutzow, M. Wilsdorf, K. Wilckens, C. Czekelius, *Org. Lett.* **2011**, *13*, 224-227;  e) X. Xu, S. H. Kim, X. Zhang, A. K. Das, H. Hirao, S. H. Hong, *Organometallics* **2013**, *32*, 164-171. 
- ¹⁸⁰ M. Kumar, G. B. Hammond, B. Xu, *Org. Lett.* **2014**, *16*, 3452-3455. 
- ¹⁸¹ a) A. S. K. Hashmi, J. P. Weyrauch, W. Frey and J. W. Bats, *Org. Lett.* **2004**, *6*, 4391-4394;  b) J. P. Weyrauch, A. S. K. Hashmi, A. Schuster, T. Hengst, S. Schetter, A. Littmann, M. Rudolph, M. Hamzic, J. Visus, F. Rominger, W. Frey and J. W. Bats, *Chem. Eur. J.* **2010**, *16*, 956-963;  c) A. S. K. Hashmi, A. M. Schuster and F. Rominger, *Angew. Chem., Int. Ed.* **2009**, *48*, 8247-8249;  d) A. S. K. Hashmi, A. M. Schuster, S. Gaillard, L. Cavallo, A. Poater, S. P. Nolan, *Organometallics* **2011**, *30*, 6328-6337. 
- ¹⁸² O. A. Egorova, H. Seo, Y. Kim, D. Moon, Y. M. Rhee, K. H. Ahn, *Angew. Chem., Int. Ed.* **2011**, *50*, 11446-11450. 
- ¹⁸³ W. Wang, M. Kumar, G. B. Hammond, B. Xu, *Org. Lett.* **2014**, *16*, 636-639. 
- ¹⁸⁴ S. R. Patrick, I. I. F. Boogaerts, S. Gaillard, A. M. Z. Slawin, S. P. Nolan, *Beilstein J. Org. Chem.* **2011**, *7*, 892-896. 
- ¹⁸⁵ Since the reaction should proceed through an anti-periplanar attack, the steric properties of L are expected not to influence both the nucleophilic attack and the breaking of the Au-C bond. C. A. Gaggioli, G. Ciancaleoni, L. Biasiolo, G. Bistoni, D. Zuccaccia, L. Belpassi, P. Belanzoni, F. Tarantelli, *Chem. Commun.* **2015**, *51*, 5990-5993. 
- ¹⁸⁶ Recent theoretical findings suggest that when BF_4^- is employed as counterion also the substrates, the products and the solvent can assist the proton shuttle: a) A. Couce-Rios, G. Kovács, G. Ujaque, A. Lledós, *ACS Catal.* **2015**, *5*, 815-829;  b) G. Kovács, A. Lledós, G. Ujaque, *Angew. Chem. Int. Ed.* **2011**, *50*, 11147-11151;  c) G. Kovács, A. Lledós, G. Ujaque, *Organometallics* **2010**, *29*, 5919-5926. 
- ¹⁸⁷ A. Zhdanko, M. Strçbele and M. E. Maier, *Chem. Eur. J.* **2012**, *18*, 14732-14474. 

- ¹⁸⁸ L. Rocchigiani, M. Jia, M. Bandini and A. Macchioni, *ACS Catal.* **2015**, *5*, 3911-3915. 
- ¹⁸⁹ a) D. J. C. Constable, A. D. Curzons, V. L. Cunningham, *Green Chem.* **2002**, *4*, 521-527;  b) M. S. Singh, S. Chowdhury, *RSC Adv.* **2012**, *2*, 4547-4592;  c) M. B. Gawande, V. D. Bonifacio, R. Luque, P. S. Branco, R. S. Varma, *ChemSusChem* **2013**, *7*, 24-44. 
- ¹⁹⁰ a) A. S. K. Hashmi, *Gold Bull.* **2004**, *37*, 51-65;  b) A. S. K. Hashmi, G. J. Hutchings, *Angew. Chem., Int. Ed.* **2006**, *45*, 7896-7936. 
- ¹⁹¹ a) M. Comotti, C. Della Pina, R. Matarrese, M. Rossi, *Angew. Chem., Int. Ed.* **2004**, *43*, 5812-5815;  b) A. S. K. Hashmi, J. P. Weyrauch, M. Rudolph, E. Kurpejović, *Angew. Chem., Int. Ed.* **2004**, *43*, 6545-6547;  c) C-Y. Zhou, P. W. H. Chan, C.-M. Che, *Org. Lett.* **2006**, *8*, 325-328;  d) Y. Xi, D. Wang, X. Ye, N. G. Akhmedov, J. L. Petersen, X. Shi, *Org. Lett.* **2013**, *16*, 306-309. 
- ¹⁹² Schrohe, *Chem. Ber.* **1875**, *8*, 367.
- ¹⁹³ a) A. Y. Fukuda, K. Utimoto, *J. Org. Chem.* **1991**, *56*, 3729-3731.  b) Y. Fukuda, K. Utimoto, *Bull. Chem. Soc. Jpn.* **1991**, *64*, 2013-2015. 
- ¹⁹⁴ J. W. Hartman, W. C. Hiscox, P. W. Jennings, *J. Org. Chem.* **1993**, *58*, 7613-7614. 
- ¹⁹⁵ a) H. T. He, C. R. Qi, X. H. Hu, Y. Q. Guan and H. F. Jiang, *Green Chem.* **2014**, *16*, 3729-3733;  b) B. Mathieu, A. Mann and A. Wagner, *Chem. Commun.* **2012**, *48*, 434-436. 
- ¹⁹⁶ a) F. X. Zhu, W. Wang and H. X. Li, *J. Am. Chem. Soc.* **2011**, *133*, 11632-11640;  b) F. Chevallier and B. Breit, *Angew. Chem., Int. Ed.* **2006**, *45*, 1599-1602. 
- ¹⁹⁷ a) N. Marion, R. Gealageas and S. P. Nolan, *Org. Lett.* **2008**, *10*, 1037-1037;  b) G. A. Carriedo, S. Lopez, S. Suarez-Suarez, D. Presa-Soto and A. Presa-Soto, *Eur. J. Inorg. Chem.* **2011**, *9*, 1442-1447;  c) N. A. Romero, B. M. Klepser and C. E. Anderson, *Org. Lett.* **2012**, *14*, 874-877;  d) G. A. Fernandez, A. S. Picco, M. R. Ceolin, A. B. Chopa and G. F. Silbestri, *Organometallics* **2013**, *32*, 6315-6323. 
- ¹⁹⁸ Y. Xu, X. Hu, J. Jing Shao, G. Yang, Y. Wu and Z. Zhanga, *Green Chem.*, **2015**, *17*, 532-537. 
- ¹⁹⁹ W. Wang, A. Zheng, P. Zhao, C. Xia and F. Li, *ACS Catal.* **2014**, *4*, 321-327. 
- ²⁰⁰ G. Mazzone, N. Russo and E. Sicilia, *J. Chem. Theory Comput* **2010**, *6*, 2782-2789. 
- ²⁰¹ C. M. Krauter, A. S. K. Hashmi and M. Pernpointner, *ChemCatChem* **2010**, *2*, 1226-1230. 
- ²⁰² J. Cordón, G. Jiménez-Osés, J. M. López-de-Luzuriaga, M. Monge, M. E. Olmos and D. Pascual, *Organometallics* **2014**, *33*, 3823-3830. 
- ²⁰³ P. Johnston, N. Carthey and G. J. Hutchings, *J. Am. Chem. Soc.* **2015**, *137*, 14548-14557. 
- ²⁰⁴ D. Gasperini, A. Collado, A. Gómez-Suárez, D. B. Cordes, A. M. Z. Slawin and S. P. Nolan, *Chem. Eur. J.* **2015**, *21*, 5403-5412. 
- ²⁰⁵ L. Hintermann, *Beilstein Journal of Organic Chemistry* **2007**, *3*, No. 22, 1-5. 
- ²⁰⁶ R. Uson, L. A. Oro, J. A. Cabeza, *J. Organomet. Chem.* **1983**, *247*, 105-116. 
- ²⁰⁷ A. S. K. Hashmi, B. Bechem, A. Loos, M. Hamzic, F. Rominger and H. Rabaa, *Aust. J. Chem.* **2014**, *67*, 481-499. 

- ²⁰⁸ a) M. Botta, F. Corelli, E. Petricci and C. Seri, *Heterocycles* **2002**, *56*, 1-2, 369-378;  b) A. Bacchi, M. Costa, B. Gabriele, G. Pelizzi and G. Salerno, *J. Org. Chem.* **2002**, *67*, 13, 4450-4457. 
- ²⁰⁹ M. Preisenberger, A. Schier and H. Schmidbaur, *J. Chem. Soc., Dalton Trans.*, **1999**, 1645-1650. 
- ²¹⁰ Z. Zhang, E. Szlyk, G. J. Palenik and S. O. Colgate, *Acta Cryst.* **1988**, *44*, 2197-2198. 
- ²¹¹ E. Y. Tsui, P. Müller and J. P. Sadighi, *Angew. Chem. Int. Ed.* **2008**, *47*, 8937-8940. 
- ²¹² A. Iglesias, K. Muniz, *Chem. Eur. J.* **2009**, *15*, 10563-10569. 
- ²¹³ S. Handa, L. M. Slaughter, *Angew. Chem. Int. Ed.*, **2012**, *124*, 2966-2969. 
- ²¹⁴ $\text{CisocyanateNC}(\text{CH}_3)_3$ not detected, please see: M. A. Celik, C. Dash, V. A. K. Adiraju, A. Das, M. Yousufuddin, G. Frenking and H. V. R. Dias, *Inorg. Chem.* **2013**, *52*, 729-742. 
- ²¹⁵ A. S. K. Hashmi, T. D. Ramamurthi and F. Rominger, *J. Organomet. Chem.* **2009**, *694*, 592-597. 
- ²¹⁶ G. Seidel, C. W. Lehmann and A. Fürstner, *Angew. Chem. Int. Ed.* **2010**, *49*, 8466-8470. 
- ²¹⁷ R. E. M. Brooner, T. J. Brown and R. A. Widenhoefer, *Chem. Eur. J.* **2013**, *19*, 8276-8284. 
- ²¹⁸ A. S. K. Hashmi, T. Lauterbach, P. Nçsel, M. H. Vilhelmsen, M. Rudolph and F. Rominger, *Chem. Eur. J.* **2013**, *19*, 1058-1065. 
- ²¹⁹ S. E. Thwaite, A. Schier and H. Schmidbaur, *Inorg. Chim. Acta*, **2004**, *357*, 1549-1557. 
- ²²⁰ A. Gimeno, A. B. Cuenca, S. Surez-Pantiga, C. Ramrez de Arellano, M. Medio-Simón and G. Asensio, *Chem. Eur. J.* **2014**, *20*, 683-688. 
- ²²¹ S. Attar, W. H. Bearden, N. W. Alcock, E. C. Alyea, J. H. Nelson, *Inorg. Chem.* **1990**, *29*, 425-433. 
- ²²² A. Zhdanko and M. E. Maier, *Chem. Eur. J.* **2013**, *19*, 3932-3942. 
- ²²³ J. Jeener, B. H. Meier, P. Bachmann, R. R. Ernst, *J. Chem. Phys.* **1979**, *71*, 4546-4553. 
- ²²⁴ R. Wagner, S. Berger *J. Magn. Reson. A* **1996**, *123*, 119-121. 
- ²²⁵ B. Lix, F. D. Sönnichsen, B.D. Sykes, *J. Magn. Reson. A*, **1996**, *121*, 83-87. 
- ²²⁶ ADF User's Guide. Release 2012.1, SCM, Theoretical Chemistry, Vrije Universiteit, Amsterdam, **2008**, <http://www.scm.com>; C. F. Guerra, J. G. Snijders, V. G. Te, E. J. Baerends, *Theor. Chem. Acc.* **1998**, *99*, 391-403;  G. T. Velde, F. M. Bickelhaupt, E. J. Baerends, C. F. Guerra, S. J. A. V. Gisbergen, J. G. Snijders, T. Ziegler, *J. Comput. Chem.* **2001**, *22*, 931. 
- ²²⁷ M. J. Frisch, G. W. Trucks, H. B. Schlegel, G. E. Scuseria, M. A. Robb, J. R. Cheeseman, G. Scalmani, V. Barone, B. Mennucci, G. A. Petersson, H. Nakatsuji, M. Caricato, X. Li, H. P. Hratchian, A. F. Izmaylov, J. Bloino, G. Zheng, J. L. Sonnenberg, M. Hada, M. Ehara, K. Toyota, R. Fukuda, J. Hasegawa, M. Ishida, T. Nakajima, Y. Honda, O. Kitao, H. Nakai, T. Vreven, J. A. Montgomery, Jr., J. E. Peralta, F. Ogliaro, M. Bearpark, J. J. Heyd, E. Brothers, K. N. Kudin, V. N. Staroverov, R. Kobayashi, J. Normand, K. Raghavachari, A. Rendell, J. C. Burant, S. S. Iyengar, J. Tomasi, M. Cossi, N. Rega, J. M. Millam, M. Klene, J. E. Knox, J. B. Cross, V. Bakken, C. Adamo, J. Jaramillo, R. Gomperts, R. E. Stratmann, O. Yazyev, A. J. Austin, R. Cammi, C. Pomelli, J. W. Ochterski, R. L. Martin, K. Morokuma, V. G. Zakrzewski, G. A. Voth, P. Salvador, J. J. Dannenberg, S. Dapprich, A. D. Daniels, Ö. Farkas, J. B. Foresman, J. V. Ortiz, J. Cioslowski, and D. J. Fox, Gaussian, Inc., Wallingford CT, **2009**. 

- ²²⁸ a) L. E. Van, E. J. Baerends, J. G. Snijders, *J. Chem. Phys.* **1993**, *99*, 4597-4610;  b) L. E. Van, E. J. Baerends, J. G. Snijders, *J. Chem. Phys.* **1994**, *101*, 9783-9792; 
- ²²⁹ S. Grimme, J. Antony, S. Ehrlich, H. Krieg, *J. Chem. Phys.* **2010**, *132*, 154104-154119. 
- ²³⁰ a) A. D. Becke, *Phys. Rev. A* **1988**, *38*, 3098-3100;  b) C. Lee, W. Yang and R. G. Parr, *Phys. Rev. B: Condens. Matter* **1988**, *37*, 785-789. 
- ²³¹ J. P. Perdew, *Phys. Rev. B* **1986**, *33*, 8822-8824;  J. P. Perdew, *Phys. Rev. B* **1986**, *34*, 7406-7406. 
- ²³² D. Marchione, L. Belpassi, G. Bistoni, A. Macchioni, F. Tarantelli and D. Zuccaccia, *Organometallics* **2014**, *33*, 4200-4208. 